Physical, chemical and thermal changes of coals and coal maceral concentrates during coke formation

A thesis submitted in partial fulfilment of the
Requirements for the degree of
Doctor of Philosophy

By

Wei Xie

Discipline of Chemical Engineering
The University of Newcastle
Australia

March, 2013

This thesis contains no material which has been accepted for the award of any degree or diploma in any university or other tertiary institution and, to the best of my knowledge and belief, contains no material previously published or written by another person, except where due reference has been made in the text. I give consent to this copy of my thesis, when deposited in the University Library, being made available for loan and photocopying subject to the provisions of the Copyright Act 1968.

Signed ----------

Wei Xie

Acknowledgements

I wish to acknowledge the financial support provided by the Australian Research Council (ARC) for the fundamental understanding of cokemaking.

There are many people I wish to thank for their help and support during my completing this thesis. Especially, I would like to express my sincere thanks to my principal supervisor Prof. Terry Wall, to whom I owe a great deal for the years scholarship, guidance, advice, criticism, help, motivation and inspiration he has provided. His wide variety of academic experiences in coal science and supervising PhD students are essential for the successful development of this thesis. The humble thanks I offer here cannot nearly express the depth of my gratitude.

I would also like to express my profound gratitude to my co-supervisor A/Prof. John Lucas, his deep understanding in CATA technique and wide knowledge in cokemaking inspired me a lot throughout my thesis. Particularly I want to express my sincere thanks to him for his help, trust, encouragement and inspiration during this thesis.

Dr. Rohan Stanger, one of my supervisors for advising and inspiring me during my thesis, is deeply thanked for his valuable supervision, the improvement of CATA technique and the development of DETA technique by him are essential for this thesis.

I would extend my gratitude to my industrial supervisor Dr. Merrick Mahoney from BHP research for his advice during this thesis. His participation in the regular weekly meeting with Prof. Terry Wall, A/Prof. John Lucas and Dr. Rohan Stanger for supervising me is appreciated.

Also, Prof. Jianglong Yu who was my supervisor during my Master degree from China is thanked for his assistance for recommending me to my principle supervisor Prof. Terry Wall, for which I had a chance to study as a PhD candidate in Australia.

I owe my deep gratitude to Dr. Liza Elliot and Dr. Zeenathul Farida Abdul Gani for their help in reading my thesis through and for their valuable comments. They also provided such valuable help and motivation during my experiments and my PhD confirmation, which gave me a lot of confidence that this thesis would be achieved.

Thanks also to Dr. Yinghui Liu and Dr. Harold Rogers for his assistance and advice during my experiments, to Dr. Kalpir Shah for his encouragement, and to Prof. Galvin Kevin, Dr. James Zhou, and Mr. Kelly Walton. Mr. Jamie Dickinson and Ms. Rashanthi Liyanaarachchi for the help during my using reflux classifier for coal macerals separation. I would also like to

thank Prof. Erich Kisi, Dr. Bob Loo and Mr Gareth for their assistance during my optical microscopy analysis for my coke samples.

I am also grateful to Ms. Jenny Martin who helped me a lot for my experimental consumables. I would extend my gratitude to the laboratory and workshop staff members for their timely help, Mr. Darren McCarthy, Mr. Con Safouris, Mr. Lonn Cooper, Mr. John Richards, Mr. Robert Jones, Mr. Jim Wilson, Ms. Jane Hamson, Mr. Mark Mason and Mr. Neil Gardner.

I wish I would never forget the help and the good company I shared with other PhD students in my lab; Renu Kumar, Zeenathul Farida Abdul Gani, Huali Cao, Hongyu Li, Dunyu Liu, Lawrance Belo, Tim Ting and Reinhold Spoerl; and the fourth year students, Jon Chao, Julian Zheng, Timothy Hopper and Andreas Scheyhing.

Finally, I would like to thank my parents, my two brothers and my cousins for their strong support and encouragement which made my PhD possible.

Table of contents

List of Figures

List of Tables

Nomenclature

Symbol	Description	Units
T	temperature	°C, K
T_R	resolidification temperature	°C, K
T_g	graphite (control) temperature	°C, K
T_s	surface temperature	°C, K
T_c	centre temperature	°C, K
T_r	temperature at radius r	°C, K
t	time	s
r	radius	m
m	mass	g
C_p	specific heat capacity	$J/m^3.K$, J/kg.K
k	thermal conductivity	W/m.K
L	length	m
D	diameter	mm, μm
wt%	concentration	wt. %
V	volume, vitrinite content	m^3, %
A	area	m^2
Q	heat rate	W
$Q_{(t)}$	heat flow for time increment Δt	W
$Q'_{R,t}$	Surface heat flux	W/m^2
ΔH	enthalpy of reactions	kJ/m^3
U	gas velocity	m/s
p	pressure	Pa
G*	overall resistance to deformation	

Greek symbols

θ	angle	degrees
δ	phase angle	degrees
ω	frequency	Hz
ν	frequency	Hz
γ_0	the maximum applied strain	
τ_0	the maximum stress response	
ρ	density	kg/m^3
α	thermal diffusivity	m^2/s
μ	viscosity	Pa.s

Subscript

Symbol	Description
max	maximum
min	minimum
vMax	vitrinite mean maximum reflectance
graphite	graphite
surface	surface
centre	centre

Abstract

The measured coke reactivity index (CRI) and coke strength after reaction (CSR) determined in experiments based on coke formed in pilot-scale coke ovens are the two main parameters that are employed to evaluate coke for its potential utilization in the blast furnace. Thermo-plasticity, such as swelling, permeability and fluidity, chemical reactions, such as the evolution of gases and tars, and thermal changes, such as heat of devolatilisation and thermal conductivity, on coal heating are known to dominate the transformation of coal to coke in the coke oven, and determine the CRI and CSR of coke. Coal properties, such as vitrinite and inertinite components, and coking conditions, such as heating rate and particle size, have also been found to influence the physical, chemical and thermal properties during coking.

Many studies have previously investigated the swelling of different coals and coal maceral concentrates as well as the influence of heating rate and particle size on swelling during coking. The literature has highlighted the correlations between swelling, mass loss and the properties of the released tars and gases for a range of coals and coal maceral concentrates using a number of techniques. However, the correlations between swelling and the dynamic evolution of total volatiles (gases and tars), and the physical and chemical properties of the evolved tars, are made from data collected from independent experiments and therefore the interpretations are not very clear. Previous work compared heat of devolatilisation between thermal coals and coking coals. For coking coals only, the differences in heat of devolatilisation and thermal conductivities between high fluidity and low fluidity coking coals also were studied. However, reasons for the differences in the thermal properties of different coals are still unclear. In particular, the effects of coal maceral components on heat of coal devolatilisation and thermal conductivity are still unknown. The potential associations of swelling and thermal changes with the properties of tars for coals and coal maceral concentrates are scarcely studied.

The main objectives of this study are therefore to identify the sequence of physical, chemical and thermal changes of heating coal and coal maceral concentrates to provide insights into the fundamental mechanisms in the transformation of coal to coke. This work in particular is focused on (a) separation of coal maceral concentrates without using chemicals; (b) simultaneous measurements of swelling and thermal changes of heating coal and coal maceral concentrates from a single experimental run; (c) characterising the dynamic evolution of gases and tars for difference coal maceral concentrates; (d) revealing the mechanisms in the

transformation of coal to coke thereby correlating the physical, chemical and thermal changes of coal and coal maceral concentrates.

To achieve the objectives, three novel techniques were employed.

A water based device called the Reflux Classifier was employed to separate coal maceral concentrates on the basis of varying settling rates of different density particles.

The existing Computer Aided Thermal Analysis (CATA) technique was modified to simultaneously estimate swelling and shrinkage, permeability, apparent volumetric specific heat and thermal conductivity of heating coal and coal maceral concentrates. Swelling and shrinkage of the heating coal and coal maceral concentrates were measured by the contraction and expansion of a compressible spring. The permeability of heating coal pellet was estimated based on Darcy's law by the measurements of swelling of coal sample bed and the pressure drop of gas flowing through the coal sample bed. The pressure drop of gas flowing through the coal sample bed was measured using a pressure sensor. Endothermic and exothermic behaviour of heating samples was evaluated based on the estimated apparent volumetric specific heat. The apparent volumetric specific heat and thermal conductivity were estimated by the measurements of the control, surface and centre temperatures of the heating sample.

A new technique, Dynamic Elemental Thermal Analysis (DETA), was used to measure the evolution of total volatiles, gases and tars from different coal maceral components. The released tars of maceral concentrates during devolatilisation were condensed using a tar condenser, while the residual tars in char were extracted using solvents of acetone and toluene. The physical properties, such as boiling point, and chemical properties, such as elemental compositions, for condensable and extracted tars also were evaluated using the DETA technique.

Based on four Australia coking coals, three different heating rates of 3, 5 and 10°C/min and two particle size ranges of 0-212 and 0-500 μm of raw coals were used to study the effects of heating rate and particle size on physical and thermal changes during coking. The experimental results indicated that rapid swelling occurred at the primary exothermic reaction (400-550°C) accompanied by an increase in thermal conductivity. The swelling was complete with the occurrence of an endothermic reaction (550-600°C) that corresponds to the onset of the secondary exothermic reaction. The secondary exothermic reaction (600-1000°C) was accompanied by the semi-coke shrinkage and a rapid increase in thermal conductivity. Increases in heating rate and particle size were found to promote maximum swelling, heat of

coal devolatilisation and thermal conductivity during the primary exothermic reaction, and shift these events to occur at lower temperatures.

Two coals were employed for coal maceral concentrate separation. A preliminary separation was conducted on a relatively low swelling coal with a particle size of 0-212 μm. The results indicated that the preliminary coal maceral concentrate separation can be affected by vitrinite content and particle size of the crushed coal. A second separation was made on a high swelling coal with size cuts of 106-212 μm and 212-500 μm. Vitrinite contents of the separated coal maceral concentrates varied from 96.0% to 26.1% (all analyses were in mmf, unless otherwise specified). A suite of carbonisation experiments of coal maceral concentrates were conducted at a heating rate of 10°C/min to evaluate the physical, chemical and thermal changes in the transformation of coal to coke.

Based on experimental observation, new insights were established into the contributions of coal maceral concentrates to the transformation of coal to coke include (a) vitrinite rich concentrates contribute to swelling, heat of exothermic reactions and the increase of thermal conductivity between 400 and 550°C; (b) with decreasing vitrinite content, a sequence of events related to the onsets of the physical, chemical and thermal changes all shifted to higher temperatures; (c) for vitrinite rich concentrate separated from a high swelling coal, heat of exothermic reactions during the primary devolatilisation, the maximum swelling, pressure drop of gas flowing through the coal sample and thermal conductivity at the maximum swelling (about 510°C) all increased linearly with vitrinite content independent of particle size. However, a linear trend did not correlate the changes of inertinite rich concentrates; (d) addition of inertinite rich concentrate to vitrinite rich concentrate suppressed swelling between 400 and 550°C and shifted the onset of swelling to a higher temperature. However, the addition had little effect on heat of exothermic reactions and thermal conductivity during this temperature region but increased the heat of endothermic reactions and decreased thermal conductivity between 550 and 600°C. Also, addition of inertinite rich concentrate to vitrinite rich concentrate gave little effect on contraction, heat of exothermic reactions and thermal conductivity between 600 and 1000°C.

Since vitrinite rich concentrates are responsible for swelling and thermal changes of heating coal, the correlations of physical, chemical and thermal changes of heating coal are detected based on one vitrinite rich concentrate and one medium vitrinite rich concentrate. The dominant event associated with coke formation is swelling during coal heating. The new findings of the present study relate to the temperature sequence of events prior to the first-detected onset of swelling and the temperature of rapid swelling during the formation of coke

from heating coal are (a) the release of measured tar identified by DETA technique was initiated at almost 180°C prior to the measured onset of swelling and is associated with endothermic and exothermic reactions identified by CATA technique; (b) the release of measured gas was initiated at less than 100°C prior to the onset of swelling; (c) the measured pressure drop of gas flowing through the coal sample indicated liquid formation and it increased about 30°C prior to the onset of swelling, decreased after this onset and increased again during rapid swelling; (d) the estimated thermal conductivity increased slightly about 30°C prior to the onset of swelling, apparently also due to liquid formation (but with less sensitivity than pressure drop), and to a greater degree during rapid swelling; (e) measured rapid swelling occurred over a temperature interval after the onset of swelling of about 40°C and was associated with an additional exothermic reaction and the release of gases.

Based on the measured sequence a suggested mechanism for rapid swelling requires the formation of metaplast, with the measured increases of pressure drop and thermal conductivity (at about 70°C prior to the onset of rapid swelling) being indicators of the onset of metaplast formation. A second requirement is the release of gases after sufficient metaplast has formed. The current measurements for gas and tar evolution, with the associated changes of pressure drop and thermal conductivity, support such a mechanism.

Chapter 1 Introduction and Objectives

1.1 Introduction

1.1.1 Coke in a blast furnace

In the blast furnace, coke not only provides heat energy and produces hot reducing gases to reduce iron oxides and carburize molten iron, it also performs a physical role of providing a permeable bed that allows the flow of gaseous and molten products while supporting the burden materials including iron ore and coke [1-4]. A high quality coke should be able to provide high thermal energy, high metal reduction and enough strength to support a smooth descent of the blast furnace burden with as little degradation as possible [5, 6].

Coke with high reactivity in the blast furnace can improve reduction efficiency and lower energy consumption but at the cost of lowering coke strength. Coke with low strength will weaken and be degraded into small particles. Excessive coke degradation leads to coke bed collapse, which could reduce permeability of the bed restricting flow of gases through the blast furnace, cause blockage of the tuyeres with coke residues and impair efficiency of blast furnaces performance [5]. An ASTM standard procedure (ASTM D 5314-93a) defines coke quality by testing CRI (Coke Reactivity Index) and CSR (Coke Strength after Reaction). For a good quality coke, the CRI should be low and the CSR index high. A strong relationship exists between the two indices [5, 6]. Results from Nippon Steel Corporation (NSC) suggested that CSR depends about 70% on coal properties and about 30% on coking conditions [7]. In general, it is considered that coke is suitable use in blast furnace operations when it has a CRI of 20-30 and a CSR of 60-75 [5, 8].

1.1.2 Coke transformation from coal

Coke is commercially produced in coke oven batteries by carbonization of coal from room temperature (25°C) to 1000°C in atmosphere with no oxygen present. During the coking process, coal passes through softening that initiates at around 300°C, fusion that initiates at around 400°C, which transform the solid coal into a meta-plastic material, followed by resolidification that occurs at around 550°C with the formation of semi-coke. These phase changes are accompanied by swelling (400-550°C) and contraction (over 550°C). The physical changes relate to chemical reactions which include depolymerisation of organic molecules with gases and tars evolution (400-550°C) and repolymerization (550-1000°C) with release of light gases and coke formation. These chemical reactions of organic molecules are accompanied by endo/exothermic processes. These physical, chemical and thermal

changes during the transformation of coal to coke can be affected by coal ranks, coal maceral content [9, 10] mineral constituents [11, 12], coal moisture content [13, 14], particle size, bulk density, coking temperature, and heating rate [15, 16].

During the transformation of coal to coke, swelling favours the development of porosity of coke, which can increase the reactivity of coke and the permeability of the coke in the blast furnace. However, high swelling tends to accompany high coking pressure, which may cause damage to the coke oven wall leading to shortened coke oven life and decreased coke strength. It was reported that swelling can be affected by softening, fusion and resolidification and the release of gases and tars [17, 18]. Therefore, it is necessary to launch ongoing work to indentify the phase changes and devolatilisation of the coal.

Coal devolatilisation due to the relaxation of organic molecules can affect swelling, contraction and endo/exothermic reactions [19]. The release of gases and tars can affect coking pressure, fluidity, thermal conductivity of meta-plastic material and the development of porosity of the char [19, 20]. Boiling point and viscosity of liquid tars have a direct link to weight loss [20] and the development of coking pressure [17] of the coal. Therefore, understanding in chemical changes for the release of volatiles, particularly the liquid tars, is a key step towards revealing the mechanisms in the transformation of coal to coke.

In an industrial coke oven, the thermal degradation of coal includes successive endo/exothermic reactions such as depolymerisation and repolymerization that cause gases and tars release, thermo-plasticity development accompanied by swelling and contraction resulting in coke formation [3]. Thus, heats of devolatilisation are related to coal properties and its transformation to coke [21]. Charged coal near the wall is firstly heated, and then conducts heat to the oven centre at a certain rate dependent on the thermal properties of the coal. In general, coal in the centre is not heated to resolidification temperature until 10 h after charging in the oven because of the low thermal conductivity. The differences of heating rates of coal between near the wall and in the centre can reduce the homogeneity of coke [22, 23]. Figures 1.1 and 1.2 show the slow coking progress from near the wall to the centre of the oven and the temperature distributions in a coke oven [24, 25]. In Figure 1.1 it still was at the metaplast stage between coke near the wall and coal at the centre when coke formed near the oven wall during coking. The other work in Figure 1.2 clearly showed the temperature distributions in a coke oven, time for reaching the resolidification temperature increased with distance from the oven wall. This Figure also showed the coke mass never asymptotically reached the wall temperature, at long times, which is consistent with the gap between coke and the oven wall in Figure 1.1. Therefore, the necessity for quantification of the heats of

endo/exothermic reactions and thermal conductivity arises from the need to better understand the coking process.

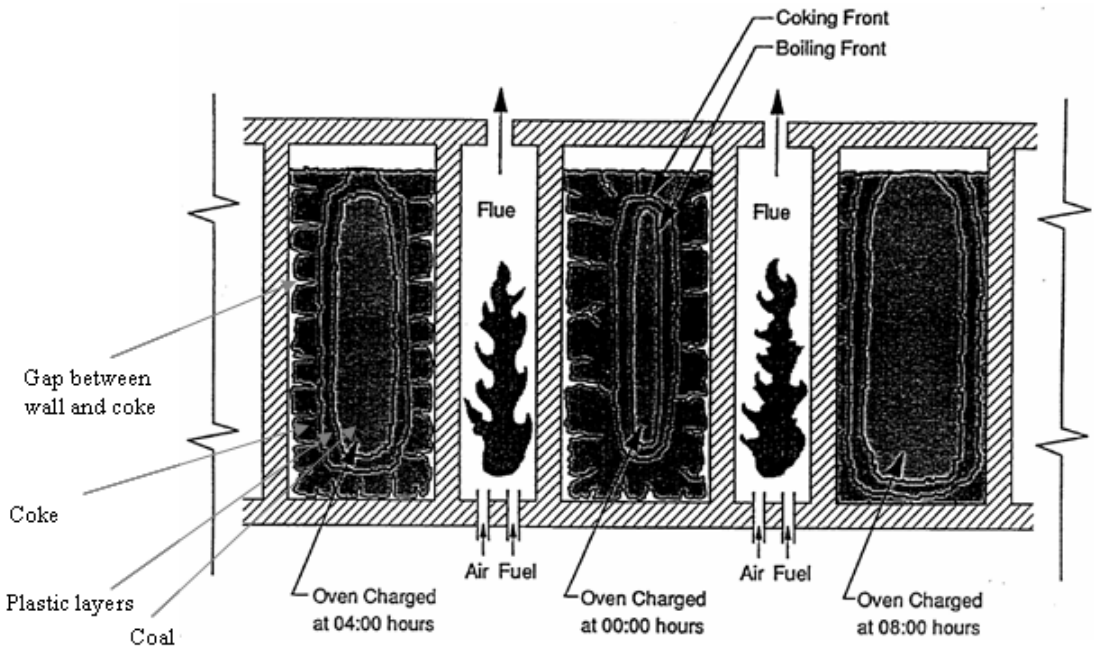

Figure 1.1. A longitudinal section of a coke oven battery [24].

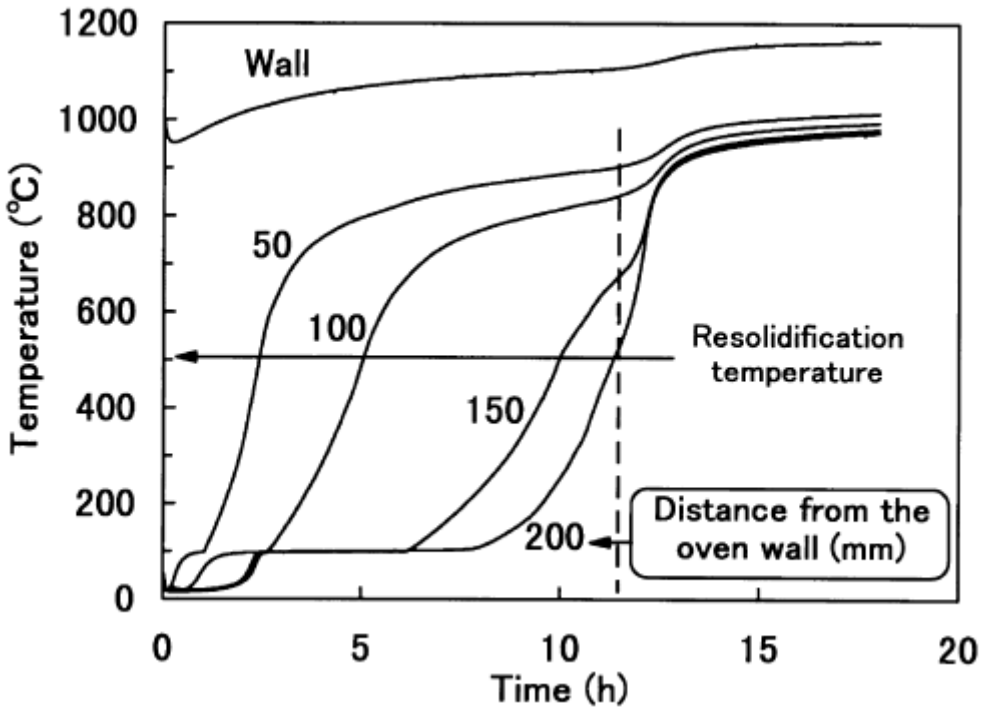

Figure 1.2. Changes in temperature with time at the relevant distance from the oven wall [25].

1.2 Objectives

This study aims to identify the physical, chemical and thermal changes during the transformation of coal to coke, including swelling and contraction, gases and tars evolved, and apparent specific heat and thermal conductivity of coal as a function of temperature. Once these properties can be accurately determined, this study aims to explore the correlations between them and finally reveal the mechanisms of coal to coke. The main objectives of this thesis therefore are to:

- Develop a Novel Computer Aided Thermal Analysis (CATA) which will be able to simultaneously measure physical (swelling and contraction) and thermal properties (apparent specific heat and thermal conductivity) of heating coal; develop a Dynamic Elemental Thermal Analysis (DETA) to describe chemical compositions of gases and tars evolved from heating coals and coal maceral concentrates.

- Synchronise measurements of swelling, apparent specific heat and thermal conductivity of heating coals; explore the relationship between swelling and endo/exothermic reactions as well as thermal conductivity of heating coal, and identify the possible effects of heating rate and particle size on swelling and thermal properties of heating coal.

- Utilize reflux classifier to separate coal maceral concentrates; clarify the contributions of vitrinite and inertinite components to swelling, permeability across the heating coal pellet, apparent specific heat and thermal conductivity; relating thermal conductivity to fluidity during the transformation of coal (coal maceral concentrates) to coke.

- Analyse chemical compositions of gases and tars evolved from vitrinite and inertinite components; exam thermodynamic characteristics (boiling point and chemical compositions) of tars from vitrinite or inertinite components.

1.3 Outline of the thesis

The thesis has been organised into ten Chapters. Each Chapter deals with one specific topic surrounding the objectives mentioned above. Brief descriptions of these Chapters are as follows.

- Chapter 1 provides an overview of the thesis.

- Chapter 2 reviews the current understanding in physical, chemical and thermal changes of heating coals, including softening, fluidity, permeability, resolidification, swelling and contraction; gases and tars evolutions and their chemical compositions; endo/exothermic reactions (characterised by apparent specific heat) and thermal conductivity. Therefore, this Chapter will identify what research needs to be done.

- Chapter 3 summarises the experimental methodology for this study.

- Chapter 4 discusses the synchronous measurements of swelling, apparent specific heat and thermal conductivity of heating coal, investigates the effects of heating rate and particle size on these physical and chemical parameters.

- Chapter 5 investigates preliminary coal maceral concentrates separation and the swelling, apparent specific heat and thermal conductivity of heating coal maceral concentrates.

- Chapter 6 investigates particle size controlled coal maceral concentrates separation and the swelling, apparent specific heat and thermal conductivity of coal maceral concentrates.

- Chapter 7 investigates thermal permeability of coal maceral concentrates.

- Chapter 8 studies dynamic gases and tars evolutions of vitrinite and inertinite components; analyses physical (boiling point) and chemical (chemical compositions) properties of tars from vitrinite and inertinite components.

- Chapter 9 summarizes the correlations between physical, chemical and thermal changes (apparent specific heat and thermal conductivity) during the transformation of coal to coke.

- Chapter 10 concludes the thesis and outlines future research recommendations.

Chapter 2 Literature review

2.1 Introduction

This literature review has broadly covered studies in coking coal properties, carbonization behaviour of coking coal and coal macerals concentrates separated from coking coal. Typically, this review will summarize three aspects: the first one introduces the concepts of physical, chemical and thermal changes during cokemaking, including coal devolatilisation, softening, plasticity (fluidity), permeability, swelling, resolidification, and shrinkage as well as specific heat and thermal conductivity; the second one is a literature review of the experimental techniques for studying the physical, chemical and thermal changes of coal during heating; the third aspect includes a literature review of physical, chemical and thermal changes of coal and coal maceral concentrates during heating. In the meanwhile, the review will also discuss the limitation of current experimental techniques, propose the possibility of developing novel techniques which can synchronously reveal the plasticity (fluidity and swelling) and thermal properties (apparent specific heat and thermal conductivity) of the heating coal and coal maceral concentrates; and analyse the chemical compositions of gases and tars evolved during coal maceral concentrates heating to reveal the contributions of coal maceral concentrates to the formation of coke.

2.2 Coal and its heterogeneity

2.2.1 Coal and its organic constituents

Coal is a chemically and physically heterogenous mineral or rock consisting principally of carbon, hydrogen, and oxygen, with lesser amounts of sulphur and nitrogen. Other constituents are the ash-forming inorganic compounds distributed as discrete particles of mineral matter throughout the coal substance. Coal varies remarkably in its chemical and physical properties depending on its maturity and geological environment of the coalification. Some coals melt and become plastic when heated and evolve gases and tars leaving a residue of coke. Coals that do not melt also evolve gases and tars when heated, but leave a residue of a friable char instead of coke. Coal may be burned to generate heat or it may be carbonized to produce coke. Coal may also be hydrogenated to produce liquid fuels, or hydrogasified to produce methane. Synthesis gases or gaseous fuels can be produced as the principal product by completely gasifying coal with oxygen and steam or air and steam [26].

In terms of the operational definitions, coal can be divided into moisture, volatile matter, fixed carbon, and ash based on the proximate analysis [27]. Moisture includes free water,

inherent moisture that is absorbed within the pore structure of coal, and water of constitution that is mainly combined with the mineral matter [3]. The volatile matter includes organic and mineral compositions. Ash is oxidised mineral matter. Volatile matter is an important parameter for evaluating coal properties because this helps to classify the coking coals and largely determines the fixed carbon limits. Since volatile matter is removed during carbonization; a coal with lower volatile will give a higher percentage of coke. However, coals below 14% volatile matter will not form coke and on the other hand, coals of extremely high volatile matter either can not form a coke or will make a poor quality coke. Possibly 38% volatile matter could be considered the upper limit [28].

Ultimate analysis indicates the chemical composition of the coal consists primarily of carbon, hydrogen, nitrogen, oxygen, and sulphur, on an ash-free basis. The rank of a coal is directly related to its carbon content, with a highly graphitic material representing the ultimate product of the coalification process [27, 29]. Carbon is the main residue in coke after coal carbonization and it plays the role of reducing iron ore to metal iron in the blast furnace. Coke strength is essential for blast furnace operation. There is a direct relationship between the oxygen content and the quality of coke produced; high oxygen coals produce relatively weak cokes [28].

There have been substantial efforts to explain the organic molecular structure of coal, but this becomes extremely difficult because of the variety of coal types, the heterogeneity of a single coal, and the complexity of individual coal constituents. It has been suggested that the chemical substance contains classical organic functional groups, e.g., mainly carbonyl and hydroxyl, aromatic and heterocyclic ring units and aliphatic bridges [20, 29, 30]. Some hypothetical structures for coal constituents have been proposed [20, 29-33]. Shinn [33] constructed the molecular structure of bituminous coal by piecing together the aromatics, functional group and aliphatics fractions that built by a “retrograde synthesis” based on the detailed chemical analyses of both coal and products from liquefactions. The structure is shown in Figure 2.1; bituminous coal is composed of the relative abundance of single and two ring structures with the absence of more than four aromatic rings. A number of cross-linking exists between aromatic clusters, but limited hydroaromatic structures. Oxygen is the predominant heteroatom within two macromolecules. Functional groups, particularly, the hydroxyl groups seem to be important to thermal processing.

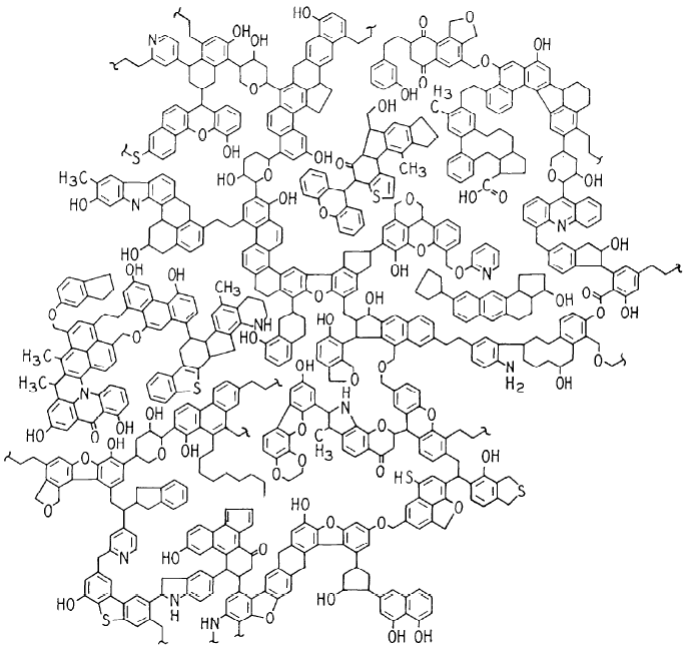

Figure 2.1. Shinn model of bituminous coal structure [33].

2.2.2 Coal maceral compositions

2.2.2.1 Coal petrography

As a heterogenous substance with a mixture of organic materials (i.e., the coal matrix) [20, 30, 31] and inorganic materials (i.e., the mineral matter) [27, 34, 35], microscopically, coal has a pronounced banded feature recognized as bright, predominantly bright or dull in appearance. The identifiable banded components are termed as lithotypes [27, 36]. Microscopically, the organic materials of coal are made up of complex maceral constituents classified mainly as three groups, i.e., liptinite (exinite), vitrinite and inertinite [35, 36]. Table 2.1 gives a survey of the three maceral groups and the individual macerals belonging to them [27]. In the reflected-light microscope the light impinges normally on the polished specimen surface. Most of the light is absorbed by the coal, but some is reflected back through the objective lens to the eye-piece. Since the proportion of incident light that is reflected is controlled by the chemical composition and molecular structure of the specimen, measurement of the reflectance can be used as a guide to the chemical properties of very small areas (volume) of coal [35]. The reflectance of each maceral groups changes in the order: liptinite < vitrinite < inertinite, as seen in Figure 2.2 [27].

Table 2.1. Maceral groups and macerals of hard coals ([27], after Techmüller [37]).

Group	*Maceral*	*Characteristics*
Vitrinite	telinite	cell walls
	collinite (telo-)	amorphous (gel or gelified (tissue))
	collinite (detro-)	amorphous (gel or gelified (detritus))
	corpocollinite	cell fillings
	vitrodetrinite	detritus
Liptinite (formerly exinite)	sporinite	spores, pollen
	cutinite	cuticles
	suberinite	suberinised cell walls (cork)
	fluorinite	plant oils
	resinite	resins, waxes, latex
	alginite	algae
	bituminite	amorphous (bacterial, algal, faunal)
	chlorophyllinite	chlorophyll
	exsudatinite	secondary exudates
	liptodetrinite	detritus
Inertinite	fusinite	cell walls (charred, oxydised)
	semi-fusinite	cell walls (partly charred, oxydised)
	sclerotinite	fungal cell walls
	macrinite	amorphous gel (oxydised, metabolic)
	micrinite	secondary relics of oil generation (mainly)
	inertodetrinite	detritus

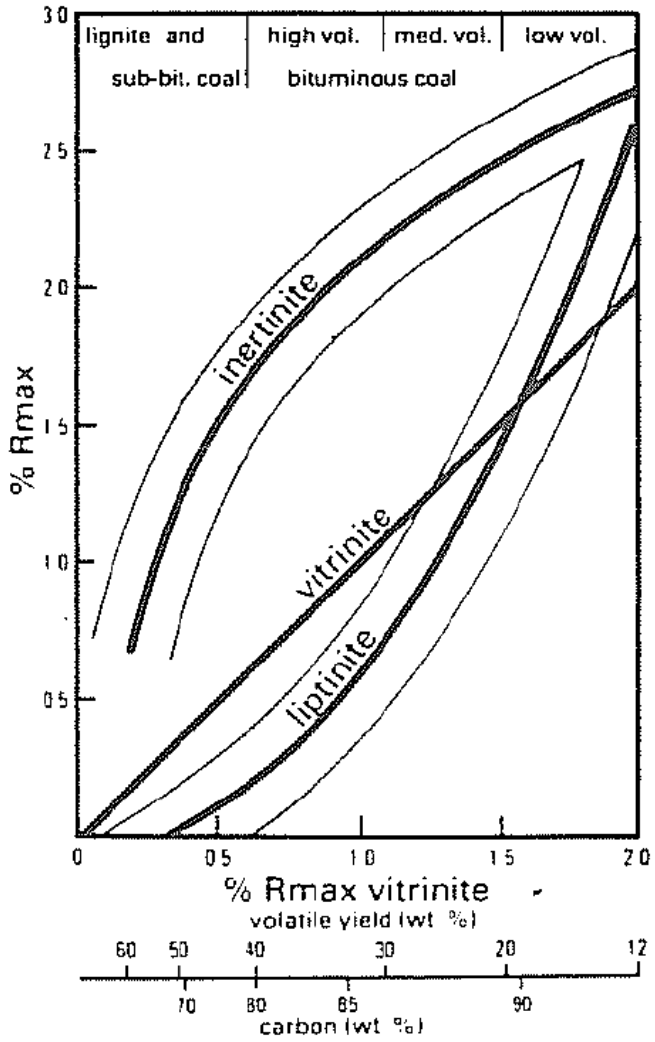

Figure 2.2. Reflectance of macerals as a function of coal rank, the maximum reflectance of vitrinite is chosen as a parameter for the coal rank, R_{Max} is mean maximum reflectance [27].

2.2.2.2 Coal maceral separation

In order to get a clear understanding in individual coal maceral group properties, one of the feasible methods is to separate macerals components from coals. It was reported that for any rank coal vitrinite is lighter than inertinite [27]. Separation of coal macerals utilises the difference in density among maceral groups. Techniques such as density gradient centrifugation (DGC) for ultrafine particle [38, 39] and sink-float separation [15, 40, 41] for larger particles are employed. The techniques have been extensively used in literature. Maceral separation with dense liquids, such as aqueous cerium chloride [38, 42], zinc chloride [43] or carbon tetrachloride and bromoform [40] not only separate macerals, but control the density range of the concentrates. The isopycnic density gradient method [38], in which the density range of the gradient encompasses the expected density range of the particles, is not dependent on particle size, but only on particle density. Sink-float techniques are easy to use, but many repetitive cycles are needed to obtain a particular enrichment level

by varying the specific gravity of the density media. Organic dense media present a safety hazard and may impact on the coking behaviour during subsequent testing [44]. Inorganic dense media solutions, such as zinc chloride [43], which may not be completely removable, may also have a deleterious effect on coking behaviour. In addition, relatively sharp maceral separation based on these techniques requires ultrafine milling of the particles (such as to 10 μm) followed by DGC to get pure vitrinite or inertinite [27], but these fine particles are not suitable for further coking analysis. Galvin et al. [45-47] introduced a relatively new technique named the Reflux Classifier (RC) for fine particles separation on the basis of the principle of gravity separation. They have successfully separated coal and mineral matter less than 2 mm in size without introducing any impurity.

2.2.2.3 Coal maceral properties

Since different macerals are derived from different original plant tissues or coalified in different geological environments, there are remarkable distinctions in their chemical and physical properties between different maceral groups. For instance, it was suggested that the liptinite and vitrinite components are the reactive components during coal carbonisation. They are related to the development of fluidity and swelling. Inertinite behaves as more or less as inert additives during carbonisation, they show little fluidity and swelling [3, 27]. In terms of chemical compositions, in general, for a given rank coal, liptinite has the highest H and lowest O contents, vitrinite shows the medium range H and O up to the anthracite rank, inertinite shows the highest C and O contents, as seen in Figure 2.3 [35]. Therefore, volatile matter content, hydrogen content and H/C ratio in different maceral groups show the variations in the order: liptinite > vitrinite > inertinite, these differences are attenuated with the increase in rank [27, 48]. The difference of H/C is a typical characteristic from vitrinite to inertinite. The changes of C, H and O concentrations before and after pyrolysis of different macerals indicate the contribution of different macerals towards devolatilisation [49].

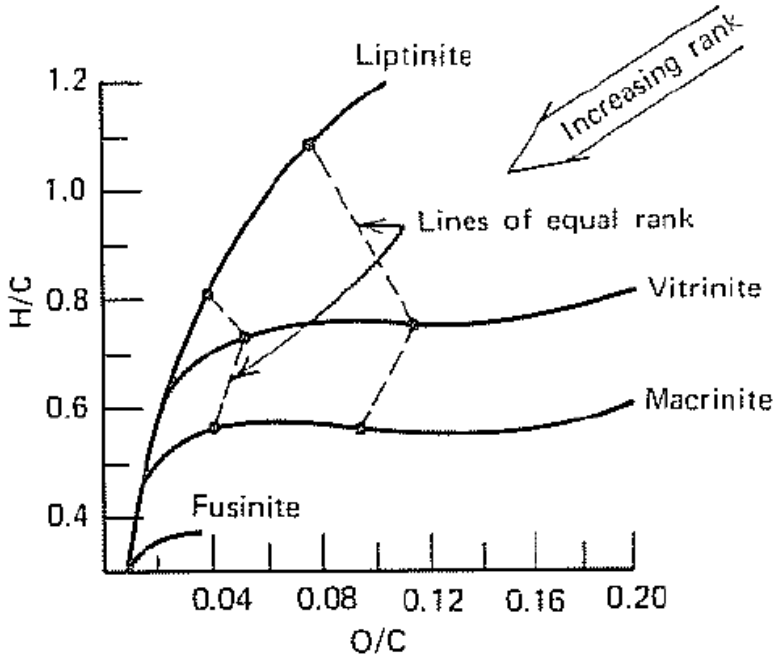

Figure 2.3. H/C and O/C content of macerals as a function of coal rank [35].

2.2.3 Coal classification

Coal is generally classified by its rank which is a way of expressing the progressive metamorphism of coal from lignite (low in rank), sub-bituminous coal, bituminous coal to meta-anthracite (high in rank). The rank is generally indicated by its heat value and fixed carbon content [34, 50]. The major transformations in coal's properties with increasing coal rank can be summarized as [36, 48]: (1) a drop in moisture and a marked decrease in the oxygen content due to the loss of hydroxyl, carbonyl and carboxyl group; (2) a removal of aliphatic and alicyclic groups which causes an important reduction in the volatile matter content with a parallel increase in the aromaticity during the bituminous coal stages; (3) the anthracite stage that is characterized by a rapid fall of hydrogen (H_2) content and a strong increase in both the reflectance and the optical anisotropy. Whitehurst et al. [51] reported an increase in the aromaticity of coal with increasing rank. The aromatic carbon content increases from 40% to 50% for sub-bituminous coal to over 90% for anthracite. Due to the changes in properties, the behaviour of coals of different ranks varies drastically during carbonization and combustion [36].

Based on Chemical Percolation Devolatilisation (CPD) model and ^{13}CNMR estimates, Fletcher et al. [52] suggested that the high rank coals have low side chain molecular weights compared to the low rank coals. This is consistent with measured aromaticities as a function of coal rank; high rank coals exhibit higher carbon aromaticities than low rank coals. The NMR data also correspond to the observation that more aliphatic -CH_2- is seen in FTIR spectra of low rank coal tars than in high rank coal tars [53]. During pyrolysis, the low rank

coals (60-75% C) attain the same total volatiles yields as the high volatile bituminous coals (80-80% C), and the total volatiles yields decrease for the high rank coals (>85% C). In general, tar yields are low for the low rank coals; they increase and reach a maximum for the high volatile bituminous coals, and then decrease for high rank coals. Also, Solomon et al. [54] and Suuberg et al. [55] suggested that the cross-linking that prevents further evolution of tars by repolymerising the molecular species occurs at low temperatures for the low rank coals compared to the high rank coals.

For most coals, vitrinite is the principal maceral [28, 35]. Reflectance of vitrinite is used as the indicator of coal rank [35, 36]. The greatest advantage of this method is that it measures a rank-sensitive property on only one petrographic constituent. In general, it is considered that vitrinite is associated with the basic properties of the macromolecular skeleton – aromaticity and size of condensed rings [27]. With increasing rank, aromaticity and molecular cluster size increase, as a result the reflectance also correspondingly increases [35].

In addition to the classification of rank based on vitrinite reflectance, coal can also be classified into coking coal and non-coking coal based on its carbonization properties [26]. Single coking coal is capable of forming coke under inert pyrolysis. Weakly coking or non-coking coals, such as anthracites, can be blended with coking coals during coke manufacture [5]. Under typical coking conditions, coking properties of coals may be determined by coal properties, such as volatile matter content, elements composition of C, H and O, and vitrinite reflectance [5, 8, 26, 56]. Some studies reported the associations of these parameters with coal coking properties, as shown in Table 2.2 [26]. Speight et al. [31] also reported that prime-quality coking coals should have volatile contents in the range 20-32% (dmmf), yield strong coke with good abrasion resistance. The main coke-forming substances in coal are the reactive vitrinite, together with liptinite and part of the semifusinites, which are called reactive macerals, becoming fluid and aiding in the development of the coke structure during cokemaking. Zimmerman [28] suggested that coals with percent reflectance of reactive macerals within the range 0.5 to 2.0 are suitable for cokemaking. Zhang et al [57] reported that cokes produced from coals with vitrinite reflections in the range 1.1-1.2% show the highest coke strength. Cokes from coking coal exhibit better resistance to breakage than their parent coals while the opposite behaviour has been observed for non-coking coals [58].

Table 2.2. Relationship between coal properties, such as elemental compositions and volatile matter, and the type of coke formed [26].

Genus	Class	Chief Uses	Percentage Composition C	H	O + N + S	% Volatiles at 900° C	% Fixed Carbon	Character of Carbonaceous Residue
A, Lignites	Noncaking	—	60–75	~ 5.0	20–35	> 45	< 55	Noncoherent
B, Bituminous	1. Noncaking, long flame	Reverberatory furnaces	75–80	4.5–5.5	15–20	40–45	55–60	Noncoherent
	2. Caking, long flame	Gas making	80–85	~ 5.0	10–15	32–40	60–68	Very porous coke
	3. Hard coking	Coke manufacture	84–89	5.0–5.6	5.5–11.0	26–32	68–74	Dense coke
	4. Hard coking, short flame	Coke manufacture and steam raising	88–90	4.5–5.5	5.5–6.5	18–26	74–82	Very dense coke
BC, Semibituminous	Noncaking, short flame	Steam raising	90–92	4.0–4.5	4.0–5.5	15–20	80–85	Weakly caking or noncoherent
C, Anthracitic and anthracites	1. Anthracitic, noncaking	Steam raising	92–94	3.0–4.0	3.0–4.5	8–15	85–92	Pulverent
	2. Anthracites, noncaking	Domestic and central heating; malting kilns				< 8	> 92	Pulverulent

All numerical data refer to the dry ashless coal.

2.2.4 Summary of coal and its heterogeneity

- Coal is a chemically and physically heterogenous substance with a mixture of organic materials and inorganic materials. Coal organic materials consist principally of carbon, hydrogen and oxygen, with lesser amounts of sulphur and nitrogen. These elements comprise coal organic matrix involving aromatic nuclei and methylene bridges. The ash-forming inorganic compounds distribute as discrete particles of mineral matter throughout the coal substance.

- Microscopically, coal organic components of complex maceral constituents can be classified mainly as three groups, i.e., liptinite (exinite), vitrinite and inertinite. Liptinite is rich in hydrogen, vitrinite has medium hydrogen and oxygen and inertinite shows the highest carbon and oxygen. Volatile matter content in maceral components changes in the order liptinite > vitrinite > inertinite. However, opposite trend in mean maximum reflectance was observed.

- Coal properties vary with coal constituents or coal rank. The reactive maceral components of liptinite and vitrinite tend to soften and fuse during carbonization while inertinite fraction tends to keep inert. Coals with vitrinite reflectance from about 0.9 to 1.7% are feasible for cokemaking. In general, bituminous coal produces a dense coke, suitable for coke manufacture.

2.3 Changes in coal during heating

2.3.1 Chemical changes

2.3.1.1 Devolatilisation

Coal is generally described as consisting mainly of hydroaromatic and aromatic clusters linked by aliphatic bridges [20, 29]. During primary devolatilisation, partial organic bonds break at temperature between 200 and 500°C, the coal softens and fuses to form a plastic material. Small molecular fragments can vaporize and be transported out of the heating coal pellet as gases and tars, heavy fragments are retained and solidify as char. During secondary devolatilisation, large molecular fragments that did not vaporize during primary devolatilisation evolve CO and H_2 by cross-link with further ring condensation [20, 36]. Saxena [59] suggested the primary devolatilisation starts initially with rupture of the weaker bonded aliphatic bridges at lower temperatures (400°C), while the secondary devolatilisation is mainly attributed to the condensation of the stronger bonds of polynuclear aromatic compounds at higher temperatures. Given [32] speculated that the devolatilisation consists of four steps: (1) a low-temperature (400-500°C) loss of hydroxyl groups, (2) dehydrogenation of some of the hydroaromatic structures, (3) scission of the molecule at the methylene bridges, and (4) rupture of the alicyclic rings.

The major compositions of gaseous products during coal devolatilisation include CO_2, CO, H_2, CH_4, NH_4, N_2, H_2S and C_xH_y [29, 59]. Tars are usually divided into low and high temperature tars [19, 60, 61]. Low-temperature tars consist of cyclic hydroaromatic structures and smaller amounts of olefines, paraffin hydrocarbons and aromatic compounds [19, 62], while high-temperature tars are composed mainly of cyclic aromatic hydrocabons ranging from single-ring benzene and alkyl benzenes to compounds containing possibly as many as 20 or more ring [61, 62]. The general trends of volatile matter during coal devolatilisation were summarized by Strezov et al. [19] based on the proposal by Saxena [59], as seen in Figure 2.4.

In addition to coal properties, the evolution of gases and tars can be affected by heating condition. Strezov et al. [63] examined the effect of heating rate on the evolutions of gases and tars. TGA was used in conjunction with FTIR for the analysis of evolved gases and tars. Details of this technique can be found elsewhere [64, 65]. They found that the rate of the evolution of gases and tars both increased with increasing heating rate at 10, 25 and 100°C/min. Temperature at which maximum rate of mass loss occurred also increased with increasing heating rate. Using TG-FTIR, Seebauer et al. [66] studied the effect of particle size on the evolution of pyrolysis products, they reported that particle size did not have a

significant effect on total volatiles, however, it was found that the use of smaller particles led to a higher extent of secondary reactions.

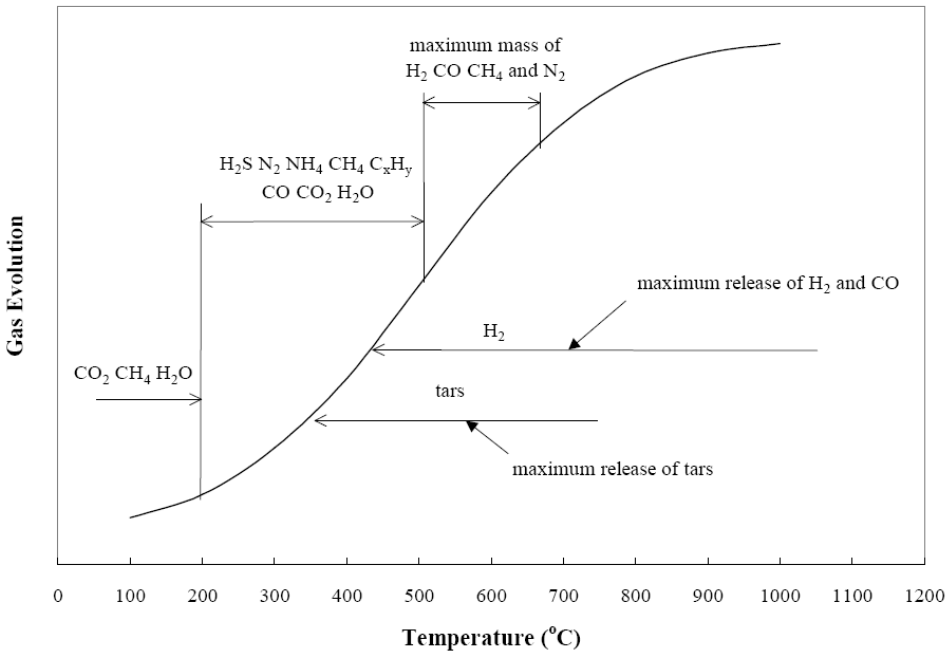

Figure 2.4. General trends for gases and tars evolution during coal devolatilisation [19].

2.3.2 Physical changes

2.3.2.1 Softening and fusion

A heating coal initially undergoes a softening and fusion process to form a meta-plastic material. The meta-plastic phase is followed by resolidification with the formation of semi-coke to coke [36, 67-71]. The visible softening of a heating coal under microscopic observation begins with the deformation of the individual particles that move into the inter-particle space [72]. Large particles further fuse with smaller particles. They show formation of pores and flowing structures. High bulk density improves the fusing of the grains immediately after the beginning of softening [73]. Habermehl et al. [73] summarized the softening and fusion mechanism, the pores due to fusion firstly begin to form followed by the formation of pores due to degasification in vitrinite. The temperature of the first formation of pores depends not only on the coal itself but also on carbonization conditions, such as the heating rate, bulk density and particle size. The shape and reflectivity of the liptinite remain unchanged at the beginning of softening, but immediately afterward their decomposition begins. The increasing softening is characterized by homogenization, which makes it impossible to distinguish between pores caused by fusion and by degasification. The viscosity of the plastic mass decreases and the gas formation increases. The disappearance of some

particle boundaries indicates certain limitations of flow. However, the particles do no flow together completely. As the temperature increases further, the properties of the plastic mass change continuously. The viscosity increases, the pore volume reaches its maximum value, and the reflectance increases.

Some experimental results implied the assumption that initial softening is not connected with decomposition, but a consequence of physical melting of a thermoplastic material [73-75]. This was shown by three observations, firstly, the softening is more or less reversible over cycles of heating, as long as pyrolysis reactions do not progress to any great extent, such as the very slow reactions below 370-380°C [74]. Secondly, the initial softening temperature depends little on the chemical composition in the range from 20% to 30% volatile matter, whereas other characteristic temperatures of pyrolysis, such as temperatures for maximum fluidity and resolidification increase with rank [3]. Thirdly, the softening temperature depends little on the heating rate [75], whereas other phenomena connected with pyrolysis show correlation with heating rate [3].

During physical changes, liptinite shows the greatest plasticity. Since vitrinite constitutes the majority of normal coals, its behaviour is not very different from that of the whole coal. At high rank (below 30% volatile matter) vitrinite is a little more fusible than the coal; at low rank it is a little less so. The difference shows up at the lower end of the range of coking coals, around 82% carbon. Inertinite tends to be infusible but not completely inert [3]. The limit between reactive and inert behaviour of semifusinites depends on the rank of the vitrinite or the coal. Semifusinites, with a reflectance of 0.1-0.2% above that of the vitrinite, are inert. The micrinite does not change during transition through the plastic zone and must therefore be considered inert [73]. Liptinite is generally found finely dispersed in the vitrinite. In the case of weakly coking coals of high volatile matter, the intimate contact between these two macerals sometimes allows the very fusible liptinite, through solvent effects, to induce fusion of vitrinite which, carbonized alone, would have remained infusible. The behaviour of a coal thus depends not only on the individual properties of its macerals and on their proportions, but also on their distribution [3].

2.3.2.2 Plasticity and swelling

Fluidity and viscosity

When coal is subjected to heating, the softening and fusion of the coal in the temperatures between 420-600°C causes it become plasticity in nature, called metaplast [3, 36] . The meta-plastic material shows fluidity and viscosity. Viscosity of coal during the meat-plastic stage is extremely important because it affects the rate of mass transport [76] and further affects the

internal pressure within the coal, thus influencing swelling. Some coals such as coking coals show significant fluidity [73]. The fluidity progress of heating coal is directly related to the coal petrographic components [27, 36, 77] and heating conditions [36, 73]. Van Krevelen et al. [27] found that liptinite becomes extremely fluid when heating; the inertinite shows no fluidity, whereas vitrinite takes an intermediate position. In maceral mixtures of vitrinite and inertinite, the non-softening inertinite has a strong depressing effect on the fluidity. Kidena et al. [78] studied the nature of plastic phenomena of vitrinite-rich and inertinite-rich fractions of two bituminous coals using a number of techniques. They reported that the vitrinite-rich fractions, which showed a larger swelling ratio, have a higher fluidity due to relatively greater number of substituents on aromatic rings, and their structures were constructed by relatively small aromatic clusters connected by aliphatic moieties and alicyclic parts. The inertinite-rich fractions, which show little fluidity in the plastic range, have larger aromatic clusters, fewer substituents (alkyl- and oxygen functional groups) on aromatic rings and a higher density of cross-linking than vitrinite-rich fractions from the same coal.

Permeability and swelling

Coal permeability can be defined by a lumped index of how well fluid passes through coal [79]. With the increase of viscosity, the permeability across the heating coal pellet decreases; it becomes difficult for gases and tars to escape from the plastic coal. Therefore, gas bubbles with very high internal pressure may form to swell the viscous mass. When primary devolatilisation is complete, the viscosity decreases so that the corresponding permeability increases. The gas pressure across the coking bed decreases through the formation of degasification pores, thus the swelling ends [73]. Therefore, considering the relationship between permeability and swelling, parameters for analysing swelling of heating coals may include the following aspects: the plastic layer thickness, the viscosity of the plastic material, permeability, the evolution rate of gases and tars and the development of degasification pores. All these parameters can be affected by coal constituents such as, petrographic components and inorganic compositions, as well as the rank and coking conditions such as packed density, particle size and heating rate. [3, 27, 36, 73, 80].

2.3.2.3 Resolidification

After softening at about 400°C and formation of the metaplast up to around 550°C, the plastic state can not be maintained because cross-linking reactions become dominant when the availability of transferable hydrogen required for free radical stabilisation diminishes [36]. With increasing temperature, the plasticity decreases and finally irreversibly disappears. The decrease in plasticity is normally described as resolidification, and the temperature at which the plasticity disappears can be regarded as resolidification temperature. Resolidification

coincides roughly with the disappearance of soluble constituents [3]. The resolidification process is strictly associated with thermal decomposition, therefore, it depends more on the chemical constituents of the coal than on its petrographic structure [81]. The influence of rank is only indirect and is determined by the difference in chemical composition of the different types of coal [73].

2.3.2.4 Shrinkage after resolidification

The product obtained during coking after resolidification (at about 550°C) is usually called semi-coke. The properties of the coke are already evident; however a further temperature increase is required to complete the formation of coke [36]. With temperature up to 1000°C, there is some rearrangement of the carbon atoms; CO is released as an important constituent between 600 and 800°C, while H_2 passes through a very characteristic maximum at temperatures around 750°C [3, 20, 36]. In the meanwhile, semi-coke shrinkage occurs, which leads to the formation of fissures in the final coke.

Compared with what occurs in the temperature range 350-500°C, coking conditions, such as heating rate are less important above 500°C. The total shrinkage is independent of the heating rate, it is determined by the state at 500°C, by the maximum temperature reached and to a secondary extent by the residence time at that temperature [3, 73].

2.3.3 Thermal changes

2.3.3.1 Endo/exothermic reactions

During heating of coal, physical and chemical changes are always accompanied by heats of reactions and the changes of thermal conductivities [19]. Endothermic and exothermic reactions are associated with devolatilisation, cross-linking and graphitisation [19, 82]. The first endothermic peak, at about 110°C, is due to the removal of moisture [19, 21, 83, 84]. The secondary endothermic peak at around 420°C is related to the primary devolatilisation [19, 21, 83]. The primary devolatilisation (450-550°C, depending on coal properties and coking condition) and the secondary (550-1000°C) devolatilisation are the major exothermic processes [19, 21], though the primary exothermic stage may include some endothermic properties due to tar vaporisation [82]. In addition to coal properties, coking conditions, such as heating rate, may affect the development of endothermic and exothermic reactions and the evolution of gases and tars [63].

2.3.3.2 Thermal conductivity

Thermal conductivity of heating coal may be affected by temperature, pyrolysis, plasticity and structural changes and atom rearrangements [19, 20, 82, 85]. It is generally considered

that the thermal conductivity of coal at room temperature is about 0.1-0.2 W/m·K [3, 85]. The actual values can show a slight decrease with temperature due to water release [85] and an increase relating to the fluidity [19] during the primary devolatilisation as well as structural changes during the secondary devolatilisation [20, 82, 85].

2.3.4 Summary of changes in coal during heating

- The transformation of coal to coke includes two major devolatilisation regions. The primary devolatilisation occurs between 400 and 550°C with major gases and tars evolving, during which the heating coal undergoes softening, formation of a metaplast and resolidification as well as volumetric swelling. The secondary devolatilisation occurs between 550 and 1000°C with the release of H_2 and CO accompanied by high temperature contraction.

- Exothermic regions are mainly observed during coal devolatilisation, whereas endothermic reactions occur prior to coal devolatilisation relating to the removal of moisture, the endothermic process also is observed relating to the onset of coal devolatilisation and tar evaporation. Thermal conductivity increases during the primary devolatilisation due to the change of fluidity.

2.4 Methods used in coal coking experiments

2.4.1 Introduction

Petrographic, proximate and ultimate analyses provide elementary information of coal constituents. During cokemaking, regardless if the coal is a single coal or a blend from various coals or coal maceral concentrates, coking progress under typical conditions is mainly determined by the combination of physical, chemical and thermal changes [20, 21, 36], in particular, the depolymerisation and repolymerization of organic constituents from different maceral fractions [20].

Physical changes mainly refers to the formation of the plastic nature of coking coal, which includes softening, fluidity, resolidification, swelling and shrinkage, this has been discussed above. The popular techniques applied to coal for studying physical changes includes: Gieseler plastometer [3, 73] and Proton Magnetic Resonance Thermal Analysis (PMRTA) [86, 87] for measuring fusibility; Rheometry for measuring phase changes [88-92]; Crucible swelling [3], Audibert-Arnu dilatometer [3, 73], Ruhr dilatometer [73] and Shock dilatometer [73] for evaluating swelling. Chemical changes may refer to the release of gases and tars due to the depolymerisation of molecular structures such as aliphatic chains on aromatic groups or part of the aromatic components itself, as well as organic functional groups such as –OH groups and –COOH groups [20, 36]. These changes in chemical structure may be quantified by Thermogravimetric Analysis (TGA), Gas Chromatography (GC), Mass Spectrometry (MS), Fourier Transform Infrared Spectroscopy (FTIR) [93] and Nuclear Magnetic Resonance (NMR) [39, 93-98]. Thermal properties such as endothermic and exothermic reactions can be investigated by Differential Scanning Calorimetry (DSC) [99-101] and Differential thermal analysis (DTA) [83]. Thermal conductivity and thermal diffusivity of heated coal has been measured using laser pulse heating methods [102], and a new thermal analytical technique Computer Aided Thermal Analysis (CATA) can simultaneously define apparent specific heat and thermal conductivity of heating coal [19, 103].

2.4.2 Fluidity and fusibility

2.4.2.1 Gieseler plastometer

The Gieseler plastometer for evaluating the plasticity of coal has evidently found worldwide application. The measuring instrument has a metal crucible in which about 5.0 g of divided coal sample with a top particle size 425 μm (less than 50% under 212 μm) can be heated by a solder bath at a heating rate of 3°C/min between 300 and 550°C in the absence of air [3, 104].

A small stirrer is located in the coal, actuated by a constant torque controlled by an electric motor (approximately 300-500 r/min) connected directly to a clutch or hysteresis brake. A dial drum, directly attached to the clutch brake shaft, is graduated into 100 divisions for 360 degrees [73, 104]. Each complete revolution, or 100 dial divisions is recorded on a counter. Rotation rates can be converted directly to dial divisions per minute and can be displayed or recorded once per minute on a suitable electronic readout. The stirrer is not rotated when the coal is in the solid state. Its speed increases as the heating coal begins to soften and reaches a maximum at the maximum fluidity at a temperature in the region of 450-480°C [3, 28, 104]. It subsequently decreases fairly rapidly and the stirrer finally stops at solidification temperature. The final report includes the initial softening temperature, maximum fluidity temperature, solidification temperature, plastic range and maximum fluidity (dial divisions per minute or dd/min) [3, 28, 73, 104].

The measured results from the Gieseler plastometer can be influenced at a wide range by measuring conditions and the limitation of the instrument itself. Habermehl et al. [73] summarized the disadvantages of the Gieseler plastometer, *(a)* results from different laboratories may not be quite reproducible because of the differences in the construction of the individual instruments; *(b)* with increasing depth of the retort immersion in the metal bath, the maximum fluidity increases while the characteristic temperature are not noticeably changed; *(c)* a smaller particle size distribution of sample than specified can lower the maximum fluidity; *(d)* an expansion of the softening coal may occur in a part of the stirred container, which does not belong to the actual measuring location, thus, the measured viscosities may erroneous; and *(e)* a foam structure may develop, which leads to viscosities measured which are often much lower than those actually present in the range of maximum fluidity.

2.4.2.2 Proton Magnetic Resonance Thermal Analysis (PMRTA)

The principle of PMRTA is on the basis of analysing the NMR signal shape from solid-echo of heating samples. During heating, solid-echo NMR signals (with a tau of 12 μs) are measured at 0.1-2 s intervals and summed over 30s based on a Bruker Minispec pc120 operating at 20 MHz by a PMRTA instrument. The summed signals are recorded every 75 s during coal pyrolysis. The method used to estimate the extent of fusion is to Fourier-transform the signal (which is first mirrored about zero time) to obtain the frequency domain response $g(v)$,v is frequency, and use $g(v)$ to calculate the fusion parameter, using the formula [87]:

$$M_{2T}16 = \int_0^{16\,kHz} v^2 g(v)dv / I(0) \qquad (2\text{-}1)$$

where I(0) is the NMR signal amplitude at zero time.

The extent of thermoplastic fusion of the specimen, $M_{2T}16$, varies from 0 for fully fused materials such as water or molten pitch to ~52 kHz^2 for rigid materials such as dry anthracite at room temperature. The $M_{2T}16$ parameter can be rescaled to give the more intuitively understood fusion parameter (F) using the formula:

$$F=100\ (52- M_{2T}16)/52 \qquad (2\text{-}2)$$

The F values range from 0 for fully rigid material, to 100 for a fully mobile material.

The PMRTA technique has been successfully used to evaluate the fusion of coals at various heating rates up to 10°C/min, the results indicate the temperature at which the maximum fusion occurs increases with heating rate, as seen in Figure 2.5. The same trend is also observed with the extent of fusion, whereas the initial softening of the coals is independent of heating rate. Particle size does not have a significant effect on the maximum fusion temperature, while there appears to be a small but significant decrease in the maximum fluidity with the decrease of top particle size from 1 to 0.1 mm [91].

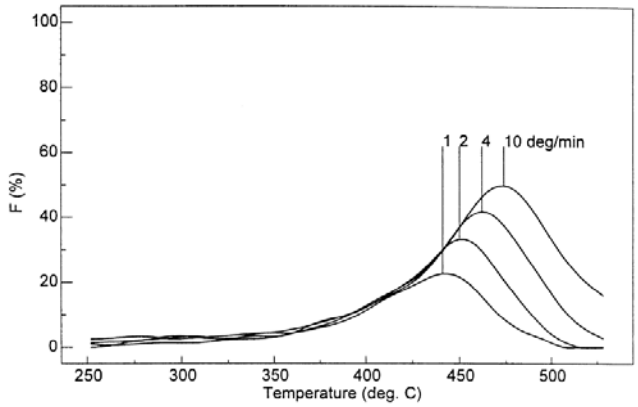

Figure 2.5. Effect of heating rate on fusibility of a coal (74% vitrinite) [91].

In the PMRTA experiment conducted by Sakurovs [91], 0.4 g of sample with a particle size less than 212 μm is heated under flowing nitrogen from room temperature to 560°C at a heating rate of 4°C /min. The maximum extent of fusion for 10 different coals with various ranks showed similar trends in the changes of maximum fluidity as measured by Gieseler

plastometry. The temperatures at which the maximum extent of fusion occurs are also very close to the maximum fluidity temperatures from Gieseler plastometry [87]. The small differences of temperatures between maximum extents of fusion and maximum fluidity values may be related to coal properties and the differences of heating rates between the two techniques.

Problems encountered in the PMRTA determination include: *(a)* the measured maximum extent of fusion of the coal increased significantly with increasing depth of sample over the range 6-20 mm, with the more fusible coals showing a greater increase; *(b)* the PMRTA determination may be affected by swelling of some samples [91]; *(c)* the operation is limited to low temperatures, up to 700°C only [92].

2.4.2.3 Permeability

Coal permeability can be defined by a lumped index of how well fluid passes through coal [79]. Two methods have been employed in literature to evaluate the permeability of the heating coal pellet. The first one is based on the Darcy's law [17, 72, 105, 106], which includes the estimation of the pressure drop across the sample bed, thickness of the bed layer, viscosity of and velocity of the flow gas. The second method directly measures the pressure of the gas passing through the heating coal pellet [107]. During carbonization, the pressure is required to be maintained at a constant value. The higher the required nitrogen pressure (mbar), to maintain a nitrogen flow rate, the lower the permeability. This measure of permeability will depend on the preparation of the sample that becomes fluid.

2.4.2.4 Rheometry

Analysis of rheological behaviour of heating coal can suggest the change in coking pressure [88, 89] and the pore structure development during coke formation [90]. Rheological measurements of heating coal have been performed by using a Rheometrics RDA-III that is controlled by stain rheometer with high torque transducer and forced air convection oven [88]. The rheometer set-up consists of two parallel plates which are housed in an oven chamber, between which the prepared sample is placed. The test involves applying an oscillatory strain to the sample via the bottom plate and measuring the resultant stress in the top plate. For a purely elastic material, which deforms instantaneously, the maximum strain occurs at the maximum stress, while for a purely viscous material that deforms at a constant velocity, the strain lags the applied stress by a phase angle δ of 90°. For viscoelastic materials $0<\delta<90°$, the exact value of the phase angle is a direct measure of the amount of elastic and viscous character that the material possesses at any given frequency, with 45° indicating the boundary

between liquid-like and solid-like behaviour. In addition, the overall stiffness or resistance to deformation can be measured by the complex modulus, G^*:

$$G^*=\tau_0/\gamma_0 \quad (2\text{-}3)$$

where τ_0 is the maximum stress response and γ_0 the maximum applied strain. A complex viscosity η^* can also be calculated which is a measure of overall resistance to dynamic shear as a function of frequency (ω) or shear rate:

$$\eta^*= \tau_0/(\gamma_0\, \omega) \quad (2\text{-}4)$$

Since the phase angle, δ, is a measure of viscoelastic character while the complex viscosity, η*, is a combined measure of its resistance to deformation and flow. The combination of δ and η* provides all the information required to characterise the linear viscoelastic behaviour of a material at any given temperature or frequency.

Standard coal sample preparation in this technique [88] includes pressing about 1.5 g of sample under 5 tonnes of pressure to form discs 25 mm in diameter and approximately 2.6 mm in thickness. The sample tablets are fixed between 25 mm parallel plates (serrated) with a constant force of 200 g applied to the top plate to reduce slippage and prevent excessive expansion during the test. The samples are firstly heated to 350°C at a heating rate of 18°C /min up to 350°C under a constant flow of inert gas, and then to 550°C at a heating rate of 3°C/min. Duffy et al. [88] reported the rheological behaviour of a heating coking coal, a typical measure of η*, the resistance to deformation and flow, as well as δ, the viscoelastic character described by phase angle, shown in Figure 2.6. This coal has vitrinite 71%, R_{vMax} 1.63, VM 18.0%, Dilatation 55%, Gieseler fluidity (ddpm) 100. During heating, the coal showed maximum fluidity at about 475°C with a maximum phase angle observed.

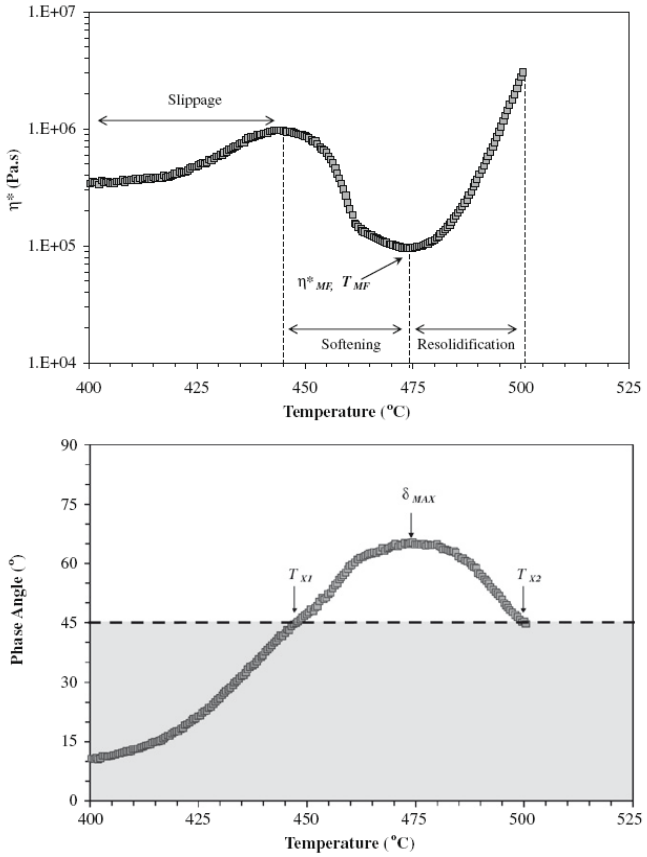

Figure 2.6. (Top) η* as a function of temperature for one heating coking coal (71% vitrinite), (bottom) phase angle (δ) as a function of temperature for the same heating coal [88].

2.4.3 Swelling/shrinkage

2.4.3.1 Crucible-swelling

The crucible-swelling index measures the change in size of a 1 g coal sample, with a total particle size of -212 μm [108] heated under certain specific conditions in a translucent silica crucible with a ring-handle pierced lid. The sample is heated to 800°C or 820°C within 2.5 mins using a Bunsen burner, or for 1.5 minutes in an electric furnace. The profile of the coke "button" formed reflects the free swelling power [3]. In general, the index of 3.5 is considered the lower limit for coking coal potential; a profile of 8 to 9 is a high swelling coal [28]. However, this index does not reflect such essential coking characteristics as plasticity and actual coke strength and should be used with caution in evaluating a coal's ultimate coking performance.

2.4.3.2 Audibert-Arnu dilatation

In the Audibert-Arnu dilatation, the experimental sample is a pencil shaped briquette, 60 mm in length, which is prepared from about 10 g of coal with a particle size less than 212 μm. The sample is inserted in a narrow calibrated tube and topped by a steel piston which slides in the

tube as the coal is heated at 3.0°C/min [16, 109]. By making regular readings of the displacement of the piston as a function of the temperature and expressing the displacement observed in percentages of the original length of the pencil, a curve of the type shown in Figure 2.7 can be plotted [109]. The significant data are as follows: T_1 represents the temperature of initial contraction; T_2 represents the temperature of maximum contraction, at which the dilatometer piston reaches its lowest point; T_3 is the temperature of maximum dilatation, at which the dilatometer piston reaches its highest point.

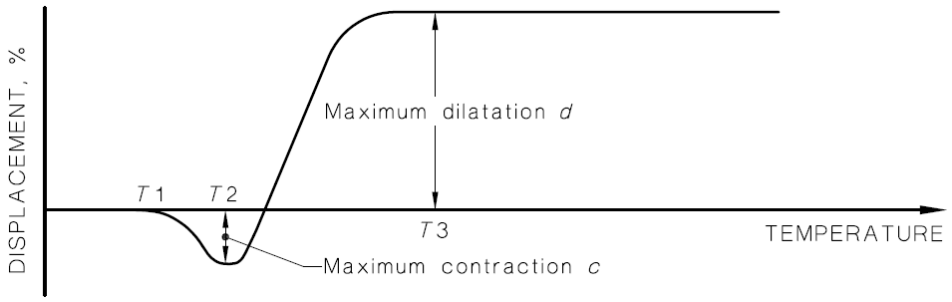

Figure 2.7. Audibert-Arnu dilatometer curve [109].

2.4.3.3 A combination measurement of swelling and rheometry

During rheological measurements (described in section 2.4.3), heating coal expands, generating a normal force which causes the rheometer to raise (or lower) the top plate in order to maintain a constant force. The swelling/shrinkage process can be followed by measuring the relative plate displacement (ΔL) with the increasing carbonization temperature. An alternative means of following the swelling process is to measure the axial force generated under constant gap conditions. This involves heating the sample under standard conditions and prior to the onset of rapid swelling (ΔL_{MIN}), holding the plate gap constant and monitoring the resultant force. This value is recorded manually at 1°C intervals until either the onset of a constant force plateau or until resolidification occurs. The corresponding swelling/shrinkage of the coal to the rheological progress shown in Figure 2.6 is shown in Figure 2.8 [88]. The advantage of this technique is the ability to synchronize rheological properties and the swelling of heating coal. In addition, the peak and subsequent drop in magnitude of axial plate force indicates cell rupture, where the rupture of closed pores to form an open pore network capable of transporting evolved volatile matter is suggested [72, 88-90].

In addition to direct recording of swelling behaviour, other methods for investigation the swelling/shrinkage of coal during coking has been developed by other researchers, such as, the transient volumetric swelling and shrinkage measured from videos taken of the process [110, 111].

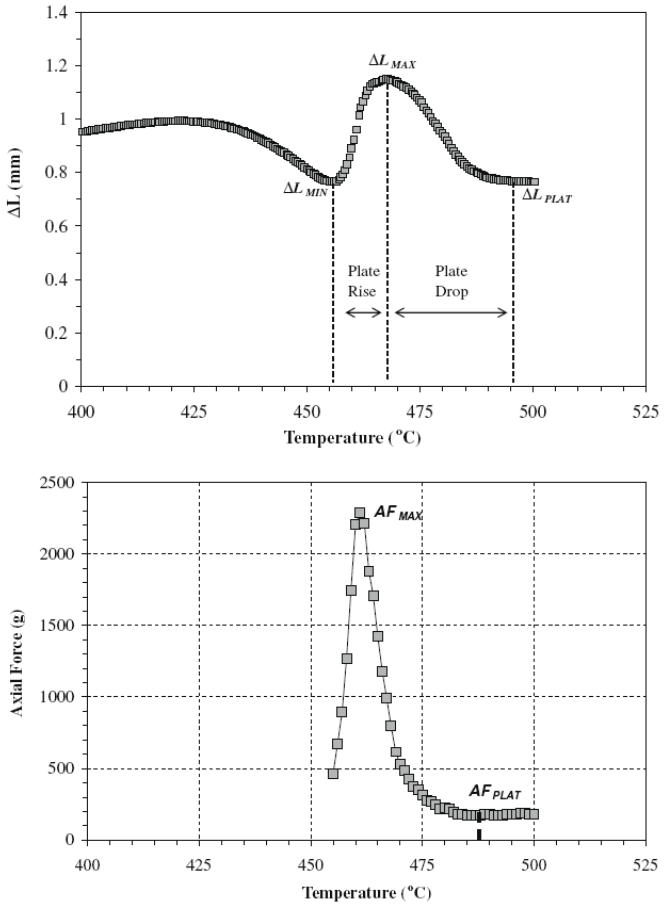

Figure 2.8. (Top) Plate displacement ΔL as a function of temperature for one coking coal (71% vitrinite), (bottom) axial force (AF) as a function of the same coal [88].

2.4.4 Gases, tars and organic structures analysis

2.4.4.1 Thermogravimetric analysis (TGA)

TGA has been employed in coal science to perform a number of characterizations including: proximate analysis, kinetics of weight loss and semi-coke and coke reactivity. TG-DTG weight loss curves are able to provide total volatile matter release with increasing temperature as well as pyrolysis rate of volatile matter [112]. Pyrolysis tests of maceral components on the basis of TG-DTG technique clarified the different contributions of various macerals towards coal devolatilisation during coke formation [49].

2.4.4.2 Matrix-Assisted Laser Desorption/Ionization (MALDI)

Matrix-assisted laser desorption/ionization (MALDI) is a soft ionization technique used in mass spectrometry, allowing the analysis of large organic molecules (such as polymers, coal tar and pitch and other macromolecules) and biomolecules, which tend to be fragile and fragment when ionized by more conventional ionization methods. It is a two-step process: The first step is desorption of matrix material triggered by an ultraviolet laser beam,

producing many species on a hot plume: neutral and ionized matrix molecules, protonated and deprotonated matrix molecules, matrix clusters and nanodroplets. The second step is ionization, protonation and deprotonation of analyte molecules which takes place in the hot plume [113].

The MALDI mass spectrometry has been employed to analyse the coal liquefaction extracts and pyrolysis tars. Molecular weight range of pyrolysis tar may change from different coals or different coal maceral concentrates. For instance, Strezov et al. [19] measured the molecular weight range was between 150 and 500 amu from six different coals. John et al. [114] found that tars from the pyrolysis of Point of Ayr maceral concentrates showed Molecular Mass (MM) distributions in the order: inertinite >Liptinite>Vitrinite. However, molecular structure and chemical types of pyrolysis tars can not be revealed based on the MALDI technique.

2.4.4.3 Fourier Transform Infra-red Spectrometry (FTIR)

Fourier Transform Infrared spectrometer (FTIR) has been employed to analyse the structural properties of coal and separated maceral concentrates, gases and tars components as well as tars and char structures of pyrolysis products, which provides evidence of pyrolysis mechanism of heating coal [39, 49, 64, 66, 82, 97]. FTIR analysis of evolved products shows advantages over mass spectroscopy (MS) in allowing the analysis of very heavy products, and over gas chromatography (GC) in speed. The FTIR can obtain spectra showing identifiable bands for CO, CO_2, CH_4, H_2O, SO_2, COS, C_2H_4, olefins, HCl and NH_3. Above 400°C, the spectra also show aliphatic, aromatic, hydroxyl, carbonyl and ether bands from tar [64]. The evolution of gases derived from the IR absorbance spectra can be obtained by a quantitative analysis program which employs a database of integration regions and calibration spectra for different compounds. However, discrepancies can occur in matching the weight loss determined of heating coal because of missing components such as H_2 which can not be detected by IR and H_2S which is very difficult to detected [97]. The combinations of TG-DTG curve and mass spectra (MS) and gas chromatography (GC) as well as Thermogravimetric–FTIR were implemented [40, 97, 115-117] to explain the mechanism of coke formation.

2.4.4.4 Nuclear Magnetic Resonance (NMR)

Nuclear Magnetic Resonance (NMR) includes ^{13}C-NMR [94] and ^{1}H-NMR measurements. ^{13}C-NMR is the application of nuclear magnetic resonance (NMR) spectroscopy to carbon. It

is analogous to proton ^{1}H-NMR and allows the identification of carbon atoms in an organic molecule just as proton NMR identifies hydrogen atoms [118]. As such NMR is an important tool in chemical structure elucidation in organic chemistry [96]. For instance, Nomura et al. [119] investigated the ratio of aliphatic to aromatic clusters from different coals by using NMR analysis. Kawashima et al. [98], studied the structural change of coal density-separated components during pyrolysis by means of solid-state ^{13}C-NMR spectra. The results show that pyrolytic reactivity is less for heavier components in all coals, and is lower for higher rank coals. Since most of the reactivity of each sample was related to the proportion of aliphatic moieties present, it can be concluded that the aliphatic moiety content in each sample determines its reactivity.

The combination of ^{13}C-NMR and FTIR further indicated the structural properties of chemical bonds of different maceral components. For instance, liptinite spectrum shows an intense aliphatic C-H absorption. Vitrinite spectrum shows a much reduced aliphatic C-H band but some evidence of aromatic C-H absorption. Oxygen in vitrinite is mainly present as the hydroxyl group on the basis of the intensity of bands [39]. Compared to vitrinite, inertinite has less aliphatic C-H, hydrogen bonding and higher aromaticity [49].

2.4.5 Thermal analysis

Physical changes such as swelling and permeability are associated with coal devolatilisation which includes complex endothermic and exothermic reactions accompanied by a change in thermal conductivity. It is difficult to evaluate the endothermic and exothermic behaviour above 300°C because of the beginning of coal pyrolysis.

2.4.5.1 Differential Scanning Calorimetry (DSC) and Differential Thermal Analysis (DTA)

Differential Thermal Analysis (DTA) [19, 120] is based on the measurement of the temperature difference between the sample and a reference material when both are heated under identical conditions. The reference material should be thermally inert with physical and thermal properties identical to the material under study. The assumption is that the thermal properties of the sample remain the same before and after transition. Coal char, coke and alumina are usually used as they have properties similar to coal.

Differential Scanning Calorimetry (DSC) [19, 121] is based on the principle of maintaining both the reference and sample temperatures the same by adding or subtracting heat to or from the sample and the reference to compensate for the energy absorbed or evolved by the sample during its transition. Generally, both sample and reference holders have individual heaters.

The maintenance of equal temperature is obtained by the use of a differential temperature control loop. The temperature control loop maintains the linear increase of the temperature in both holders [19].

In DTA, the sample mass is assumed to remain constant with temperature, however, the mass actually changes during pyrolysis. In DSC, the changes of mass and volume can cause drift in the baseline required for calculation of the heats of reactions. This leads to the need to couple additional TGA measurements to the DSC runs to adjust for mass loss. Thus, changes in mass and volume of samples in both DTA and DSC measurements can cause uncertainty in the results. Therefore, these instruments may not be suitable for quantitative determination. In addition, both DTA and DSC measurements use samples that are usually very small, in the range of few milligrams, which may also limit the suitability of these techniques[19, 83, 99-101, 122].

2.4.5.2 Computer Aided Thermal Analysis (CATA)

In addition to the DTA and DSC techniques, the heats of devolatilisation have been determined by measuring the real apparent specific heat. The real specific heat C_p* is the heat capacity of the inert char. The apparent specific heat, Cp, is the real specific heat with the heats of reactions ΔH included. The correlation between the apparent and real specific is shown by the following equation:

$$Cp = Cp^* + d\Delta H / dT \qquad \text{(J/kg·K)} \quad \text{(2-5)}$$

C_p* is the real specific heat of the inert char and C_p is the apparent specific heat representing the real specific heat with the heats of reactions, ΔH, included [117]. Differences between C_p* and C_p with thermal decomposition reveal the processes of endothermic and exothermic reactions with temperature.

Strezov et al. [19, 103] have recently developed a Computer Aided Thermal Analysis (CATA) technique which is able to synchronously measure the apparent specific heat and thermal conductivity of heating samples. The difference between apparent specific heat and real specific heat has been used to characterise the heats of coal pyrolysis [21], iron ore/coal blends [123] and ore/biomass blends [124].

2.4.6 Coke properties analysis

2.4.6.1 Coke Reactivity Index and Coke Strength after Reaction (CRI & CSR)

Coke reactivity index (CRI) can be determined directly by reaction of coke with CO_2 followed by a tumbler test to determine coke strength. In Australian standard (AS 1038.13-

1990) [125] of determination of coke reactivity index (CRI) and coke strength after reaction (CSR), about 200 g of a 10 kg or greater mass representative sample of +25 mm coke should be applied into the reaction and strength tests. The reaction vessel has 72 mm to 78 mm internal diameter, manufactured from stainless steel and partially filled with inert porous packing for gas diffusion and preheating. Coke sample in the reaction vessel should be heated to 1100°C within 1 h under nitrogen condition, and maintained at this temperature for 10 min. To test the reactivity between coke and CO_2, the gas flow should be changed into CO_2 at a flow rate of 5 L/min, and maintained heating for 120 min. The following step is to change the gas flow to nitrogen at 10 L/min; remove the reaction vessel from the furnace and allow to cool to room temperature. The reactivity index of coke can be determined based on the mass change of coke sample after reaction with CO_2.

Coke sample after reactivity test should be transferred into a strength tumbler that has 130 mm internal diameter and 700 mm internal length and is capable of rotating on its transverse axis at 20 r/min. After rotating at 20 r/min for 30 minutes, sieve the residual test sample from the strength tumbler through a 10 mm sieve and weigh the material retained by the sieve. Coke strength after reaction (CSR) can be determined based on the content of coke sample with size larger than 10 mm.

The coke reactivity index and the coke strength after reactions should be calculated from the following equations:

$$CRI = \frac{Mass\ of\ test\ sample - mass\ of\ sample\ after\ reaction}{Mass\ of\ test\ sample} \times 100 \qquad (2\text{-}6)$$

$$CSR = \frac{Mass\ of\ sample > 10\ mm\ after\ strength\ test}{Mass\ of\ sample\ after\ reaction\ test} \times 100 \qquad (2\text{-}7)$$

Selective small scale experimental test for coke strength and reactivity due to the limited amount of sample has been developed in literature [126]. Each strength test used 25 g of the crushed sized coke at -9.5+6.3 mm, this was placed in a cylinder with an inside diameter of 76 mm onto which a 1000 g weight was dropped, three times from a height of 1000 mm. The coke being tested was then resized at 6.3 mm, 3.15mm, 1mm and < 1mm. The mechanical strength of the coke can be calculated through the surface area of the coke tested, and the surface area was calculated based on the coke density, weight distribution and size.

2.4.6.2 Morphology

Optical microscopy [72, 127] and Scanning electron microscopy (SEM) [128-130] have been extensively used to study morphologic properties of materials. For cokemaking, they were employed to evaluate the development of porosity during coke formation. Results of morphological analysis of coke provide support in understanding the transformation of coal to coke. For instance, MacPhee et al. [131] suggested that coke produced from high-volatile coal has a predominantly mosaic texture with a substantial amount of flow texture while low-volatile coke is mostly domain texture with some flow.

2.4.6.3 Relationship between coke properties and morphology

Coke reactivity and coke strength is considered to be related to coke morphology that was characterised by SEM and/or optical microscopy [132, 133]. Morphological and microtextural types of coke particles can be characterised by observing homogeneity, isotropic/anisotropic texture, thickness of cell walls and pore structures [134]. Coke with more anisotropic texture [133], thicker cell walls and fewer pores is considered to show stronger mechanical strength than that of coke rich in isotropic texture or thinner cell walls.

2.4.7 Summary of methods used in coal coking experiments

- For coking coal, fluidity is mainly evaluated using the Gieseler Plastometer, Proton Magnetic Resonance Thermal Analysis (PMRTA) and Rheometer; swelling is mainly investigated using the Gieseler Plastometer and Audibert-Arnu dilatation.

- Gas and tar evolutions is mainly analysed using Thermogravimetric Analysis (TGA), Gas Chromatography (GC), Mass Spectroscopy (MS), Fourier Transform Infrared (FTIR), Nuclear Magnetic Resonance (NMR) and Matrix-Assisted Laser Desorption/Ionization (MALDI), which can provide fundamental understandings in gases compositions and tars structural properties during the transformation of coal to coke but not molecular arrangements.

- Thermal properties measured during coal coking are mainly evaluated based on Differential Thermal Analysis (DTA), Differential Scanning Calorimetry (DSC) and Computer Aided Thermal Analysis (CATA).

- Microscopic properties of coke can be evaluated based on optical microscopy and SEM analyses. Coke reactivity index (CRI) and Coke strength after reaction (CSR) can be evaluated by reaction vessel and strength tumbler.

Overall, techniques for evaluating thermo-plasticity and swelling/shrinkage [3, 8, 28], coal devolatilisation, [39, 49, 82, 97, 98, 135, 136] endothermic and exothermic reactions [19, 21, 83, 99-101] as well as thermal conductivity [19, 21] of heating coals can be summarised in Table 2.3.

Table 2.3. A summary of methods used in coal coking experiments [3, 8, 28, 99-101, 137].

Coal			
Objective	Techniques	Conditions	Advantage/Disadvantage
Fluidity (Fluidity index, Viscosity)	Gieseler Plastometer [3, 104]	5g, 425 μm ,3°C/min	Difficult to achieve agreement from different labs
	Rheometry [88]	1.5g tablet 3°C/min	May be affected by expansion.
	PMRTA [87, 91, 92]	0.4 g, ~212 μm [87]; 4°C/min	May analyse inertinite and hydrogen behaviour, but may be affected by expansion [91]; low temperature (up to 700°C only) [92]
Swelling/Shrinkage	Crucible swelling [3, 28, 108]	212 μm [108], 800 or 820°C in 2.5 or 1.5 mins	Good reproducibility; Difficult to differentiate quality of coking coal
	Audibert-Arnu dilatation [16, 109]	<212 μm, 3°C/min	Determines the swelling; not indicates pressures exerted on the walls of industrial coke oven
Organic structure (Aliphatic, Aromatic)	TGA [112, 137]	Changeable sample mass and heating rate, but in milligrams	Total weight loss, but not gases and tars chemical compositions
	MALDI [113, 114]	Solvent matrix is needed	Determine molecular weight range, but is not able to reveal molecular structure and chemical types
	FTIR [39, 49, 66, 82, 97]	About 1 mg sample of char	Reveal chemical structure, may have a large error
	NMR [94, 96]	Small mass sample used, such as 0.3-0.5 g [96]	Reveal coal chemical structure. can quantitative for tars but only qualitative for solid coal [94]
Heat of reactions (Kinetics)		Endo/exothermic	
	DTA [19, 120]	Changeable mass, particle size and heating rate	Lack of resolution, sensitivity; dependent on reference; not good for quantitative analysis.
	DSC [19, 121]		
	CATA [19, 103]		Synchronously apparent specific heat and thermal conductivity, may be affected by expansion and mass loss
Coke			
CRI & CSR	Reaction vessel for CRI; Strength tumbler for CSR [125]	200 g, +25 mm coke, 1100°C for reaction test; 20 r/min for strength test	Directly determine the CRI and CSR but fail to represent the process conditions of the coke in the blast furnace [5]
Morphology	Optical microscopy [72, 127]	Needs to be mounted in resin	May directly describe the microscopic development of porosity of coke but not directly quantify the distribution of pores with different sizes
	SEM [128-130]	Needs to be mounted in resin & carbon coated	

2.5 Literature on chemical changes of coal and coal macerals during heating

2.5.1 Mechanisms

The mechanism for the transformation of coal to coke has been summarized in the literature [20, 36, 59, 138]. The pyrolysis process includes bond rupture, vaporization of micromolecule and condensation or cross-linking, accompanying changes in the density of aliphatic group and aromaticity. Saxena [59] summarized that primary devolatilisation commences with the rupture of weak bonds at the bridge between ring systems at about 400°C. The formed free radical groups combine to produce gases and tars. Light tars can vaporize and be transported out of the char particles with gases as they formed. The heavy polynuclear aromatic compounds diffuse slowly even at high temperatures and start to condense with the elimination of H_2. The ultimate product due to the condensation reaction is coke/char. In addition, CO is also produced through the cracking of heterocyclic oxygen groups. The reactions that occur in these stages can be described as below.

Solomon et al. [20] proposed nine steps of the pyrolysis reactions to interpret the evolution of volatile matter.

- When heated, three processes occur in the temperature range of 200-400°C. These processes are the disruption of hydrogen bonds (Step 1), the vaporization and the transport of the non-covalently bonded 'molecular phase' (Step 2) and low-temperature cross-linking in coals with more than 10% oxygen (Step 3) which coincides with CO_2 or H_2O evolution.

- During primary pyrolysis, the weakest bridges (labelled 1 and 2 in Figure 2.9 a [138]) can break by producing molecular fragments (depolymerisation) (Step 4). The fragments abstract hydrogen from the hydroaromatics or aliphatics, thus increasing the aromatic hydrogen concentration (Step 5). These fragments will be released as tar if they are small enough to vaporize and be transported out of the char particle (Step 6) under typical pyrolysis conditions and do not undergo moderate temperature cross-linking reactions before escaping from the particles. The moderate temperature cross-linking reactions (Step 7) are slightly slower than the bridge breaking reactions and appear to correlate with CH_4 evolution. The other event during primary pyrolysis is the decomposition of functional groups to release gases (Step 8), mainly CO_2, light aliphatic gases and some CH_4 and H_2O. The release of CH_4, may produce cross-

linking by a substitution reaction in which the attachment of a larger molecular weight releases the methyl group. Cross-linking also release CO_2 by condensation after a radical is formed on the ring when a carboxyl is removed. Similarly, H_2O is released by the condensation of two –OH groups or an –OH group and a –COOH group to produce an ether link (in Figure 2.9 b [138]). The cross-linking is important to promote the release of tar and the visco-elastic properties of the coke. The primary pyrolysis completes when the donatable hydrogen from hydroaromatics of aliphatics is depleted.

- During secondary pyrolysis, there is additional gas formation when CH_4 evolves from methly groups, HCN from ring nitrogen compounds and CO from ether links, and finally hydrogen evolves by ring condensation (Step 9) (in Figure 2.9 c [138]).

Stanger [82] found that the devolatilisation process occurred initially with the breakdown of oxy-functional groups primarily weakened with the removal of water. The low temperature evolution of CO_2 and CO began at temperature between 100 and 200°C. The early breakdown process of oxy-functional groups (100-375°C) acted as a precursor to the primary devolatilisation (300-500°C) in which large structural changes occurred (450-500°C) alongside peak volatile evolution. The secondary devolatilisation (500-600°C) occurred as a result of tar vaporisation. These tars were formed during the primary devolatilisation process but too heavy to vaporize and be transported out of the char structure until reaching their boiling point. The formation of light hydrocarbon (C_2H_4, C_2H_6) at around 400-600°C was indicative of cross-linking reactions occurring at the end of hydrogen transfer.

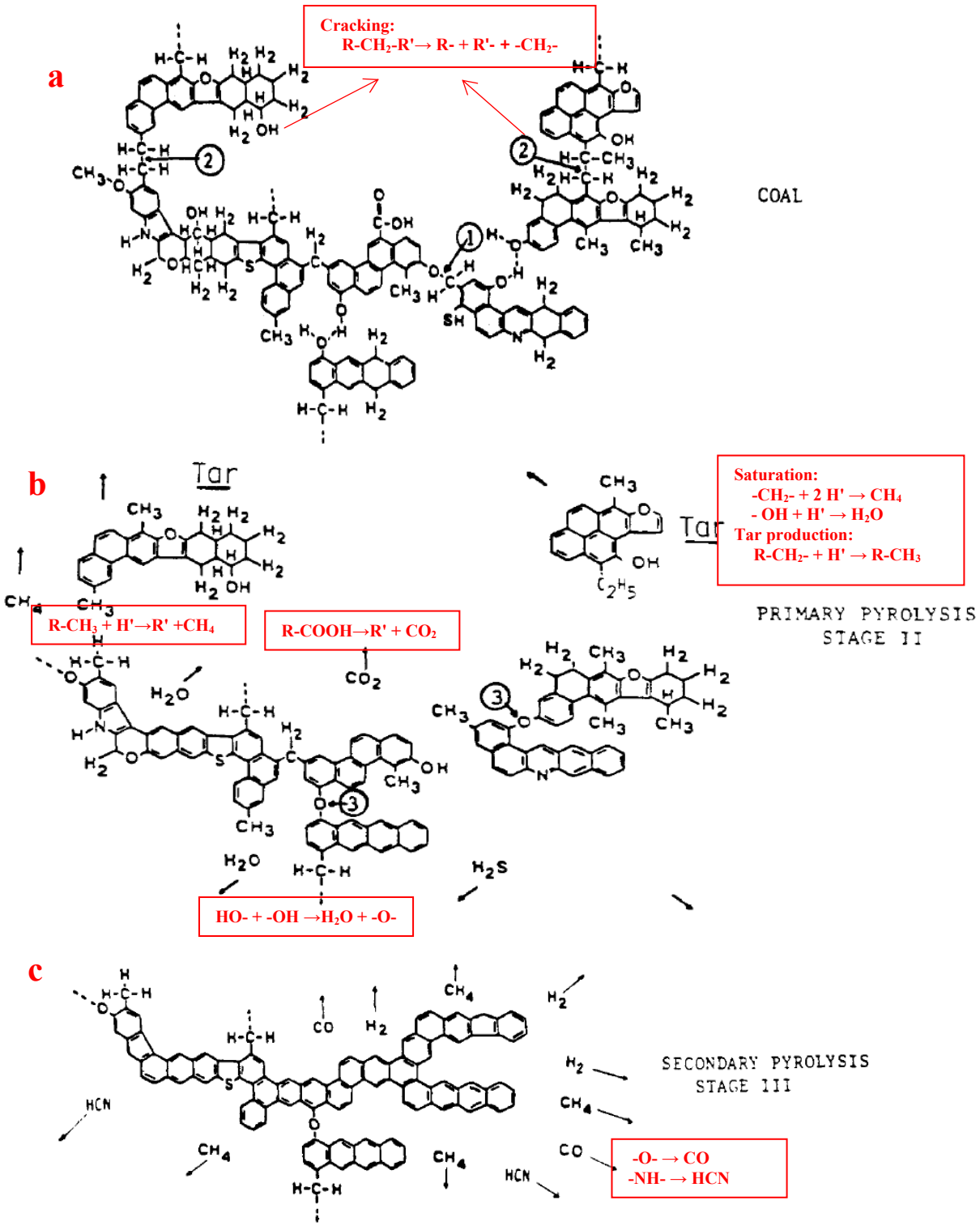

Figure 2.9. Hypothetical coal molecule during stages of pyrolysis [138].

2.5.2 Gas and tar evolution

During pyrolysis, light gases such as CO_2, CO, H_2, CH_4, NH_4, N_2, H_2S, C_xH_y and tars are released from the plastic coal with incremental temperature accompanied by swelling [16]. The C-C bond at the bridge between ring systems breaks to produce molecular fragments [36, 139]. The fragments abstract hydrogen from the hydroaromatics or aliphatics, thus increasing the aromatic hydrogen concentration. These fragments will be released as tar if they are small enough to vaporize and do not undergo retrograde reactions before escaping from the particles, as seen in Figure 2.9 b.

Coal tar impregnated coals was found to increase fluidity but also to extend the thermoplastic range to lower temperature, causing an increase in the swelling range and showing an association with high coking pressure [89]. There are two sorts of coal tars, low temperature and high temperature coal tars. Coal tars from low temperature pyrolysis consist of mainly aromatic and low molecular weight hydrocarbon compounds [60, 61]. The main components of high temperature coal tar are cyclic aromatic hydrocarbons ranging from single-ring benzene and alkyl benzenes to compounds containing possibly as many as 20 or more rings [61].

Strezov et al. [63] studied the evolution rate of tars and volatiles of a high volatile bituminous coal heated at a heating rate of 10°C/min. Tars and seven volatile species (CH_4, C_2H_4, H_2O, CO, CO_2, NH_3 and HCN) were analysed using the TG-FTIR, the apparent specific heat of heating sample was also simultaneously estimated, the results were shown in Figure 2.10 [63]. The results indicated that tars started to evolve at 250°C, while gases were evolving at lower temperature. The onset for the release of gas and tar may relate to other theories, for instance, it was considered that at low heating rates, such as lower than 1°C/s [59, 140], the entrapped CO_2 and CH_4 were driven off at about 200°C. Above this temperature, internal condensation occurred among the macromolecular structure of low-rank coal with the evolution of CO_2 and H_2O. In the range 200-500°C, CH_4 began to evolve with its higher homologues and olefins; most of the oxygen in coal structure was eliminated as water and oxides of carbon. At 400-500°C, H_2 began to evolve with a critical point at about 700°C, which was characterized by a rapid evolution of H_2 and CO. Between 500 and 700°C, the volume of gases such as H_2, CO, CH_4 and nitrogen increased with temperature while most hydrocarbons decreased. Tar formation began at around 300-400°C with a maximum yield that occurred at approximately 500-550°C. The main tars were due to the release of coal fragments during the break-up of the macromolecular coal structure by bonds breaking, evaporation and transport.

The proportion of gases and tars vary widely with various coal ranks. In general, it is believed low-rank coals generate a high yield of gases and a low yield of tars during pyrolysis. By comparison, high volatile bituminous coals generate a high yield of tars and a moderate yield of gases while high rank coals generate a moderate or low yield of tars and a low yield of gases [20, 138, 141].

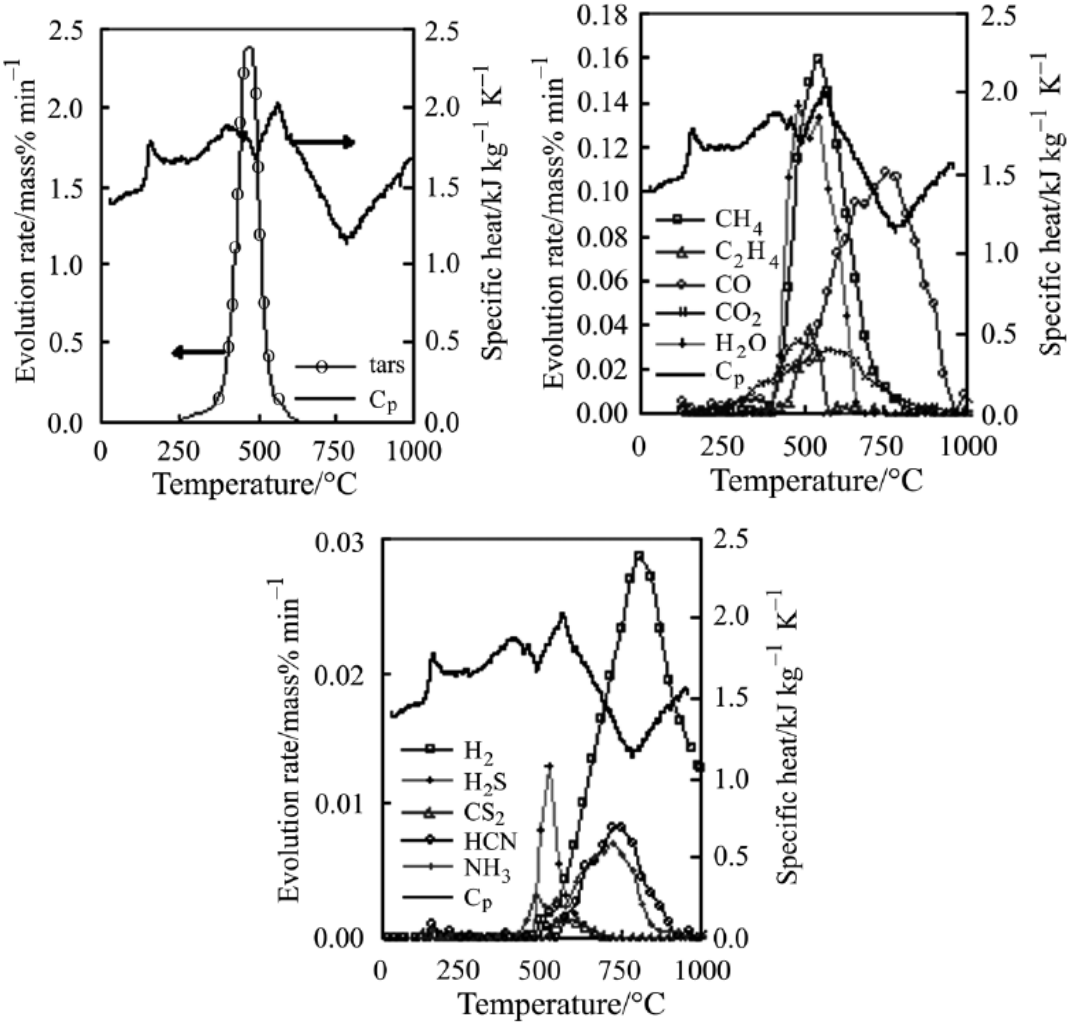

Figure 2.10. Evolution rate of tars and volatiles of heating coal at a heating rate of 10°C/min [63].

2.5.3 Functional groups

Functional groups of hydrogen and oxygen may play an important role in coal pyrolysis. Hydrogen is a key element released from macromolecules, particularly for the evolution of tars [59]. In general, oxygen is considered to be particularly important during the depolymerisation of the coal macromolecules due to cleavage of oxygen ether linkages as well as in the radical mechanism of thermal decomposition [142]. Inertinite-rich coals containing more aromatic ring structure and more oxy-functional groups showed more thermal stability than vitrinite at low temperatures due to the difficulty in breaking the

aromatic rings. However, these rings could decompose further at the second devolatilisation when temperature is over 600°C [135, 141].

H_2 produced during coal pyrolysis plays a vital role in forming other compounds. It saturates the OH and O radicals to produce water; it produces aliphatics by CH_2A radicals; and produces tar molecules by saturating the larger radicals. Arenillas et al. [115] drew the conclusion that the oxygen content of coals plays a vital role in the release of hydrogen as the product of H_2O formed by hydrogen and oxygen increased with the increase of oxygen content in the parent coals. The evolution of the nitrogen compounds followed a similar trend to other pyrolysis compounds. No nitrogen species were detected in anthracite, while the peak temperatures for NO release increased from 500°C for the high volatile bituminous coal to 510°C and 525°C for the medium and low bituminous coals [115].

Nomura et al. [119] investigated the relationship between the Gieseler MF (Maximum Fluidity) and a normalized parameter of *Rmax/WL* (the maximum rate of weight loss *Rmax* divided by the amount of total weight loss WL up to 1000°C) with the analysis of the tar fraction from 16 coal samples. They found that lower rank coals (C<86%) have lower fluidity than higher rank coals (C>86%) at the same *Rmax/WL* values. This may be explained by the following concepts: *(a)* aromatic clusters, which are the frame of the fluid matrix, are smaller in lower rank coals than those in higher rank coal; *(b)* the ratio of aliphatic components to aromatic compounds. Aliphatic compounds act as effective lubricants against the fluid matrix. Lower rank coals have a larger ratio of aliphatic compounds than higher rank coals. Therefore, both the small size of aromatic rings and the relatively larger ratio of aliphatic components to aromatic compounds in metaplast lead to less fluidity.

2.5.4 Coal macerals concentrates

Kidena et al. [78] reported that vitrinite-rich samples have lower physical density, contain relatively more long aliphatic chains and bridges, and a greater number of substituents on aromatic rings, showing higher fluidity. Inertinite-rich samples have higher physical density, contain relatively high aromaticity, showing lower fluidity. On carbonisation, inertinite rich samples, whatever the rank of the coal, produces around 20% of its volatile matter as CO and CO_2 and very little tar [3]. By comparison, Das [143] reported that vitrinite rich concentrates characterise the higher content of volatiles, higher values of maximum rate of weight loss, higher weight loss for tar formation and lower weight loss for gas formation. However, vitrinite-rich concentrate produced a smaller amount of loss than fusinite-rich concentrates during secondary devolatilisation.

Sun et al. [49] reported that vitrinite has lower carbon content, more alphatic C-H and hydrogen bonding, higher evolution of light hydrocarbon (C_2-C_4) and lower aromaticity than inertinite. Vitrinite char always has higher H and lower C content than inertinite char at the same pyrolysis temperature. Using FTIR, Xie et al. [39] found that the liptinite spectrum shows an intense aliphatic C-H absorption. Vitrinite spectrum shows a much reduced aliphatic C-H band but some evidence of aromatic C-H absorption. Oxygen in vitrinite is mainly present as the hydroxyl group on the basis of the intensity of bands. The inertinite spectrum shows less aliphatic C-H absorption but a considerably stronger aromatic C-H signal.

Wang et al. [141] studied the pyrolysis of inertinite-rich coal and reported the pyrolysis reactions during the primary devolatilisation come mainly from the decomposition of hydrogen functional groups, however, the second devolatilisation at high temperature is mainly attributed to the decomposition of stable oxygen functional groups in the coal matrix. Inertinite-rich coal contain more aromatic ring structures and more oxy-functional groups than vitrinite-rich coals, which implies that coals with more inertinite content have more thermal stability at low temperature due to the strong aromatic rings. However, these rings could decompose further at the second devolatilisation when the temperature is over 600°C.

2.5.5 Summary for chemical changes of coal and coal macerals

- Coal pyrolysis includes two-step devolatilisation, the primary devolatilisation between 400 and 550°C begins with weak bonds breaking between aromatic rings with the major gases and tars evolution; the secondary devolatilisation is mainly attributed to macromolecules condensation with H_2 and CO release.

- Hydrogen is a key element released from macromolecules, particularly for the evolution of tars; the end of hydrogen transfer during the primary devolatilisation may mean the beginning of cross-linking.

- Vitrinite concentrates contain a relatively large proportion of long aliphatic chains and bridges as well as a greater number of substituents on aromatic rings, thus, they can release more gases and tars and show higher fluidity than inertinite concentrates.

2.6 Literature on physical changes of coal and coal macerals during heating

2.6.1 Introduction

During pyrolysis under inert conditions, coal will initially melt and contract at temperatures around 400-430°C, depending on coal rank and coking conditions, followed by swelling due to the generation of volatiles during coal decomposition between 400 and 600°C, which becomes trapped inside the plastic mass causing an increase in the internal gas pressure [144-146]. As temperature continues to increase, high temperature contraction can be observed resulting from the resolidification process which includes release of secondary gases H_2 and CO.

The swelling and contraction behaviour of coals during pyrolysis are mainly dependent on coal rank, maceral components, volatile matter and minerals, and coking conditions such as heating rate, particle size and bulk density of coal in the coke oven [3]. The swelling and contraction can be directly investigated by measuring coal volume change with temperature [16]. It may also be indirectly evaluated by studying coal thermo-plasticity properties and coking pressure development. Thermo-plasticity properties can affect gas and tar release and thus affects coking pressure. Coking pressure is one of the major concerns in a coke oven because of its effects on swelling and shrinkage [25]. Previous published work on the development of thermo-plasticity and coking pressure of heating coal is summarised below, allowing the mechanism of swelling and shrinkage of heating coal to be discussed.

2.6.2 Swelling/shrinkage of coal

Fu et al. [111] gave the schematic diagram of the swelling and shrinkage of coal during pyrolysis, shown in Figure 2.11. It is supposed that microscopic interspace among fine particles will augment when major destruction of the coal matrix takes place in the particle. This allows the volatile matter to escape uniformly from microscopic interspace within particles. Volatile matter continues to form larger bubbles with the development of pyrolysis, which forces the particles to swell along the interspace. With increasing temperature, contraction may be observed when the gas escapes from the channels followed by bubble rupture.

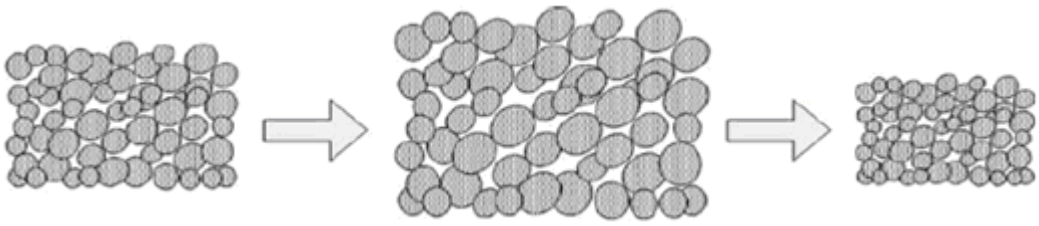

Figure 2.11. Schematic diagram of the swelling and shrinkage of coal during pyrolysis [111].

Fu et al. [111] investigated the effect of volatile matter on swelling and contraction ratio of heating coal, the swelling and contraction ratio are the relative volume changes (after heating versus before heating) against the original volume. The coals were firstly crushed to the particle size of 90% < 50 μm, and then the coal powder was pressed into coal cakes with different densities. Contrasted to the original volume of coal samples, significant shrinkage but slight swelling was observed. The coal high temperature contraction ratio increased with the volatile matter content. However, the volumetric shrinkage ratios at the temperature 1000°C did not change linearly with the volatile matter content over a range of different coals. They considered that one possible reason for this is that the volumetric shrinkage depends on not only the volatile matter content of coal but also the structural transformation by heating coal itself. After coal samples undergoing the chemical changes, such as primary devolatilisation and secondary devolatilisation as well as tars evaporation, the extent of orderly arrangement of molecules increased and the structure become more compact than that before heating.

Marzec et al. [147] reported that the high temperature volumetric contraction is mainly dependent on:

(a) The yield of thermally decomposed products that were generated on coal heating to the resolidification temperature T_R; semi-coke layer showed satisfactory shrinkage and good semi-coke permeability if the heating coal produced at least 14 wt % of the thermal degradation products on heating to T_R and showed a high content of alkylated aromatics in the products. The following explanation could be that formation of solid material (a precursor of semi-coke) is a continuous process that is initiated when the coal is in a plastic state (approximately at a temperature of maximum fluidity) and is continuously accompanied by generation of thermal degradation products. These molecules, either gaseous or liquid, penetrate the gradually resolidifying material and contribute in this way to formation of open porosity in the material and, hence, to a permeability of the semi-coke layer.

(b) Chemical compositions of the decomposed products; the contraction of the semi-coke layer increased with the predominance of components that represented various aromatic hydrocarbons containing alkyl carbon atoms in the range of C_3-C_9.

2.6.3 Thermo-plasticity of coal

During the transformation of coal to coke, heating coal undergoes a meta-plastic intermediate phase in the temperatures between 420-600°C showing viscosity and fluidity [36, 146]. Viscosity of heating coal can affect the rate of mass transport [76, 146] and further affects the internal pressure within the coal, thus influencing swelling. Strezov et al. [146] reported that the difficulty for the volatiles to diffuse and release from the highly viscous plastic mass in high viscosity coals with high swelling index can potentially be source for developing pressure during cokemaking. By comparison, a coal with a low viscosity thermoplastic phase can be applied for blending purposes in order to reduce the expected excessive pressures. Gao et al. [148] suggested that swelling may relate to thermo-plastic properties such as the fluidity and the surface tension. High fluidity and low surface tension will lead to more frequent bubble ruptures, as volatile gases are easier to escape from the liquid particles. On the other hand, high surface tension and low fluidity of the meta-plastic will result in less frequent bubble rupture and a high swelling.

Sakurovs et al. [91] investigated the factors controlling the thermoplastic behaviour of coals by Proton Magnetic Resonance Thermal Analysis (PMRTA). When coal is fluid, the material responsible for the thermo-plasticity of coal is volatile [3]. The extent for fusion of a coal depends on the equilibrium between the amount of plasticising material in the coal and its concentration in the gas surrounding the coal particles. The concentration in the gas phase is dependent on the ratio between the rate of evolution of the plasticising material and the rate of its release from the bulk coal. Therefore, thermo-plasticity of coking coals is controlled by the gas-phase concentration of volatile plasticising material in the atmosphere surrounding the coal particles. The fluidity of coals can be altered by changing the atmospheric concentration of the volatile plasticising material. Charcoals, brown coals and high volatile bituminous coals can reduce the extent of fusion of bituminous coals due to inert diluents.

Marsh et al. [149] suggested the plasticity commences at the temperatures 350-400°C at which depolymerization occurs. Smaller molecules formed from the coal, serve as a necessary solvating vehicle and possibly as hydrogen donors within this plasticity. With increasing temperature, the viscosity decreases so that the mean molecular size is reduced commensurate with thermal rupture of bridging structures and the stabilization of free-radicals by donor-hydrogen. However, with a further increase in the temperature, the limited inventory of

donor-hydrogen becomes consumed and evolved as volatile matter. Free-radical which continue to be formed will become stabilized by repolymerization. Therefore, they viewed hydrogen donor ability as the decisive factor that determines coal thermo-plasticity.

Spiro [150] constructed space-filling models to propose the thermal decomposition and plasticity of coal based on four proposed coal molecular models. The constructed model contains aryl planarity. The mechanism for thermo-plasticity includes thermolysis of aliphatic, alicyclic and hydroaromatic groups which protrude from aryl planes. These smaller fragments act as spacers and lubricants, enabling the resultant parallel aryl planes to flow in two dimensions, unhindered and protected from cross-linking. The mobility cause thermoplastic behaviour in bituminous coals.

Schulten et al. [71] reported that coals with a large proportion of unsubstituted aromatic hydrocarbons, as well as sparsely substituted multi-ring aromatics and hydroxyl compounds, showed poor thermoplastic properties. The higher their content in the coal, the lower the thermo-plasticity is. On the other hand, coals consisting of alkylated aromatic hydrocarbons have good thermoplastic properties.

Schulten et al. [71] summarized that maximum fluidity of coal material depends on four properties:

(a) For the covalent bonding structures of C atom with in coal molecules, the amount and distribution of $C(sp^2)$-$C(sp^3)$ bonds as well as $C(sp^3)$-$C(sp^3)$ and $C(sp^3)$-O bonds in coal material (sp^2, sp^3 represent electron configuration). This amount and distribution can directly affect the molecular size of thermal degradation products, and thus the fluidity of the heating coal.

(b) The content of hydroaromatic structures that produce highly reactive intermediates named cyclohexadienyl radicals. These can be formed either by reaction of the hydroaromatics with aromatic structures or with other radicals.

(c) The content of unsubstituted or sparsely substituted hydrocarbons containing at least five aromatic rings. These can either be present in the original coal or formed pyrolytically, and can undergo condensation reactions at a relatively low temperature that is below the temperature of maximum fluidity. Their condensation interferes with the development of high fluidity caused by coal thermal decomposition.

(d) And finally, the content of species that are inactive in polymerization and condensation reactions, such as C_1-C_2 naphthalenes, C_1-C_3 fluorenes, C_1-C_2 acenaphthenes representing two-ring aromatics. Their presence imposes a diluting effect on the concentrations of the reactive species. This brings a delay of condensation and polymerization. The delay is manifested by higher temperatures of maximum fluidity and resolidification in standard measurements carried out at a constant heating rate with the use of Gieseler plastometer.

Duffy et al. [89] found that addition of a coal tar pitch to a high fluidity and high pressure coal can increase fluidity but also extend the thermoplastic range to lower temperatures. This caused an increase in the swelling range and was accompanied by a long plateau in viscosity. Elasticity and viscosity at the onset of expansion were also higher for both the pitch impregnated coals and the high pressure blends, which supports their previous findings [88, 90] for singly charged high pressure coals, and confirms the potential use of such criteria for identifying potentially dangerous coals/blends. Addition of a low rank, high fluidity, low coking pressure coal, with a high rank, low fluidity, high coking pressure coal can significantly reduce the coking pressure associated with the latter [89]. The blend, however, does not result in a midway fluidity between the two coals. Sometimes the resulting fluidity is lower than that of the low fluidity coal, especially when the coals are significantly different in rank. The viscosity of the resultant blend can be estimated from the viscosity of each component coal using a logarithmic additivity rule commonly employed for polymers.

2.6.4 Coking pressure and swelling pressure of coal during heating

2.6.4.1 Mechanisms

Pressure generated by trapped gas and tar in the plastic layer during carbonisation is undoubtedly an important factor in the swelling mechanism. For the pressure field in loading coking chambers, coking pressure is the maximum pressure in the middle of the furnace and the swelling pressure is the maximum pressure at the charge-wall contact [151].

Coking pressure can be affected by plastic layer properties such as internal gas pressure, tars and gases evolution, permeability and viscosity. Low permeability of the heating coal pellet can restrict the escape of gas from coal bed, which corresponds to an increase of internal gas pressure. Tar migration in the coke oven is also considered to show a direct effect on coking pressure because tar directed towards the oven centre can build up and contribute to the final gas pressure, while tar escaping can relieve pressure at the oven centre [105, 107, 152]. The

viscosity/elasticity properties of the mesophase will determine volatile retention in the plastic layer, which will affect the internal pressure of meta-plastic and ultimately impact on swelling propensity. High fluidity coals are associated with high coking pressures [89], results from Zubkova [153] also indicated that high fluidity coals are more likely to generate high intralayer pressure within the plastic layer. Coking pressure is also affected by the contraction behaviour of the coke layer near the oven walls. A large contraction can decrease the coal bulk density in the oven centre and hence the internal gas pressure in the plastic layer [17]. Koch et al. [107] investigated thermoplastic properties and semi-coke contraction of 42 coals. They reported that wall pressure decreased with an increase of the semi-coke shrinkage, and was not related to the maximum fluidity.

Strezov et al. [146] studied the swelling pressure of two different coals and their blends. The first coal was a high swelling pressure coal (HP) with high vitrinite and low inertinite, and the second coal was a low swelling pressure coal (LP) with low vitrinite and high inertinite. The coal with high vitrinite and low inertinite exhibited a stable pressure at 105 kPa after reaching resolidification, while the second coal, with low vitrinite and high inertinite produced a pressure which was below zero. Evolution rates of the lower molecular weight volatiles were similar for both coals. However, the evolution of tars between the two coals or their blend showed a significant difference. The high swelling pressure coal exhibited a smaller amount of tars within a narrower temperature range and a higher initial decomposition temperature than the low swelling pressure coal. Similar results were also observed by Duffy et al [88]. In addition, the viscosity and thermo-plasticity evidently influenced the properties of the coal plastic mass and its potential to either develop or reduce the excessive pressure during pyrolysis. High viscosity of the plastic phase and high swelling index may potentially be the source for developing pressure. Therefore, it is believed that the major influence on the swelling pressure capacity for coals originates from the evolution and properties of the tars and the thermo-plasticity of the remaining semi-coke.

Duffy et al. [72] suggested that to understand the mechanisms that control oven wall pressure, it is the mesophase and semi-coke that need to be investigated, not the fully formed coke. They studied the potential correlations of expansion/contraction, fluidity and coking pressure by using high temperature rheometry, ^{1}H NMR, thermogravimetric analysis and SEM. They [72, 88-90] suggested that pore structure development is critical for coking pressure development, and is relevant to the rheological behaviour of the molten coal. The maximum expansion represents a cell opening process which was considered important for coking pressure since it provided a potential mechanism for volatile escape and subsequent charge contraction. They suggested that high fluidity, low coking pressure coals are capable of

forming a highly interconnected pore network, if or when the pore network is established, it facilitates volatile escape and subsequently a large degree of contraction at the end of the softening process. On the other hand, high coking pressure coals resist cell rupture in the early stages of fluidity leading to the formation of a stable foam close to resolidification. Therefore, these coals contain a higher proportion of closed cells both at and during resolidification, reducing permeability in both the semi-coke and high temperature plastic layers and increasing fluid elasticity and lowering volatile evolution rate at the onset of expansion, producing a greater degree of swelling. This expansion is considered to be a potential reason for its high coking pressure [88].

Duffy et al. [72] proposed that the bubble growth region represents the major barrier to the passage of volatiles. For coals that produce high oven wall pressure, considerable bubble growth occurs with very little coalescence prior to resolidification or the time for bubble growth is considerable prior to coalescence. Duffy et al. [88, 90] suggested that this bubble coalescence provides a route for the release of volatiles for single coals and is hence considered a primary mechanism for coking pressure, with bubble coalescence restricted by high viscosities. However, this mechanism does not fully explain coking pressures for coal blends. Duffy et al. [89] found that when coals of different ranks whose thermoplastic regions do not overlap greatly are blended together, the viscosities/elasticities of the resultant blends are often higher than that of the parent coals. High coking pressures for these coal blends in the movable wall oven tests were not observed although the bubble coalescence mechanism would predict high coking pressures. They proposed that the volatiles from each coal in the blend are able to pass through the voids created by the accompanying coal, whether it is though unsoftened or resolidified material. This suggested a secondary mechanism for coking pressure, on which is also thought to be relevant to low fluidity single coals high in inertinite, which was found to exhibit low coking pressures.

Using polarised light microscopy, Duffy et al. [89] found that the degree of mixing between coals of different rank is minimal, with fusion restricted to the particle surface. This limited fusion is significantly important for understanding the coking pressure mechanism for blends. They proposed the components of blends with varying thermoplastic regions do not interact, and therefore the thermoplastic properties cannot be viewed as that of a single material. The lower rank coal, which softens at lower temperature, is able to expand into the inter-particle voids between the high rank coal that is yet to soften, and these voids can create channels for volatiles to traverse. With rising temperature, when the high rank coal begins to expand, the pore structure developed in the resolidified structures of the low rank coal can facilitate removal of volatiles, while the resolidified materials may also act as a suitable sorbent for

volatile matter. This is considered to be the primary mechanism by which coal blending is able to alleviate coking pressure, and applies to the addition of inert materials. Nomura et al. [154] described the same mechanism for suppression of internal gas pressure by blending low rank and slightly coking coal. Nomura et al. [17] found addition of high volatile matter coking coal, semi-anthracite and coke breeze can act as an inert material to help the gas to escape from the heating coal pellet of a low volatile matter, high coking pressure coal, which greatly decrease the permeability of the heating coal pellet and coking pressure. However, for the same permeability, high volatile matter coking coal can decrease coking pressure at a higher degree than semi-anthracite, which means coking pressure in a movable wall coke oven is not only determined by plastic coal permeability, but other factors such as semi-coke contraction and fissure formation close to the coke oven wall and coal bulk density. Organic additives can not only decrease the coking pressure for good plastic properties coking coal, but also increase the coke strength, however, it also deteriorates the coke strength of poor plastic properties coal [18].

2.6.4.2 Permeability during coking

Permeability of the heating coal pellet is a key function in evaluating the ability of a coal to generate coking pressure because it determines the flow of the evolved gas and tar or their entrapment in the heating coal pellet. Based on Darcy's law, permeability of heating coal pellet can be evaluated on the basis of pressure drop of gas flowing through the coal sample, thickness of the coal bed layer, viscosity of and velocity of carrier gas [17, 106]. Nomura et al. [17] studied the permeability of plastic coal to the flow of nitrogen through an isothermal sample and found that for coking coal, the pressure drop increases to a maximum before decreasing as the temperature approaches the resolidification temperature. In a coke oven the temperature gradient from the wall to the plastic layer results in some regions of the bed contracting and this contraction of the coke layer near the oven walls is not replicated in laboratory isothermal experiments and is believed to impact the properties of the plastic layer in the oven modifying the pressure generated. They found that a large contraction near the coke oven wall can decrease the coal bulk density in the oven centre and hence the internal pressure in the plastic layer.

The permeability of the semi-coke/coke layer depends on both the pore structure and the fissure pattern present. When the pores are narrow and few fissures are present, the permeability is low, it is difficult for gas to escape, thus the internal gas pressures develop [105]. Duffy et al. [72] suggested that gas permeability is dependent on open pore structure that corresponds largely with intergranular porosity prior to softening, and a ruptured pore network at higher temperatures. The yield values of closed pore volume measured for high

oven wall pressure samples quenched at various stages of coal swelling are higher than that of low oven wall pressure samples.

Casal et al. [106] studied the permeability of a coal bed as it was heated in the laboratory as a function of temperature and compared the permeability with other factors such as coal devolatilisation rate. The aim of the work was to understand the characteristics of dangerous coals and safe coals. They found that all coals tested produced a low permeability zone in the thermoplastic regions. For dangerous coals the low permeability zone is maintained longer and to higher temperatures (beyond the resolidification temperature) than in the case of safe coals. It was proposed that the difference between the temperature of the end of the low permeability zone and the temperature of resolidification may be used to indicate the degree of dangerousness of a coal.

Koch et al. [107] determined that the low permeability of the heating coal pellet is not a causative factor of high coking pressure. Some experiments showed that permeabilities the heating coal pellet for safe coals were lower compared with the permeabilities found for dangerous coals. Furthermore, they found that for the safe coals the low permeability zone was situated before the plastic layer range, while for the dangerous coals it was located in a temperature range beyond those of resolidification. In a coke oven, it was expected that volatile matter will flow mainly towards the semi-coke for safe coal, while flowing towards the non transformed coal for dangerous coals. They studied the tar migration during carbonization on the basis of N-methyl-2-pyrrolidinone (NMP) extraction by withdrawing and quenching the coal charge during the coking process. The experimental results indicated that for dangerous coals, the tars tend to migrate to the cold side through the plastic layer but to the hot side for safe coal (the semi-coke and coke side). They considered that a reason of such behaviour could be found in the permeability of the phases next to the plastic layer. Being low in semi-coke of dangerous coals, it could therefore be a hindrance for higher molecular volatile species to flow towards the heated side of the oven. Therefore, the accumulation of tars in the cold side of the coke oven can be used for assessing whether a coal is dangerous or not.

2.6.5 Effect of heating rate

Coking conditions such as heating rate, particle size and charge bulk density, affect the carbonization process including release and composition of volatiles, swelling progress and resultant coke strength, and are important parameters for process optimisation and achieving coke with good thermal properties.

Pyrolysis reactions of softening coal give rise to sufficient labile bond breaking of the macromolecular network; producing low molecular mass gases or liquid components which are often referred to as metaplast. The metaplast phase which is responsible for the swelling of heating coal [3, 36, 73], is transient, it ends up partly volatilized and partly transformed into coke. The swelling of heating coal increases with increasing plastic layer thickness. High heating rates can increase the plastic layer thickness and thus increase the swelling of heating coal.

There are a couple reasons suggested in literature to explain the influence of high heating rate on plasticity and swelling of heating coal:

(a) High heating rates lead to an increase in the heat flow which results in more coal becoming plastic per unit time [73];

(b) High heating rates can shift the maximum rate of gas evolution to higher temperature ranges, resulting in a more extensive thermal fragmentation of coal's molecular structure, raising the softening, metaplast and resolidification temperatures. However, softening and resolidification temperatures do not increase to the same extent, there is usually an increase in the plastic range, which lowers the minimum viscosity, enhancing the plastic properties of the heating coal [3, 29, 36, 73, 112, 155];

(c) At a low heating rate from 3 to 10°C/min, the rate of weight loss is approximately proportional to the heating rate but does not significantly vary the proportions of products during the primary devolatilisation process [155];

(d) For low-rank oxygen rich coals, in which cross-linking occurs early at normal heating rates preventing any possibility of fusion, a high heating rate will probably allow a degree of plastic fusion before the pyrolysis reactions begin [3].

Sakurovs et al. [91] concluded that from 1 to 10°C/min the temperature of maximum fusion and the maximum extent of fusion both increased with increasing heating rate for bituminous coals. The swelling ratio and maximum devolatilisation rate increase with rising heating rate [16]. Zeng et al. [129] reported at low heating rates, volatiles can diffuse through the pores without causing an internal pressure high enough to cause the particle to swell.

Since heating rate can cause a significant influence on swelling/shrinkage development of heating coal, the semi-coke and coke porous structures also correspondingly change with various heating rates, which may influence coke strength and coke reactivity as well as its

utilization in the blast furnace. It was observed that chars prepared at high heating rates contained more micro-pores and meso-pores and had a greater internal surface area, resulting in a higher reactivity [156].

2.6.6 Effect of particle size

Fu et al. [111] reported that the swelling ratio increased while the contraction ratio decreased as the sample size increased. They suggested that one of the possible reasons is that the internal volatile pressure build-up is in competition with the changes of liquid viscosity and surface tension in coal. An increase in size favours the coalescent of coal particles [111] and restricts the release of volatiles. For instance, tar escape decreases with increasing particle size [3] and therefore results in an increase of pressure within the particles [73], which in turn leads to condensation of the pyrolysis products. These events greatly affect the subsequent thermal changes in the coal substance, especially its plastic behaviour. On the other hand, small particles can increase softening temperature but decrease plastic temperature range [155]. It was also reported that smaller particles can lead to a higher extent of secondary reactions, although there was no significant difference in total volatile yield during carbonization [66], this may be one of the reasons for explaining its high contraction ratio.

Sakurovs et al. [91] concluded that the magnitude of the interactions between blended coals decreased with increasing particle size over the range of 0.1-1 mm. However, it is expected the interaction would still play a role in determining the fluidity of blends in coke ovens, when the particle size is typically -3 mm.

2.6.7 Effect of charging density

Fu et al. [111] studied the effect of coal density on swelling and shrinkage. The coals were firstly crushed to the particle size of 90% < 50 μm, and then the coal powder was pressed into coal cakes with different densities. They found that with increasing coal density the swelling ratio increased and the shrinkage ratio decreased. Nomura et al. [154] studied the generation of coking pressure by dry coal blends charged into a pilot oven. They reported that the internal gas pressure and fluidity of coal blends increased as the bulk density increased.

2.6.8 Coal maceral concentrates

The maceral compositions influence to a great extent both the degradation of the coking process and the chemical and mechanical properties of the resulting coke [10]. Liptinite is the lightest maceral. It is the most fluid maceral during the coking process. Vitrinite appears to be cement which surrounds the other macerals and mineral matter and is easily fractured. They have more aliphatic C-H and hydrogen bonding and lower aromaticity than inertinite. They

swell and agglomerate during the meta-plastic process. Inertinite contains relatively high aromaticity and is rich in carbon, poor in hydrogen and volatile matter. It remains inert during the coking process, except for a few semifusinites at the boundary [3, 10]. Therefore, liptinite and vitrinite melts and becomes fluid, forming vesicles or pores and then resolidify to form isotropic coke or a mosaic texture during coking [157].

2.6.9 Effect of swelling/shrinkage on coke properties

2.6.9.1 Development of porosity

Using microscopic technique, Hays et al. [127] found that pore first appeared in large particles slightly below the softening point observed on the Ruhr dilatometer. As the temperature increased, partial fusion occurred and pores increased in size and number. More particles contained pores and most of the large particles became multi-pored. At higher temperature, continued swelling of larger particles resulted in the smaller ones being swept and concentrated into the diminishing void spaces. Continuation of these processes led to partial fusion and eventually to complete fusion when the small particles were completely engulfed within the expanding larger particles. Therefore, the original pore structure of a coal may diminish due to the combination of coal fusion and the blockage caused by the fluidity. The char structure is therefore determined by the thermoplastic properties and swelling/shrinkage of the coal rather than by its original pore structure. SEM images also confirmed that the expansion process develops the pore structure and this occurs relatively quickly when the coal is in its most fluid state [90].

Duffy et al. [72] investigated the microstructure development of coal with increasing temperature. SEM and optical microscopy results clearly indicated coal fusion, volume swelling, permeability and pore development with increasing temperature. These can be described in four steps:

Step 1, at the onset of expansion, there are only sporadic bubbles inside the coal grains and at their boundaries, the individual coal grains are clearly distinguishable and retain angular edges. A large proportion of the porosity is inter-granular and the porosity allows some gas flow to occur, but the permeability remains relatively low because of the packing density.

Step 2, when the grains soften with swelling and fusion clearly visible, the total porosity increases, however, most of the newly formed pores remain closed. Consequently there is an overall drop in permeability.

Step 3, with increasing temperature, more bubbles are formed and a high extent of volume swelling occurs, the visible porosity and pore size increase. However, the permeability is still lower than that at the onset of swelling because most of the porosity is still not interconnected, and the structure as a whole still cannot facilitate significant gas transport, since the initial inter-granular porosity has all but disappeared.

Step 4, when the sample is approaching maximum swelling, cell rupture occurs and pore network increases, and consequently a large increase in permeability is observed.

Vitrinite and liptinite develop fluidity during heating. Coals with high liptinite and vitrinite and low inertinite show high swelling pressure, therefore, these macerals are the main contributors to the swelling of coal and the population of porous chars [3, 146]. The homogeneous and rich fusible maceral particles swell in an isotropic way and produce cenospheres and honeycomb types of char, whereas the coal particles rich in infusible macerals produce unfused blocks [58]. The development of areas of anisotropy occurs in the plastic zone and is visible under the microscope. The size of these areas of anisotropy are fixed when the particle zone changes into the resolidified zone, and they do not change further [73].

2.6.9.2 Coke strength

In the blast furnace, coke produces reducing gases for the reduction of iron ore, and it provides heat for the endothermic requirements of chemical reactions and the melting of slag and metal. Coke also supports the burden of iron ore and coke itself and give a permeable matrix through which reducing gases can flow and molten material can percolate in the lower blast furnace region. Coke strength is related to coke size and its resistance to breakage and abrasion. Coke with a large mean size and a narrow size distribution is good for permeability. Most operators consider a mean optimum size of coke in the blast furnace to be in the range of 50-55 mm [5].

Coke mechanical strength such as surface breaking provides a useful assessment of coke performance. However, the tests used to assess coke mechanical strength are carried out at ambient temperature and hence do not represent the process conditions of the coke in the blast furnace. Therefore, a combined test for determining the coke reactivity and post-reaction strength was introduced. This test has been adopted as an Australian standard (AS 1038.13-1990) [125]. The procedure of this standard for determination of coke reactivity index (CRI)

and coke strength after reaction (CSR) has been described in section 2.4.6.1. There is an approximate relationship between coke reactivity index (CRI) and coke strength after reaction (CSR), a high CSR corresponds to a low CRI, as seen in Figure 2.12 [6]. For a good quality coke, the CRI should be low and the CSR index high. If the coke in the blast furnace reacts excessively with CO_2, coke will weaken and will be degraded into smaller particles. Excessive coke degradation leads to permeability reduction and lowered efficiency of blast furnace performance. The Australian BHP Port Kembla considers a CSR to be 74.1 [158]. Other operators consider a CSR to be in the range of 50-65 [5]. There is an approximate relationship between coke reactivity index (CRI) and coke strength after reaction (CSR),

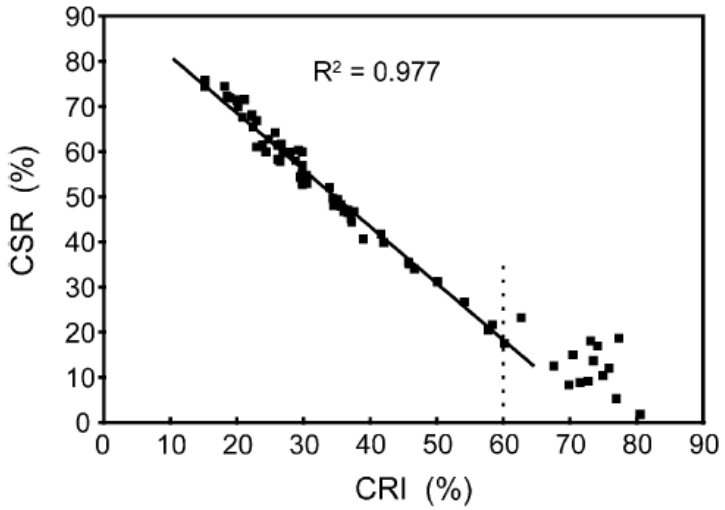

Figure 2.12. Relationship between CRI and CSR indices [5].

During coke formation, swelling significantly influences coke strength. Nomura et al. [154] found that the surface breakage of coke decreases steeply when the total dilatation decreases below a certain value, which shifts to a lower total dilatation range as the bulk density increases. The reason was explained as follows: when coal was charged in the coke oven chamber, the coal particles only partly came into contact with each other. At around 400°C, the coal grains began to soften and expand into the inter-particle space. If the volume of coal expansion was larger than that of inter-particle space, the fused coal particles would stick together and finally form strong bonds. On the other hand, if the volume of coal expansion was smaller than that of inter-particle space, the fused coal particles cannot adhere very well and thus weak bonds were formed. Therefore, the volume of inter-particle space and the expansion of fused coal are important for the strong adhesion of coal particles, which will finally affect surface breakage of coke.

Díez et al. [5] summarized the factors that determine coke strength after reactivity (CSR) and coke reactivity index (CRI) during cokemaking, which include coal rank, coal rheology, coal

composition (organic and inorganic inerts) and coking conditions. The rank of coal is the dominate factor determining CSR and CRI. Zhang et al. [57] suggested that a coke with good thermal properties can be made from a coal with an mean vitrinite reflectance of 1.1-1.2%. Nakamura et al [7] also reported that the CSR passes through a maximum for prime coking coals with mean vitrinite reflectance of 1.2% to 1.3% and falls towards coals of lower or higher rank, as shown in Figure 2.13.

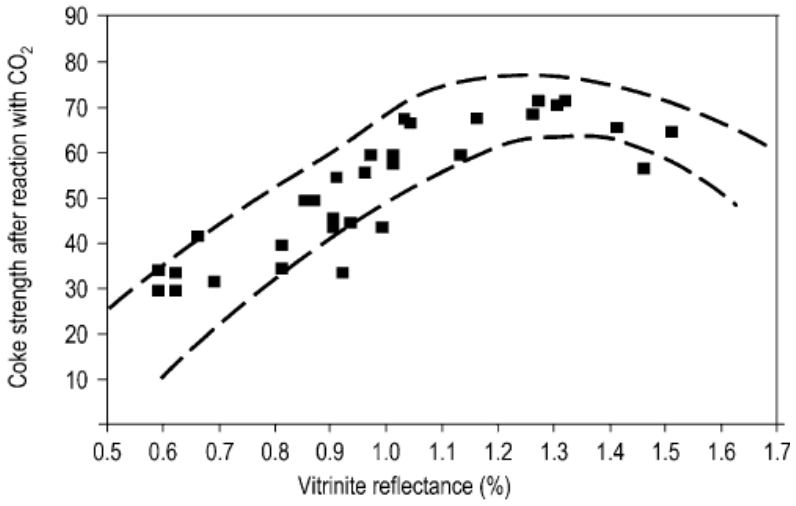

Figure 2.13. Relationship between vitrinite reflectance and coke strength after reaction with carbon dioxide (CSR) [7].

2.6.10 Summary for physical changes of coal and coal maceral concentrates

- Swelling is caused as a result of the obstruction of generated gas and tar in the plastic phase between 400 and 600°C depending on coal properties and coking conditions. Volatiles released during coal pyrolysis coalesce in the plastic mass forming bubbles which increases the size of the plastic mass. Foaming process, fluidity/viscosity, permeability, gases and tars evolution, internal pressure and pore coalescence and their correlations are key points for understanding the swelling behaviour of heating coal [88, 111, 147, 159].

- There are two stages for coal contraction. The first stage occurs at about 420°C due to the softening of coal, the second one begins to develop only after the end of the maximum swelling, which is also regarded as the resolidification process with secondary gases H_2 and CO release.

- Low permeability of the semi-coke layer does not allow vapour species generated in the plastic layer to migrate through the semi-coke to the coke layer. In such a case, the species are trapped in the plastic layer and build up pressure in the layer, corresponding to the swelling to occur [147].

- Heating rate, particle size and bulk density can affect the coal's plastic behaviour, volatiles release, thermal degradation, coalescent of coal particles and internal coking pressure. Thus, affecting the swelling of heating coal.

- Vitrinite and liptinite have more aliphatic C-H and hydrogen bonding and lower aromaticity than inertinite. They melt and show higher fluidity and weight loss, contributing to plasticity and swelling while inertinite keeps inert during the meta-plastic process, except for a few semifusinites at the boundary [3, 10]. However, aromatic rings could be decomposed further at the second devolatilisation above 600°C.

- SEM images and optical microscopy confirm that the foaming and expansion processes relate to pore structure development and also show this occurs relatively quickly when the coal is in its most fluid state [90]. The pores started to develop at temperatures close to the onset of plasticity and increased in size and number up to a critical temperature, above which the number of pores decreased, which was again attributed to pore coalescence [127].

- Coal rank, such as vitrinite reflectance dominates coke strength after reactivity (CSR), although other factors, such as coal composition (organic and inorganic inerts) and coking conditions also need to be considered. There is an approximate relationship between coke reactivity index (CRI) and coke strength after reaction (CSR). In general, a high CSR corresponds to a low CRI.

2.7 Literature on thermal changes of coal during heating

2.7.1 Specific heat and heats of reactions

The specific heat of coal and semi-coke depends on four factors [160, 161]:

(a) It increases with increasing temperature;

(b) At a given temperature it increases with the volatile matter content;

(c) It increases with the moisture content and

(d) It decreases with the ash content.

The specific heat of coal is measured mainly below the temperature of thermal decomposition. There is a wide scatter among the reported results, with the specific heats ranging from 1000 to 1400 J/kg·K at room temperature and increasing to 1300-1800 J/kg·K at about 300°C, as shown in Figure 2.14 [160].

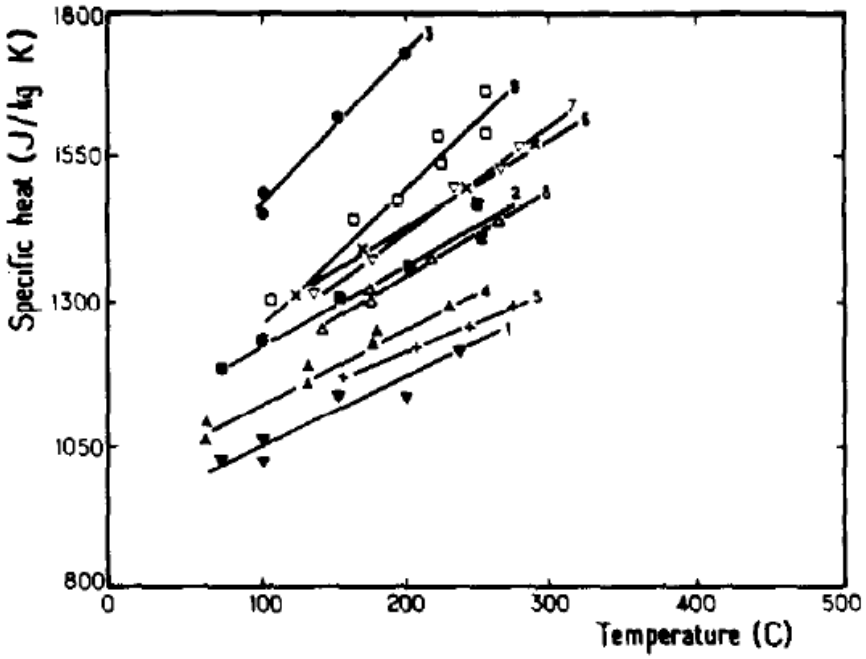

Figure 2.14. Mean specific heat of coal versus temperature [160].

Previous work based on the differences between real specific heat and apparent specific heat reported endothermic reactions of coal in the range between 300 and 700°C and an exothermic reaction above 700°C [122, 160, 162]. Agroskin et al. [162] reported two endothermic peaks, the first at 400-450°C and the second at 550-575°C. An exothermic trough was observed at 800°C. The heats of the endothermic reaction ranged between 150 and 300 kJ/kg and 100-300 kJ/kg for the exothermic reactions.

Lopez-Peinado et al. [163] studied 17 different coals from lignite to anthracite using TG-DSC. They reported the heat events were principally endothermic heats in nature below 780°C; with only some exothermic heats found between 180 and 480°C for low rank coals. The endothermic heats in the temperature range 25-180°C are attributed to desorption of moisture and increase with decreasing rank of coal, especially for lignites. For bituminous coals and coals lower in rank, there are no large heat events associated with the principal pyrolysis weight losses that occurred between 180 and 480°C. The major part of the endothermic heat event occurred above 480°C and is attributed to C-H bond breaking reactions, which cause dehydrogenation of the coal char matrix. The endothermicity at 630-680°C reached a maximum, and then increased again with temperature due to the condensation reaction, which are probably exothermic. For the overall heat of pyrolysis in the temperatures between 180-780°C, a maximum in endothermicity in the order of 450-550 kJ/kg (daf) was found for coals with a volatile matter content in the range 10-15 wt% (daf).

Using DTA, Glass et al. [83] suggested that low volatile bituminous coals show three endothermic reactions. The initial peak at 130°C is caused principally by loss of water. The two major reactions, at about 500°C and 620°C, are referred to as the primary and secondary devolatilisation, respectively. The first reaction occurs as the coal becomes fluid and the second reaction represents a post-solidification gas evolution. For high volatile type coals, the primary devolatilisation peak is interrupted by an exothermic reaction which usually occurs between 400 and 430 °C.

Similar results were also reported using TG-DSC. Rosenvold et al. [84] examined 21 bituminous coals and reported three endothermic peaks. The first (25-150°C) corresponds to removal of moisture, the second in the range 400-500°C corresponds to devolatilisation of organic matter and the third, a partially resolved endothermic event above 550°C relates to thermal cracking and coking processes subsequent to the pyrolysis step. Elder and Harris [101] examined 6 coals and reported that the exothermic reactions occurred between 300 and 550°C, and they were associated with the primary devolatilisation process involving plastic development and the onset of secondary reaction. They also measured a large endothermic reaction between 560 and 590°C, depending on heating rate.

Strezov et al. [21] have previously used the CATA technique to quantify five pyrolytic regions in both coking and thermal coals: dehydration, transition, resolidification, secondary reaction and contraction reaction, as seen in Figure 2.15. The endothermic dehydration region between 100 and 200°C was attributed to removal of moisture. The second endothermic region (380-420°C) was found to correlate with a pre-plastic transition involving structural relaxation with early release of CO_2 and CO. The first exothermic region between 420-550°C was related to the fluidity of the coal. The fourth region (550-620°C) was attributed to another endothermic reaction involving devolatilisation. The fifth and largest region involved an exothermic reaction with the release of H_2 and a contraction of carbon hexagonal planes. They also reported that the heats of the exothermic reactions at 420-550°C ranged from 15 to 45 MJ/m^3 and 15-25 MJ/m^3 at 650-925°C [19].

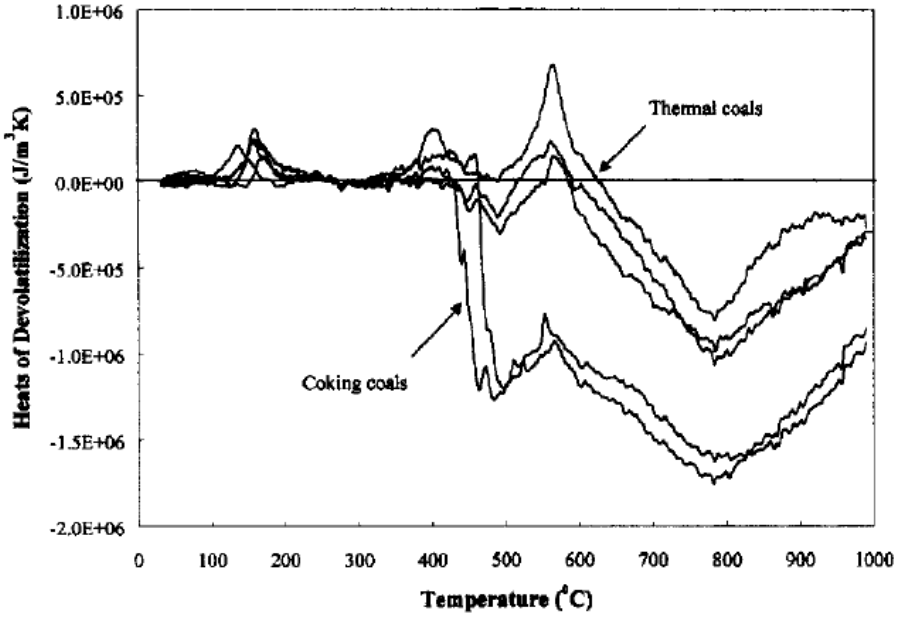

Figure 2.15. Heats of devolatilisation with temperature, calculated by subtracting the apparent specific heat from the real specific heat [21].

Using CATA technique with the combinations of micro gas chromatograph and Fourier Transform Infra-Red (FTIR), Stanger [82] summarized thermal behaviours along with a series of chemical changes. The description of endo- and exothermic reactions taking place in pyrolysis with temperature by Stanger is presented in Table 2.4. The endothermic processes are mainly occurring at coal desorption (25-200°C) and tar vaporisation (500-600°C), while the exothermic processes occur at primary (100-500°C) and secondary devolatilisation (500-1000°C). Heats of exothermic reactions are about 54 kJ/kg coal at breakdown of oxy-functional groups and primary devolatilisation and 364 kJ/kg coal at secondary devolatilisation, respectively. The heat of endothermic desorption is 1.54 MJ/kg coal and the heat of endothermic tar vaporisation is around 22 kJ/kg coal.

Table 2.4 A description of reactions taking place in coal pyrolysis [82]

Products	H_2O	CO_2, CO Light oils (R-OH&R-COOH	CO_2, CO, H2 Light C_xH_y Heavy liquid tars formed	Light CxHy Heavy liquid tars vaporised	H_2&CO CO_2, CH_4
Coal	Coal drying	Breakdown Of oxy-functional groups	Primary Devolatilisation process	Secondary Devolatilisation process	Charring, Graphitisation
	25-200°C	100-375°C	375-500°C	500-600°C	500-1000°C
Mechanism	Endothermic desorption	Exothermic desorption	Exothermic desorption	Endothermic tar vaporisation	Exothermic desorption
	ΔH des=+1.54MJ/kg H_2O	ΔH=-27kJ/kg coal	ΔH=-27kJ/kg coal	ΔH=+22.2kJ/kg coal	ΔH=-364.4kJ/kg coal

In 2004, Strezov et al. [63] examined the effect of heating rate on apparent specific heat and the evolution of gaseous species of coal. The evolved volatiles were analysed using TG-FTIR. They reported the apparent specific heat was approximately 1.4 kJ/kg·K at room temperature and increased to 1.9 kJ/kg·K at 410°C at heating rates of 10, 25 and 100°C/min. When the sample commenced its decomposition and consequent devolatilisation, the apparent specific heats were considerably different. The heating rates influenced the overall devolatilisation process affecting changes in the decomposition products. Using TG, they found that the decomposition point and maximum rate of mass loss shifted towards higher temperatures with increasing heating rate. Correlating the evolution of tars and apparent specific heat, they concluded that the release of the same quantities of tars in a shorter period of time consumes larger energy for bonding breaking and coincides with endothermic heat release which was insignificant at 10°C/min and became stronger at higher heating rates.

The strongest endothermic reaction correlated to the secondary devolatilisation between 500 and 600°C, was observed at the heating rate of 10°C/min. Most of the volatile constituents that evolved during this event were the hydrocarbons (CH_4 and C_2H_4), secondary water H_2O and CO_2, exhibiting peaks in the similar range as the endothermic heat release evident from the apparent specific heat data. The exothermic trough for contraction reactions exceeding 600°C increased with increasing heating rate.

2.7.2 Thermal conductivity and thermal diffusivity

The thermal conductivities of various coals were reported by Badzioch et al. [164] and Butorin and Matveeva [85], as around 0.1-0.2 W/m·K depending very much on size distribution, packing and moisture content [3]. The values showed a slight decrease from room temperature to 200°C due to moisture loss [85], then increased to about 0.2 W/m·K at 400-500°C followed by a rapid increase to around 2-3 W/m·K at 900°C. It was proposed that the increasing thermal conductivity is attributed to the combination of three effects [20, 85]: (a) radiant heat transfer across pores and cracks; (b) changes in the conductivity of the coal due to pyrolysis; (c) changes in the intrinsic conductivity with temperature [85]. Badzioch et al. [164] also suggested that rapid changes of conductivities at higher temperature are attributed to the continuous changes in the coal structure and increase in radiation heat transfer through coal pores.

Thermal diffusivity of dried coal was found to be 1.5×10^{-7} m^2/s below 200°C, a small decrease at 300°C followed by a slow increase up to 600°C and a rapid increase up to 50×10^{-7} m^2/s at 850°C [85]. Dindi et al. [165] reported that the thermal diffusivity is around 1×10^{-7} m^2/s at low temperature (110°C).

Using CATA, Strezov et al. [19] reported that the initial values of thermal conductivity and thermal diffusivity for different coals were in the range between 0.17-0.31 W/m·K and 0.78×10-7-1.26×10^{-7} m^2/s, respectively, as seen in Figures 2.16 and 2.17. The thermal diffusivity was found to have a similar trend with thermal conductivity at elevated temperature. When temperatures reached the thermoplastic range, thermal conductivities and diffusivities increased rapidly with the change in the fluidity of the coals. The increase of thermal conductivity and diffusivity for high fluidity coals occurred at lower temperatures than low fluidity coals [19]. The values of thermal conductivities in Figure 2.16 produced a maximum thermal conductivity (k_{max}) of 4 W/m·K above 450°C or higher temperatures. When the thermal conductivity reaches 3-4 W/m·K and beyond, the difference between the measured surface temperature and the temperature at the centre of the coal pellet is very small, and the calculation breaks down.

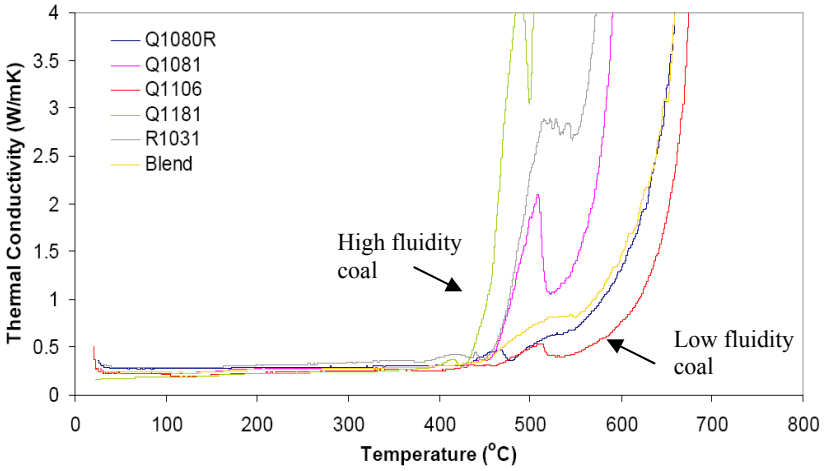

Figure 2.16. Effective thermal conductivity for the coal samples at a heating rate of 5°C/min heated from room temperature to 1000°C [19].

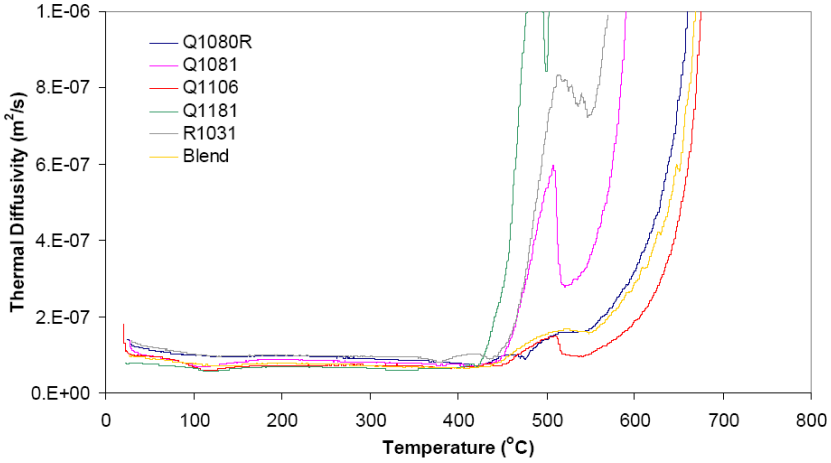

Figure 2.17. Effective thermal diffusivity for the coal samples at a heating rate of 5°C/min heated from room temperature to 1000°C [19].

2.7.3 Summary for thermal changes of heating coal

- During the primary and the secondary devolatilisation, coking coals show larger exothermic heats than thermal coals.

- During the transformation of coal to coke, there are three endothermic regions relating to the removal of moisture (110°C), and pre-devolatilisation of primary (450°C) and secondary (550°C) devolatilisation. Primary (450 and 550°C) and secondary (550 and 1000 °C) devolatilisation are the major exothermic regions.

- The changes of thermal conductivities and diffusivities are relevant to the development of fluidity and char/coke structures. High fluidity coals exhibit an increase in thermal conductivity and diffusivity at lower temperatures, while lower fluidity coal exhibit rapid increases in thermal conductivity and diffusivity at higher temperatures.

2.8 Summary from the literature

On review of the literature, the following conclusions can be drawn.

2.8.1 Techniques

- Vitrinite and inertinite concentrates can be separated using inorganic or organic dense phase media, by changing the densities of the selected liquid media.

- Gieseler Plastometer, Proton Magnetic Resonance Thermal Analysis (PMRTA) and Rheometer as well as Gieseler Plastometer and Audibert-Arnu dilatation have been widely used to evaluate fluidity and swelling properties of coking coal. Differential Thermal Analysis (DTA), Differential Scanning Calorimetry (DSC) and Computer Aided Thermal Analysis (CATA) have also been employed to investigate thermal properties during cokemaking. Thermogravimetric Analysis (TGA) can generally reveal the total weight loss during coke formation. Gas Chromatography (GC), Mass Spectroscopy (MS) and Fourier Transform Infrared (FTIR) can provide fundamental understanding in gases compositions and tars structural properties during coke formation

2.8.2 Physical changes

- Foam formation, gases and tars evolution, fluidity/viscosity, permeability, internal pressure and pores coalescence are key points for understanding the swelling behaviour of heating coal.

- Vitrinite and liptinite show higher fluidity and weight loss during heating compared to inertinite, contributing to plasticity and swelling while inertinite remains inert during the meta-plastic process, except for a few semifusinites at the boundary. High heating rates and large particle sizes can increase plastic layer thickness and promote swelling.

2.8.3 Chemical changes

- The mechanism for coal devolatilisation proposed by Solomon et al [20] states that the formation and evolution of gases and tars begins from the breaking of weak bonds between aromatic rings. Aliphatic and aromatic structures play a significant role in determining the formation and release of gases and tars.

- Tars can affect the fluidity and viscosity of the plastic layer. Vitrinite concentrates are more aliphatic, show a higher ratio of gases and tars evolution and higher fluidity than inertinite concentrates.

2.8.4 Thermal changes

- During coke formation, the removal of moisture and pre-devolatilisation are endothermic reactions. Primary (450 and 550°C) and secondary (550 and 1000°C) devolatilisation are the major exothermic regions.

- Changes of thermal conductivities can be produced by the development of fluidity and char/coke structures. The higher fluidity of meta-plastic, the higher thermal conductivity can be observed.

2.9 Gaps in knowledge

- Previous work for coal maceral separation based on inorganic or organic media may have some disadvantages, this includes, a) inorganic or organic media may affect coking properties of coal; b) this technique limits the coal maceral concentrates to a small particle size range; c) only a small number of coal maceral concentrates can be obtained for one experimental run, it needs multi-repeats to get enough coal maceral

concentrates. Therefore, a technique for coal maceral concentrates separation, which can reduce the disadvantages mentioned above, is needed.

- Current techniques for evaluating physical and thermal properties of coking coal have their own advantages and disadvantages. Correlations between the changes of endothermic and exothermic reactions, thermal conductivity and swelling can only be understood by collecting data from individual experiments. However, the associations of these changes summarized from different studies can be affected by coal properties and different experimental conditions. The synchronized measurements of physical and thermal changes are still lacking. In addition, the current techniques for chemical analysis also have limitations in that they cannot directly correlate chemical compositions of tars to the physical and thermal changes during the transformation of coal to coke.

- The correlations between the physical changes, such as fluidity and volumetric swelling, and thermal changes, such as apparent specific heat and thermal conductivity, for coking coal are still unclear.

- The effects of vitrinite and inertinite concentrates on apparent specific heat and thermal conductivity are rarely reported. Correlations of endothermic and exothermic reactions and plastic layer properties such as permeability, swelling and thermal conductivity for different maceral concentrates are not well understood.

- Different coal maceral components tars properties and their contributions to physical and thermal changes during the transformation of coal to coke are not well known.

2.10 Hypothesis and objectives

2.10.1 Hypothesis

Based on the reports from the previous studies in coal compositions and the physical, chemical and thermal changes during the transformation of coal to coke, the hypothesis for the current work is stated as follows

"The fundamental changes that coal undergoes during coking are a complex mixture of physical, chemical and thermal mechanisms. The maceral components in the coal will affect these mechanisms, coking behaviour and final coke product. Techniques which measure the mechanisms together as coal heats can be used to gain new insights into the dynamic interactions of these components during coking."

2.10.2 Objectives

The research objectives include technique developments, experiments and their interpretations, including:

- Use the reflux classifier to separate coal maceral concentrates separation without introducing any inorganic or organic media.

- Introduce a compressible spring and a pressure sensor to the existing CATA technique, which can synchronously determine the swelling, permeability, apparent specific heat and thermal conductivity of heating coal; develop a Dynamic Elemental Thermal Analysis (DETA) technique to evaluate the gases and tars properties during coke formation.

- Synchronously determine the swelling, endothermic and exothermic reactions (characterised by apparent specific heat) and thermal conductivity of heating coal and analyse the effects of heating rate and particle size on these parameters.

- Evaluate the contributions of vitrinite rich and inertinite rich concentrates on the changes of swelling, apparent specific heat and thermal conductivity during coal heating, and investigate the possible interaction between vitrinite rich and inertinite rich concentrates.

- Correlate the swelling and permeability with simultaneous investigation of apparent specific heat and thermal conductivity of different coal maceral concentrates to reveal the mechanisms responsible for the physical and thermal changes during coal heating.

- Study physical and chemical properties of tars obtained from different coal maceral components, explore the impact of tars properties on swelling, apparent specific heat and thermal conductivity.

Chapter 3 Experimental work

3.1 Apparatus and techniques

3.1.1 Reflux classifier for coal macerals separation

The Reflux Classifier is relatively a new technique for solid particle separation which operates on the principle of "particle settling rates" in an inclined plane. Figure 3.1 shows the schematic of the Reflux Classifier set-up. It is a combination of a system of parallel inclined channels above a conventional fluidized bed. The inclined channels, defined by the plate length, L, perpendicular channel spacing, Z, and angle of inclination with the horizontal, θ, provide a significant hydraulic advantage over conventional fluidized bed.

The reflux classifier has been developed and successfully employed for mineral and coal particle separation at the University of Newcastle by a mineral processing research group headed by Professor Galvin. The concept and the design of the apparatus were detailed by Galvin et al [46, 47]. Zhou et al. [166] has shown that an optimal performance of the classifier can be attained with the angle of inclination (θ) in the range 60°-80° for solid particle separation. In the present work an angle of inclination of 70° is employed for coal macerals separation. The plate length (L) was 1000 mm with 24 channels, and the gap of the inclined channel was 1.77 mm. The cross-sectional area was 60×100 mm in the vertical section and the length of the vertical section was also 1000 mm. This allowed about 500 g of sample to be separated in each run.

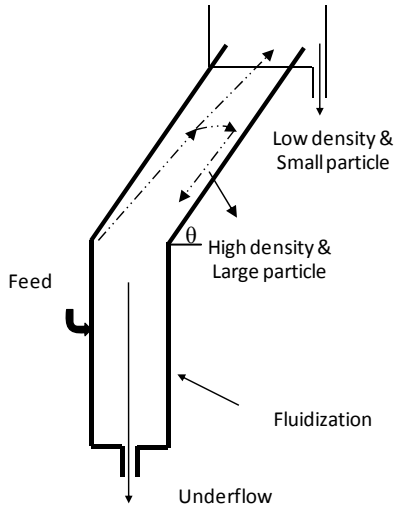

Figure 3.1. Schematic representation of the reflux classifier showing the feed and a fluidized bed housing, 24 parallel channels in the inclined equipment were not directly presented.

After crushing the coal to the expected size, the crushed coal samples were then soaked in water for 24 hours. During coal macerals separation, the coal slurry was fed into the vessel,

forming a bed of coal particles that was fluidized by pumping water from below. The fluidized suspension passed up into the inclined channels, where the coal particles segregated onto the upward facing surfaces of the inclined channel. With the fluidization controlled by the water flow rate, coal particles either were conveyed upwards out of the inclined channel with the water or back into the fluidized bed, depending on the density and particle size. Therefore, coal particles of a given density and size would be separated at a typical water flow rate.

A nylon bag with a mesh size of 22 μm was used at the outlet to collect the coal samples. Lighter, less dense, smaller particles have the slowest settling rate and were removed firstly as the sample overflowed. Further increase in water flow rate aids in removing higher density particles. The water flow rate was controlled by a single flowmeter or a combination of two flowmeters depending on the flow rate required. The initial water flow rate was set at 0.5 l/min, at which there was no sample collected, then gradually increased until the lightest and smallest particles were collected. With a specified water flow rate, the nylon bag for collecting sample was replaced every 30 minutes. The procedure was repeated until no particles get into the nylon bag, which guaranteed a complete separation for concentrates with different densities.

3.1.2 Computer Aided Thermal Analysis (CATA)

Computer Aided Thermal Analysis (CATA) is an advanced thermal analysis technique that allows simultaneous solution of both the specific heat and thermal conductivity of materials as a function of temperature. The material under study was made into a cylindrical bed of known dimensions. By measuring the surface and centre temperatures of a cylindrically packed bed, and using a pre-calibrated heat flux profile, the temperature profiles are incorporated into a cylindrical coordinate heat model that inversely solves the thermal properties.

A heating chamber is fitted inside a Sin-ku Riko Gold Image infrared heating furnace and is controlled by a thermocouple set into a graphite annulus inside the heating chamber. Heat is supplied to the sample from the furnace through the surrounding graphite cylinder at a constant heating rate, as shown in Figure 3.2. Graphite was used as it has well characterised thermal properties, is relatively inert and has no significant thermal reactions under argon flow. A larger silica glass tube was placed around the graphite annulus allowing the chamber to be flushed with inert gas to prevent the graphite from combusting. The gold heating furnace was capable of controlled heating rate up to 500°C/min and operated by reflecting infra-red radiation towards the central tubing. Therefore, the overall thermal inertia was small

and allowed for rapid heating or cooling. The upper picture shows the main features of the heating chamber. The lower diagram describes the use of the surface, centre and control thermocouples to solve the thermal properties (apparent specific heat and thermal conductivity) under a calibrated radial heat flux.

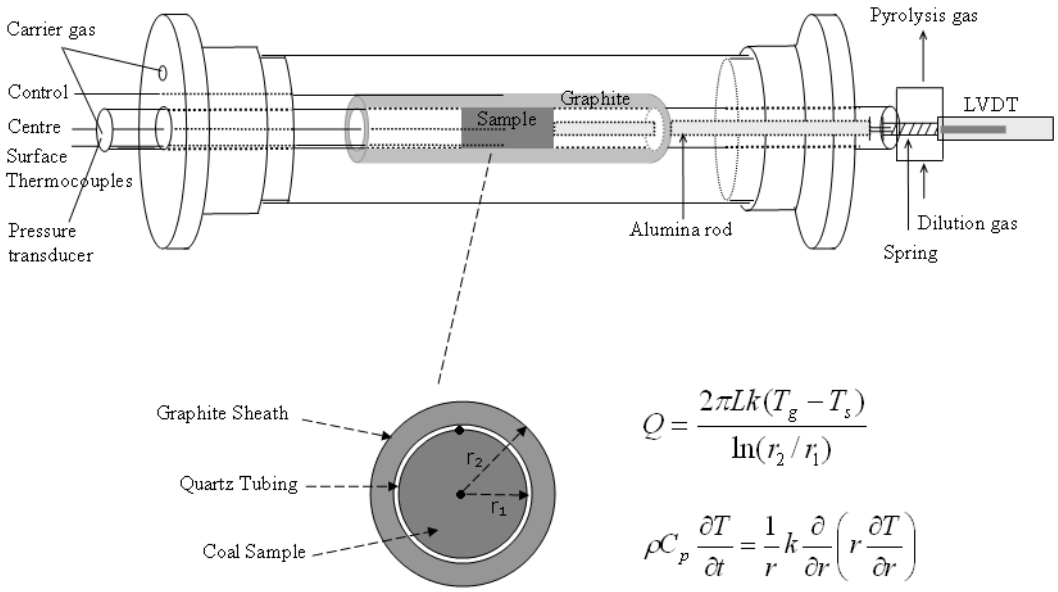

Figure 3.2. Schematic representation of the thermo-swelling test setup.

All raw coal samples were packed inside the 11.80 mm ID quartz tube to a length of 30 mm. Some samples that may show a huge swelling were packed to a length of 20 mm. Packed samples were heated from room temperature (25°C) to 1000°C under an inert atmosphere using a continuous argon flow. A nominal 200 ml/min flow rate was selected for the outer chamber and 30 ml/min was used inside the inner tubing. Both flow rates were controlled by Mass Flow Controllers (MFC). The temperatures of the graphite heating element, surface and centre of the samples were measured using three Type K thermocouples with a diameter of 1 mm.

Three different heating rates of 3, 5 and 10°C/min were used in this thesis. A nominal run would set the furnace to heat at a desired heating rate to 40°C and hold for half an hour, thereby purging the system of air and equilibrating the sample to a standard temperature. Pico software logged the time, and three temperature (control, surface and centre) in a data file. At the completion of the run, the data file was then processed using a specially written program that subsequently converts the temperature profiles into temperature dependant apparent specific heat (ρC_p), thermal conductivity (k), thermal diffusivity (α) and surface heat flux

($Q'_{R,t}$). The properties are considered apparent because they also contain energy requirements for endo/exothermic reactions, properties changes, such as softening, melting, boiling and decomposition.

3.1.2.1 Calculation of the heat flux

The heat flux to the sample surface was determined by calibrating a graphite sheath, which is also used as the furnace control temperature. The heat transfer rate from the graphite heating tube to the sample is [167]:

$$Q = \frac{2\pi Lk(T_g - T_s)}{\ln(r_2 / r_1)} \qquad (3\text{-}1)$$

Where Q is the heat rate (W); k is the thermal conductivity of the graphite (W/m.K); L (m) is the length of the sample; r_1 is the distance from the centre to the surface of the sample and r_2 is the distance from the centre of the sample to the graphite surface where the graphite control thermocouple is positioned (m). T_g and T_s are the temperatures of the graphite and the surface of the samples (K), respectively.

In this thesis, $\ln(r_2/r_1)/2\pi Lk$, which is defined as apparent thermal resistance [167], is determined through calibration using pure copper with known specific heat properties. Pure copper was used for calibration because of its high thermal conductivity [167] so that the measured centre and surface temperatures of cylinder copper in the quartz were considered the same. The apparent thermal resistance obtained from the calibration were used for numerically calculating the volumetric apparent specific heat and thermal conductivity of samples.

3.1.2.2 Calculation of the apparent specific heat and thermal conductivity

Following the definition in the CATA technique, the apparent specific heat and thermal conductivity of samples at elevated temperatures were calculated by applying an inverse numerical technique [103] to the measured temperatures: the conduction heat transfer is assumed to occur in one dimensional and the heat conduction equation in cylindrical coordinate is given in equation (3-2):

$$\rho C_p \frac{\partial T}{\partial t} = \frac{1}{r} k \frac{\partial}{\partial r}\left(r \frac{\partial T}{\partial r} \right) \qquad (3\text{-}2)$$

Where ρ is the density of the sample (kg/m^3), C_P is the specific heat (J/kg·K), k is the thermal conductivity (W/m·K), T is the temperature (K), t is the time, and r is the radius (m).

Boundary conditions were the measured centre temperature with zero heat flux and surface temperature of the samples with known heat flux. The numerical solution provides an

apparent thermal diffusivity α (m^2/s) and the discretised temperature profile (equation 3-3), which is then used to calculate the specific heat (equation 3-4) and thermal conductivity (equation 3-5). Volumetric specific heat is derived from the ratio of net heat input to volumetrically weighted temperature increase; while thermal conductivity is calculated from the heat balance of the surface node.

$$\frac{1}{\alpha}\frac{V_r}{\Delta t}\left(T_{r,t}-T_{r,t-1}\right)=\frac{A_{r+1}}{\Delta r}\left(T_{r+1,t}-T_{r,t}\right)-\frac{A_{r-1}}{\Delta r}\left(T_{r,t}-T_{r-1,t}\right) \quad (3\text{-}3)$$

$$\rho C_P=\frac{Q\Delta t}{\sum V_r\left(T_{r,t}-T_{r,t-1}\right)} \quad (3\text{-}4)$$

$$k=\frac{\frac{\pi\Delta r^2\left(R-\frac{1}{4}\right)}{\Delta t}\left(T_{R-1,t}-T_{R,t}\right)\rho C_P-Q\Delta t}{2\pi\left(R-\frac{1}{2}\right)\left(T_{R-1,t}-T_{R,t}\right)} \quad (3\text{-}5)$$

Where V_r is the node volume, A_r is the node area of heat transfer, T_r, t is the temperature expressed in K of the node r for the time t (s) and $Q_{(t)}$ is the heat flow expressed in W for time increment Δt.

3.1.3 Swelling of heating samples

For the purpose of synchronously including the swelling when the thermal properties were evaluated using a CATA technique, a linear variable differential transducer (LVDT) with a range of ±75 mm was introduced to measure the transient swelling and contraction of heating coal sample. Measurement of swelling of heating coal is shown in Figure 3.3. The coal bed was restrained on one side by a restrained alumina rod and allowed to expand on the other side against a moveable alumina rod. The moveable alumina rod in the core of the inner quartz tube was named the first alumina rod that has a diameter of 5.5 mm. It was surrounded by 10 smaller alumina rods that have a diameter of 3 mm to match the diameter of the packed sample. Kaowool was packed between the alumina rod and sample, which prevented the heating coal moving into the hole of the hollow alumina rods. The second alumina rod was covered by a washer at the tip. A calibrated spring with a diameter of 7.8 mm coated on the second alumina rod, one side was against the washer on the first alumina rod, the other side was against the sheath surrounding the LVDT magnetic core. Upon setting up the experiments, the spring was slightly compressed. During cokemaking, the spring was able to be further compressed or released depending on swelling or contraction of the heating coal

sample. The LVDT readings recorded the compression or release of the spring, which exactly implied the swelling or contraction of the heating sample. Temperature and LVDT readings were collected every second. In order to reduce possibly artificial errors from different measurements, all experiments were started under the same spring compression of 5 kPa. The spring constant was 142.7 N/m^2 and the maximum pressure was 155 kPa.

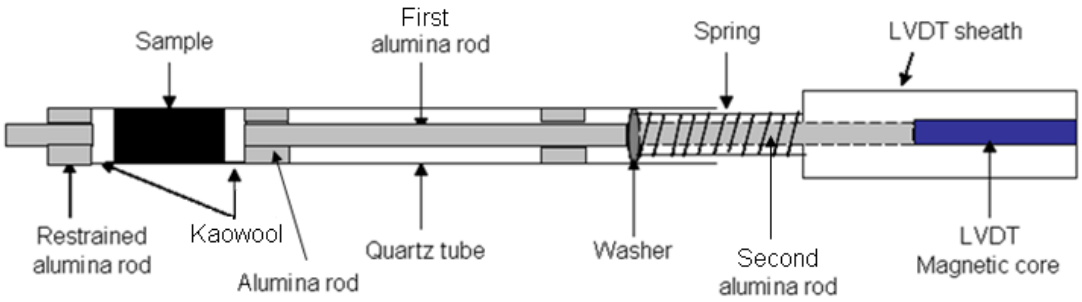

Figure 3.3. Schematic representation for measuring swelling of heating coal and coal maceral concentrates.

Swelling of samples was determined by the transient value of the LVDT measured during heating, calculated by the following equation:

$$Swelling = \frac{\Delta L}{L_0} \times 100\% \qquad (3\text{-}6)$$

Where ΔL is the dimension change which is the difference between the original length and the transient length of coal bed measured by the LVDT, L_0 is the original length of the packed sample of 20 or 30 mm in the quartz tube depending upon the sample nature and was already discussed. In addition to swelling which occurred at temperatures between 400 and 550°C, the contraction that occurred between 550 and 1000°C was also evaluated in the current study. The value of the contraction is the difference between the maximum swelling at around 510°C and the final swelling at 1000°C. Since the contraction occurred from 550-1000°C, it was named high temperature absolute contraction. The instantaneous swelling and contraction of all heating samples are presented in Chapters 4 to 7, all results are the horizontal swelling and contraction against the measured surface temperature of heating samples. The measured surface temperature is about 5°C higher than the temperature used to describe the apparent specific heat and thermal conductivity, depending on coal properties and heating conditions. This temperature applies to all results in Chapters 4-10, unless otherwise specified. The final length of coke was also measured by vernier calipers, which was used to calculate the density of coke.

3.1.4 Pressure drop and permeability

The pressure drop of gas flowing through the coal sample was recorded every second by a pressure transducer. The maximum pressure that could be measured by the transducer used in current work was 400 kPa. The permeability coefficient k (m^2) of the sample was then estimated according to Darcy's law [17, 106].

$$\frac{\Delta P}{L} = \frac{1}{k}\mu U \tag{3-7}$$

ΔP is the pressure drop of gas flowing through the coal sample expressed in Pa, μ is the viscosity of the carrier gas argon expressed in Pa.s, changes of argon viscosity with temperature was based on data in Perry's chemical engineer's handbook [168]. U is the carrier gas velocity in m/s, L is the transient length of the coal bed in m, which was calculated according to the LVDT measurement. Down stream pressure was assumed to be atmospheric. The effect of gases flow from the release of volatile matter on the calculation of permeability coefficient k (m^2) was also discussed. The results for the instantaneous pressure drop and permeability are presented in Chapter 7, the instantaneous temperature was the measured surface temperature of heating samples.

3.1.5 Coke density

The mass of the coke was weighed with an accuracy ± 0.00001 g using the HR-202 mass balance. Volume of the coke was calculated based on the measurements of the length and diameter of the final coke using the vernier calipers. The density of coke on daf was calculated based on mass, volume and the proximate and ultimate analysis for coal or coal maceral concentrate.

3.1.6 Thermogravimetric Analysis (TGA)

The mass change of the coal sample on heating was recorded using the Setaram TG/DSC analyser. About 20 mg of sample was accurately weighed in the sample crucible. Sample top size was less than 200 μm. All samples were heated with a constant argon flow rate of 30 ml/min over the sample crucible. Pyrolysis behaviour was assessed from room temperature up to 1000°C at a heating rate of 10°C/min. For the work with air, systems were purged with argon at room temperature for 60 minutes prior to heating.

3.1.7 Optical microscopy analysis

Olympus optical microscopy was used to assess the development of porosity of heating coal maceral concentrates. Char samples were prepared at critical temperatures, such as the onset of swelling, minimum permeability, maximum swelling and the onset of contraction. Microscopic properties of cokes from different coals or different coking conditions were also

compared. All samples were resin embedded and polished for optical microscopy analysis. The results for optical microscopy analysis are reported in Chapters 4, 6 and 7.

3.1.8 Dynamic Elemental Thermal Analysis (DETA)

Dynamic Elemental Thermal Analysis (DETA) is an advanced thermo-chemical analysis technique that is based on the concept of converting the volatile matter into combustion products as they are evolved using a custom built O_2 lance. By analysing the combustion products the results can be used to back-calculate the elemental compositions of CHNOS as they are evolved from the coking material. The lance is placed downstream of the evolving volatile matter and separately heated to 950°C. Figure 3.4 below shows the lance and flue gas analysis equipment added to the back end of the furnace described in Figure 3.2. By using this in situ method of conversion the tars are prevented from condensing downstream and can be included in the on-line analysis. The combustion products were analysed using a LiCor A CO_2/H_2O infrared analyser and a Testo 350XL flue gas analyser (O_2, CO, H_2, NO, NO_2, SO_2, hydrocarbons). Infrared analysis of H_2O was found to be important over more conventional relative humidity or dew point probes because such probes do not allow moisture determinations at low concentrations in the time scales measured.

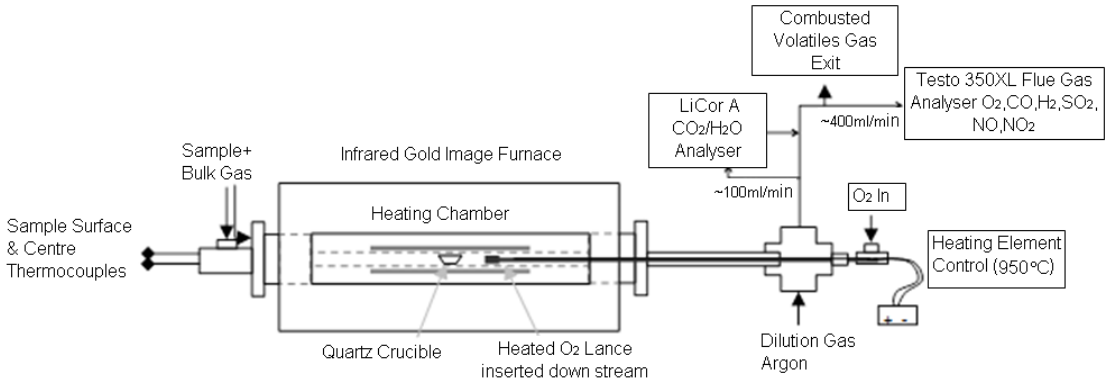

Figure 3.4. DETA apparatus for measurements of chemical compositions (CHNOS) of tars and gases during evolution.

There are four (4) modes of operating the DETA apparatus, as shown in Figure 3.5. The first mode combusts the total volatiles (tars plus light gases) evolved during heating. This configuration is the same as shown in Figure 3.4. About 500 mg of coal sample was loaded in a quartz crucible and inserted into an inner quartz tube, heated independently to 1000°C at a heating rate of 10°C/min. Argon was used as both the carrier sweep gas (200 ml/min) and a secondary dilution gas (1250 ml/min) to prevent condensation of H_2O and produce a flow rate suitable for the gas analyser (about 1500 ml/min required). Oxygen was injected through the lance at 100 ml/min. This produced a system whereby volatiles evolved from the coal sample during controlled heating rate mixed with O_2 downstream and combusted over a hot,

independently heated section of quartz tubing and alumina lance. The volatiles, both light gases and condensable tar species, were fully combusted to form CO_2 and H_2O as the main products, with minor amounts of CO, NO, NO_2 and SO_2. For a nominal test, the lance temperature was set to 950°C. Combustion gases exiting the furnace were air cooled to 50-100°C and diluted with the secondary stream of argon before being analysed using a LiCor A CO_2/H_2O infrared analyser and a Testo 350XL flue gas analyser.

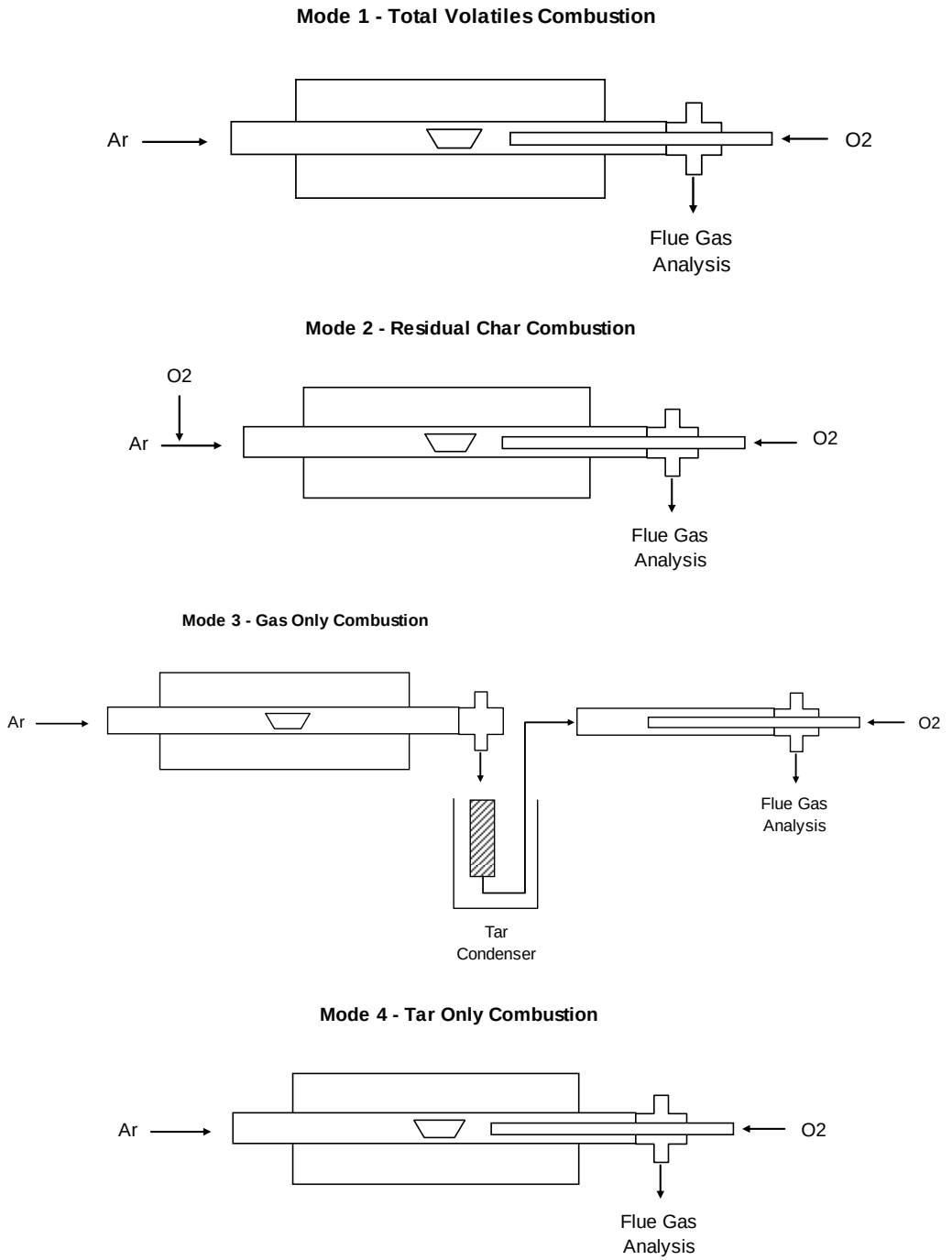

Figure 3.5. Modes of operation using the DETA apparatus for analysing tars plus gases, char, gases only and tars only.

The second mode, char combustion shown in Figure 3.5, adds a second stream of O_2 to the front end of the furnace to combust the residual coke/char. Total oxygen flow introduced through the second stream at the front end of the furnace plus injected O_2 through the O_2 lance stream was at the same flow rate of 100 ml/min during mode 1. Argon flows for other streams were not changed as a result that the total gas flow through the LiCor A CO_2/H_2O infrared analyser and the Testo 350XL flue gas analyser were at the same as that in mode 1.

Mode 3, Gas Only combustion, uses the same heated O_2 lance and gas analyser arrangement, however, the volatiles were swept through an ice cooling condenser prior to being combusted in a separate quartz tube. In practice this created a residence time delay of approximately 10 s. The benefit of this arrangement is that by comparing the Total Volatile combustion with Gas Only combustion, the combustion products produced from the evolved tars, and by extension the main elements involved, can be readily determined. For this separate test, 800 mg of coal sample was used – the greater sample size was used so as to target a CO_2 concentration between 10,000 and 20,000 ppm with the expected light gases combustion. The high CO_2 concentration was expected to reduce the measured errors during experimental runs. All comparative results between Total Volatiles combustion and Gas Only combustion have weighed the Gas Only results for the Total Volatiles sample mass.

Mode 4, Tar Only combustion utilized the same lance configuration as the mode 1 Total Volatile, however, it completed on tar. Tar was collected in the Gas Only test or washed from quenched char between 400 and 600°C. Tar species collected in the Gas Only test were condensed with ice cooling and in a tar condenser. For this test, acetone was used as the solvent to wash the quartz tubing and tar condenser clean. This solvent was selected due to the ease of use and relative safely, and though other solvents have been shown to be more suitable (i.e. pyridine, THF, methanol-chloroform), acetone may be safely used in greater abundance to overcome solubility issues. The washed mixture of tar and solvent acetone was allowed to evaporate in a fume cupboard at room temperature until the tar appeared to be glutinous or dry. This process took approximately 10 hours and included some re-wetting of the walls of the container to ensure tar species were not lost. Tars collected from quenched char were completely washed by two steps. The first step was to wash relatively small molecular tars that were capable of completely dissolving into acetone. Washing would not end until there was no colour change for acetone as it passed through the char sample. Washed tar was kept in a tar container, acetone evaporation from tar was the same process as described above. The secondary step was to wash out the relatively large molecular tars using a relatively heavy solvent of toluene. Washed tars were kept in a separated container and

treated in the same manner as acetone washing. Glutinous or dry tars were transferred into a crucible for further combustion analysis.

3.2 Calibration

3.2.1 Furnace temperature distribution

All experiments, such as coals/macerals pyrolysis for swelling and thermal properties analysis, volatile matter (gases plus tars) generation and collected tars reheating for chemical analysis were conducted in a Sin-ku Riko Gold Image infrared heating furnace. The available Infra-red zone in the heating furnace is about 30 cm in length. Temperature distribution measured with thermocouple displacement is attached in Appendix A. It indicates that about 15 cm in the centre of the furnace can be considered a stable temperature zone where it is suitable for conducting isothermal experiments. During coals/macerals pyrolysis experiments, the length of the packed sample beds were only 20 or 30 mm which guaranteed the heating samples would not move out of the stable isothermal zone even if a huge pyrolytic swelling occurred. The quartz crucible used during tar only combustion experiments was about 40 mm in length, which ensured the experiments occurred within a stable temperature zone.

3.2.2 Mass flow controllers

Five Brooks series mass flow controllers (MFC) were used for all the physical, chemical and thermal analysis experiments. This included all swelling, apparent specific heat and thermal conductivity and chemical elemental dynamic measurements.

All MFC were calibrated to the set flow rate by the use of a bubble flow meter and a digital stop watch. For every run above 5 ml/min, the MFC were set and allowed to equilibrate over 2 minutes. The gas flow was connected to the 50 ml bubble flow meter and timed using the movement of the soapy bubble interface. When 3 measurements were completed, the difference of each measurement was less than 0.1 ml/min, the gas was reconnected to the apparatus and the MFC was considered calibrated.

3.2.3 Compressible spring

A compressible spring was used to record the instantaneous horizontal swelling or shrinkage of the heating samples. The spring was calibrated to ensure its compression or release was within the limit and corresponded to the equivalent force. A known mass is applied to the spring to get the linear strain of the spring. From the calibration

the equivalent force can be calculated and the value can be used for the experimental observation. The relationship between LVDT displacement and equivalent force is attached in Appendix A.

3.2.4 Apparent thermal resistance

The apparent thermal resistance as indicated by Equation 1 defines the rate at which heat is transferred from the graphite heating tube to the sample surface. The term $\ln(r_2/r_1)/2\pi Lk$ is defined as apparent thermal resistance. Apparent thermal resistance can be determined at different heating rate because of its effect on the thermal conductivity of the graphite. Considering the high thermal conductivity of pure copper (401 W/m·K at 400 K), copper with known specific heat was selected to calibrate the apparent thermal resistance of the heating furnace at a fixed heating rate. After being shaped to the same volume as a packed coal sample bed, 11.80 mm diameter and 30 mm length, the copper surface was blacked by combusted acetylene soot increasing the thermal conductivity between the copper surface and the quartz tube. Only one thermocouple was used to measure the copper centre temperature, as the copper surface temperature was considered to be exactly the same as the centre temperature due to its high thermal conductivity. The calibration process was conducted at three different heating rates of 3, 5 and 10°C/min. The results for the calibration of heat flux and the apparent thermal resistance with temperature at different heating rates are attached in Appendix A.

3.2.5 Pressure transducer

Pressure drop of gas flowing through the coal sample was measured using a GEMS pressure sensor, with instantaneous pressure drop recorded every second. Permeability coefficient k through the heating coal pellet was calculated based on measured pressure drop, swelling, viscosity and velocity of carrier gas. The results are presented in Chapter 7.

3.2.6 Dynamic Elemental Thermal Analysis (DETA)

The measurements of elemental compositions using the Dynamic Elemental Thermal Analysis (DETA) were calibrated based on the organic chemicals of Benzoic acid ($C_7H_6O_2$), Diphenylamine ($C_{12}H_{11}N$) and Sulfolane ($C_4H_8O_2S$). The experiments were based on the DETA mode 4 technique. About 200 mg of sample was weighed for each calibration. The released C, H, S, N and O matched the elemental compositions of the used sample. Results for these calibrations are attached in Appendix A.

3.3 Coal samples

3.3.1 Preparation of coal samples

Four coal samples were selected for synchronously investigation of the swelling and thermal properties of heating coal: two bituminous coking coals B and C with relatively high vitrinite reflectance; two bituminous coal samples D and E with relatively low vitrinite reflectance. The Proximate analysis, Petrographic analysis, Gieseler Plastometer and Dilatation analysis are presented in Table 3.1. Coal sample C was ground to 0-212 μm and 0-500 μm for the purpose of evaluating the effect of particle size on swelling and thermal properties of coking coal, the others were ground to 0-212 μm. All samples were stored under refrigeration to stop oxidizing. Following the original names of the coals came from, the samples were named B, C, D and E rather than the order of A, B, C and D.

Table 3.1. Coal samples analysis.

	B	C	D	E
Proximate analysis (ad)				
Fixed carbon (%)	70.3	72.6	62.1	61.6
Volatile matter (%)	19.1	19.1	27.7	27.2
Ash (% ad)	9.3	6.9	7.5	8.3
Air dried moisture (%)	1.3	1.4	2.7	2.9
Mineral, (% vol)	3.2	2.2	3.2	2.4
Petrographic analysis				
R_{vMax} (%)	1.59	1.46	0.97	0.98
Liptinite (%mmf)			2.6	1.5
Vitrinite (%mmf)	73.6	51.2	63.6	67.5
Inertinite (%mmf)	26.4	48.8	33.8	31.0
Gieseler Plastometer (AS 1038.12.4.1)				
Crucible Swelling Number	>9		8.5	8.0
Initial Softening Temperature, °C	440	435	415	420
Maximum Fluidity Temperature, °C	475	470	455	450
Maximum Fluidity, ddpm	170	45	250	60
Solidification Temperature, °C	500	495	480	480
Plastic Range, °C	60	60	60	60
Dilatation (AS 10.38.12.3)				
Initial Softening Temperature, °C			380	385
Maximum Contraction Temperature, °C	455	455	425	435
Maximum Dilatation Temperature, °C	490	490	450	460
Maximum Contraction, %	19	25	18	18
Maximum Dilatation, %	84	23	40	8

3.3.2 Preparation of coal macerals samples

3.3.2.1 Coal maceral separation

Two bituminous coking coal samples B and C were selected for coal maceral separation. Coal sample C, with relatively a small Maximum Dilatation, was selected for the preliminary maceral separation without controlling the coal particle size. Coal sample C was firstly crushed to less than 212 μm, and then coal slurry was obtained after soaking up coal sample in water for 24 hours. During washing of coal slurry, slight and small particles were firstly separated. With continuously increasing water flow rate, denser and larger particle were subsequently separated through the Reflux Classifier. Collected maceral samples were dried at 80°C in an oven with an argon atmosphere. Cooled samples were stored under refrigeration for further testing.

For the purpose of getting a large difference in swelling for separated vitrinite rich and inertinite rich coal maceral concentrates. The second coal macerals separation was based on coal sample B that shows relatively a large maximum Dilation. Meanwhile, in order to eliminate the effects of particle size on swelling and thermal changes of coal maceral concentrates, particles sizes of coal sample B were controlled before being separation. Coal sample B was crushed to 0-1000 μm, then wet sieved into 106-212 μm and 212-500 μm size fractions. Using the reflux classifier, they were separated into different vitrinite and inertinite concentrates. Separated coal macerals were dried and stored under refrigeration for further testing.

3.3.2.2 Density, ash and particle size distribution of coal macerals

Density measurements of separated maceral concentrates were based on Australian Standards (AS 1141.6.2-1996). Maceral samples were dried to constant weight at 105°C under a nitrogen atmosphere. A ~5 g sample mass was weighed to ± 0.00001 g for each density test. The weighed coal samples were soaked in distilled water over 24 hours in a 50 ml pycnometer. All experiments were conducted at room temperature, with the temperature measured by a thermometer for the purpose of determining the density of water. Details for calculating the relative density of coal sample can be seen in this Standard. Results for relative densities of maceral concentrates in these experiments were reproducible. Ash contents were analysed on the basis of AS 1038.3-2000. Laser particle size analysis for all maceral samples was conducted on a Mastersizer 2000 particle size analyser. The results are referred to Chapters 4-6.

3.3.2.3 Petrographic, proximate and ultimate analysis of coal macerals

Standard petrographic analysis (ISO7404) was carried out to determine the coal maceral compositions for each maceral concentrate. Proximate and ultimate analyses were based on Australia Standards 1038.1, 1038.3 and 1038.6. The results are referred to Chapters 4-6.

3.4 Experimental summary

3.4.1 Swelling and thermal properties

Swelling and thermal properties (apparent specific heat and thermal conductivity) analysis applied to all parent coal samples and coal maceral concentrates. Experiments were carried out using CATA with three temperatures (control, sample surface and centre) with instant LVDT reading measurements. Apparent specific heat and thermal conductivity were calculated based on calibrated apparent thermal resistance. TGA experiments were conducted to observe the weight loss of coal maceral concentrates as a function of temperature. Interactions between vitrinite and inertinite to affect swelling and thermal properties were conducted based on coal macerals concentrates from coal sample C. Experiments for this section are listed in Tables 3.2-3.4. The results are referred to Chapters 4-7.

3.4.2 Permeability

In order to study the mechanisms of swelling during coal heating, permeability of gases and tars through the coal sample was investigated on the basis of one high vitrinite coal maceral concentrate (86.4% vitrinite) and one medium vitrinite coal maceral concentrate (64.4% vitrinite) separated from coal sample B. Pressure drop of gas flowing through the coal sample with increasing temperature was measured by a pressure transducer. In combination with swelling, velocity and viscosity of carrier gas, permeability was calculated based on equation 3-7. To check the reproducibility, the experiments were repeated thrice and the experimental results are presented in Chapter 7. Permeability experiments are summarized in Table 3.4.

3.4.3 Porosity analysis of coke/char

The porosities of cokes prepared from different coals and coal maceral concentrates were analysed using the optical microscopy. Porosities of cokes produced from parent coals at different heating rates and different particle sizes, and the development of porosity with temperature for maceral concentrates were observed using optical microscopy. Chars were prepared at critical temperatures, such as the onset of swelling, minimum permeability, maximum swelling and the onset of contraction. Porosity experiments are summarized in Table 3.2 and Table 3.4. Since this work aims to study the mechanism in the transformation

of coal to coke, and only 2-3 g of a single coal sample was used for one experimental run, which is not enough for coke strength test, the coke strength after reaction (CSR) was not determined in this work. The experimental results are presented in Chapters 4, 6 and 7

Table 3.2. A summary for physical and thermal changes tests of all coals.

Coal sample	3°C/min, -212 μm	5°C/min, -212 μm	10°C/min	
			-212 μm	-500 μm
B	CATA, OM	CATA	CATA, OM	---
C	CATA	CATA	CATA, OM	CATA, OM
D	CATA	CATA	CATA	---
E	CATA	CATA	CATA	---

OM: Optical Microscopy

Table 3.3. A summary for physical and thermal changes tests of coal maceral concentrates from coal C.

Maceral samples C	10°C/min, 22-212 μm
Vitrinite-rich	CATA
Medium-vitrinite	CATA
Inertinite-rich	CATA
Blends of vitrinite and inertinite	CATA

3.4.4 Chemical analysis of total volatile, gases only, tars only and char

Dynamic elemental thermal analysis for total volatiles (gases plus tars) and gases only was applied to all coal macerals concentrates with a particle size of 106-212 μm separated from coal B. One coal maceral concentrate rich in vitrinite (86.4% vitrinite) and one rich in inertinite (32.4% vitrinite) were selected for chars and tars (condensable and extractable tars) properties analysis. All experiments were carried out at a fix heating rate of 10°C/min. DETA experiments are summarized in Table 3.4. The experimental results are presented in Chapter 8

Table 3.4. A summary for physical, thermal and chemical changes tests of coal maceral concentrates from coal B.

Maceral samples B	10°C/min	
	106-212 μm	212-500 μm
Vitrinite-rich	CATA, DETA, TGA, P, OM	CATA
Medium-vitrinite	CATA, DETA, TGA, P, OM	CATA
Inertinite-rich	CATA, DETA, OM	CATA

P: Permeability

Chapter 4 Swelling and thermal properties of heating coal

4.1 Introduction

The heating of coking coal is associated with physical and chemical changes that include successive endothermic and exothermic reactions and volumetric changes with the residue left as a coke. Endothermic and exothermic reactions are mainly related to coal devolatilisation [19]. Volumetric changes for heating coal include a slight low temperature contraction (300-450°C) followed by medium temperature swelling (400-600°C) and finally a high temperature shrinkage (600-1000°C) [111].

Previous studies have studied the changes of fluidity, viscosity [71, 89, 91, 169], swelling and shrinkage [111, 147, 170] apparent specific heat [21, 163] and thermal conductivity [19, 21] of different heating coals using various techniques. The change of apparent specific heat was utilized to identify the heats of endothermic and exothermic reactions during coal devolatilisation [19, 21]. Heats of coal devolatilisation and physical changes were found to be strongly dependent on the formations and evolutions of gases and tars [63, 91, 111]. Changes in the properties of heating coal, such as fluidity, viscosity and porosity, influence the thermal conductivity which determines the heat energy conducted from the coke oven wall to the centre [19, 20]. Correlations between the changes of endothermic and exothermic reactions, thermal conductivity and swelling can only be understood by collecting data from individual experiments. However, the associations of these changes summarized from different studies can be affected by coal properties and different experimental conditions. The synchronized measurements of physical and thermal changes are still lacking.

This Chapter reports results for swelling and thermal changes of heating coals using the CATA technique which simultaneously measures swelling, apparent specific heat and thermal conductivity. Analyses of the correlations between swelling, apparent specific heat and thermal conductivity of heating coal samples are also detailed. Four coal samples including two relatively high rank bituminous coking coals B and C with vitrinite reflectance (R_{vMax}) of 1.59 and 1.46, respectively; two relatively low rank bituminous coal samples D and E with vitrinite reflectance (R_{vMax}) of 0.97 and 0.98, respectively, were employed. In addition to coal properties, the effects of coking conditions, such as heating rate and particle size on swelling, apparent specific heat and thermal conductivity were also investigated. A sample bed length of 30 mm was used for all experimental results reported in this Chapter. The other sample packed bed length, such as 20 mm, was used in Chapter 6. The effects of packed bed lengths

on swelling, apparent specific heat and thermal conductivity during coal heating, based on coal sample E, is discussed in Appendix B.

4.2 Swelling and contraction of heating coal

In this section, the swelling and contraction of four coal samples B, C, D and E with a particle size 0-212 μm were investigated. Each coal sample was heated from room temperature (25°C) to 1000°C at a heating rate of 10°C/min. The results for swelling are shown in Figure 4.1. The temperature of x axis is the measured surface temperature of sample, which also applies to Chapters 5-10, unless otherwise specified. Figure 4.1 indicates that all the four coal samples experienced a rapid swelling between 470 and 520°C and a slow contraction above 600°C. Prior to the rapid swelling, a slight contraction appeared (between 420 and 470°C), as shown in the insert in Figure 4.1.

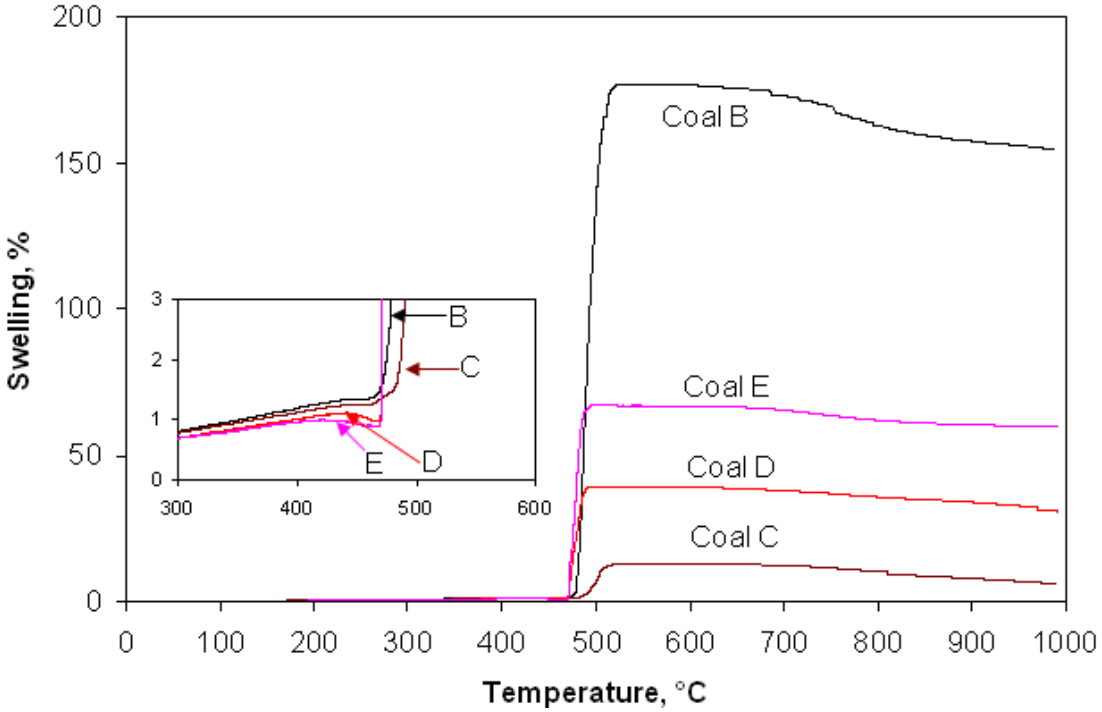

Figure 4.1. Swelling of four coal samples at a heating rate of 10°C/min from 25 to 1000°C.

Prior to the rapid swelling, the two lower rank coal samples, D and E, produced a higher degree of contraction than the two higher rank coal samples, B and C. There was no significant difference in the temperatures for the onset of rapid swelling between the two low rank coals, D and E, but this temperature was lower than that of the two high rank coals, B and C. By comparison, for the two high rank coal samples B and C, the high vitrinite content sample, B, produced a lower initial swelling temperature than the low vitrinite sample, C. Loison et al. [3] suggested that coal undergoes intra-particles swelling and bed swelling during heating. Coal undergoes intra-particles swelling first due to bubbles growing within

the particles. With the progress of pyrolysis, coal particles deform and become closer together, though still leaving some inter-particles pores that allow the pyrolysis gases to escape. Pressure in coal bed increases with the accumulation of tars and gases, the corresponding bed swelling occurs. In the current work, the bed swelling can be measured by using a compressible spring. Therefore, the measured onset of swelling at a lower temperature for coal sample B may relate to the rate of the formation of gases and tars, with the rate of bubble growing, and the viscosity of metaplast, which may affect the release of gases and tars.

Figure 4.2 indicates, for all the four coal samples, the maximum swelling increased with increasing vitrinite plus liptinite content, particularly for coal samples that have a high vitrinite plus liptinite content. This can be seen for coal samples B and E that have vitrinite plus liptinite contents of 73.6% and 69.0%, respectively. However, the high temperature absolute contraction (the difference between the maximum swelling at around 510°C and the final swelling at 1000°C) did not show a distinct increase with the vitrinite plus liptinite content.

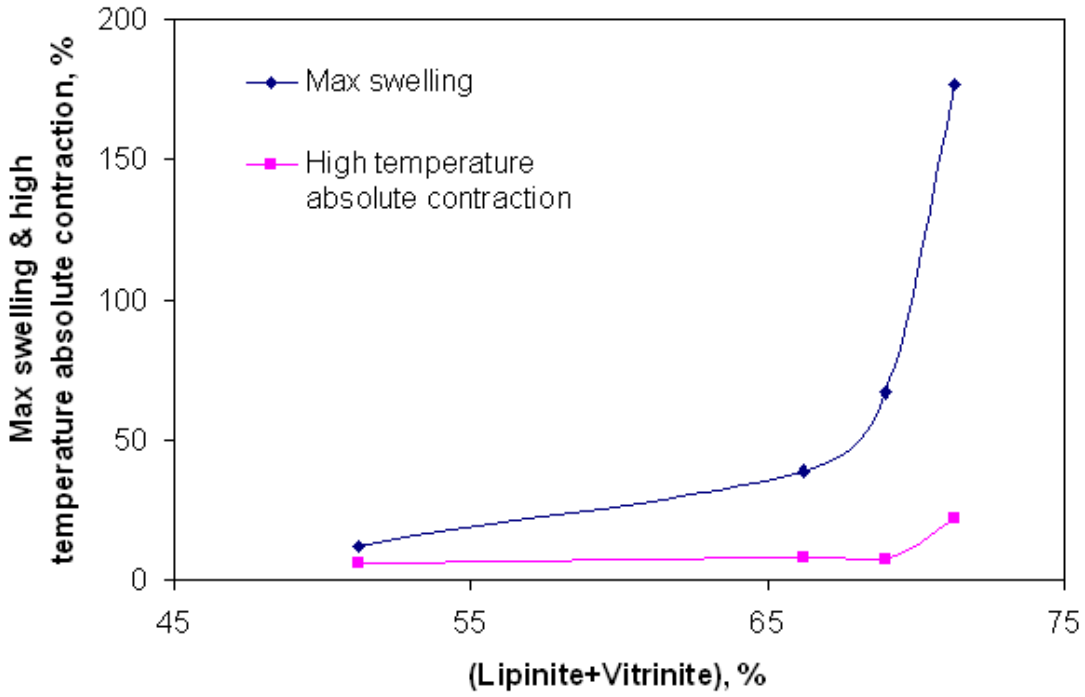

Figure 4.2. Relationship between maximum swelling and high temperature absolute contraction with vitrinite plus liptinite content for four coal samples at a heating rate of 10°C/min from 25 to 1000°C.

4.3 Apparent specific heat and thermal conductivity of heating coal

4.3.1 Apparent specific heat of heating coal

4.3.1.1 Apparent specific heat and endo/exothermic reactions

Figure 4.3 presents the estimated apparent volumetric specific heat of heating coal samples from 25 to 1000°C at a heating rate of 10°C/min. The temperature of x axis is the mean temperature estimated using CATA technique based on the control temperature and the measured surface and centre temperatures of heating sample (section 3.1.2.2), which is 5-10°C lower than the measured surface temperature used to describe swelling, depending on coal properties and heating conditions. This temperature also applies to Chapters 5-10, unless otherwise specified. The results show that the apparent volumetric specific heats for the four coal samples are in the range 1200-1400 kJ/m^3·K at 80°C and 1590-1990 kJ/m^3·K at 300°C. As the packed densities of coals were between 820 and 910 kg/m^3, the estimated apparent mass specific heat is in the range 1.3-1.7 kJ/kg·K, which is very similar to the results reported by Strezov et al. [19] and Hanrot et al [160]. They reported that the apparent specific heat of coal is 1.0-1.4 kJ/kg·K at 25°C and up to 1.3-1.8 kJ/kg·K at 300°C.

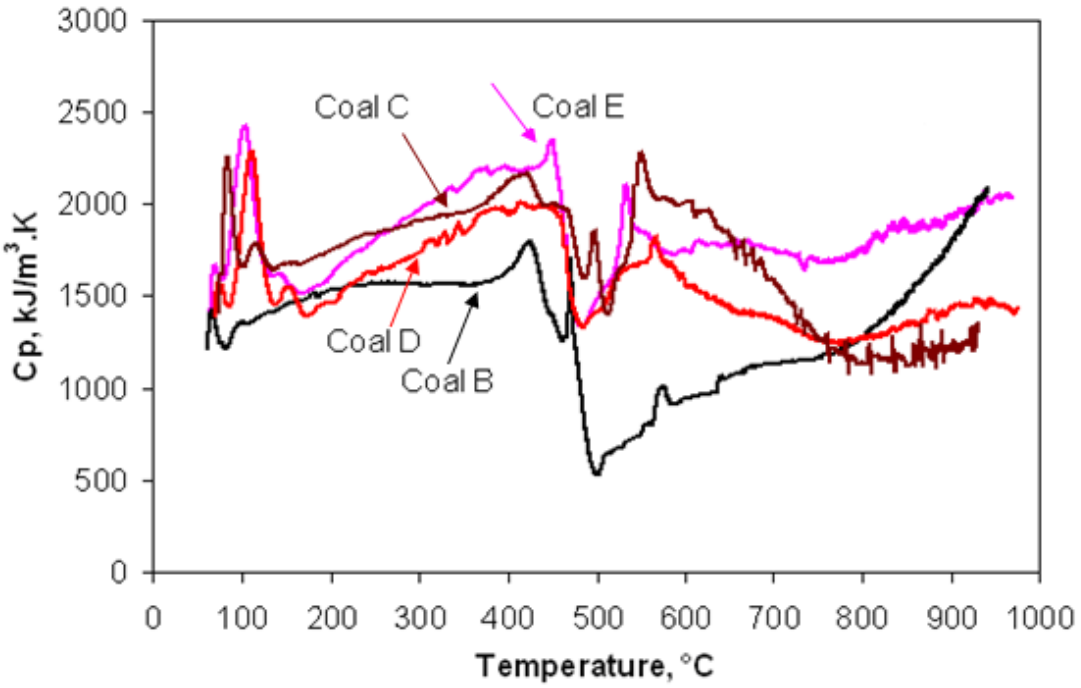

Figure 4.3. Comparison of the apparent specific heat for four coal samples at a heating of 10°C/min from 25 to 1000°C.

The changes in the estimated apparent volumetric specific heat and thermal conductivity of heating coal were previously quantified by Strezov et al. [21] using the CATA technique. Endothermic and exothermic reactions of heating coal can be indicated by the change of

specific heat [19, 21]. This has been summarized in literature in Chapter 2. Based on their work, the peak of the apparent specific heat represents the endothermic process, while the trough of the apparent specific heat indicates the exothermic reaction. Therefore, for the estimated apparent volumetric specific heat in Figure 4.3, the endothermic dehydration region between 80 and 180°C was attributed to removal of moisture. The second endothermic region (380-450°C) was found to correlate with a pre-plastic transition involving structural relaxation. The first exothermic region between 420-550°C was related to the fluidity development of the coal. The fourth region (520-580°C) was attributed to another endothermic reaction involving devolatilisation and resolidification. The fifth and largest region involved an exothermic reaction with the release of light gas and a contraction of carbon hexagonal planes. The differences for the events occurring in the temperature regions depend on the coals.

The results in Figure 4.3 indicate that the two low rank coal samples D and E have larger endothermic peaks in the temperatures between 80 and 180°C compared to the two high rank coal samples B and C, which are attributed to the higher moisture and bounded secondary water content. These results are consistent with the air dried moisture contents in Table 3.1 that presented in Chapter 3. With increasing temperature from 180 to 420°C, the apparent volumetric specific heat for coal samples D and E increase at a higher rate than that of coal samples B and C. At even higher temperatures, between 420 and 580°C, coal sample B shows the maximum exothermic trough, corresponding to the highest swelling and the maximum R_{vMax} (vitrinite maximum reflectance). Coal sample C, with a medium R_{vMax} produced the lowest swelling during the primary exothermic reaction, but it has the largest exothermic trough during the secondary devolatilisation from 570 to 950°C.

4.3.1.2 Volumetric specific heat and mass specific heat

At 300°C or higher, tars and gases begin to evolve from coal due to thermal reactions [63]. The heating coal becomes metaplastic and swells with the release of gases and tars [36]. The estimated apparent volumetric specific heat can be affected by this volumetric swelling, while the estimated apparent mass specific heat of heating coal can be affected by weight loss due to coal devolatilisation. In the current work, the apparent volumetric specific heat was estimated using the CATA technique. To estimate the apparent mass specific heat, the weight loss of coal sample B as a function of temperature was obtained from Thermogravimetric Analysis (TGA) at a heating rate of 10°C /min. The density of coal sample B as a function of temperature was estimated based on the instantaneous mass change and volume swelling. Apparent mass specific heat was estimated based on the estimated apparent volumetric

specific heat and density of heating coal. A comparison between the apparent volumetric specific heat and the apparent mass specific heat is shown in Figure 4.4. The results indicate that the apparent volumetric specific heat and the apparent mass specific heat have the same trend of endothermic and exothermic reactions. The only minor difference is the apparent mass specific heat produced a larger proportional change during the primary exothermic reaction (from 420-580°C) due to the decrease on the coal density. Therefore, all experimental results in this work will be reported as apparent volumetric specific heat, estimated using the CATA technique, unless otherwise specified.

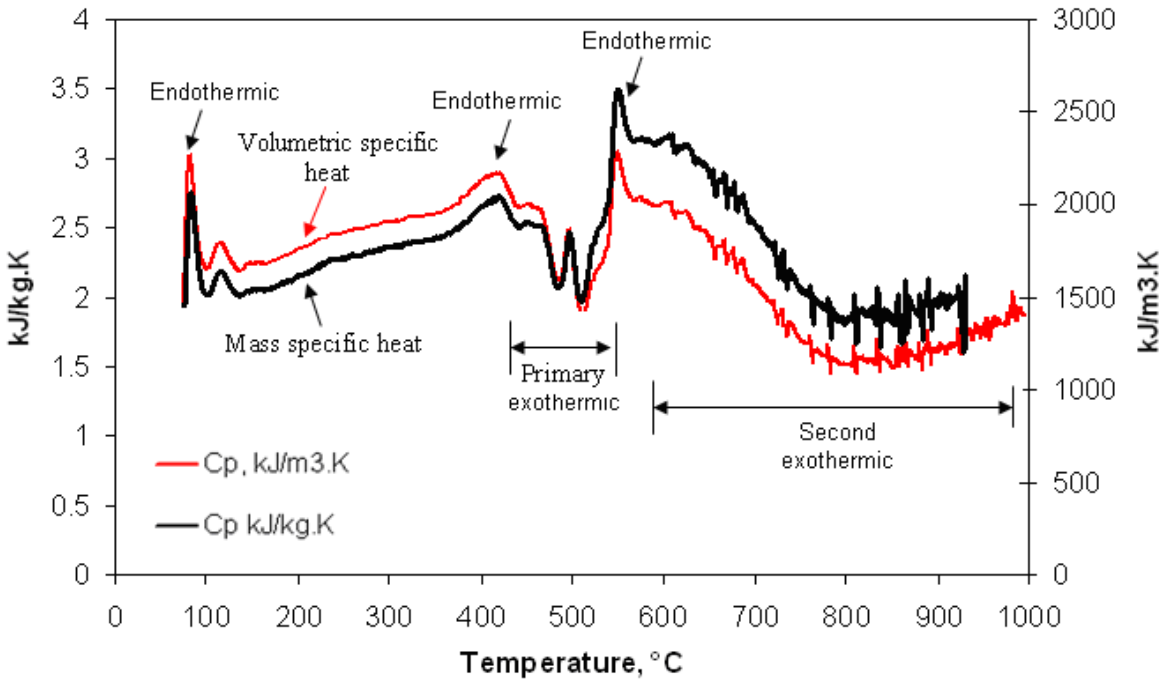

Figure 4.4. Comparison of the apparent volumetric specific heat and the apparent mass specific heat for coal sample C at a heating rate of 10°C/min from 25 to 1000°C.

4.3.2 Thermal conductivity of heating coal

The estimated thermal conductivities of the four coal samples at a heating rate of 10°C/min from 25 to 1000°C are shown in Figure 4.5. The thermal conductivities of all the coal samples are similar with values between 0.14-0.17 W/m·K up to 450°C, which is in agreement with data reported by Butorin et al [85]. All the coal samples, except for coal sample D, produced peaks in the thermal conductivities between 450 and 580°C. The peaks are particularly distinct for high swelling coal samples B and E, which indicate the association of thermal conductivity with swelling. Strezov et al. [19] found that a high thermal conductivity between 400 and 600°C relates to a high fluidity. The increase of thermal conductivity estimated using CATA is indicative of the increase in fluidity of heating coal. Therefore, in the current work, a high thermal conductivity between 400 and 600°C is also considered high fluidity. Above

600°C, a rapid increase in thermal conductivity was observed which could be associated with other effects, including:

(a) radiant heat transfer across pores and cracks;

(b) changes in the thermal conductivity of the coals due to pyrolysis;

(c) changes in the intrinsic conductivity with temperature of char [20, 85],

(d) a numerical artefact (the estimated thermal conductivity is affected by heats of reactions) associated with heat build-up in the packed bed. When thermal conductivity reached 2-3 W/m·K and beyond [19], the difference between measured surface and centre meta-plastic material temperatures was in a very narrow range or thermal inversion between surface and centre of heating sample occurred, hence results became unstable.

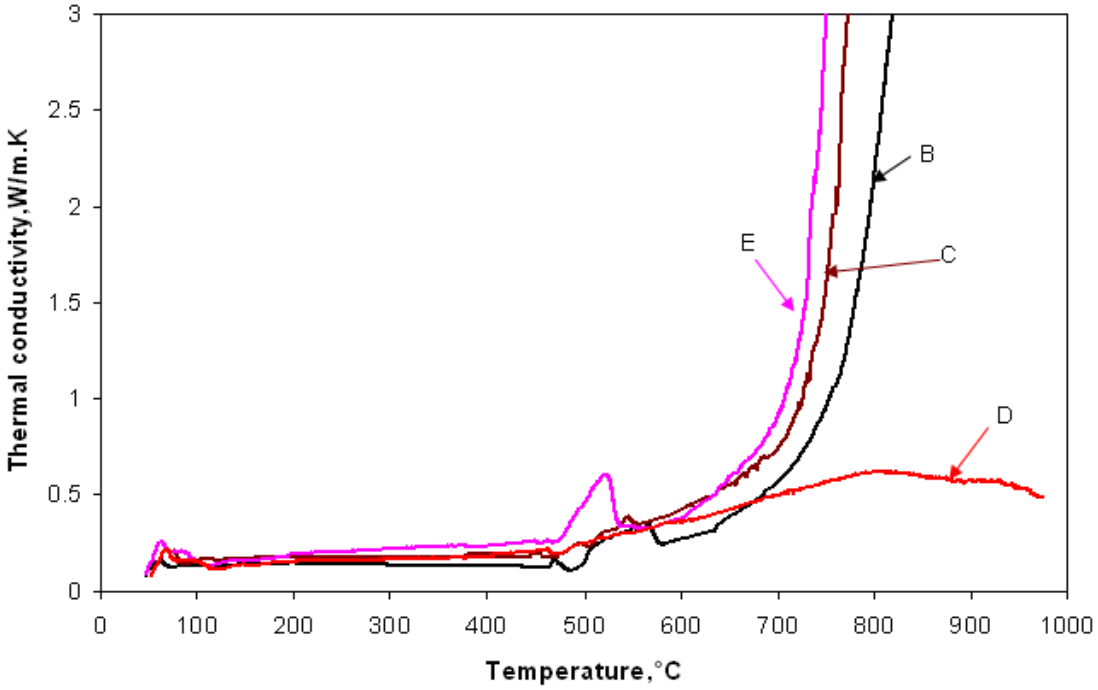

Figure 4.5. Comparison of the thermal conductivities of the four coal samples at a heating of 10°C/min from 25 to 1000°C.

4.4 Relationship between swelling and thermal properties of heating coal

This section discusses the correlations between swelling rate, the apparent specific heat and thermal conductivity of heating coal. Results for correlating the physical and thermal changes based on a high rank coal sample B and a low rank coal sample E are shown in Figures 4.6 and 4.7. Prior to the rapid swelling, both the coal samples produced an endothermic reaction, described as a prepyrolytic transition [21]. Between 420 and 580°C, rapid swelling occurred. The swelling was accompanied by a large exothermic trough and a peak in thermal

conductivity, which implied that the changes of swelling and thermal conductivity relate to the endothermic and exothermic reactions.

Comparing the two coal samples of B and E, there are some differences in the developments of swelling, apparent specific heat and thermal conductivity, although the general trends are similar. Between 460 and 480°C, the thermal conductivity for coal sample B increased slightly forming a small peak prior to rapid swelling, but this was not observed for coal sample E. Correspondingly, a small peak in the apparent specific heat for coal sample B was observed, but it did not appear for coal sample E. As the coal began to rapidly swell at around 480°C, the thermal conductivity of coal sample B dipped prior to the peak, whereas this did not happen for coal sample E. The reason for this may be that the high swelling rate of coal sample B decreases the concentration of liquid in the metaplast, which also leads to a decrease of fluidity, as a result the thermal conductivity slightly decreased. However, this did not happen for coal sample E due to the relatively low swelling rate. With increasing temperature, the concentration of liquid in the metaplast of coal sample B increased again due to the release of more tars so that the thermal conductivity correspondingly increased with the appearance of a peak between 500 and 580°C. When swelling reached the maximum, a dip in the thermal conductivity for both the coal samples was observed between 570 and 600°C, which is consistent with an endothermic peak relating to the end of the primary devolatilisation. Above 600°C, a rapid increase in thermal conductivity for both coal samples was observed which can be associated with other effects as discussed in section 4.3.2.

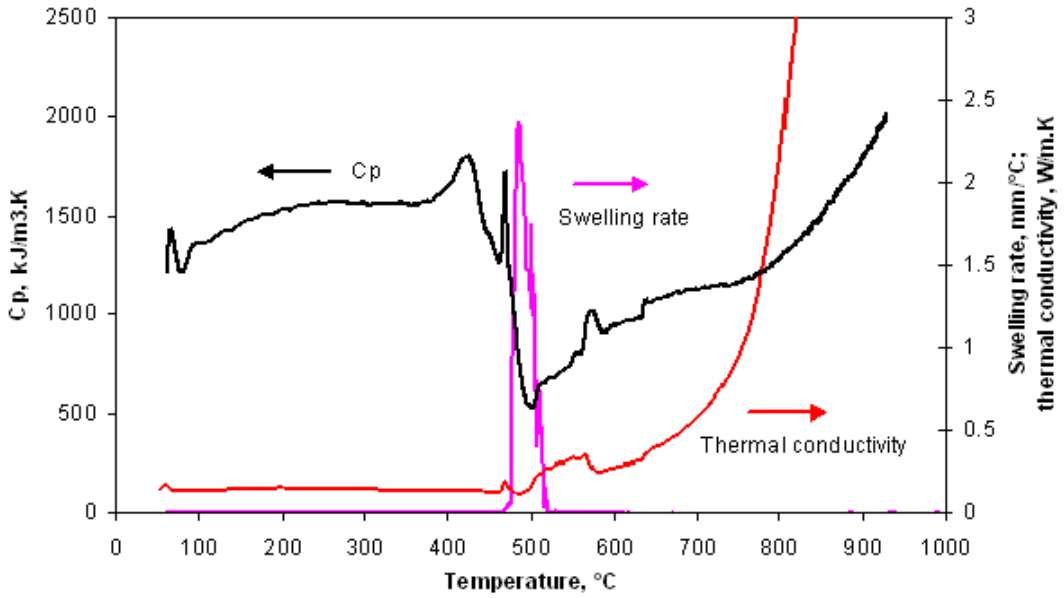

Figure 4.6. Correlations between the apparent specific heat, thermal conductivity and swelling rate with temperature for coal sample B at a heating rate of 10°C/min from 25 to 1000°C.

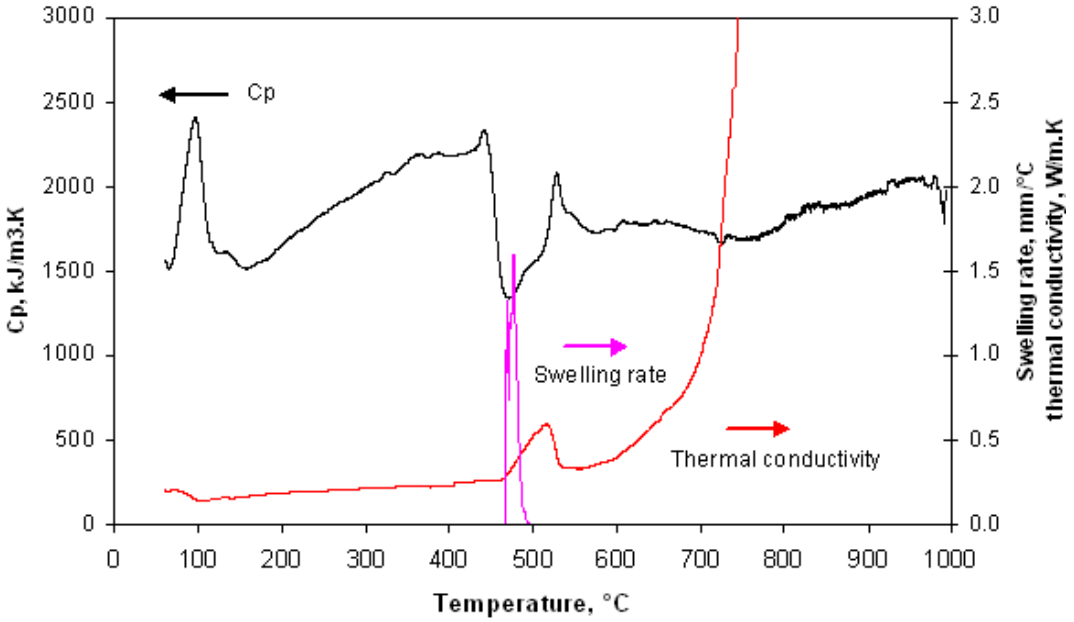

Figure 4.7. Correlations between the apparent specific heat, thermal conductivity and swelling rate with temperature for the coal sample E at a heating rate of 10°C/min from 25 to 1000°C.

4.4.1 Effect of heating rate on swelling and thermal properties

4.4.1.1 Effect of heating rate on swelling

This section examines the effect of heating rate on swelling. To investigate the effect of heating rate on swelling during coke formation, all four coal samples B, C, D and E with a particles size 0-212 μm were subjected to heating at heating rates of 3, 5 and 10°C/min from 25 to 1000°C. The results in Figures 4.8-4.11 clearly show that, at higher heating rate, the initial swelling begins at higher temperatures and swelling during the primary devolatilisation also increases. The reason is that the high heating rate increases the temperature and extent of maximum fusion [91]. The higher heating rate leads to an increase in the heat flow, which causes more coal particles to become plastic for a given time so that a thicker plastic layer is formed [73]. Also, the thermoplasticity of coking coals is controlled by the gas-phase concentration of volatile plasticising material in the vicinity of the coal particles. The fluidity of coal increases by increasing the ambient volatile concentration [91]. The higher the heating rate, the higher the fluidity [91], which implies higher volatile concentrations around the coal particles. Therefore, the thermoplasticity and swelling increase with increasing heating rate.

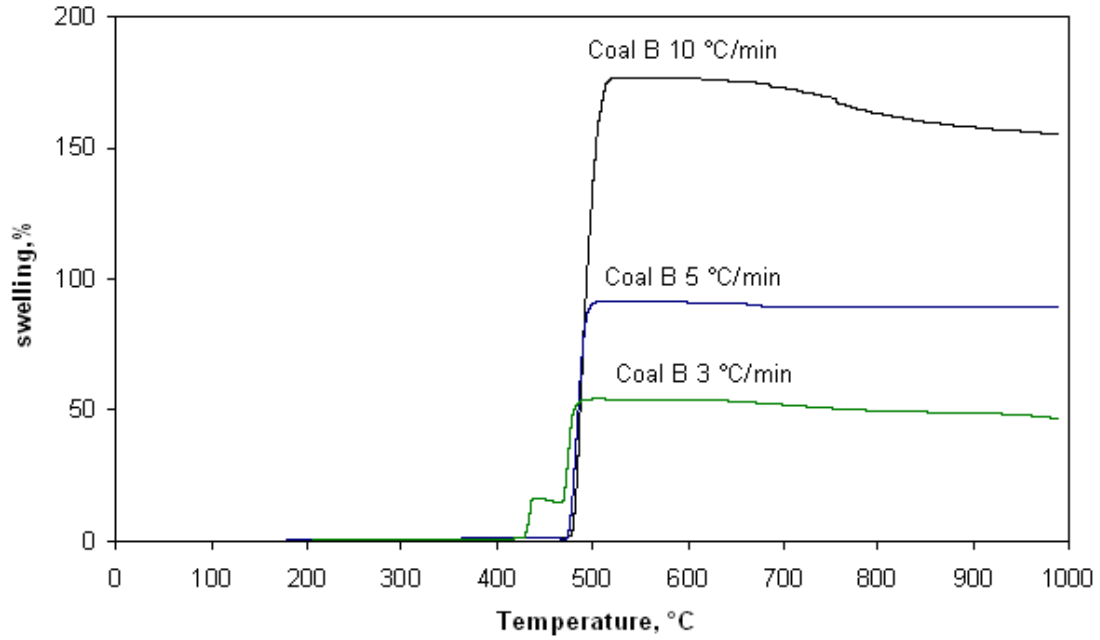

Figure 4.8. Swelling of coal sample B at three different heating rates of 3, 5 and 10°C/min from 25 to 1000°C.

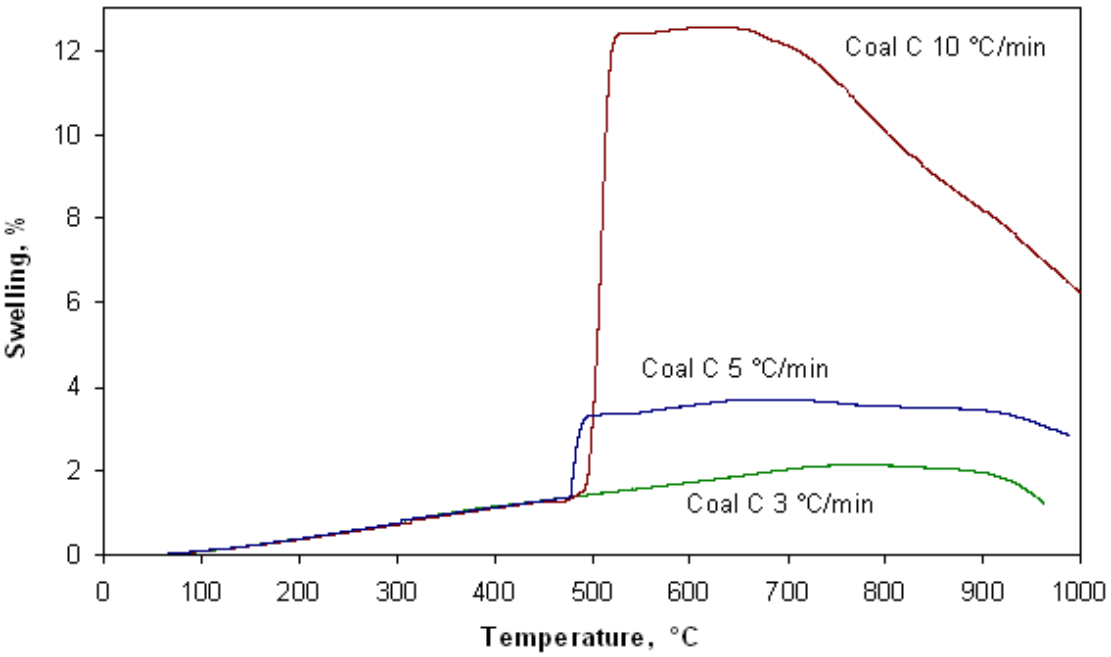

Figure 4.9. Swelling of coal sample C at three different heating rates of 3, 5 and 10°C/min from 25 to 1000°C.

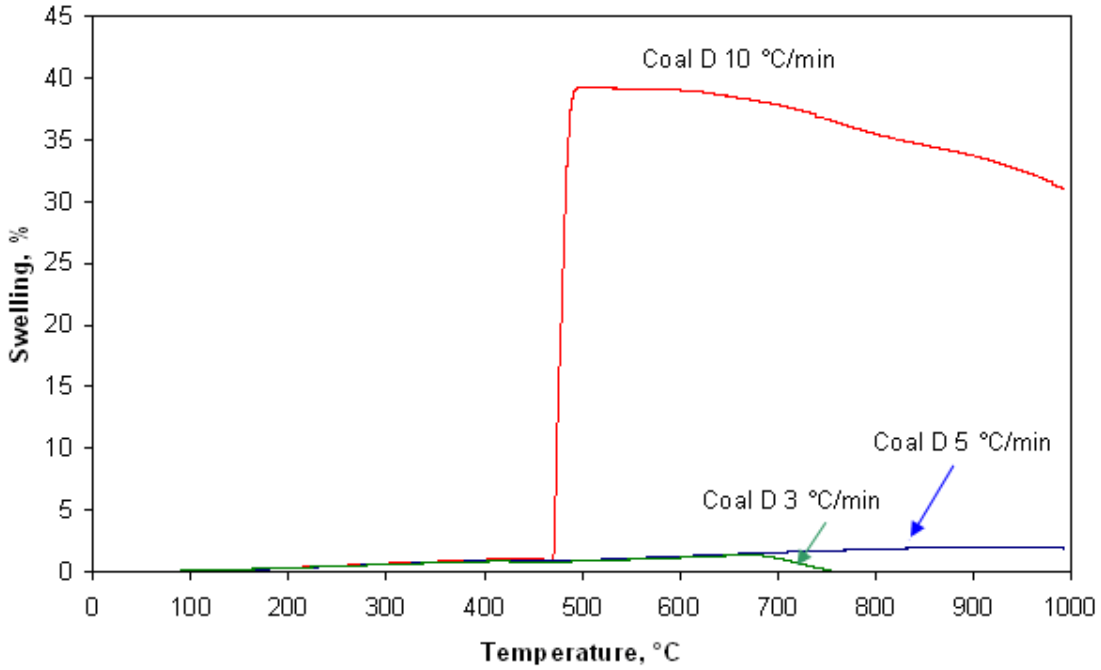

Figure 4.10. Swelling of coal sample D at three different heating rates of 3, 5 and 10°C/min from 25 to 1000°C.

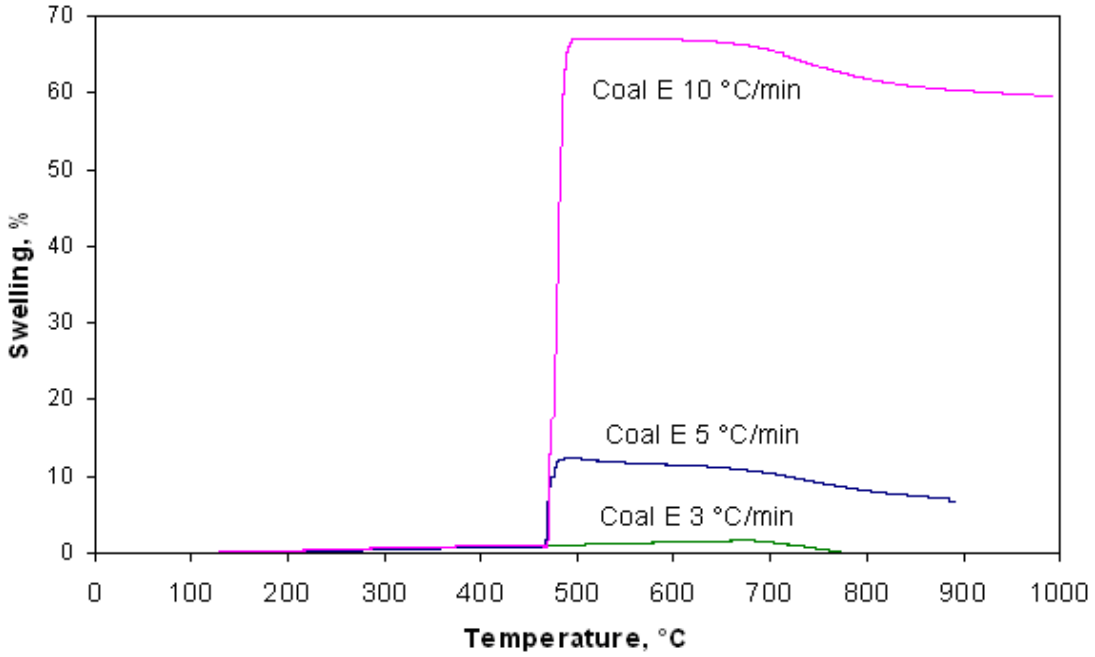

Figure 4.11. Swelling of coal sample E at three different heating rates of 3, 5 and 10°C/min from 25 to 1000°C.

Figures 4.9-4.11 indicate that, for the relatively low swelling coal samples C, D and E at a low heating rate of 3°C/min, the volume change was linear with temperature and occurred over a wide temperature range (from 25-690°C), therefore this "swelling" is considered to be due solely to thermal expansion of materials with temperature, rather than associated with a plastic transition relating to metaplast during coal pyrolysis. Figure 4.8 shows the swelling

characteristics of the relatively high swelling coal sample B at three different heating rates of 3, 5 and 10°C/min. It was found that the swelling at a heating rate of 3°C/min occurred in two stages; a sharp swelling occurred from 430°C to 450°C and again a rapid swelling occurred from 470 to 505°C. However, this phenomenon has not been observed at higher heating rates of 5 and 10°C/min. As swelling of heating coal relates to softening and fusion [3, 36], the two steps swelling at the 3°C/min heating rate can be explained based on the mechanisms of coal devolatilisation suggested by Solomon et al [20]. In the mechanisms, prior to the primary devolatilisation (rapid swelling), the heating coal starts to soften (at 450°C) due to disruption of hydrogen bonds, vaporization and transport of the non-covalently bonded "molecular phase", and low temperature cross-linking in coals with more than 10% oxygen which coincided with H_2O and CO_2 evolution. Therefore, for coal B, it is possible that the heating rates of 5 and 10°C/min may shift the softening to higher temperatures than that at 3°C/min, which causes the softening that occurred prior to the primary devolatilisation to merge with the softening that occurred during the primary devolatilisation, as a result only one swelling stage was observed. Nevertheless, one swelling stage may not be achieved at a low heating rate of 3°C/min because the mergence of the softening prior to the primary devolatilisation and the softening during the primary devolatilisation did not occur.

Figures 4.8-4.11 also present the effects of heating rate on high temperature absolute contraction between 550 and 1000°C for the four coal samples. The results indicate that heating rate had a mild effect on high temperature absolute contraction for coal samples B and E, while it had a significant effect on high temperature absolute contraction for coal samples C and D. The high temperature absolute contraction for coal sample C at the heating rate of 10°C/min was 6.2%, while it was only 0.9% at the heating rate of 3°C/min. There was no distinct contraction for coal samples D and E until 680°C at the low heating rate of 3°C/min, and no contraction was observed for coal sample D up to 900°C at the heating rate of 5°C/min. A possible reason for this is that the high temperature absolute contraction depends on not only the increasing gases and tars evolution rate with heating rate [63, 155], but also the weight percent of coal material converted to the large molecular decomposition products on heating coal to the temperature of resolidification [147].

In addition to the effects of heating rate on instantaneous swelling and contraction of heating coal, the effects of heating rate on the properties of final coke products were also analysed. Figure 4.12 indicates that, for coal sample B, coke produced at a heating rate of 10°C/min has more visible pores than that of a lower heating rate of 3°C/min, which is consistent with earlier reports [156].

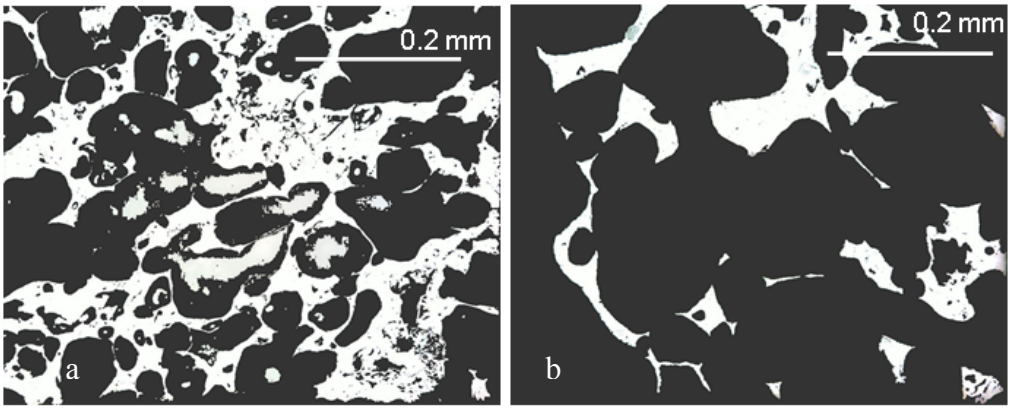

Figure 4.12. Optical microscopy images of cokes obtained from 0-212 µm coal sample B at the heating rate of 3°C/min (a) and 10°C/min (b), both images obtained near the centre of the cross section of the cylinder coke sample.

4.4.1.2 Effect of heating rate on apparent specific heat

This section details the effect of heating rate on the apparent specific heat for all the four coal samples. The results are shown in Figures 4.13-4.16. Peaks of the apparent specific heat at around 110°C related to moisture removal. The apparent specific heat slowly increases with temperature prior to the primary devolatilisation. At this stage, coal samples B, D and E exhibited the same specific heat at about 200°C at three different heating rates and this has not been observed until 350°C for coal sample C. The second peak of the apparent specific heat relating to the primary devolatilisation appears at higher temperature between 420 and 470°C with increasing heating rate. This can be particularly seen for the high swelling coal samples B and E. Exothermic troughs during the primary devolatilisation for all the four samples appear between 400 and 600°C, corresponding to rapid swelling. The maximum exothermic troughs during the primary devolatilisation for all four coal samples were observed at the highest heating rate of 10°C/min, which is consistent with the maximum swelling at the heating rate of 10°C/min. Overall, at higher heating rates, larger exothermic troughs are observed, corresponding with larger swelling. The maximum difference in the apparent specific heat with various heating rates was produced by coal sample C, in which no distinct exothermic trough was observed during the primary devolatilisation at the heating rate of 3°C/min, corresponding to its minimal swelling at this stage.

The third endothermic peak between 500 and 600°C occurs at higher temperatures with increasing heating rates, although there was no distinct endothermic process during this temperature range for coal samples B and C at the heating rate of 3°C/min. During the secondary devolatilisation, for coal samples B, C and D, the apparent specific heat at the lowest heating rate of 3°C/min showed the maximum increase, apart from coal sample E which exhibited the opposite trend. Strezov et al. [63] studied the effect of heating rate (from

10 to 100°C/min) on the apparent specific heat and coal devolatilisation. They found that a lower heating rate corresponds to lower evolution rates of gases and tars during primary devolatilisaton and secondary devolatilisation, which implies a less decrease of apparent specific heat that relating to exothermic reactions. For coal samples B and C, there was no distinct exothermic trough during the secondary devolatilisation from 550 to 1000°C at the heating rate of 3°C/min. This is because above 700°C it is difficult to calculate the apparent specific heat based on the heat conduction equation because the centre of the bed becomes hotter than the outside of the bed, which causes an inversion in temperatures between the surface and centre of the sample at low heating rates. This thermal inversion may be attributed to the low heating rate which generally means there is very little difference between the wall and the centre temperatures of the bed, exothermic reactions which provide extra heat to the bed, and the actually low thermal conductivity of the char which limits the heat loss from the centre of the bed. For samples B and D, higher heating rates of 5 and 10°C/min produced similar results for the exothermic troughs during the secondary devolatilisation. However, for coal sample E, the exothermic trough extended from 735°C at 3°C/min, 760°C at 5°C/min, to 780°C at 10°C /min. The bed temperature is the mean temperature estimated during calculating apparent specific heat based on the control temperature and measured surface and centre temperatures of sample (section 3.1.2.2). The same displacement of the secondary exothermic troughs with heating rate was also observed by Strezov et al. [63] and they considered that this change related to the evolution of hydrogen.

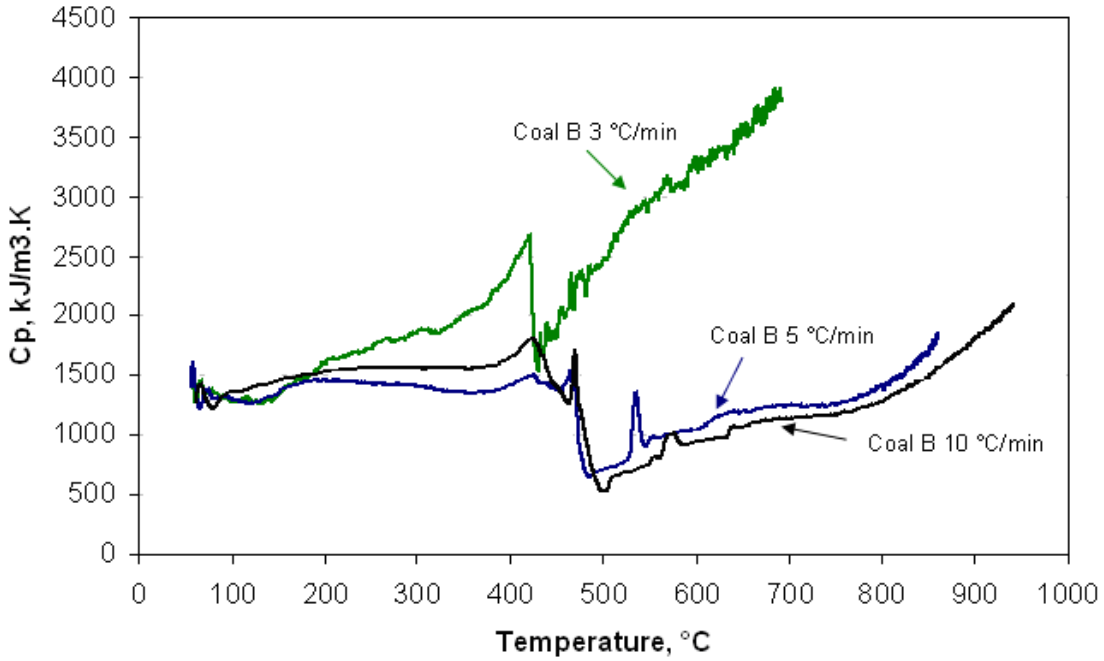

Figure 4.13. Apparent specific heat of coal sample B at three different heating rates of 3, 5 and 10°C/min from 25 to 1000°C.

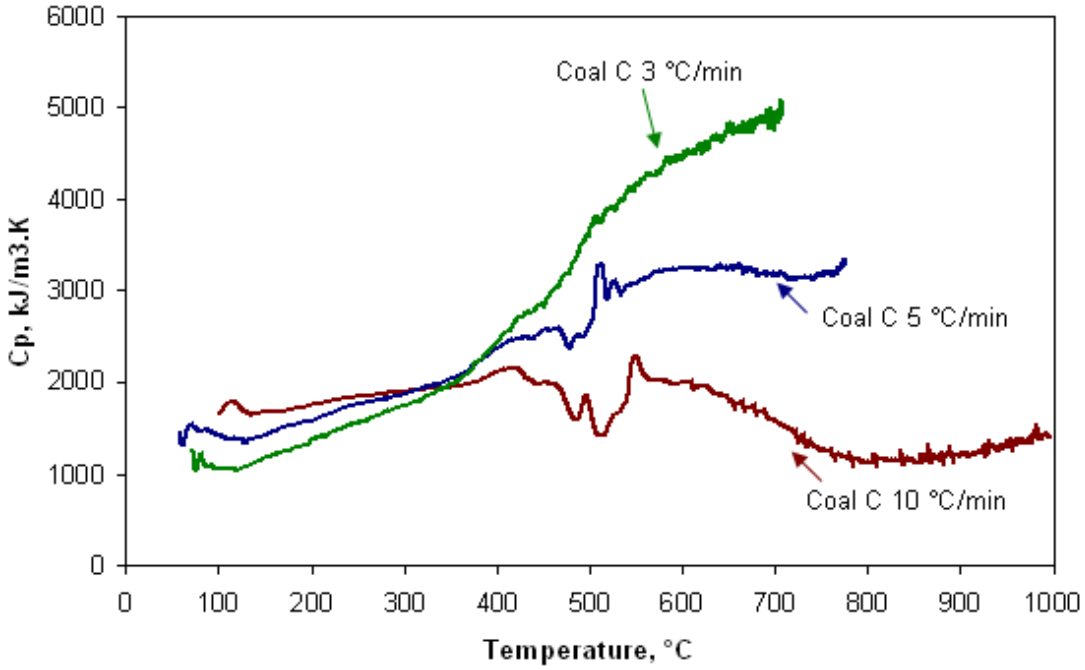

Figure 4.14. Apparent specific heat of coal sample C at three different heating rates of 3, 5 and 10°C/min from 25 to 1000 °C.

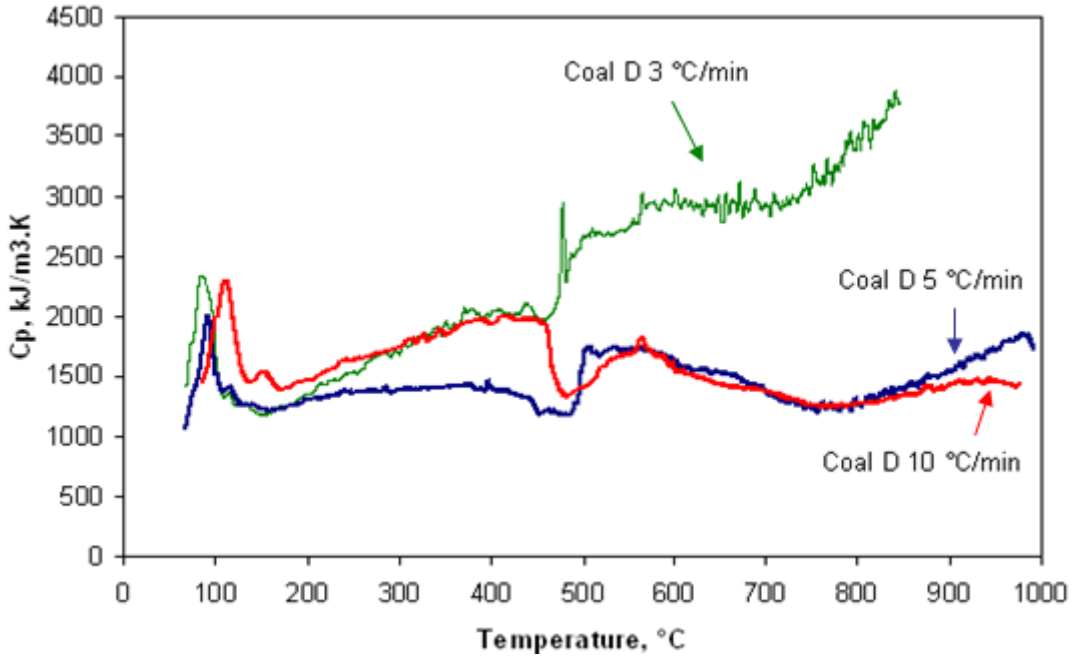

Figure 4.15. Apparent specific heat of coal sample D at three different heating rates of 3, 5 and 10°C/min from 25 to 1000°C.

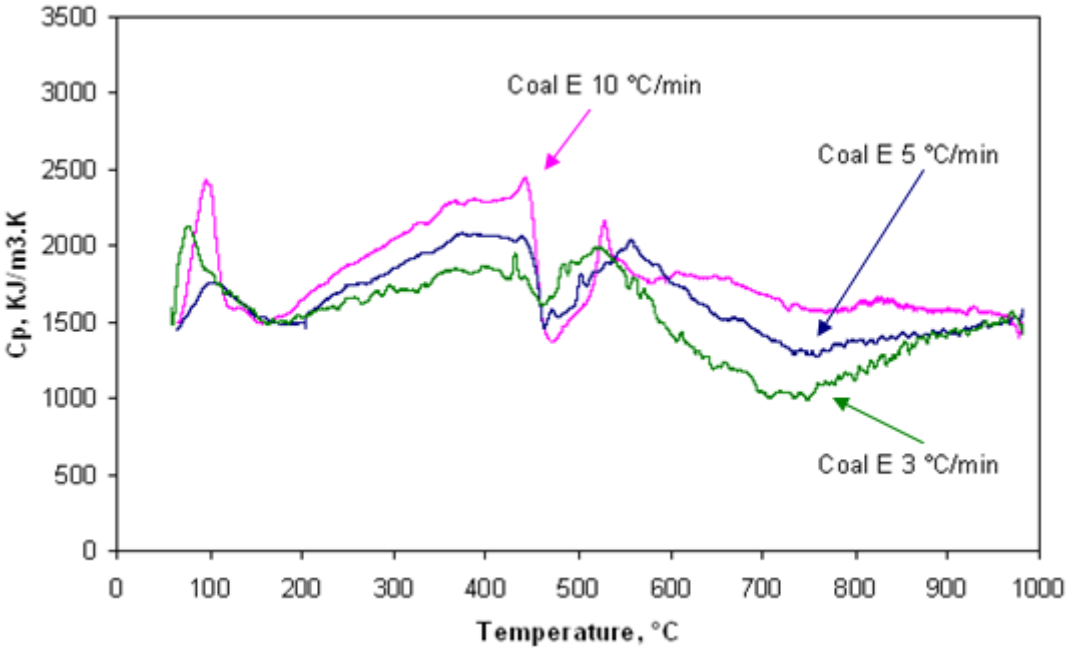

Figure 4.16. Apparent specific heat of coal sample E at three different heating rates of 3, 5 and 10°C/min from 25 to 1000°C.

4.4.1.3 Effect of heating rate on thermal conductivity

This section explains the effects of heating rate on thermal conductivity of the four coals samples. The results are shown in Figures 4.17-4.20. For all three different heating rates, the estimated thermal conductivities of all four coal samples were almost the same and did not changed until the temperature reached the primary devolatilisation. Combining the results from coal samples B, C and E, it can be observed that during the primary devolatilisation the peak thermal conductivity at the heating rate of 10°C/min is higher than that of 5°C/min. The higher thermal conductivity is consistent with the larger exothermic trough and swelling. However, for coal sample D, the maximum thermal conductivity was observed at the heating rate of 3°C/min rather than 10°C/min. The reasons for this are still unknown.

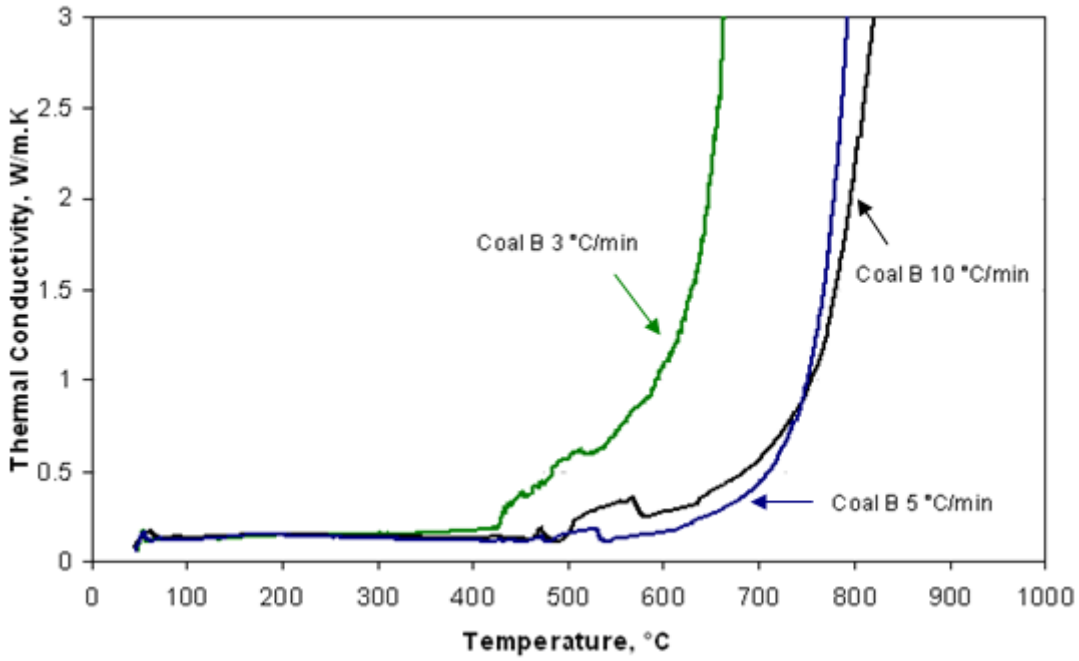

Figure 4.17. Thermal conductivities of coal sample B at three different heating rates of 3, 5 and 10°C/min from 25 to 1000°C.

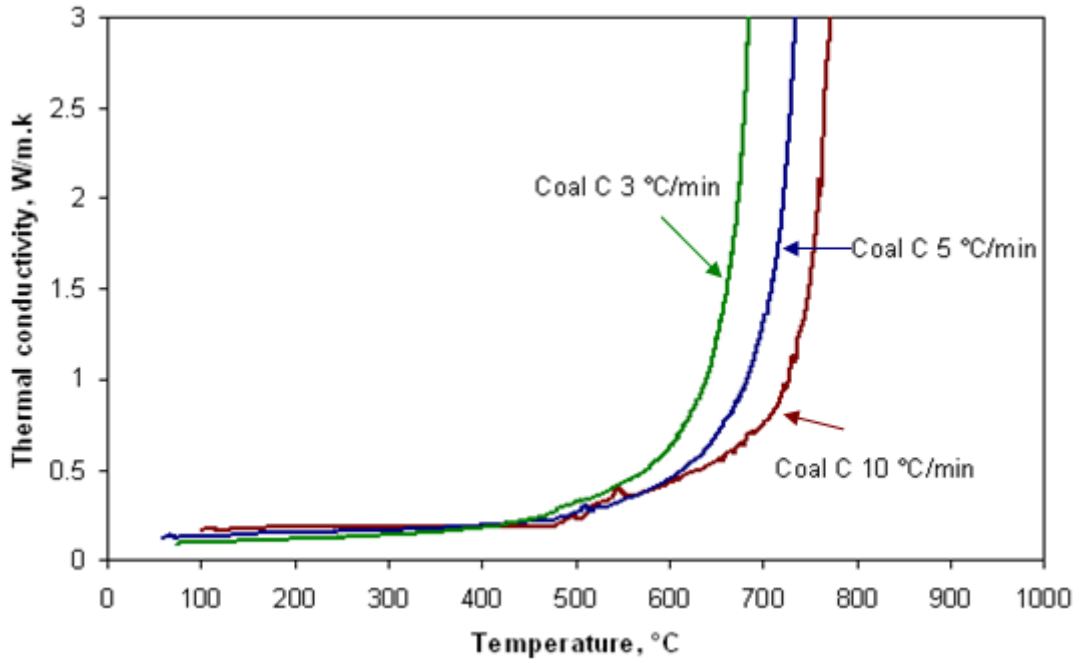

Figure 4.18. Thermal conductivities of coal sample C at three different heating rates of 3, 5 and 10°C/min from 25 to 1000°C.

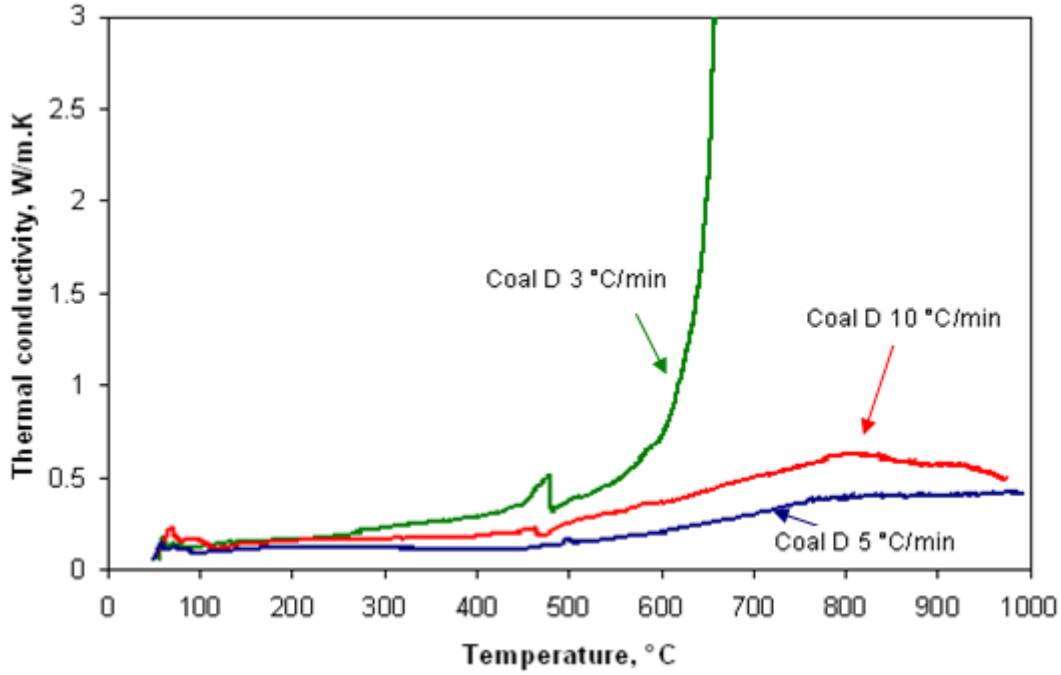

Figure 4.19. Thermal conductivities of coal sample D at three different heating rates of 3, 5 and 10°C/min from 25 to 1000°C.

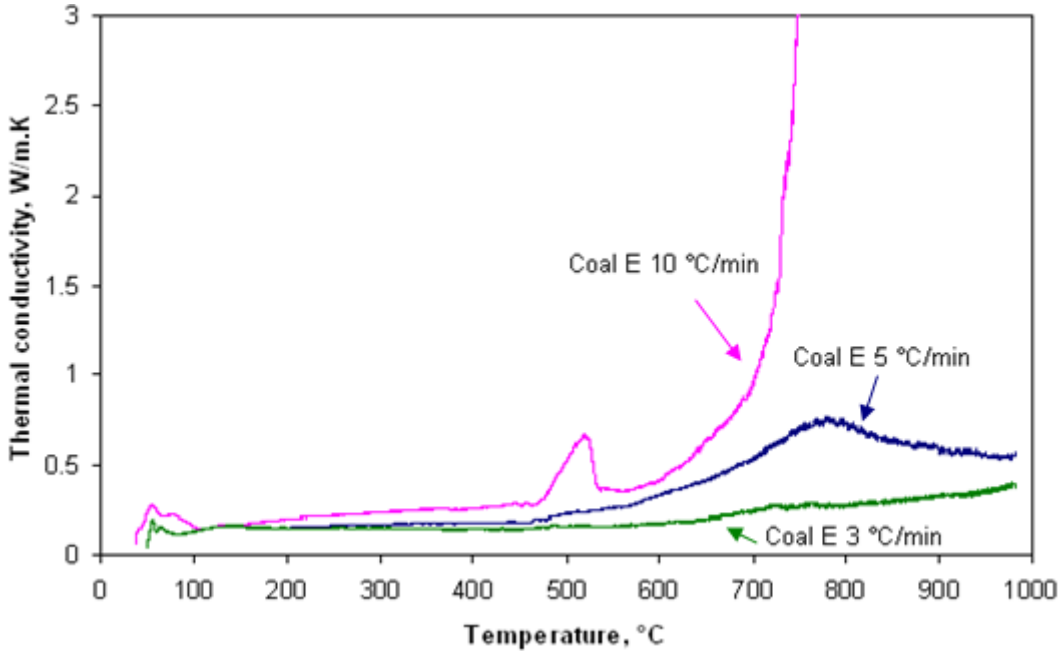

Figure 4.20. Thermal conductivities of coal sample E at three different heating rates of 3, 5 and 10°C/min from 25 to 1000°C.

4.4.2 Effect of particle size on swelling and thermal properties

4.4.2.1 Effect of particle size on swelling

The effects of particle size on swelling, apparent specific heat and thermal conductivity were studied on the basis of coal sample C at a heating rate of 10°C/min. Two particle size ranges of 0-212 μm and 0-500 μm of coal sample C were employed in the experiments. Figure 4.21

shows that the onset of the temperatures for swelling were 471°C for the 0-500 µm particle size sample and 481°C for the 0-212 µm particle size sample, respectively. However, the maximum swelling for the two different particle size samples both appeared at 512°C, which indicated that the large particle size sample has a wider temperature range for swelling. This is consistent with the previous observation by Habermehl et al [73], namely the sample with a large particle size has a wider temperature range for plasticity in comparison with the sample with a small particle size. The maximum swelling at 512°C for the large particle size sample was 74.4% compared to 11.8% for the small particle size sample. A possible explanation for this is due to the higher volume to surface area ration for larger particles, which favors the coalescent of coal particles and restricts the release of volatiles. High temperature absolute contraction, between 550 and 1000°C, was 9.24% for the large particle size sample but 5.94% for the small particle size sample.

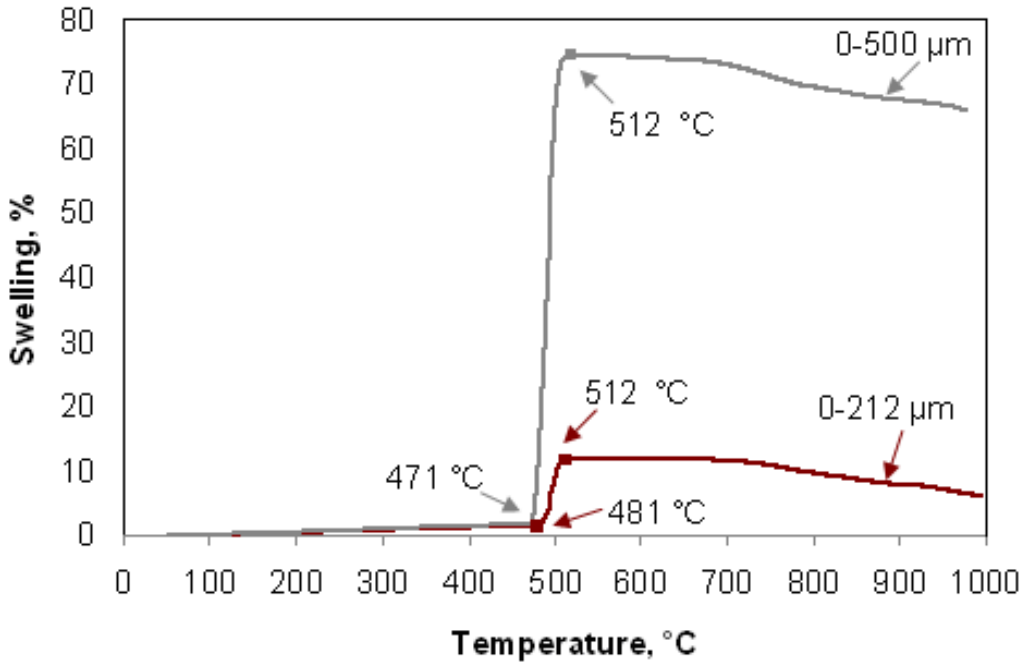

Figure 4.21. Effect of particles size on swelling for coal sample C at a heating rate of 10°C/min from 25 to 1000°C.

Combining the swelling and contraction from 25 to 1000°C, the final volume of coke obtained from the large particle size coal was larger than coke volume produced by the small particle size coal. Optical microscopy analyses of final cokes obtained from two samples with different particle sizes are shown in Figure 4.22 (a) and (b), where it can be seen that the final coke formed from the large particle size coal sample is more porous, with larger pore diameters than the coke formed from the small particle size coal sample. The pores in the centre for both the samples are much larger than that at the surrounding, which is attributed to the thermal gradient across the sample from the surface to the centre [127], and gas and tar

migration which relates to the pore coalescence [19, 88-90]. During pyrolysis, the surrounding particles were heated first, with gases bubble formed. Part of the gases was directly capable of escaping from the packed sample cylinder, while part of them contributed to bubble coalescence. With increasing temperature, more gases and tars were produced in the centre of the packed cylinder; however, it is more difficult for these gases and tars to escape from the centre comparing to the gases and tars from the exernal layer of the packed sample cylinder due to the increasing viscosity of the metaplast. Also, the pressure gradient from the centre to the surface of the sample cylinder affects the escape of gases and tars so that it affects the pore coalescence.

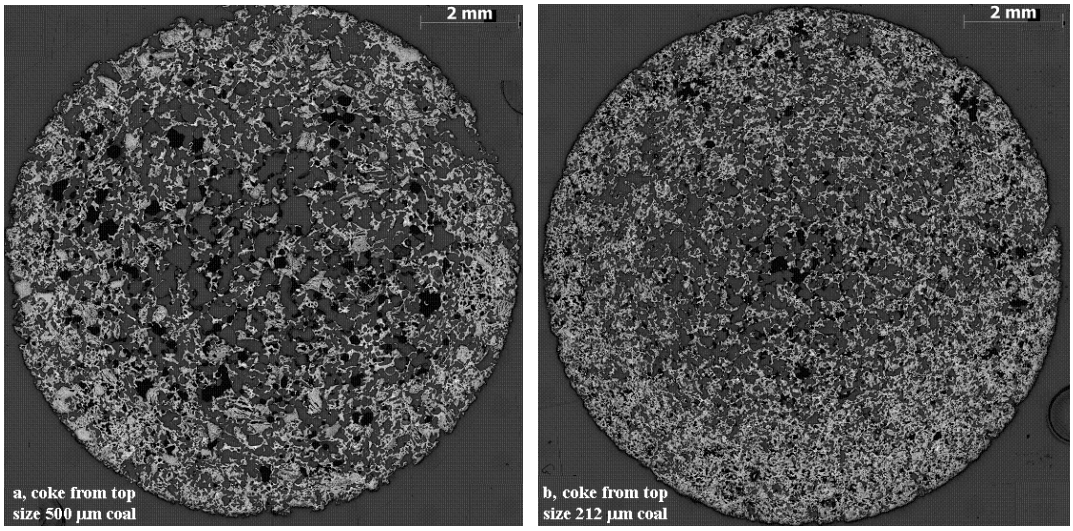

Figure 4.22. Overview of optical microscopy images of cokes formed from coal sample C at a heating rate of 10°C/min from 25 to 1000°C; (a) coke formed from 0-500 μm particle size coal, (b) coke formed from 0-212 μm particle size coal.

4.4.2.2 Effect of particle size on apparent specific heat

Figure 4.23 indicates the effect of particle size on the apparent specific heat of heating coal. Prior to the primary devolatilisation, for the two different particle size samples, the curves for the apparent specific heat are almost overlapped, apart from the endothermic peaks at around 110°C due to the removal of moisture. The samples were stored in the fringe; they sucked moisture at room temperature during preparing experiments. The small particles have larger areas than the large particles so that they sucked more moisture, showing a larger peak around 110°C. During the primary devolatilisation, the apparent specific heats of the two samples differ. For the small particle size sample, the temperature for the onset of the decrease in apparent specific heat was higher, which is consistent with the higher temperature for the onset of swelling. However, both samples, with different particle sizes, produced the same temperature (550°C) for the endothermic peak that relates to the secondary exothermic

reaction. These are consistent with the same properties that the two samples have the same temperatures for the completion of swelling (at 512°C). Also, the large particle size sample produced a larger exothermic trough during the primary devolatilisation than the small particle size sample, corresponding to a greater extent of swelling. However, the small particle size sample produced a larger exothermic trough between 600 and 1000°C. Strezov et al [63] reported the a large exothermic trough between 600 and 1000°C corresponds to a large secondary devolatilisation. Seebauer et al [66] also reported that small particle size samples showed a higher extent of secondary reaction than large particle size samples.

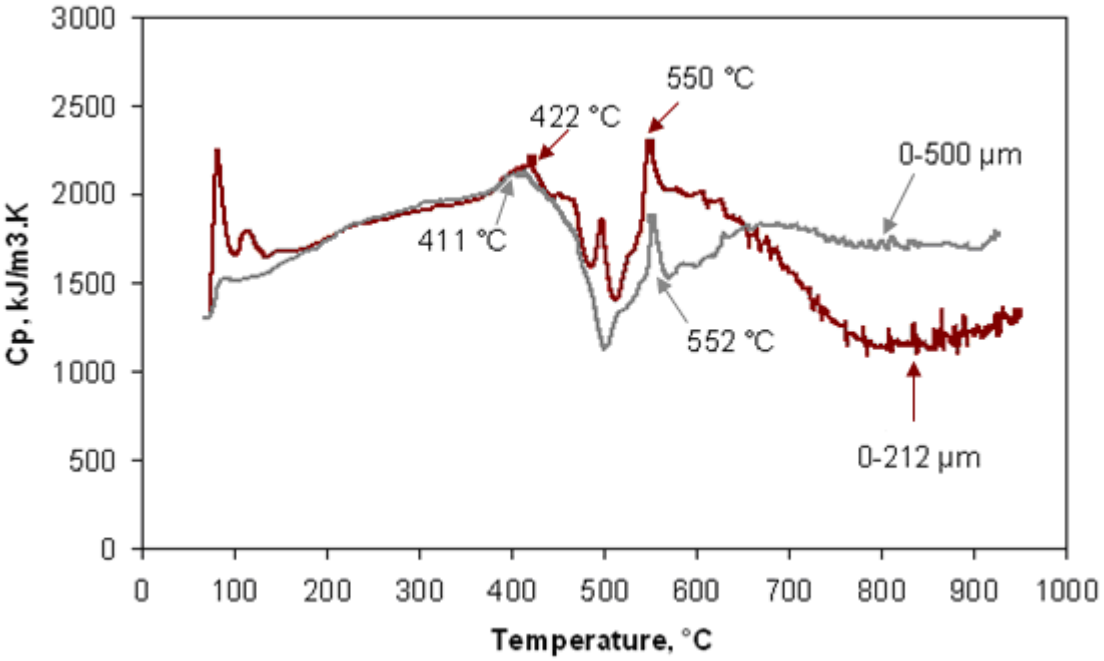

Figure 4.23. Effect of particles size on the apparent specific heat for coal sample C at a heating rate of 10°C/min from 25 to 1000°C.

4.4.2.3 Effect of particle size on thermal conductivity

Fig 4.24 presents the effect of particle size on thermal conductivity of heating coal. The thermal conductivities of the two different particle size samples begin to increase at around 480°C, corresponding to the initial swelling temperature. A slight decrease of the thermal conductivity occurred at the end of the primary devolatilisation. The extent of this decrease was larger for the sample with the larger particle size, which may be due to the larger swelling of this sample, which increases the pores of the semi-coke obtained from this sample. Above 600°C, the thermal conductivities of both samples rapidly increase, the reasons for which have been discussed in section 4.3.2.

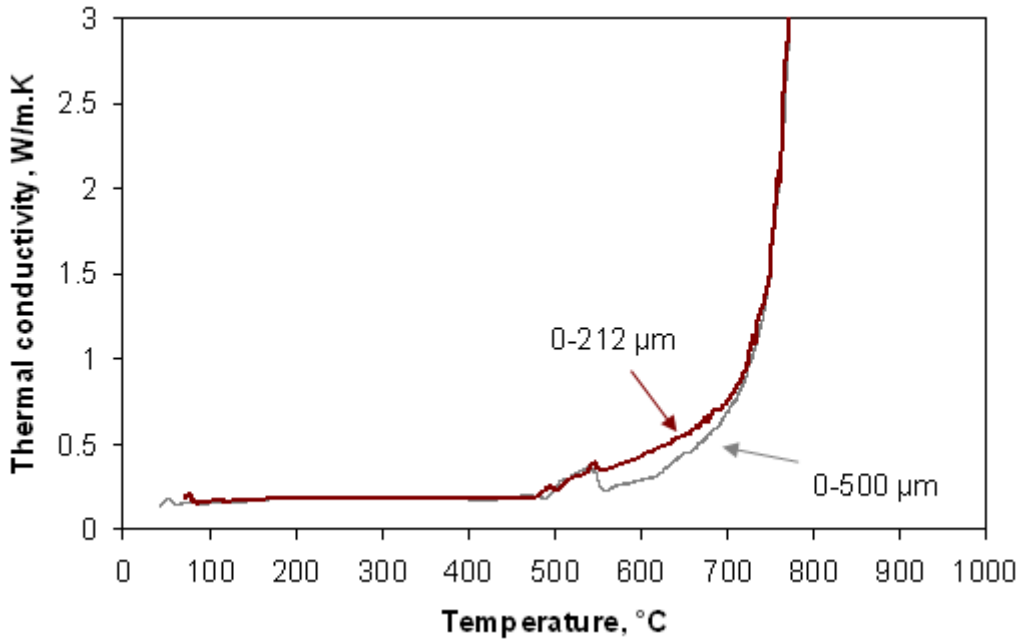

Figure 4.24. Effect of particles size on the thermal conductivity for coal sample C at a heating rate of 10°C/min from 25 to 1000°C.

4.5 Conclusions

Experiments on four coal samples have been employed to explore the relationship between swelling, apparent specific heat and thermal conductivity of heating coal. Effects of heating rate and particles size on swelling and apparent specific heat and thermal conductivity during coke formation were also simultaneously studied. The following conclusions were drawn based on the experimental results:

- Prior to rapid swelling, the heating coal samples underwent an endothermic reaction in the temperature range between 380 and 420°C. Rapid swelling occurred during the primary exothermic reaction between 420 and 580°C accompanied by an increase of thermal conductivity. The increase of thermal conductivity during the rapid swelling related to the increase of fluidity of the plastic phase. Swelling was complete at the onset of the secondary endothermic reaction between 550 and 600°C accompanied by a slight decrease in thermal conductivity. Above 600°C, during the secondary exothermic reaction, the semi-coke started to shrink accompanied by a rapid increase of thermal conductivity.

- Heating rate can affect thermal-swelling of heating coal, between 400 and 550°C, a high heating rate can shift the onsets of the initial exothermic reactions and swelling to higher temperatures, leading to a higher swelling, a higher thermal conductivity and a larger exothermic reaction trough. Between 550 and 1000°C, the initial

temperatures for the onsets of endothermic (550-600°C) and exothermic (600-1000°C) reactions and the rapid rise of thermal conductivity (600-1000°C) also increased with increasing heating rate.

- Between 400 and 550°C, the large particle size sample showed a wider temperature range for swelling and the primary exothermic reaction. The swelling and primary exothermic trough increased with increasing particle size. Between 550 and 1000°C, the small particle size sample produced a larger exothermic trough than the large particle size sample.

Chapter 5 Coal macerals separation, swelling and thermal properties of separated coal maceral concentrates

5.1 Introduction

Coal maceral components consist of mainly liptinite, vitrinite and inertinite [27]. Using the novel CATA, the previous Chapter concluded that swelling, contraction, endothermic and exothermic reactions (identified by the apparent specific heat) and thermal conductivity of heating coal relate to the vitrinite content. Therefore, the understanding in swelling and thermal behaviour of vitrinite rich concentrate and inertinite rich concentrate is an essential step towards investigating the mechanisms in the transformation of coal to coke. However, the fundamental understanding in the nature of swelling, endothermic and exothermic reactions and thermal conductivity for individual maceral concentrate has not yet been achieved.

This Chapter focuses on the swelling and thermal behaviour of a suite of coal maceral concentrates separated from the same parent coal for the purpose of determining the link between the physical and thermal changes. Blends were also studied to reveal the potential interactions of different coal maceral components. A mild swelling coal sample C with a particle size of 0-212 μm was selected for coal maceral separation. All experiments for coal maceral separation were conducted on the reflux classifier. Details for the reflux classifier were presented in Chapter 3. The principle for this separation is based on the different settling rate of various coal maceral concentrates on the inclined plates with a controlled water flow rate. With the upflow of water in the reflux classifier, light coal particles were separated at a low water flow rate, while heavier coal particles were separated at a higher water flow rate. As the vitrinite has a lower density than the inertinite [27], the separated coal particles was vitrinite rich concentrates at relatively low water flow rates and inertinite rich concentrates at relatively high water flow rates. A nylon bag with a mesh size of 22 μm was used at the outlet of the reflux classifier to collect the separated coal particles. Therefore, the collected coal maceral concentrates have a particle size range between +22 and -212 μm. Separated coal maceral concentrates with increasing water flow rate were named a, b, c, d, e and f. Swelling, contraction, endothermic and exothermic reactions and thermal conductivity of heating coal maceral concentrates were evaluated using the novel CATA technique.

5.2 Petrography, particles size, ash and density analysis of coal maceral concentrates

This section presents the petrography, particle size, ash and density analysis of separated coal maceral concentrates. Techniques for conducting the above analysis were presented in Chapter 3. Table 5.1 shows the results of petrography, ash and relative density analysis for all separated coal maceral concentrates. The parent coal sample C has a vitrinite content of 52.4% (mmf). Vitrinite percentages for the separated coal maceral concentrates of a-f vary from a maximum of 81.6% to a minimum of 29.0% with increasing water flow rate. Under low water flow rates, vitrinite rich samples a, b, c and d have similar vitrinite proportions and similar ash contents. Laser sizing of each coal maceral concentrate revealed a successive size classification with increasing water flow rate, as seen in Figure 5.1. The volume weighted mean diameter of particles for these separated coal maceral concentrates is also shown in Table 5.1. With increasing water flow rate, inertinite content in the separated coal maceral concentrates increases dramatically, ash content and relative density also correspondingly increase. This indicates that the separation of inertinite rich concentrates is attributed to a combination of three factors, namely inertinite content, ash content and mean particle size.

Table 5.1. Properties analysis of the parent coal C and separated coal macerals concentrates.

Maceral name	Water flow L/min	Vitrinite % (mmf)	Inertinite % (mmf)	D^{α} [4,3] μm	Density g/ml	Ash %	Maximum Swelling$^{\beta}$ %	Absolute contraction$^{\beta}$ %
a	1.150	78.0	22.0	40.6	1.30	2.83	20.8	5.4
b	1.725	81.8	18.2	40.7	1.27	2.53	40.7	8.7
c	2.300	79.0	21.0	47.1	1.29	2.78	25.3	4.3
d	2.875	81.6	18.4	70.7	1.31	2.80	40.7	2.7
e	3.450	64.0	36.0	92.5	1.34	4.40	3.9	2.7
f	4.025	29.0	71.0	131.5	1.38	10.40	1.9$^{\gamma}$	2.4
---	(Parent coal)	52.4	47.6	69.6	---	6.90	11.8	6.0

α Volume weighted mean diameter.

β Swelling/contraction % of packed bed length.

γ Due to thermal expansion, rather than swelling.

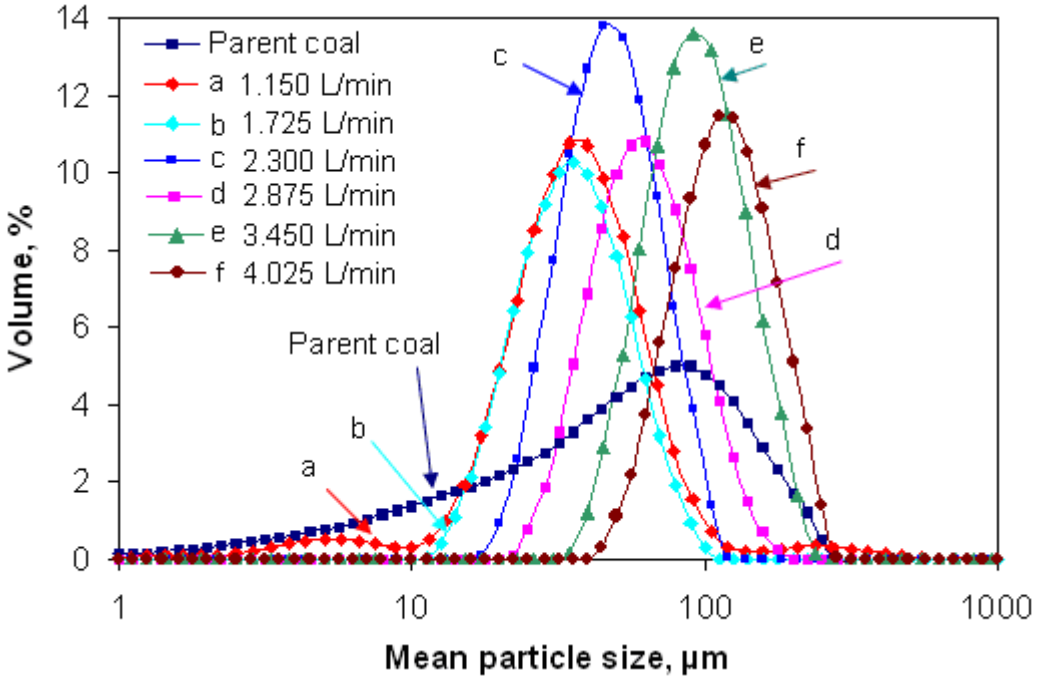

Figure 5.1. Mean particle size analysis of the parent coal C and separated coal maceral concentrates.

5.3 Swelling and thermal properties of separated coal maceral concentrates

The swelling and thermal properties of the parent coal and various coal maceral concentrates are presented in this section. Results for swelling are shown in Figure 5.2. Maximum swelling and high temperature absolute contraction are summarised in Table 5.1. All samples exhibited a gradual increase in volume due to thermal expansion, however only the highest inertinite concentrate (f) showed no swelling behaviour. The parent coal showed a swelling of 11.8% at around 500°C. The inertinite richest concentrate with a vitrinite percentage in 29.0% swelled only 1.9% at about 650°C. Because the inertinite rich concentrate volume change is linear with temperature and occurs over a wide temperature range (from 25-650°C), this "swelling" is considered to be due solely to thermal expansion, rather than be associated with a plastic transition. By comparison, the two vitrinite richest coal maceral concentrates (with vitrinite proportions at 81.8% and 81.6%, respectively) both swelled 40.7% at almost the same temperature as the parent coal. Of particular note is that these high vitrinite concentrates both produced the same swelling extent despite having a different particle size distribution. A general trend is for higher swelling behaviour with increasing vitrinite content of coal maceral cocnentrates, however, this relationship non-linear in nature.

For all coal maceral concentrates and parent coal, high temperature absolute contraction began between 600 and 700°C and continued beyond 1000°C. A general trend is for higher

absolute contraction behaviour with increasing vitrinite content, however, this relationship non-linear in nature, as shown in Figure 5.2 and Table 5.1. Of the two vitrinite richest concentrates, sample b (81.8% vitrinite) showed a greater absolute contraction than sample d (81.6% vitrinite) for the same swelling extent. This is significant in that the difference between b and d samples is a shift in particle size distribution, which would not intuitively be considered a factor once the material has plastically deformed. Chapter 4 concluded that small particles have a higher extent of the secondary reaction than large particles. It also has been validated in literature that small particles have a higher extent of the secondary devolatilisation than large particles [66], and the secondary exothermic reactions at high temperature are associated with coke graphitisation and contraction during dehydrogenation [19]. However, there is no literature found that only a very small change in vitrinite percentage could cause distinct effects on high temperature contraction and one possible explanation may be that the difference is caused by inertinite particles rather than vitrinite particles.

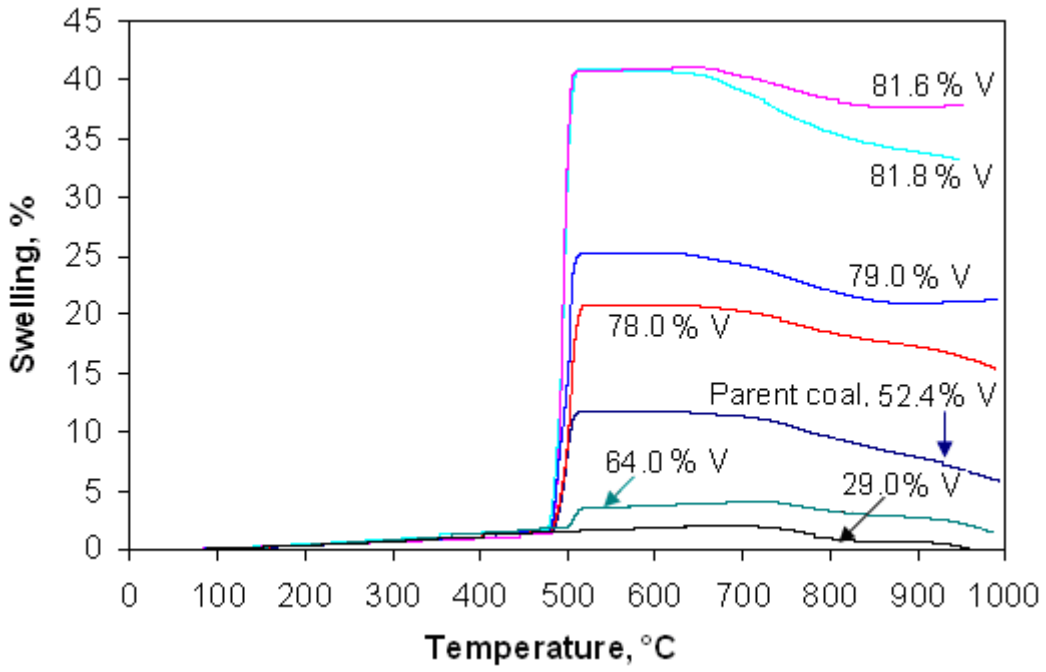

Figure 5.2. Swelling behaviour of coal sample C and coal maceral concentrates separated from parent coal sample C at a heating rate of 10°C/min from 25 to 1000°C.

Comparing the changes in the apparent specific heat between the parent coal and separated coal maceral concentrates in Figure 5.3 (a) and (b), all pyrolysis experimental results showed an endothermic peak at about 100°C due to the removal of moisture, as well as an exothermic trough at around 750-800°C. The exothermic region associated with primary devolatilisation (between 400 and 600°C) appears to contain smaller endothermic peaks at around 500°C and 550°C. This exothermic region is significant for the high vitrinite concentrates (78.0-81.6%

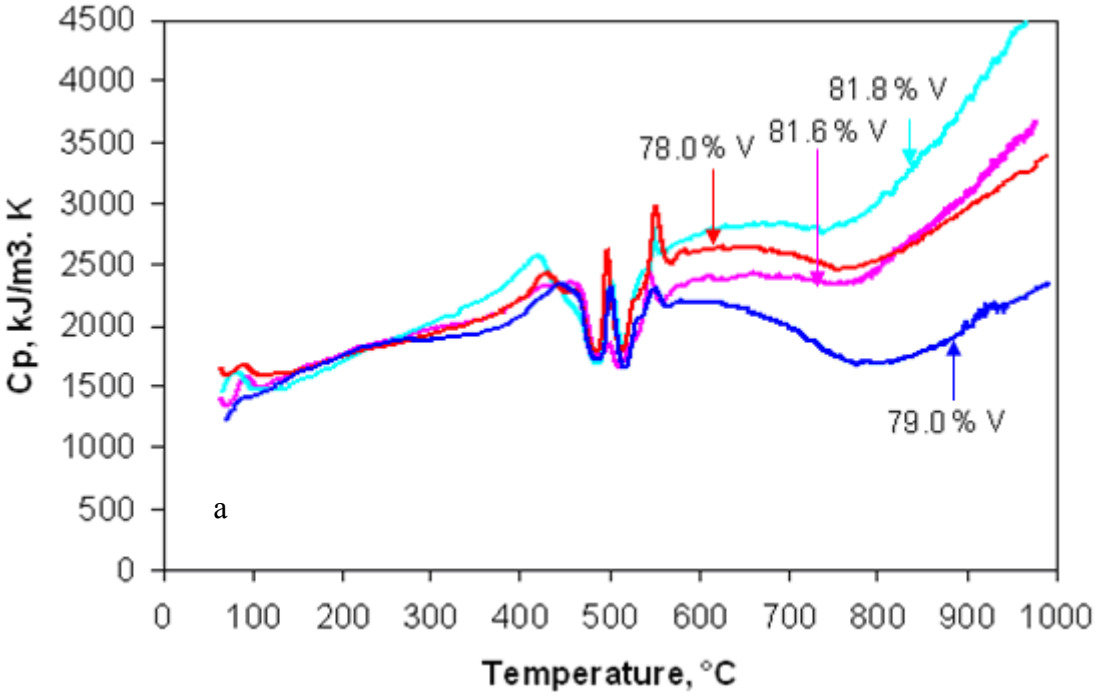

Figure 5.3 (a). Apparent specific heat of four vitrinite rich concentrates separated from the parent coal sample C at a heating rate of 10°C/min from 25 to 1000°C.

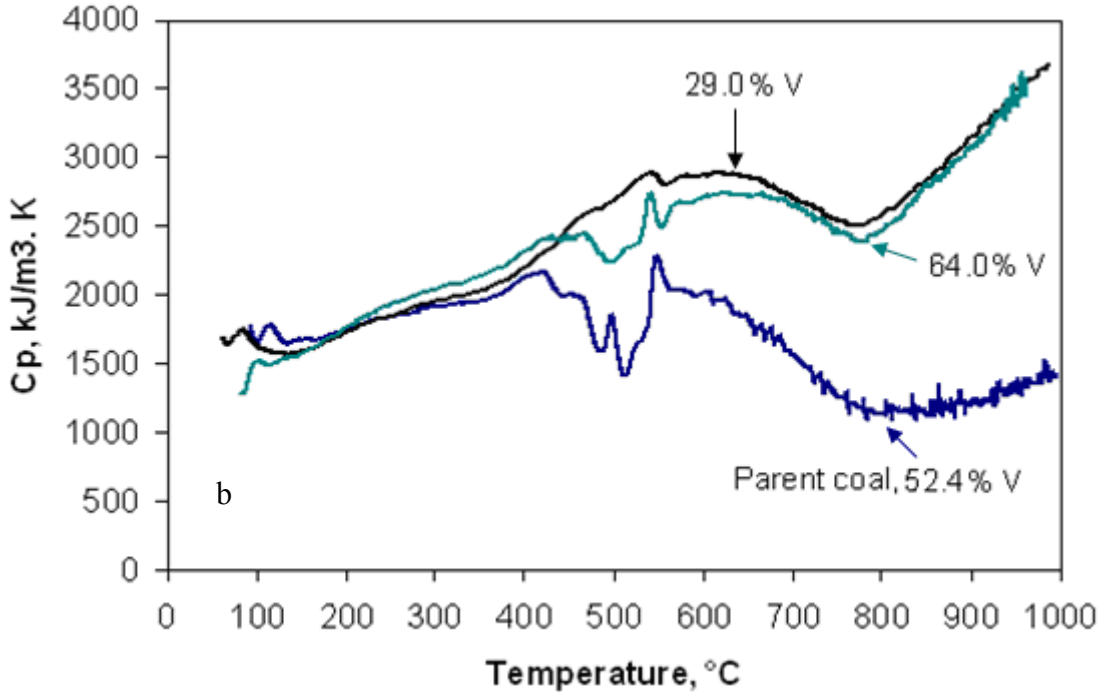

Figure 5.3 (b). Apparent specific heat of the parent coal C and two inertinite rich concentrates separated from the parent coal C at a heating rate of 10°C/min from 25 to 1000°C.

vitrinite) and parent coal, but is reduced in the 64.0% vitrinite sample and removed in the low vitrinite (29.0% vitrinite) sample. Within the coal maceral concentrates it is clear that the exothermic trough is related to vitrinite content, but the parent coal result suggests that the

significant amount of fine material may also have an impact, as with the swelling results. The endothermic peaks within this region do not occur for all coal maceral concentrates, but are prevalent in the 78.0, 79.0, 81.6 and 81.8% vitrinite samples. One observation is that for these vitrinite rich concentrates the endothermic peak within the exothermic trough occurs at the same temperature (500°C) as the maximum swelling, suggesting a link between the two events. However, there is insufficient data to draw further conclusions. At higher temperatures the exothermic trough (750-800°C) occurs at the same temperature as the maximum contraction rate, indicating a common mechanism across coal maceral concentrates and parent coal.

Apparent thermal conductivity was also derived from the numerical solution using CATA technique based on the control temperature and measured surface and centre temperatures of sample. The results for the apparent thermal conductivity are given in Figure 5.4 (a) and (b), corresponding to the high and low vitrinite concentrates, respectively. A distinct rise in thermal conductivity was observed from 475-550°C during the primary devolatilisation. The extent of this rise corresponds to similar trends observed in exothermic activity and swelling. Previous work has shown that the increase of the thermal conductivity may be associated with the development of fluidity of meta-plastic material; the higher fluidity, the larger thermal conductivity [19]. By comparison, inertinite rich concentrates which show a low extent of swelling and little to no exothermic reaction during the primary devolatilisation and correspondingly, do not show any peak in thermal conductivity, as shown in Figure 5.4(b). Prior to this increase, thermal conductivity showed an almost constant value around 0.16-0.18 W/m·K. A rapid increase in thermal conductivity above 600°C was observed which could be associated with other effects that were discussed in Chapter 4. They include:

(a) radiant heat transfer across pores and cracks;

(b) changes in the thermal conductivity of the coals due to pyrolysis;

(c) changes in the intrinsic conductivity with temperature of char [20, 85];

(d) a numerical artefact (the estimated thermal conductivity does not represent the real thermal conductivity) associated with heat build-up in the packed bed. When thermal conductivity reached 2-3 W/m·K and beyond, the difference between measured surface and centre meta-plastic material temperatures was in a very narrow range or thermal inversion between surface and centre of heating sample occurred, hence results became unstable [19].

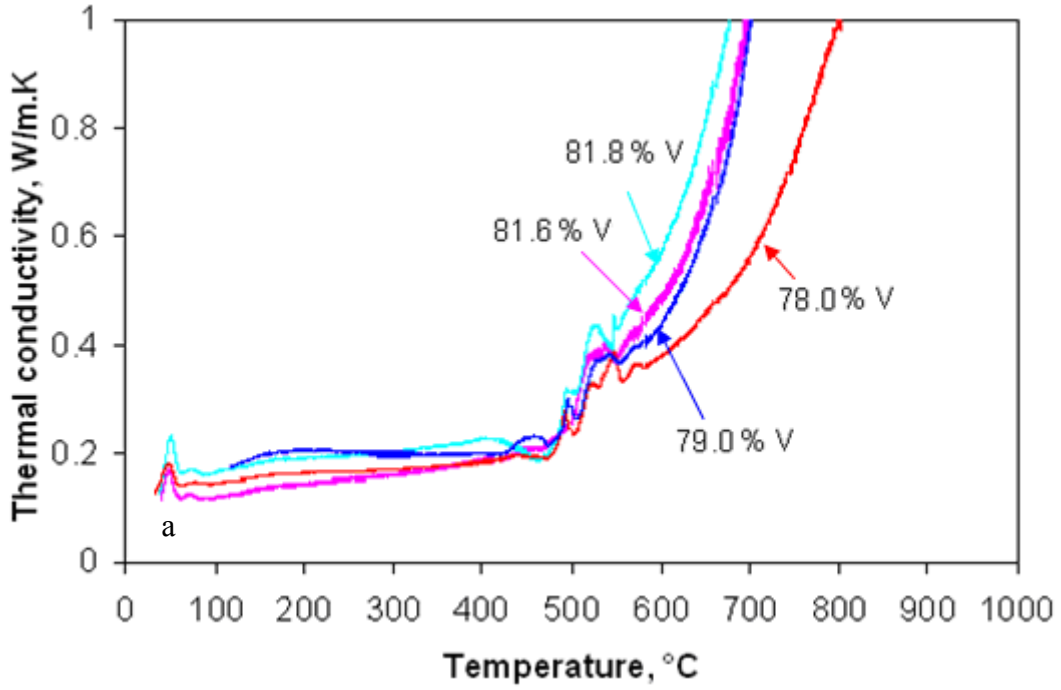

Figure 5.4 (a). Thermal conductivity of four vitrinite rich concentrates separated from the parent coal C at a heating rate of 10°C/min from 25 to 1000°C.

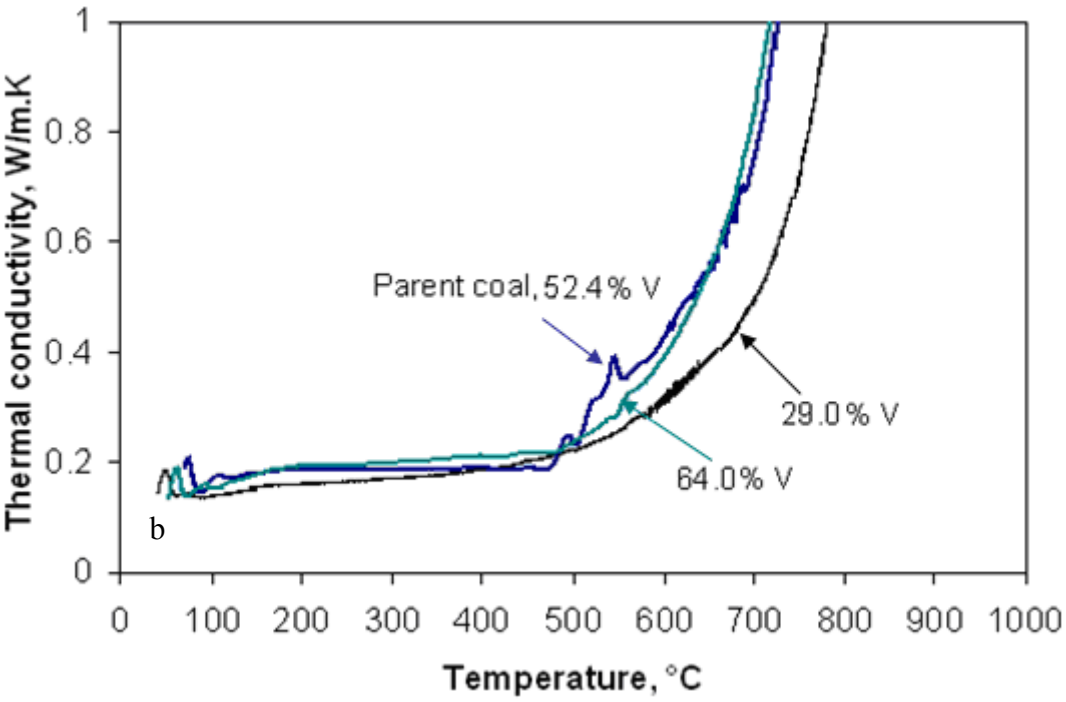

Figure 5.4 (b). Thermal conductivity of the parent coal C and two inertinite rich concentrates separated from the parent coal C at a heating rate of 10°C/min from 25 to 1000°C.

5.4 Interaction of different coal maceral concentrates

5.4.1 Interaction of vitrinite rich concentrates

The high vitrinite concentrates, being of comparable ash and maceral content, provide a unique opportunity to examine the effect of particle size distribution in a blend. A mixture of three vitrinite rich concentrates (a 78.0%, b 81.8% and d 81.6% vitrinite) at a ratio of 1:1:1 by mass was carbonized at 10°C/min. The swelling and thermal results are shown in Figures 5.5-5.7. The difference between the measured and calculated (based on mass averaged results of three concentrates) results indicates where additive and non-additive (i.e. not predictable) events occur. In general, there appears to be a small effect within the primary devolatilisation region which suppresses swelling and exothermic activity but does not affect the high temperature contraction. The swelling values for calculated and measured results are 32.7% and 28.8%, and the high temperature absolute contractions are 7.0% and 6.8%, respectively. The high temperature exothermic activity for the measured values (Figure 5.6, 600-1000°C) shows the same trends as calculated values, though slightly diminished in its extent. Little difference in the thermal conductivity was observed during the primary devolatilisation, as shown in Figure 5.7.

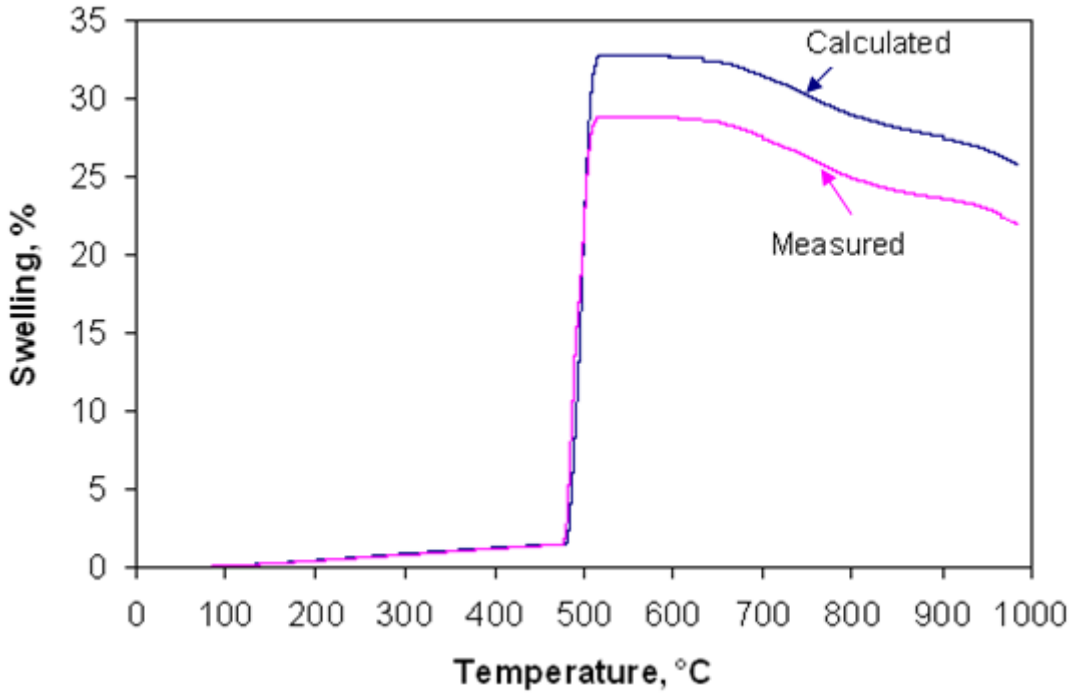

Figure 5.5. Measured and calculated swelling results at a heating rate of 10°C/min from 25 to 1000°C for the blend made up of three vitrinite rich concentrates of a, b and d (78.0%, 81.8% and 81.6% vitrinite) at a ratio of 1:1:1 by mass.

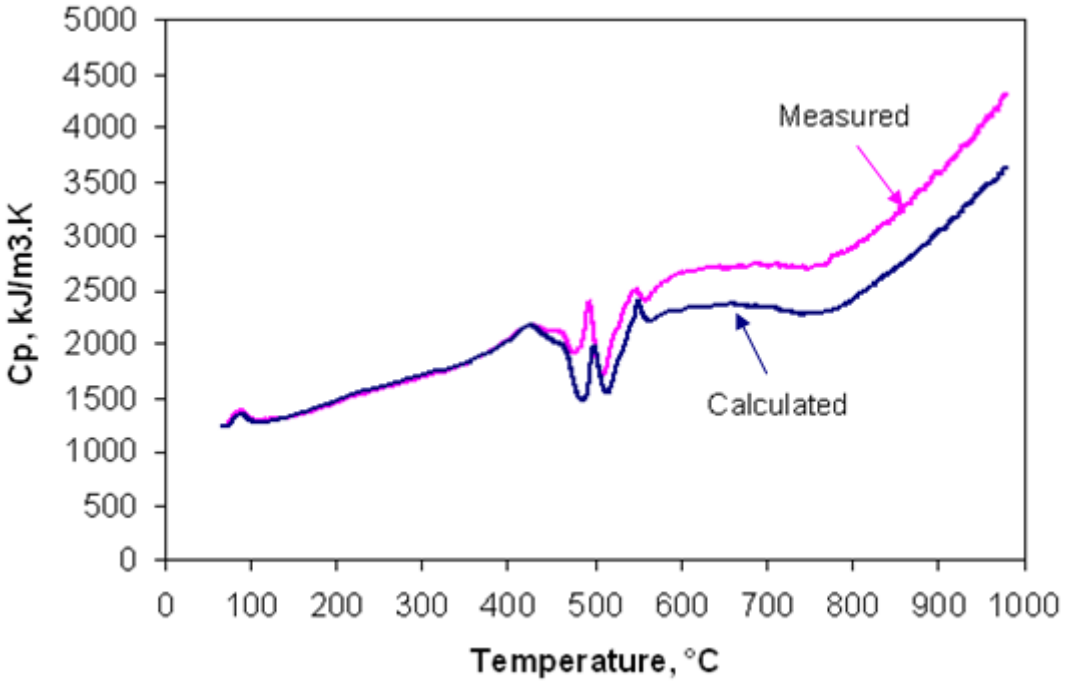

Figure 5.6. Measured and calculated apparent specific heat results at a heating rate of 10°C/min from 25 to 1000°C for the blend made up of three vitrinite rich concentrates of a, b and d (78.0%, 81.8% and 81.6% vitrinite) at a ratio of 1:1:1 by mass.

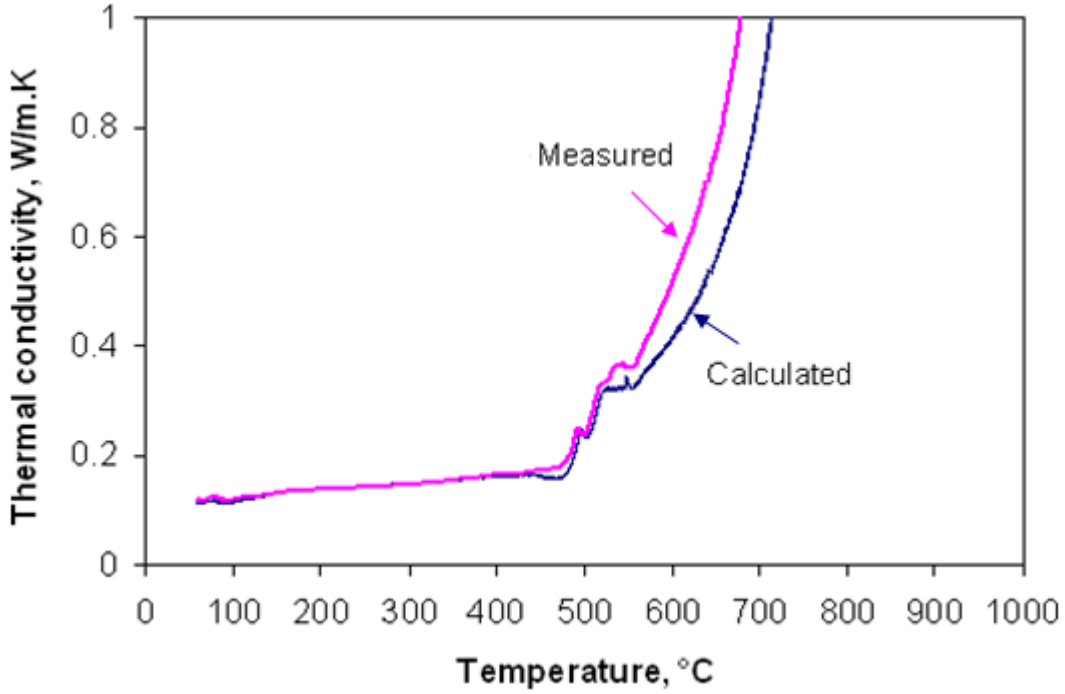

Figure 5.7. Measured and calculated thermal conductivity results at a heating rate of 10°C/min from 25 to 1000°C for the blend made up of three vitrinite rich concentrates of a, b and d (78.0%, 81.8% and 81.6% vitrinite) at a ratio of 1:1:1 by mass.

5.4.2 Interaction of vitrinite rich and inertinite rich concentrates

To examine the influence of inertinite rich concentrate and its interaction in a vitrinite rich blend, a mixture of two vitrinite rich concentrates (b 81.8% and d 81.6% vitrinite) and one

inertinite rich concentrate (f 29.0% vitrinite) was blended at a ratio of 1:1:1 by mass. The swelling and thermal results are given in Figures 5.8-5.10 and indicate a larger influence on swelling behaviour but little effect on thermal properties. The swelling values for calculated (based on mass averaged values of three concentrates) and measured results at the primary devolatilisation are 26.3% and 14.0%, respectively, as shown in Figure 5.8, and the temperature of swelling onset appears to be shifted to higher temperatures. The corresponding high temperature absolute contraction at the secondary devolatilisation are 5.8% and 4.4%, respectively, which indicates inertinite could suppress swelling during primary devolatilisation but does not have a significant influence on high temperature absolute contraction. This is consistent with the results of the blend of vitrinite rich concentrates.

The measured apparent specific heat in Figure 5.9 shows that the exothermic trough (420-550°C) produced similar results to the calculated values. A larger endothermic peak between 550 and 600°C can be observed, though the reasons for this are not clear. Thermal conductivity in Figure 5.10 also shows similar results to the theoretical values except for a smaller trough between 550 and 600°C, which are consistent with the results of apparent specific heat. At higher temperatures, the exothermic activity gives a similar trend to calculated values, also consistent with the blend of vitrinite rich concentrates.

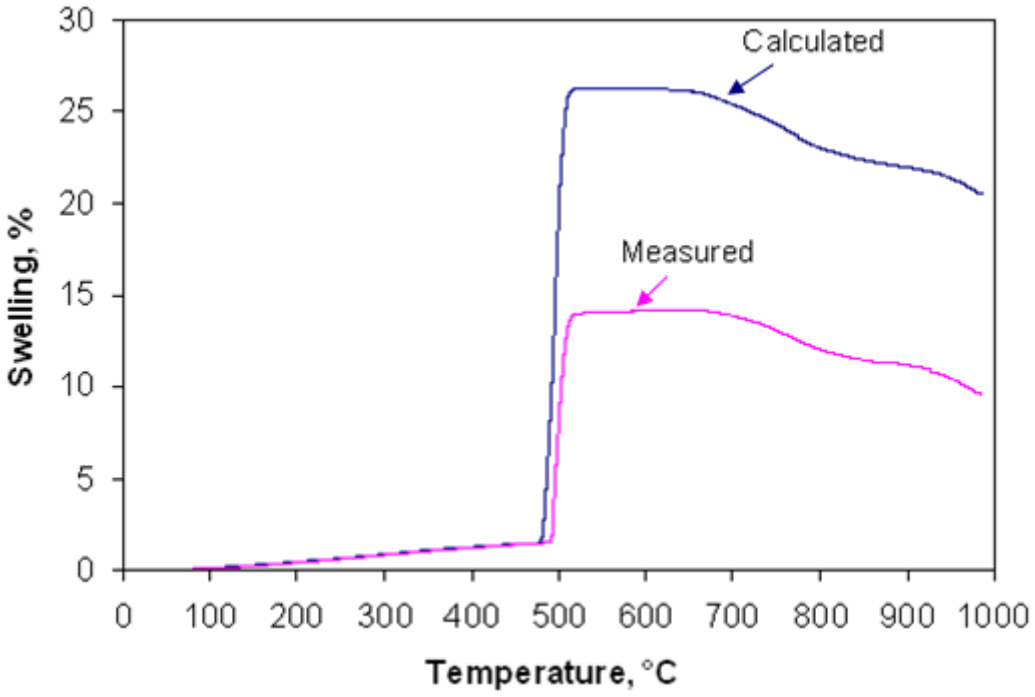

Figure 5.8. Measured and calculated swelling results at a heating rate of 10°C/min from 25 to 1000°C for the blend made up of two vitrinite rich and one inertinite rich concentrates of b, d and f (81.8%, 81.6% and 29.0% vitrinite) at a ratio of 1:1:1 by mass.

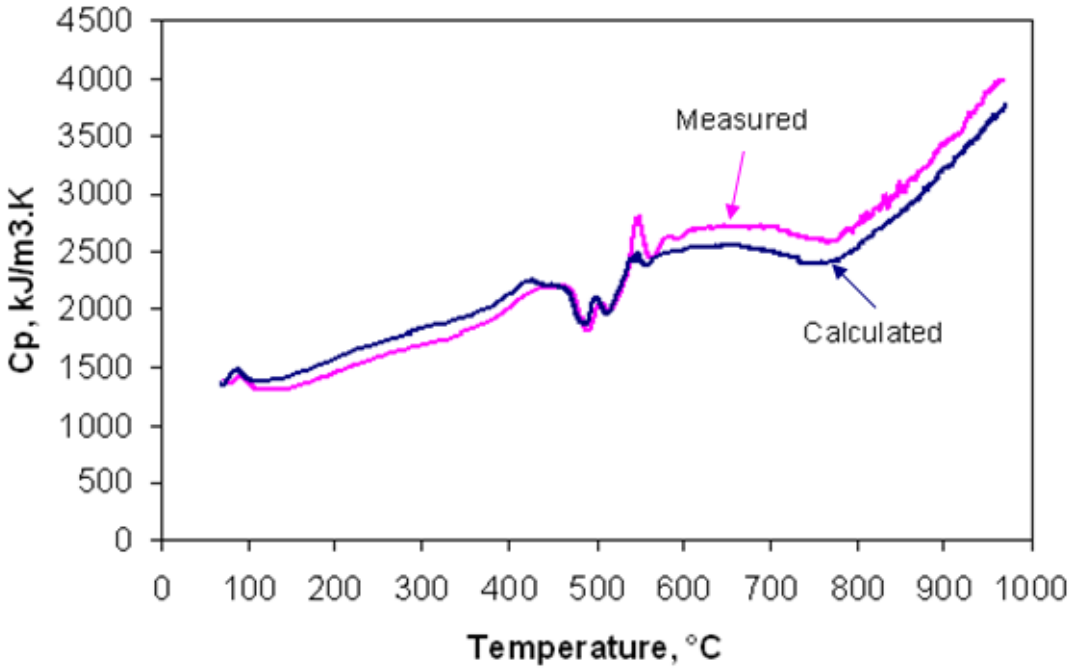

Figure 5.9. Measured and calculated apparent specific heat results at a heating rate of 10°C/min from 25 to 1000°C for the blend made up of two vitrinite rich and one inertinite rich concentrates of b, d and f (81.8%, 81.6% and 29.0% vitrinite) at a ratio of 1:1:1 by mass.

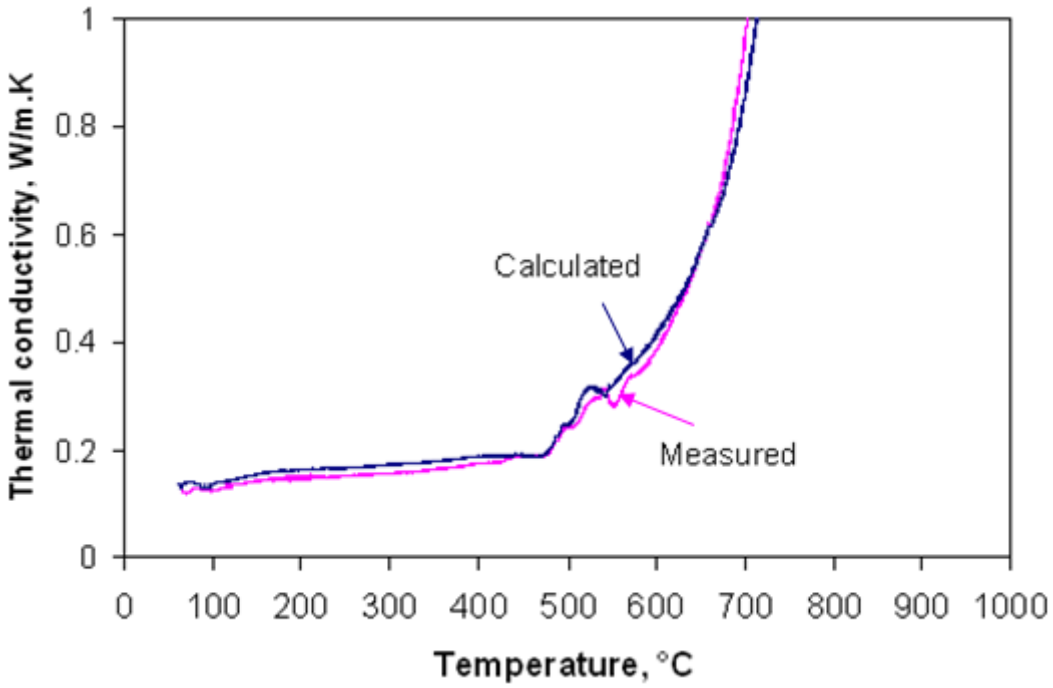

Figure 5.10. Measured and calculated thermal conductivity results at a heating rate of 10°C/min from 25 to 1000°C for the blend made up of two vitrinite rich and one inertinite rich concentrates of b, d and f (81.8%, 81.6% and 29.0% vitrinite) at a ratio of 1:1:1 by mass.

5.5 Discussion

5.5.1 Coal maceral separation

Relying on gravitational settling, the standard float-sink analysis separates coal maceral concentrate by using chemical media [27]. However, the chemical media may affect the swelling and thermal behaviour of coking coal. The reflux classifier separation method in this work has shown that it can produce concentrated coal maceral fractions for further analysis without the use of heavy media. The highest concentration of vitrinite was 81.8% (sample b) and the highest inertinite concentration was 71.0% (sample f). This method was particularly useful given the particle size range that was targeted. More concentrated coal maceral fractions could no doubt be produced with further particle size reduction, as this would liberate coal macerals from mixed (heterogeneous) particles. However, it has been shown previously in Chapter 4 that particle top size has an influence on swelling characteristics and there is a natural limit to the particle size that the reflux classifier can separate [45-47]. Such limitations are also prevalent in standard float sink analysis. For this work, effect of size classification has proven valuable in producing similar concentration vitrinite fractions with different particle size distributions. In comparison to float sink separation, it could be expected that all of these fractions would report to the same sample. Instead, the particle size distribution in float-sink analysis would be more closely aligned with the fragmentation pattern of individual coal macerals. In either case this represents an uncontrolled aspect of the process which could be alleviated with tighter control of initial size distribution in the feed sample (i.e. use of a single size fraction). From the results here it is also clear that good separation of inertinite rich concentrate is challenged by the rising ash content in the denser particles. A common method to remove this effect is through acid wash treatment (typically hydrogen fluoride), however given the highly corrosive nature of the acid and the unknown effects on coking parameters, such treatment has not been used in this work.

5.5.2 Coking behaviour of coal maceral concentrates

From the results presented in this work, it is clear that swelling is associated with exothermic behaviour and a rise in thermal conductivity. Given the sharp temperature region in which swelling occurs (475-500°C) and the broader range of exothermic activity (400-550°C), it suggests that swelling occurs as a consequence of the changes incurred by such exothermic activity. Previous work with CATA has shown that peak tar release also occurs with peak exothermic behaviour [117]. Rheological measurements of coking coals have shown that peak weight loss (in TGA) occurs at the same temperature of maximum fluidity and maximum swelling, essentially at the cross-over point between softening and resolidification

mechanisms [88, 89]. Swelling was considered to occur via a bubble growth and coalescence mechanism as a means of volatile escape in a plastic medium. After resolidification, the resulting pore structure provided a means of volatile escape, particularly in a coke oven. Of particular interest is the suggested role of inertinite in coke blends, which retains it solid structure and thus creates a porous pathway for escaping volatiles. This suggested mechanism is consistent with the results of the coal maceral blends in this work, which showed that the addition of an inertinite rich concentrate reduced the swelling extent below what is predicted by the additivity rule. Duffy et al. [88, 89] also found that blend components mainly interact at the boundary between coal particles, while inter-particle behaviour occurred in isolation.

Bubble nucleation and growth have been previously associated with a mass transfer operation involving a liquid media with a supersaturated concentration of gas molecules [171]. Attar [171] derived the governing equations for bubble nucleation during pyrolysis. Under pyrolysis conditions the viscosity of the fluid phase and the kinetic rate of gas formation are the driving factors. Importantly, it was found that a critical path length existed (approx 1-10 mm) below which gas diffusion out of the particle was sufficient to prevent bubble nucleation. However as the coal underwent plastic transition, the diffusion path length was extended beyond the boundary of the particle, resulting in a higher transport resistance and thus exceeding the critical gas concentration needed for bubble nucleation. Attar's concept is supported by the results in this work, particularly in the shift in swelling onset observed in the 64.0% vitrinite coal maceral concentrate and the vitrinite/inertinite blend. By "diluting" the mix with a solid component, the plastic material must reach a greater extent of fluidity development to reach the critical point at which bubble nucleation occurs. This may also explain why the parent coal, with its greater portion of ultra-fine particles (<10 μm), behaves outside of the coal macerals trends. Such small particles can fit into the interstitial voids in a packed bed, improving bulk density and thus gas generation per unit volume. The calculated packing bulk density of raw coal in coking bed is 0.77 g/ml (ash free) while it varies in the range 0.67-0.72 g/ml (ash free) from vitrinite rich concentrate to inertinite rich concentrate.

Measurement of apparent specific heat has shown that vitrinite rich concentrate and inertinite rich concentrate have very different behaviour during primary devolatilisation. Interpreting such behaviour as either endothermic or exothermic can be problematic in that quantification is heavily reliant on the method in which the real specific heat (i.e. without reactive heat) is determined [160]. In the current work, thermal events, such as endothermic peaks and exothermic troughs have been identified but the specific temperature at which the coal switches from endothermic to exothermic has been generalised. Within the literature there has been no fundamental studies exploring the mechanistic nature behind such thermal events.

Early work [172] has suggested that thermal degradation and softening is an endothermic process while re-solidification processes are exothermic. Poorly coking coals showed little to no exothermic activity during primary devolatilisation, while plastic coals exhibited greater exothermicity. This trend has also been previously measured using the CATA technique [21] on thermal and coking coals and has been observed here in the difference between coal macerals behaviour. Overall, it suggests that a common mechanism exists between thermoplasticity and exothermicity, the nature of which resides within the vitrinite portion of the coal.

5.6 Conclusions

The conclusions from this Chapter may be summarised as:

- The reflux classifier can successfully separate coal maceral concentrates on the basis of an alternative water based method without the need for dense media.

- Exothermic behaviour measured during primary pyrolysis appears to be related to the vitrinite portion of the coal.
    - Synchronous measurements of swelling and thermal properties of separated coal maceral concentrates indicated that increasing the vitrinite content produced a higher extent of volumetric swelling, exothermic reactions and thermal conductivity between 400 and 550°C.

    - At higher temperatures (600-1000°C), all coal maceral concentrates underwent a second significantly exothermic event which was related to high temperature volumetric contraction.

- Blending several vitrinite rich concentrates (of different particle size distributions) showed that swelling of the mixed sample was slightly lower than the calculated averaged result based on the individual concentrates. This trend was reflected in the exothermic activity. However, addition of inertinite rich concentrate to vitrinite rich concentrates showed that inertinite can suppress volumetric swelling and shift the swelling to a higher temperature during the primary devolatilisation. Inertinite rich addition did not have a significant influence on high temperature contraction. Such behaviour is consistent with previous theories that inertinite can provide a porous pathway for escaping volatiles in a fluid medium, however, the effects on high temperature contraction have yet to be explained.

Chapter 6 Swelling and thermal properties of the particle size cuts of coal maceral concentrates

6.1 Introduction

In the previous Chapter, coal maceral concentrates with different vitrinite and inertinite contents were successfully separated from coal sample C (particle size 0-212 μm) using the reflux classifier. Pyrolytic experiments with the separated coal maceral concentrates indicated that vitrinite rich concentrates produce larger exothermic heats and swelling during the primary devolatilisation (400-550°C) compared with inertinite rich concentrates. Meanwhile, the endothermic and exothermic reactions, swelling and shrinkage of coal maceral concentrates can also be affected by their particle size. Therefore, in order to evaluate the individual effect of vitrinite content and particle size on swelling and thermal properties of heating coal, coal maceral concentrates with selected particle sizes were separated and experiments were completed, as outlined in this Chapter. The swelling, endothermic and exothermic reactions and the thermal conductivity for a single particle size cut of coal maceral concentrate and the blend of two coal maceral concentrates with the same vitrinite content but different particle sizes were also investigated.

Results in Chapter 4 found that coal sample B produced the maximum swelling in comparison with the other coal samples. To enable the largest possible difference in swelling for separated vitrinite rich and inertinite rich coal maceral concentrates, coal B therefore was selected for the investigation of swelling and thermal properties of particle size cuts of coal maceral concentrates. Coal macerals separation was conducted using the reflux classifier. Swelling, apparent specific heat and thermal conductivity of the separated particle size cuts of coal maceral concentrates were evaluated using the CATA technique. Details of the reflux classifier and the CATA techniques can be seen in Chapter 3. Due to the large swelling of coal sample B (see Chapter 4), all samples in CATA experiments considered in this Chapter were packed to a length of 20 mm. Pyrolysis experiments were conducted from room temperature (25°C) to 1000°C at a heating rate of 10°C/min.

6.2 Analysis of particle size cuts of coal maceral concentrates

6.2.1 Coal maceral separation and petrography analysis

The separation of size cuts of coal maceral concentrates included three steps. Firstly, coal B was crushed to a size range of 0-1000 μm. Secondary, two particle size cuts of coal with size

range of 106-212 µm and 212-500 µm were obtained by wet sieving. Finally, the size cuts of coal were separated using the reflux classifier, resulting in a suite of particle size cuts of coal maceral concentrates. The results of petrography analysis are shown in Figure 6.1. With increasing water flow rate, for both size ranges of coal maceral concentrates, vitrinite content decreased, while inertinite content increased. Smaller particle size concentrates can be separated at a relatively lower water flow rate due to the smaller surface tension in comparison with larger particle size concentrates. At about 10 L/min the inertinite richest concentrate from the large particles was successfully separated.

The parent coal sample B has a maceral component of 73.6% vitrinite and 26.4% inertinite (mmf). Petrography analysis in Figure 6.1 indicates that the vitrinite contents of separated coal macerals vary from 26.1% to 91.2% for 106-212 µm size samples and 38.2% to 96.0% for 212-500 µm size samples, respectively. In comparison with the separation in Chapter 5 where coal particle size distributions were not controlled, size cuts of coal can obtain more coal maceral concentrates with various vitrinite contents, particularly, more concentrates with various medium vitrinite contents can be separated, which indicated that the separation of macerals is better when size cuts of coal are completed first.

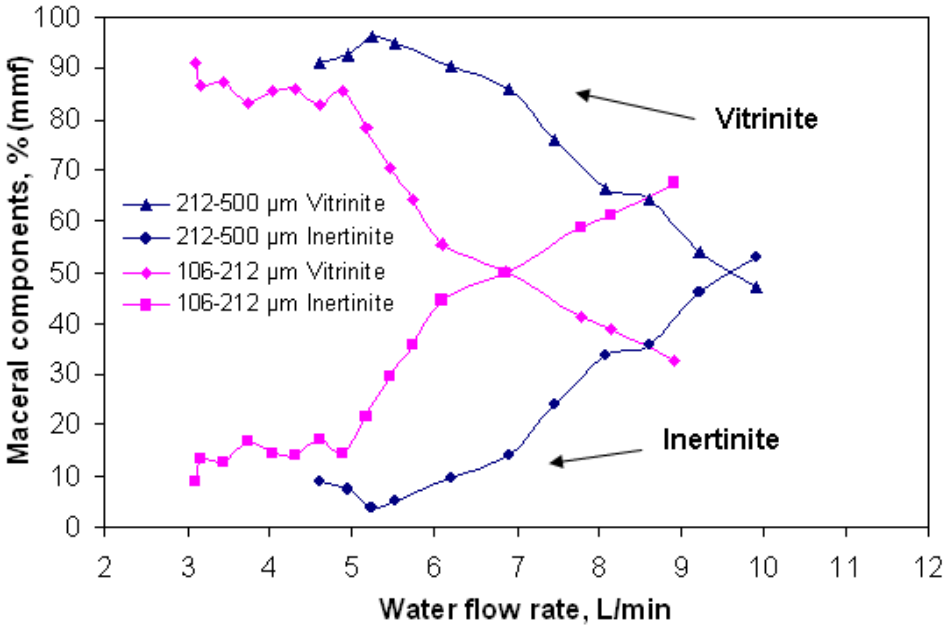

Figure 6.1. Coal maceral components versus water flow rate within the reflux classifier for all 106-212 µm and 212-500 µm size cuts of coal maceral concentrates.

6.2.2 Ash and density analysis

Figure 6.2 indicates that the ash content decreased approximately linearly with vitrinite content for coal maceral concentrates with vitrinite content above 63%, and this linear relationship is not significantly affected by particle size. However, the large particle size

concentrates have higher ash contents than the small particle size concentrates for inertinite rich particles with vitrinite contents below 63%. By comparison, Figure 6.3 indicates that for all 106-212 µm and 212-500 µm size cuts of coal maceral concentrates, the ash content increases linearly with density independent of particle size. Combining the fact that vitrinite has a lower density than inertinite [27], Figures 6.2 and 6.3 imply that for size cuts of coal maceral concentrates with vitrinite content below 63%, the small particles are more porous than the large particles. As a result, coal maceral concentrates with the same ash contents from both particle size cuts of coal have the same densities.

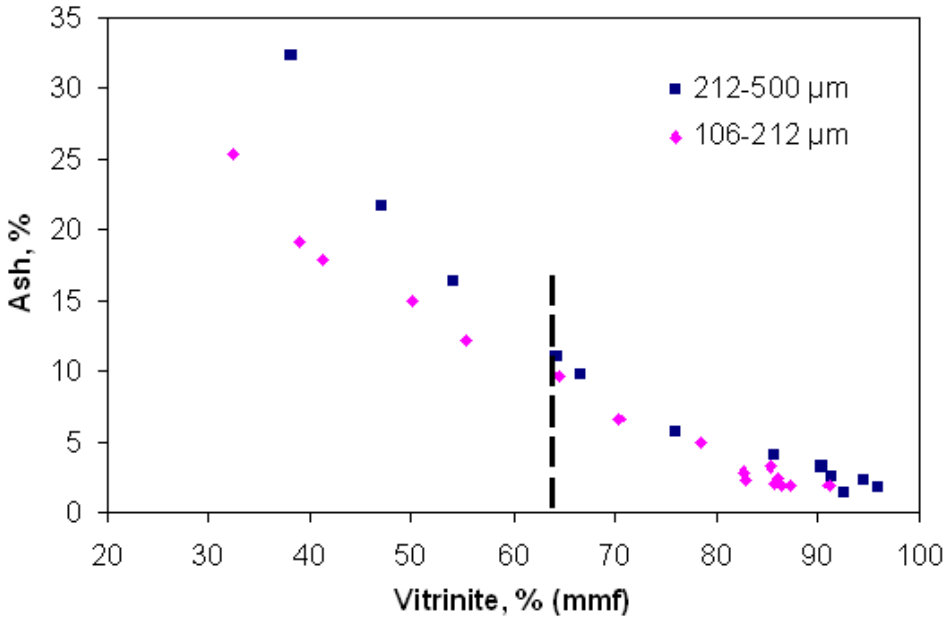

Figure 6.2. Relationship between vitrinite content and ash content for all 106-212 µm and 212-500 µm size cuts of coal maceral concentrates.

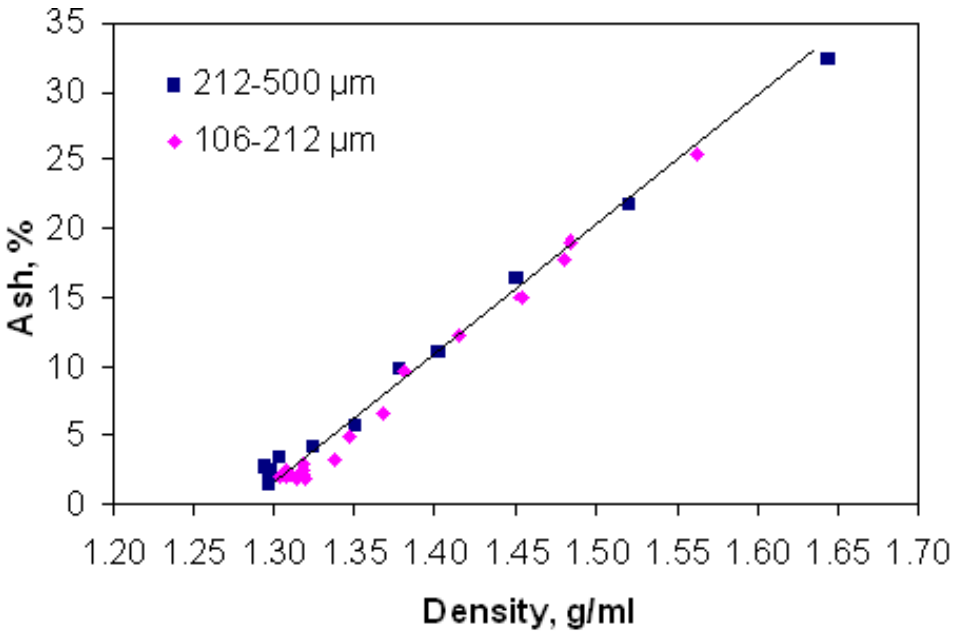

Figure 6.3. Relationship between density and ash content for all 106-212 µm and 212-500 µm size cuts of coal maceral concentrates.

6.3 Swelling and thermal changes of the particle size cuts of coal maceral concentrates

6.3.1 Effect of coal maceral components

6.3.1.1 Swelling

This section discusses the effect of vitrinite content on the swelling of coal maceral concentrates separated into different size cuts. Swelling at a heating rate of 10°C/min from 25 to 1000°C produced similar trends to that of the preliminary separated coal maceral concentrates, as detailed in Chapter 5. Figures 6.4 and 6.5 indicate that for all 106-212 µm and 212-500 µm size cuts of coal maceral concentrates, the vitrinite rich concentrates began to swell at lower temperatures and produced higher swelling between 400 and 550°C than the inertinite rich concentrates. Also, the high temperature absolute contraction (600-1000°C) increased with vitrinite content for all heating coal maceral concentrates.

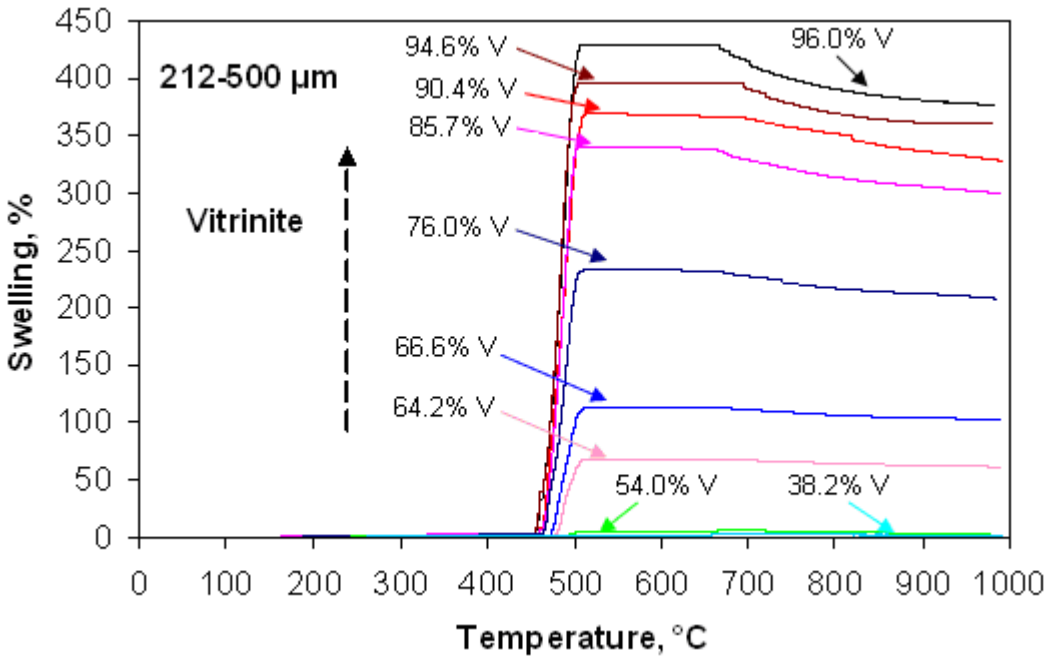

Figure 6.4. Swelling for 212-500 µm coal maceral concentrates at a heating rate of 10°C/min from 25 to 1000°C.

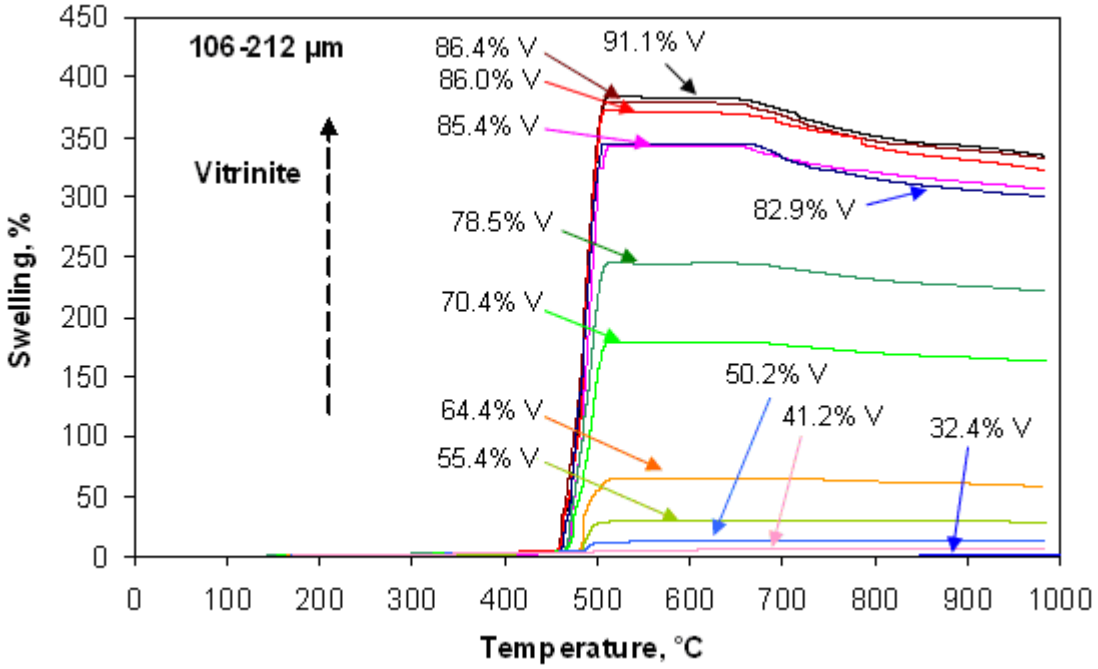

Figure 6.5. Swelling for 106-212 µm coal maceral concentrates at a heating rate of 10°C/min from 25 to 1000°C.

6.3.1.2 Apparent specific heat and thermal conductivity

Endothermic and exothermic reactions for all size cuts of coal maceral concentrates were identified by measuring the apparent specific heat, as shown in Figures 6.6 and 6.7. The peak of apparent specific heat represents an endothermic reaction, while the trough indicates an exothermic reaction [21]. Overall, the vitrinite rich concentrates have larger primary exothermic troughs (400-550°C) than the inertinite rich concentrates, although some experimental errors may exist between vitrinite rich concentrates. For instance, the exothermic trough for the 82.9% vitrinite concentrate is a little larger than that of the 91.1% vitrinite concentrate in Figure 6.7. A large exothermic trough corresponds to a high extent of swelling (Figures 6.4 and 6.5). This is consistent with the finding in Chapter 5. Prior to the primary exothermic reaction, all coal maceral concentrates underwent an endothermic reaction around 380°C, which can be identified by the endothermic peak. However, this endothermic peak extends to a higher temperature with increasing inertinite content. The 86.4% vitrinite concentrate produced this endothermic peak at 425°C, while the 41.4% vitrinite concentrate reached 475°C.

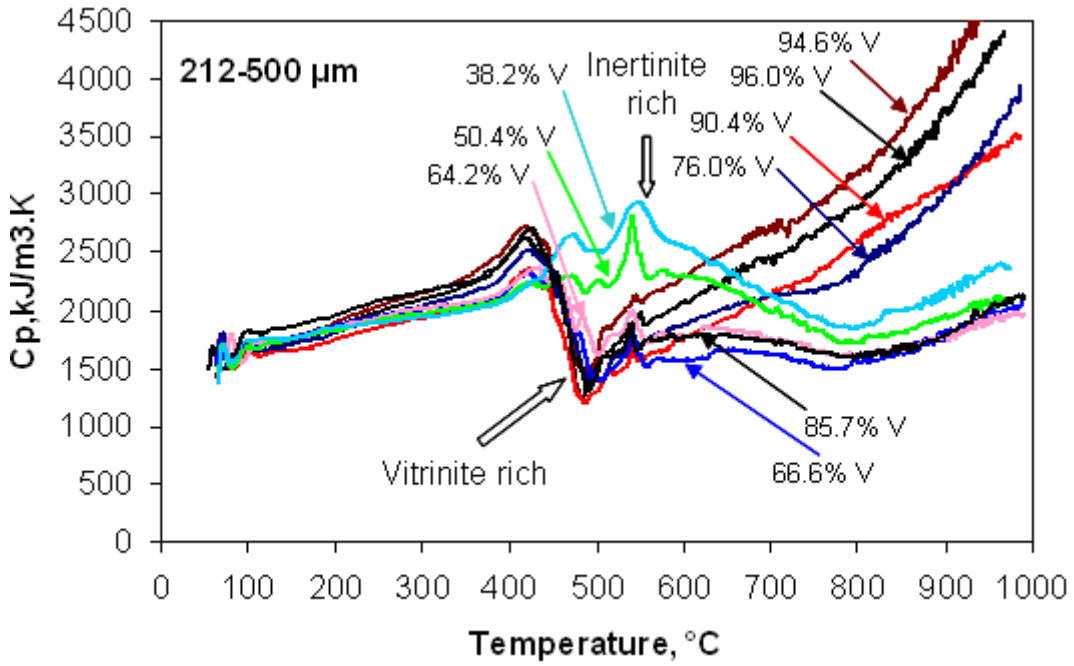

Figure 6.6. Apparent specific heat for 212-500 µm coal maceral concentrates at a heating rate of 10°C/min from 25 to 1000°C.

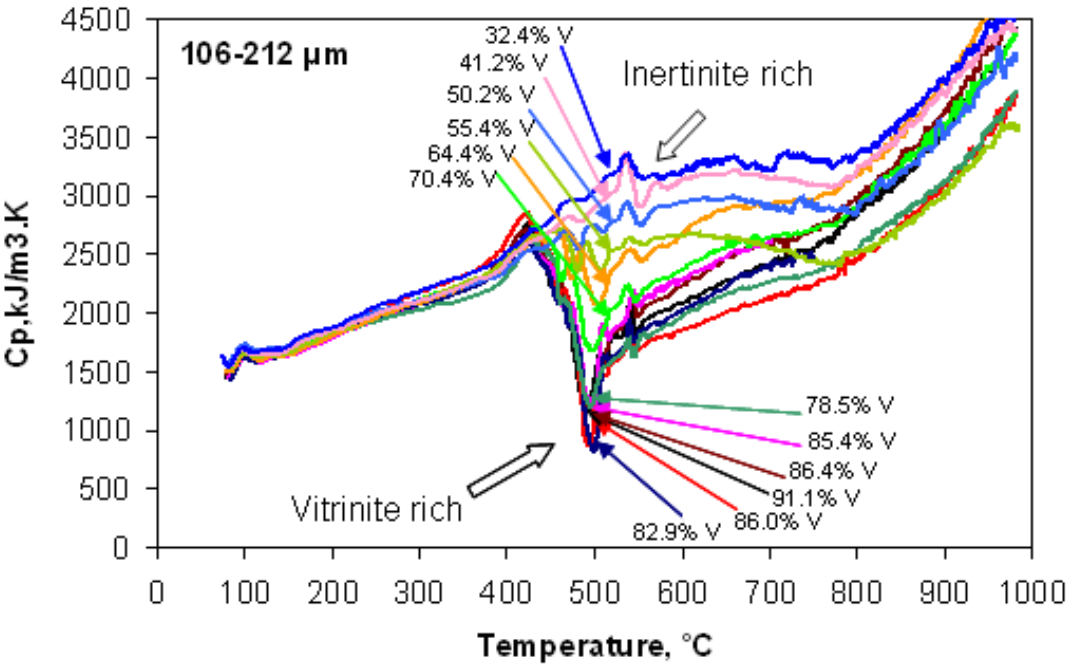

Figure 6.7. Apparent specific heat for 106-212 µm coal maceral concentrates at a heating rate of 10°C/min from 25 to 1000°C.

Figures 6.8 and 6.9 show that for all the particle size cuts of coal maceral concentrates, the estimated thermal conductivities were around 0.16-0.18 W/m·K from 25 to 475°C. With increasing temperature, a distinct increase in thermal conductivity occurs between 475 and 550°C for vitrinite rich concentrates, while no significant increase was observed for inertinite

rich concentrates. The changes of thermal conductivity are consistent with the swelling characteristics and exothermic reactions, as shown in Figures 6.4-6.7. For one vitrinite rich concentrate, a high swelling and a large exothermic trough corresponds to a sharp increase in thermal conductivity between 400 and 550°C. Comparing with the values of other concentrates in Figures 6.8 and 6.9, the relatively high thermal conductivity of 32.4% vitrinite concentrate below 500°C in Figure 6.9 is considered experimental errors. At the onset of the secondary exothermic reaction, the thermal conductivities for all coal maceral concentrates rapidly increase with temperature, and the same results were also observed and discussed in Chapters 4 and 5. The reasons include

(a) radiant heat transfer across pores and cracks;

(b) changes in the thermal conductivity of the coals due to pyrolysis;

(c) changes in the intrinsic conductivity with temperature of char [20, 85],

(d) a numerical artefact (the estimated thermal conductivity is affected by heats of reactions) associated with heat build-up in the packed bed. When thermal conductivity reached 2-3 W/m·K and beyond [19], the difference between measured surface and centre meta-plastic material temperatures was in a very narrow range or thermal inversion between surface and centre of heating sample occurred, hence results became unstable.

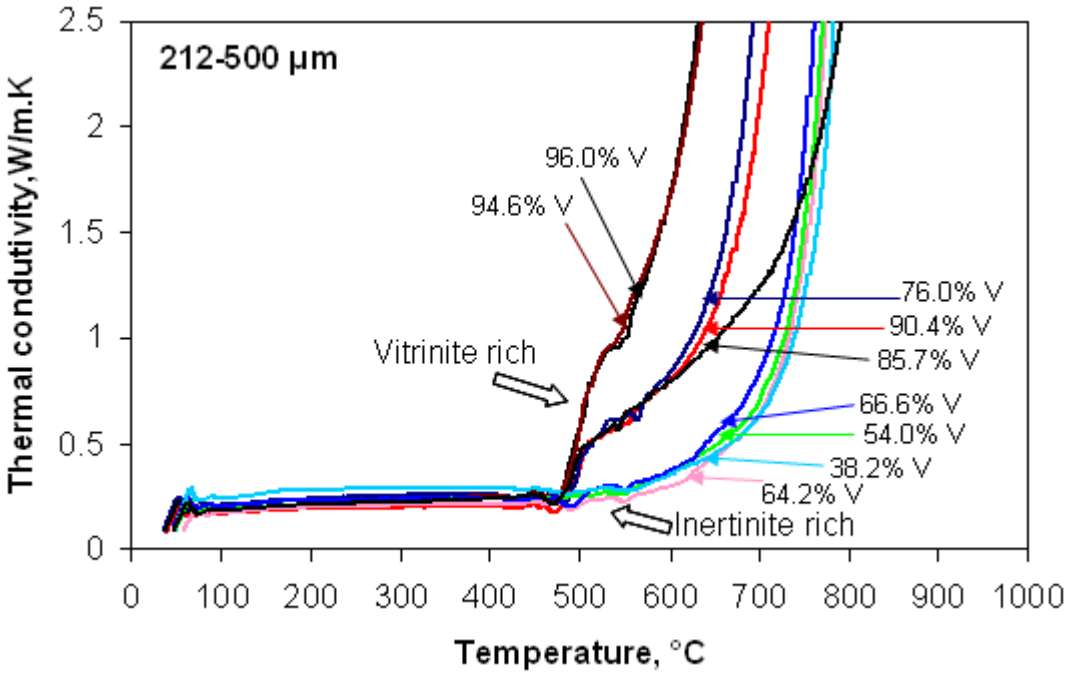

Figure 6.8. Thermal conductivity for 212-500 µm coal maceral concentrates at a heating rate of 10°C/min from 25 to 1000°C.

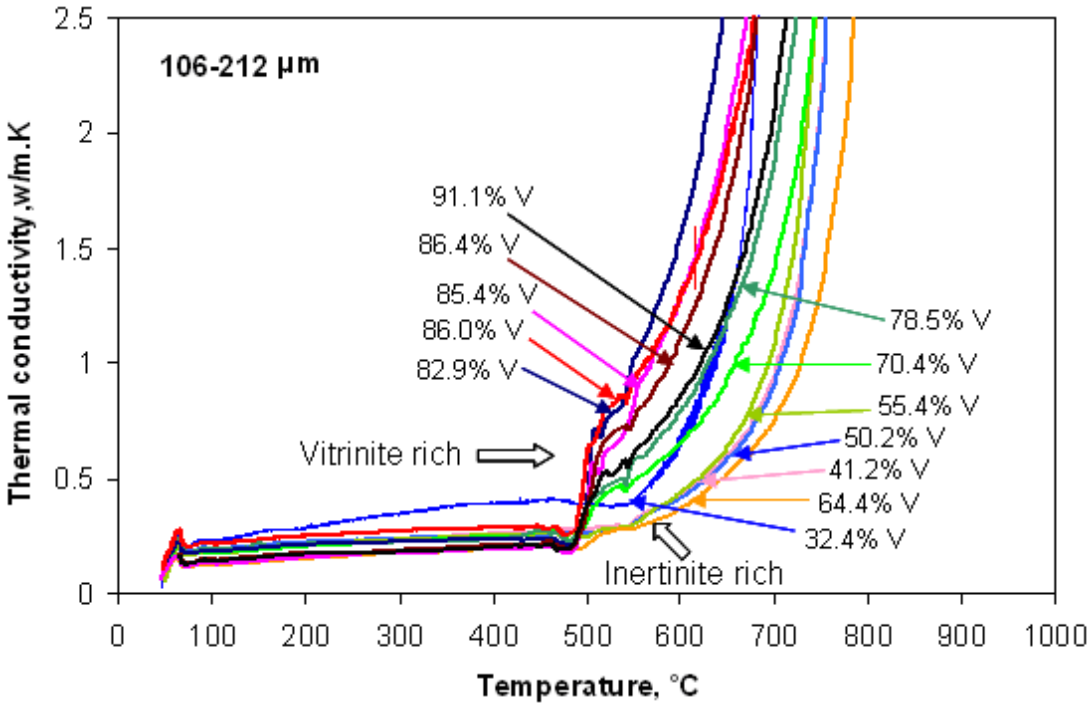

Figure 6.9. Thermal conductivity for 106-212 µm coal maceral concentrates at a heating rate of 10°C/min from 25 to 1000°C.

6.3.1.3 Microscopic properties of coke

Combining the results in Figures 6.4-6.9, it can be concluded that vitrinite concentrates contribute to swelling, exothermic activities and the increase of thermal conductivity during the primary devolatilisation. Therefore, one maceral with high vitrinite content (86.4% V) and one maceral with medium vitrinite content (64.4% V) were selected to observe the effect of vitrinite content on the development of porosity of coke. Figure 6.10 (a) and (b) show the optical microscopy images of the overview of the cross section of the cylindrical cokes that obtained from the 86.4% vitrinite and 64.4% vitrinite concentrates (106-212 µm) at a heating rate of 10°C/min from 25 to 1000°C. The images indicated that the coke sample obtained from the 86.4% vitrinite concentrate was found to be more porous, with the average pore size being larger compared to that of the 64.4% vitrinite concentrate. The cross sectional views at the centre of the cylindrical cokes are more porous in comparison with the surrounding for both cokes obtained from the two coal maceral concentrates. This is attributed to the thermal gradient across the sample from the surface to the centre [127], and gases and tars transferred and escaped from the axis towards the periphery of the cylindrical coke bed, which relates to the pore coalescence [19, 88-90]. This was also discussed at section 4.4.2.1 in Chapter 4.

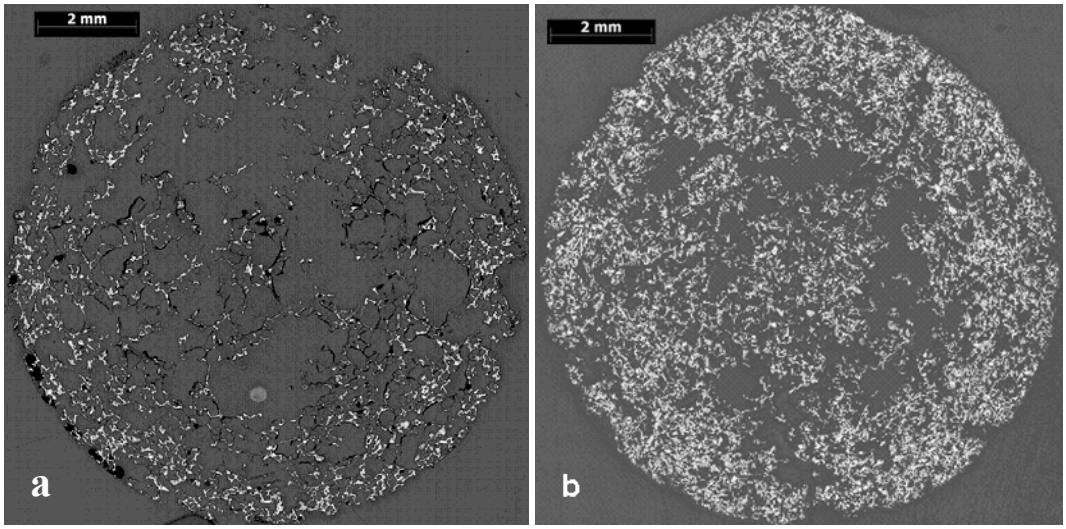

Figure 6.10. Optical microscopy overview images of the cross section of the cylindrical coke obtained from 106-212 μm (a) 86.4% vitrinite concentrate, (b) 64.4% vitrinite concentrate at a heating rate of 10°C/min from 25 to 1000°C.

6.3.2 Effect of particle size

This section discusses the effect of particle size only on swelling, endothermic and exothermic reactions and thermal conductivity of heating coal maceral concentrates. Results in Chapter 4 found that the large particle size coal sample underwent a higher extent of swelling than the small particle size coal sample. In Chapter 5, it was found that the general trend for heating coal maceral concentrates was that the swelling increased with increasing vitrinite content. However, there was no discernible linear relationship for swelling with vitrinite content or with particle size because the contributions of vitrinite content and particle size to swelling can affect each other. In order to further investigate the effect of particle size only on swelling, endothermic and exothermic reactions and thermal conductivity for coal maceral concentrates, a blend was produced by mixing two vitrinite rich coal maceral concentrates that have different particle size distributions but similar vitrinite content. The 85.4% vitrinite concentrate (106-212 μm) was mixed with the 85.7% vitrinite concentrate (212-500 μm) in the ratio of 1:1 by mass. The blend was carbonised at a heating rate of 10°C/min from 25 to 1000°C. The experimental results for swelling, apparent specific heat and thermal conductivity of the blend are shown in Figures 6.11-6.13. The theoretical results for swelling, apparent specific heat and thermal conductivity calculated based on mass averaged results of two coal maceral concentrates also are synchronously shown in Figures 6.11-6.13. These theoretical results are presented as calculated results, while the experimental results are named measured results.

6.3.2.1 Swelling

Figure 6.11 indicates that the measured maximum swelling which occurs around 510°C for the blend was 333%. Based on mass averaged results of two coal maceral concentrates, the calculated temperature at which maximum swelling occurs is also 510°C and the calculated maximum swelling was found to be 341%. The calculated values and the trends followed are consistent with the measured values. The measured and calculated high temperature absolute contraction between 600 and 1000°C were 49.8% and 37.5%, respectively. This indicated that particle size in the blend shows little effect of around 2.4% ((341-333)*100/333) difference on swelling but a significant effect of around 24% ((49.8-37.5)*100/49.8)) difference on high temperature contraction for this sample. The difference in high temperature absolute contraction between calculated and measured values may be due to [147]:

a) yields of thermal degradation products generated in coals on their heating to the resolidification temperature;

b) interactions of the volatile resulting in a change in the chemical compositions of the decomposed products, such as the predominance of components that represent various aromatic hydrocarbons containing alkyl carbon atoms in the range of C_3-C_9.

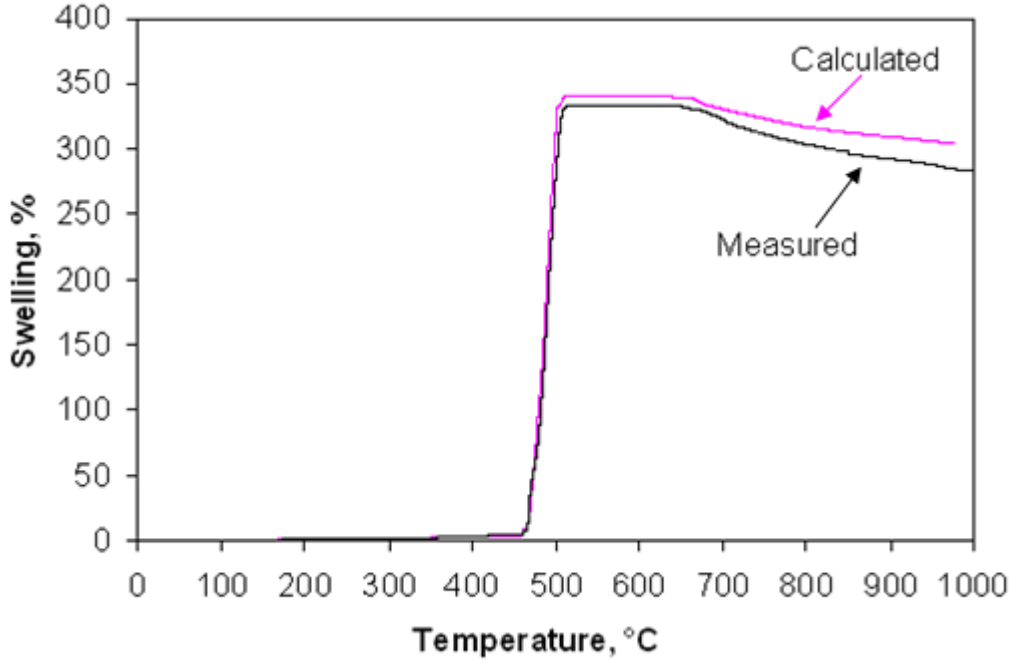

Figure 6.11. Calculated by mass average and measured swelling for a blend of 85.4% vitrinite concentrate with a particle size of 106-212 µm and 85.7% vitrinite concentrate with a particle size of 212-500 µm, blended at a ratio of 1:1 by mass, at a heating rate of 10°C/min from 25 to 1000°C.

6.3.2.2 Apparent specific heat and thermal conductivity

Based on mass averaged results of two coal maceral concentrates, the calculated apparent specific heat and thermal conductivity are shown in Figures 6.12 and 6.13 together with the

measured results. The figures show that prior to the maximum swelling (510°C), apparent specific heat and thermal conductivity for the measured and the calculated results are almost the same, as indicated by the overlap of the two curves. Between 510 and 550°C, the measured apparent specific heat is lower than the calculated result. With increasing temperature, the endothermic peaks relating to the onset of secondary devolatilisation are observed at 550°C and 565°C for the calculated and measured results, respectively. This indicates that the blend initiates the secondary devolatilisation at a higher temperature than expected. Corresponding to the difference in apparent specific heat between the measured result and the calculated value, the measured thermal conductivity is higher than the calculated value between 510 and 550°C. In addition, a small dip of thermal conductivity is observed around 565°C for the measured result, while it does not exist for the calculated value, as seen in Figure 6.13. Above 625°C, the measured apparent specific heat and the thermal conductivity deviated from the calculated values, which was consistent with the difference in the high temperature absolute contraction (Figure 6.11). Therefore, during primary devolatilisation, particle size has little influence on swelling, apparent specific heat and thermal conductivity for vitrinite concentrates. However, it has been observed that particle size can significantly affect high temperature absolute contraction and has somewhat influence on apparent specific heat and thermal conductivity during secondary devolatilisation.

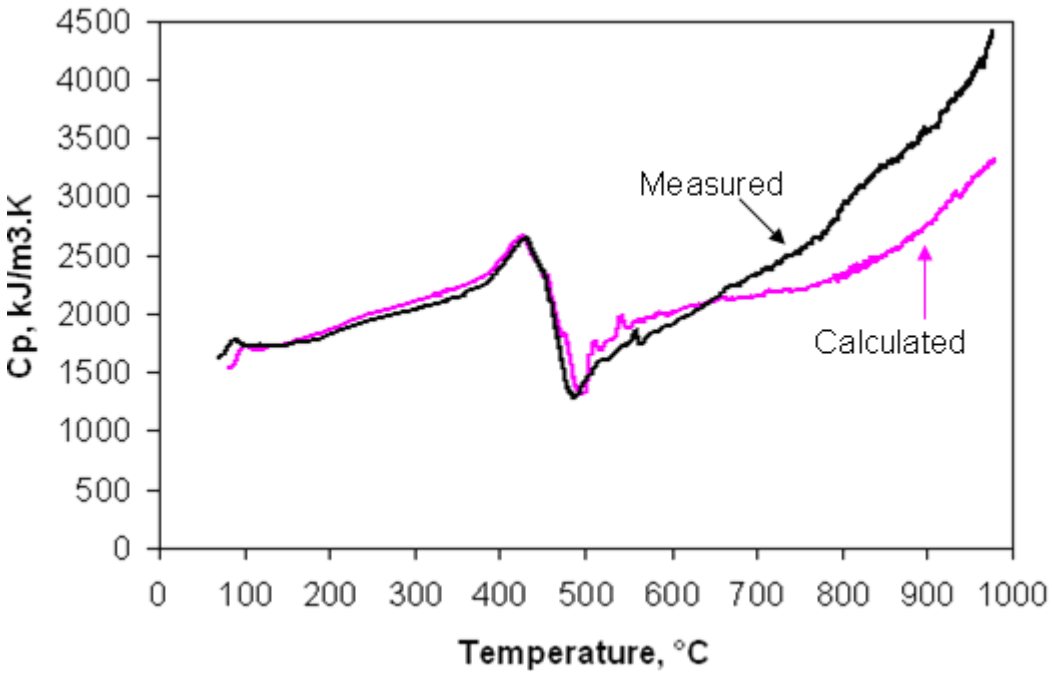

Figure 6.12. Calculated by mass average and measured Cp for a blend of 85.4% vitrinite concentrate, with a particle size of 106-212 µm and 85.7% vitrinite concentrate with a particle size of 212-500 µm, bended at a ratio of 1:1 by mass, at a heating rate of 10°C/min from 25 to 1000°C.

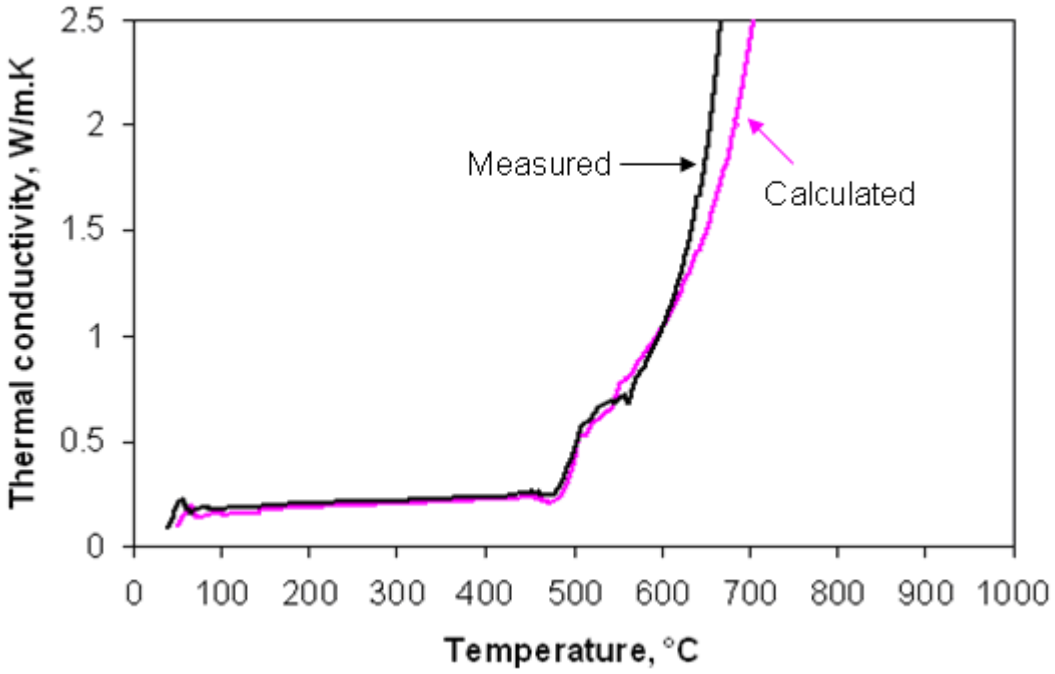

Figure 6.13. Calculated by mass average and measured thermal conductivity for a blend of 85.4% vitrinite concentrate with a particle size of 106-212 µm and 85.7% vitrinite concentrate with a particle size of 212-500 µm at a blending ratio of 1:1 by mass, at a heating rate of 10°C/min from 25 to 1000°C.

6.3.3 Effects of the combination of coal maceral components and particle size

6.3.3.1 Swelling

The impact of the combination of vitrinite content and particle size on swelling, endothermic and exothermic reactions and thermal conductivity of heating coal maceral concentrates are discussed in this section. Figure 6.14 indicates that, for all coal maceral concentrates with vitrinite contents above 63%, the maximum swelling (around 510°C) when heated at a rate of 10°C/min, increases linearly with vitrinite content independent of the particle size distributions. Similarly, the high temperature absolute contraction (550-1000°C) also increases linearly with the vitrinite content, as shown in Figure 6.15. In addition to separated coal maceral concentrates, the maximum swelling (around 510°C) and high temperature absolute contraction (550-1000°C) of the raw coal with a vitrinite content of 73.6% and particle size distribution of 0-212 µm, heated at 10°C/min from 25 to 1000 °C, lies on the linear relationship produced by the maximum swelling and high temperature absolute contraction (550-1000°C) of all the different vitrinite content samples.

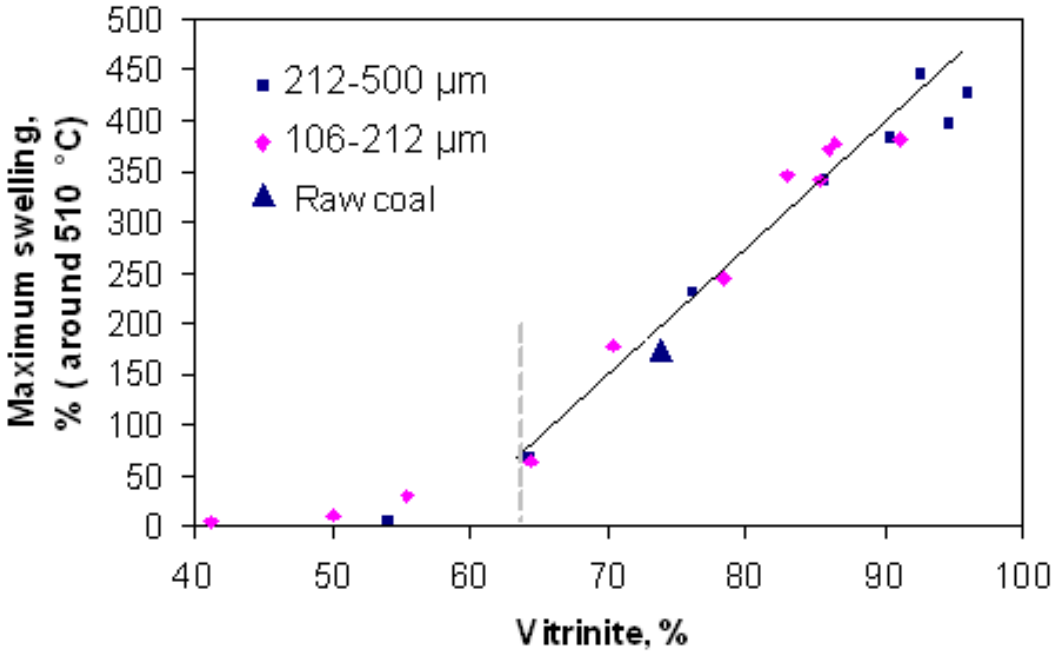

Figure 6.14. Relationship between vitrinite content and maximum swelling (at about 510°C) for the 106-212 µm and 212-500 µm size cuts of coal maceral concentrates at a heating rate of 10°C/min.

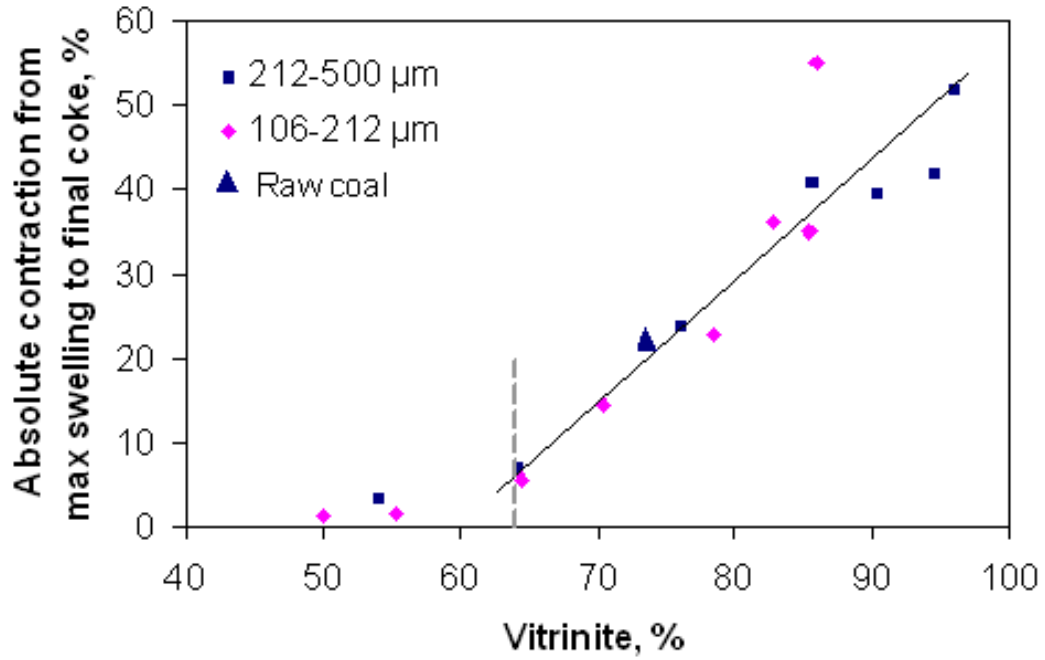

Figure 6.15. Relationship between vitrinite content and high temperature absolute contraction (550-1000°C) for the 106-212 µm and 212-500 µm size cuts of coal maceral concentrates at a heating rate of 10°C/min.

To explain the linear relationship observed between swelling and vitrinite content for the coal maceral concentrates containing more than 63% vitrinite, the mechanisms of intragranular and intergranular swelling are discussed [3]. Intragranular swelling, which represents the swelling within coal particles, depends on the coal type, particle size and heating rate, while the intergranular swelling, which represents the swelling between coal particles, depends on

packed bed of coal and the pressure caused by gaseous bubble on the solid phase. Upon heating, intragranular swelling initiates first, bubbles that are more or less spheroidal in form arise and grow due to the evolution of gases inside particles. These gases do not have an easy exit; the larger the particle, the more difficult it becomes for the gas to come out. Because of this, the external periphery of the particles deform due to the gas pressure building inside the particles. Therefore, the particles move closer together, though still leaving some intergranular pores that allow the pyrolysis gases to escape. The intergranular pores are of less regular shape than the intragranular voids formed by a gas bubble within a plastic particle. If the coal does not show a relatively high extent of plasticity during heating, the particles will swell little and fuse together. After resolidification, the semi-coke will be solid, losing viscosity and hence the swelling remains very low. By comparison, if the coal shows a relatively high level of plasticity, swelling of individual particles will then cause closure of the intergranular pores. The gases released during pyrolysis will no longer freely escape and the pressure subsequently increases in these intergranular pores, giving rise to swelling of the whole mass of coal and hence closure of intergranular pores. The result of this is a renewed increase in pressure until the large bubbles of imprisoned gas burst. The overall swelling can be several times the initial volume of the coal.

In accordance with this description, the distinction between intragranular and intergranular pores cannot be determined when there is sufficient plasticity, because the boundaries between the particles are eliminated by agglomeration. When large bubbles form, the internal pressure in the metaplast will promote plastic material to swell as a whole and this swelling is larger than that caused purely by intragranular gas for low plastic coal. The swelling process can be described based on the representation in Figure 6.16. In this model,

(a) prior to pyrolysis, the gas flow (carrier gas) is only hindered by a packed bed of solids, but it can still pass through the coal bed;

(b) when the temperature is up to 280-400°C, coal particles begin to soften, the gas flow (carrier gas and small parts of volatiles) is hindered by a combination of the packed bed and softening particles;

(c) at the early stage of the primary devolatilisation (400-450°C), the gas flow (carrier gas and large parts of volatiles) is restricted to diffusion through liquid metaplast and bubble coalescence occurs, which causes the metaplast to swell;

(d) during the primary devolatilisation (450-510°C), the gas flow (carrier gas and mainly volatiles) is restricted to diffusion through the liquid metaplast and a pore network forms, the swelling reaches a maximum at approximately 510°C.

According to this model, the vitrinite content relates to the amount of metaplast formed; the amount of metaplast relates to the degree of swelling; the metaplast is involved in "melding" of all particles and is therefore particle size independent; therefore, swelling is linearly proportional to vitrinite content and independent of particle size when the plasticity is high.

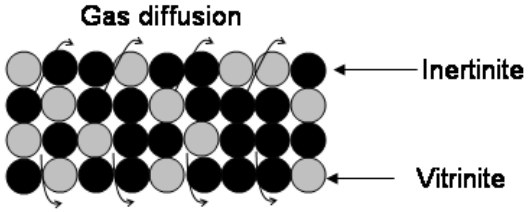

(a) Gas flow (carrier gas) is hindered by a packed bed of solids (25°C).

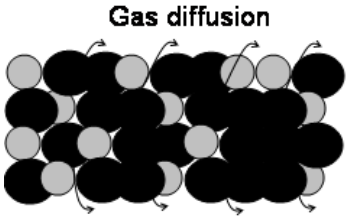

(b) Gas flow (mainly carrier gas and some volatiles) is hindered by a packed bed of solids and softening particles (280-400°C).

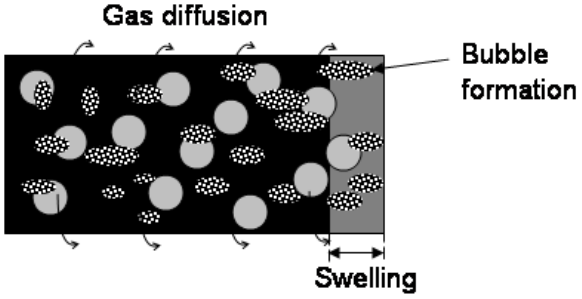

(c) Gas flow (mainly volatiles and some carrier gas) is restricted to diffusion through liquid metaplast and bubble formation (400-450°C) occurs, the swelling portion is indicated by a different colour to the original coal bed.

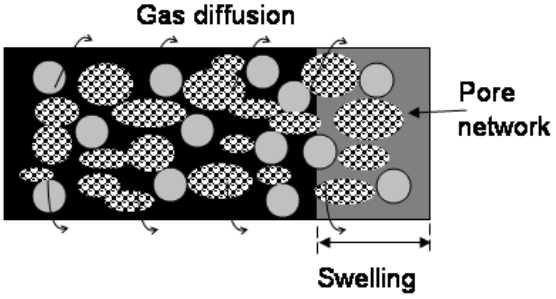

(d) Gas flow is restricted to diffusion through the liquid metaplast and a pore network forms (450-510°C), the swelling portion is indicated by a different colour to the original coal bed.

Figure 6.16. A physical model to explain the swelling of high swelling vitrinite concentrates.

In the current work, coal maceral concentrates with vitrinite above 63% exhibit swelling behaviour that appears to match this model. However, when the vitrinite content is blow 63% this model no longer matches the observed swelling, because the effect of intragranular swelling on the overall swelling cannot be neglected. Optical microscopy images in Figure 6.17 indicate that the particles of vitrinite rich concentrate (86.4% V) underwent a completely intergranular swelling with no boundaries between particles remaining. However, individual particles and boundaries still can be clearly observed in pyrolytic residue from inertinite rich concentrate (32.4% V), implying there was very little intergranular swelling in inertinite rich concentrates.

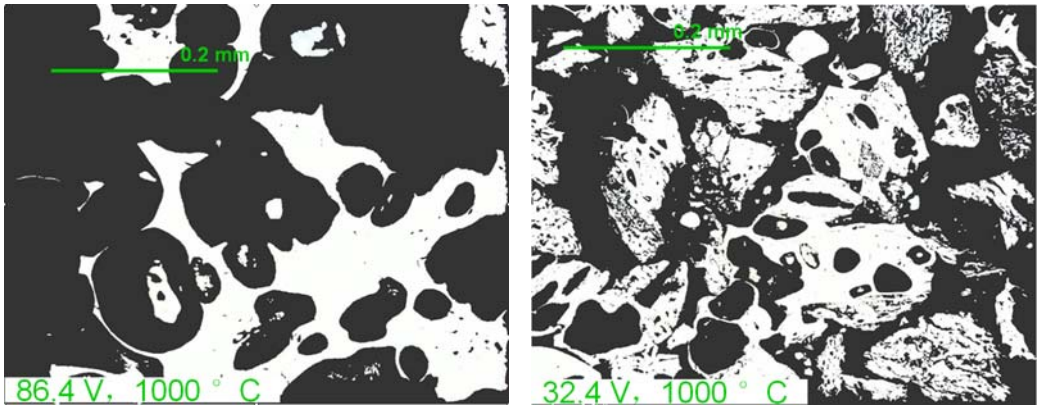

Figure 6.17. Optical microscopy images of coke obtained from 106-212 µm (a) 86.4% vitrinite concentrate, (b) 32.4% vitrinite concentrate at a heating rate of 10°C/min from 25 to 1000°C, both images obtained near the centre of the cross section of the cylinder coke sample.

6.3.3.2 Heat of exothermic reactions and thermal conductivity

In section 6.3.1, it was found that, during the primary exothermic reaction between 400 and 550°C, the higher the vitrinite content, the larger the primary exothermic reaction trough. This section further discusses the relationship between heat of the primary exothermic reaction and vitrinite content. A typical example for calculating heat of the primary exothermic reaction of a vitrinite rich concentrate (86.4% vitrinite, 106-212 µm) is shown in Figure 6.18. The exothermic heat was integrated based on the apparent volumetric specific heat trough between one endothermic peak around 420°C and another endothermic peak around 540°C [19]. This method for calculating heat of the primary exothermic reactions applied to all coal maceral concentrates that have vitrinite contents above 63%. As coal maceral concentrates with lower vitrinite contents (below 63%) did not show distinct exothermic troughs during the primary exothermic reaction, the exothermic heat for these inertinite rich concentrates was not integrated in this work. Figure 6.19 indicates that the integrated heat (MJ/m^3) of the primary exothermic reaction produced a linear increase with vitrinite content for all coal maceral concentrates independent of particle size. In addition to the heat of the primary exothermic

reaction, thermal conductivity at the maximum swelling (around 510°C) also increases linearly with vitrinite content, as seen in Figure 6.20. The relationships of heats of the primary exothermic reaction and thermal conductivity at the maximum swelling (around510°C) with vitrinite content of coal maceral concentrates (above 63% Vitrinite) are aiding in explaining the linear relationship between swelling and vitrinite content.

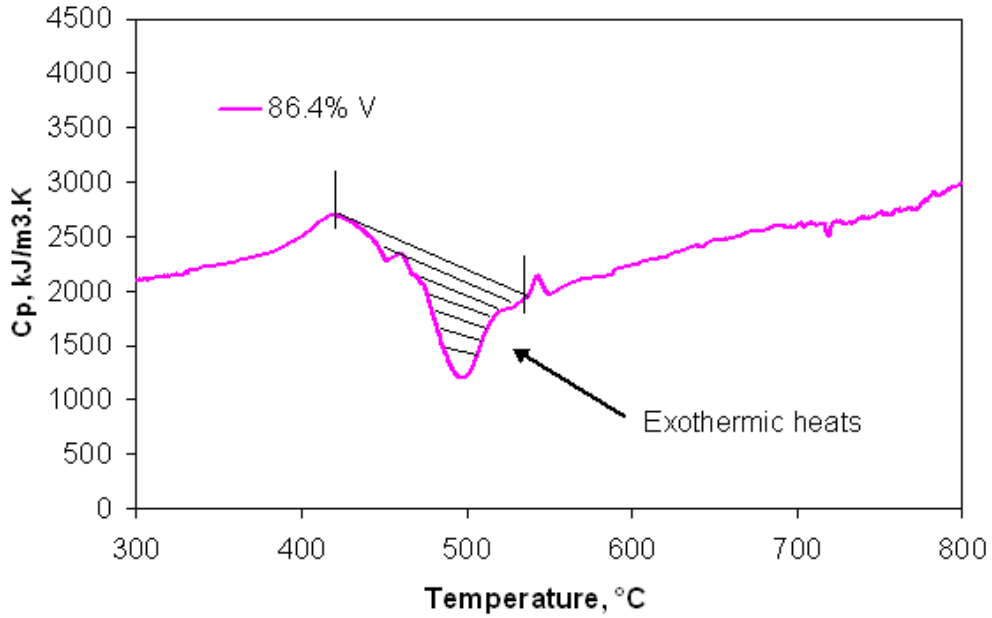

Figure 6.18. A typical example for the calculation of heat of the exothermic reaction during the primary devolatilisation (420-540°C) for the 86.4% vitrinite concentrate with 106-212 µm size range at a heating rate of 10°C/min.

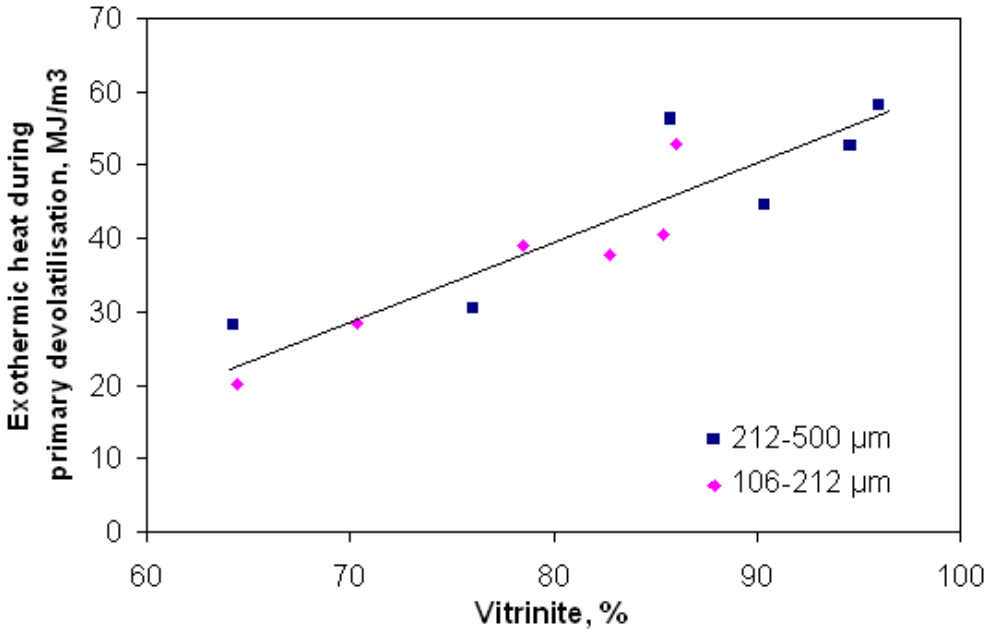

Figure 6.19. Relationship between exothermic heat during the primary devolatilisation (420-540°C) and vitrinite content for the 106-212 µm and 212-500 µm size cuts of coal maceral concentrates at a heating rate of 10°C/min.

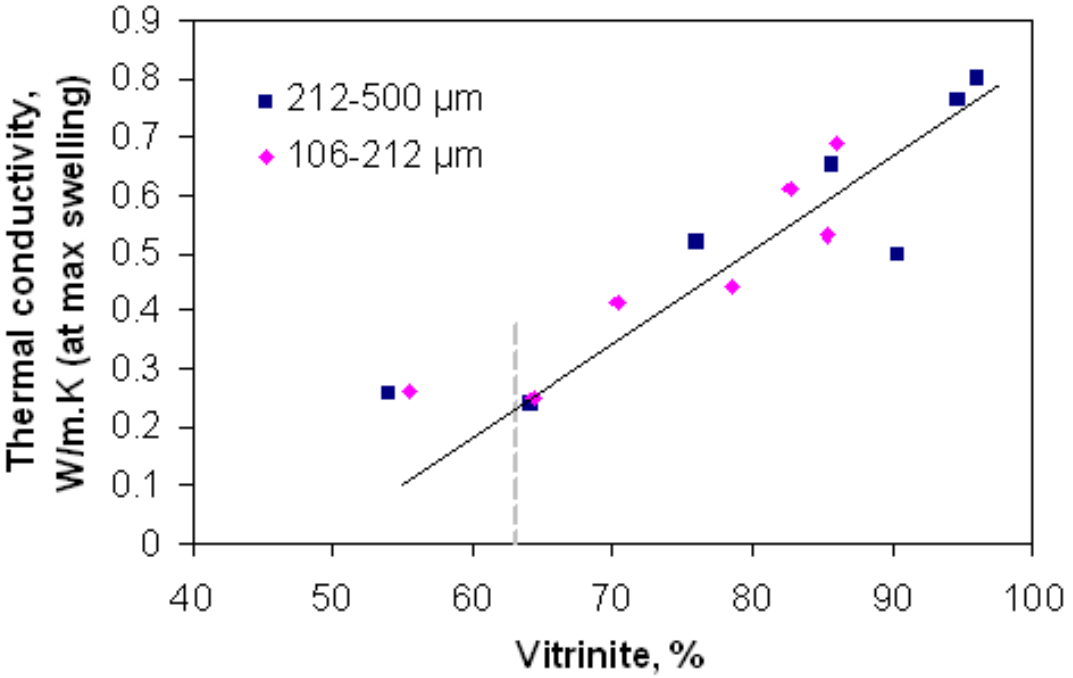

Figure 6.20. Relationship between the thermal conductivity at the maximum swelling (at about 510°C) and the vitrinite content for the 106-212 µm and 212-500 µm size cuts of coal maceral concentrates at a heating rate of 10°C/min.

Figure 6.21 indicates that the temperatures for the onsets of swelling and the primary exothermic reaction decrease linearly with increasing vitrinite content independent of particle size. The difference between temperatures for the onsets of swelling and the primary exothermic reaction slightly broadened with increasing vitrinite content. As swelling relates to exothermic reactions, therefore, it can be concluded that, for the concentrates with high vitrinite content, the initial exothermic reactions progress at a lower rate, although they begin at a lower temperature.

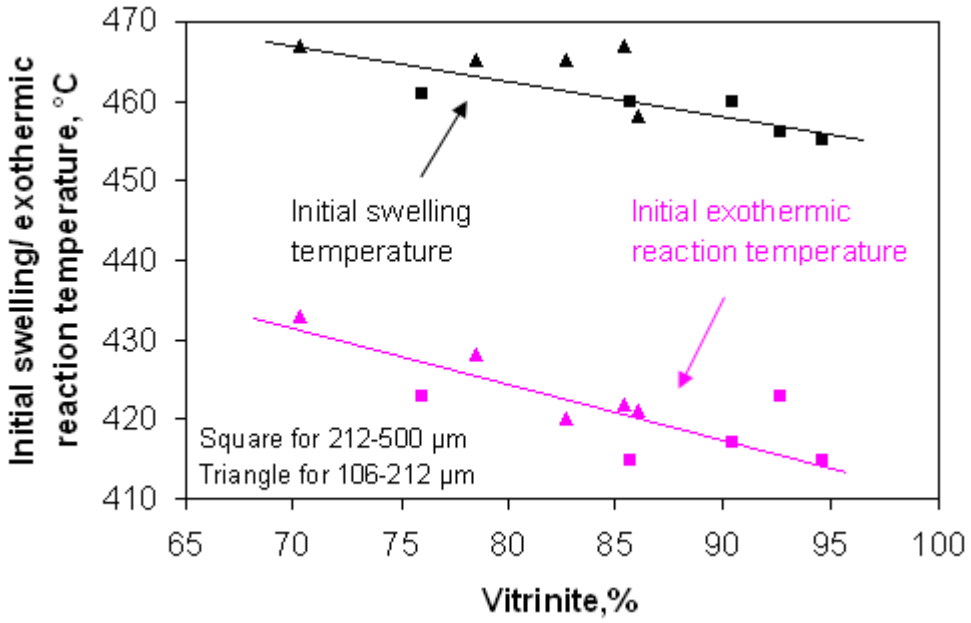

Figure 6.21. Relationship between the temperatures for the onset of swelling, primary exothermic reaction and the vitrinite content for the 106-212 µm and 212-500 µm size cuts of coal maceral concentrates at a heating rate of 10°C/min.

6.3.3.3 Results for coke properties

This section reports the densities of cokes formed from different coal maceral concentrates for the purpose of studying the porosity of cokes. The density of coke on a dry ash free (daf) basis was calculated based on mass and the final length of coke, moisture and ash contents of coal maceral concentrate.

During the transformation of coal to coke at a heating rate of 10°C/min from 25 to 1000°C, all samples were packed to a length of 20 mm. The final length of coke was measured using vernier callipers. Figure 6.22 indicates that the final length of coke increased linearly with the vitrinite content when the vitrinite content was above 63%, which was consistent with the relationships of the maximum swelling at about 510°C (Figure 6.14) and high temperature absolute contraction from 600°C to 1000°C (Figure 6.15) with vitrinite content. Coke lengths for all samples were close to the original packed coal lengths (20mm) when the vitrinite content was below 60%, which was consistent with the observations that there was little swelling for inertinite rich concentrates.

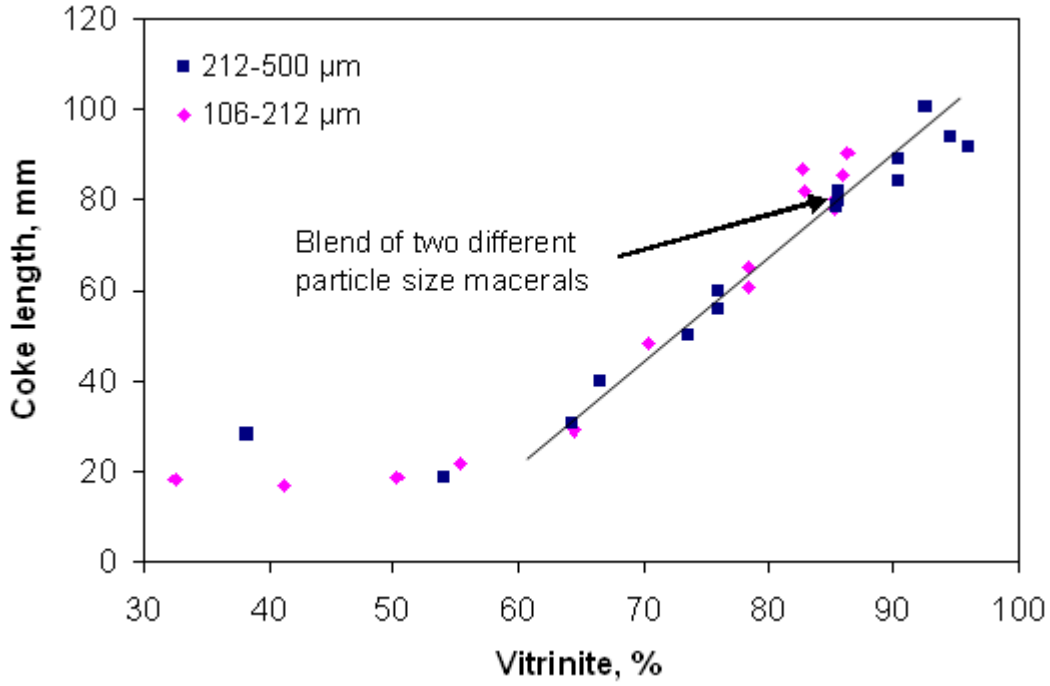

Figure 6.22. Final coke length for all coal maceral concentrates at a heating rate of 10°C/min from 25 to 1000°C.

Figure 6.23 shows that the coke density decreased with increasing vitrinite content, which indicates that cokes formed from high vitrinite content samples were more porous than that of the low vitrinite content samples. This complements the observation from the optical microscopy results in Figure 6.10. In terms of coal maceral concentrates with the vitrinite content above 90%, there was no distinct difference in coke density due to the high degree of swelling and low ash content. However, for coal maceral concentrates with vitrinite contents less than 40%, the coke density decreases with decreasing vitrinite content. This may be attributed to the high ash content (Figure 6.2). For the blend consisting of two vitrinite rich concentrates (85.4% vitrinite, 106-212 µm and 85.7% vitrinite, 212-500 µm), the final length and density of coke also match the relationships observed in Figure 6.22 and Figure 6.23. This is because particle size has little effect on the high extent of swelling, although it causes a significant effect on high temperature absolute contraction.

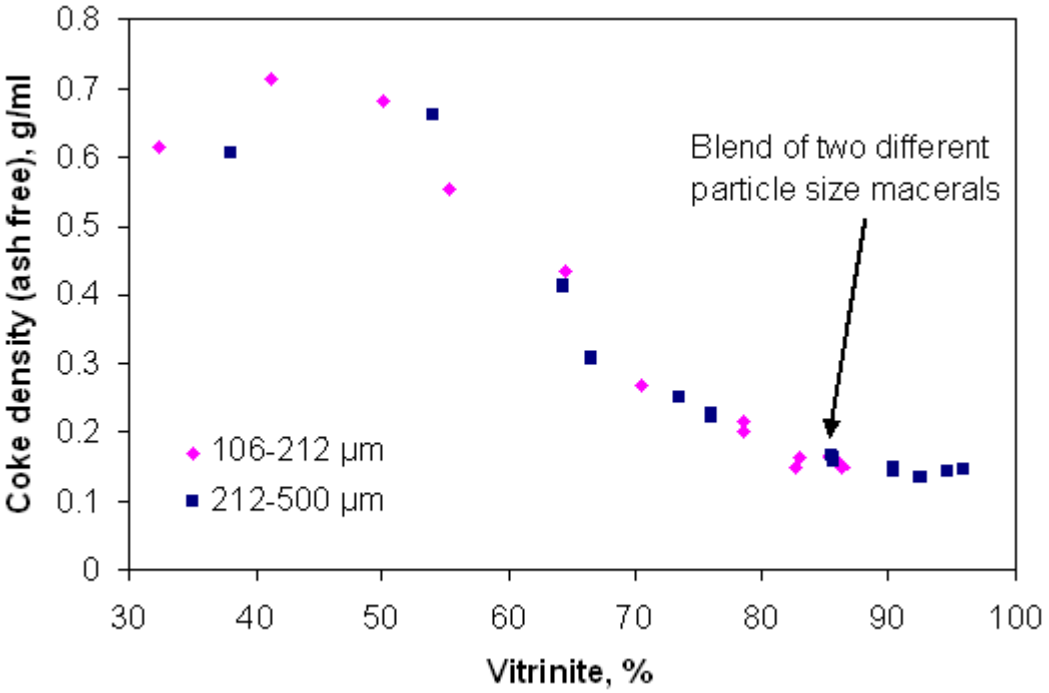

Figure 6.23. Coke densities (ash free) against vitrinite content for all coal maceral concentrates at a heating rate of 10°C/min from 25 to 1000°C.

6.4 Conclusions

- It is possible to obtain a wide range of vitrinite and inertinite rich concentrates using the reflux classifier to separate coal maceral concentrates by density and particle size. In comparison with separation for the original coal slurry without controlling particle size distributions, completing size cuts to the coal prior to separation based on density using the reflux classifier results in a better separation of the coal maceral components.

- For all separated coal maceral concentrates, ash content and relative density decreased with increasing vitrinite content. For vitrinite rich concentrates, particle size did not significantly influence ash content and relative density. However, for coal maceral concentrates with low vitrinite content, in particular, when the vitrinite content was below 63%, ash content and relative density increased with particle size.

- For both particle size ranges of 106-212 µm and 212-500 µm, vitrinite rich concentrates were found to contribute to swelling, exothermic reactions and the increase of thermal conductivity between 400 and 550°C. For the coal maceral concentrates studied, temperatures for the onsets of swelling and exothermic reactions decreased with increasing vitrinite content.

- For coal maceral concentrates with vitrinite contents above 63%, maximum swelling (around 510°C), high temperature absolute contraction (between 600 and 1000°C), exothermic heat of reactions during the primary devolatilisation, and thermal conductivity at the maximum swelling all increased linearly with increasing vitrinite content independent of particle size. This observation can be explained based on a swelling model, namely, vitrinite content relates to the amount of metaplast formed, which directly impacts the degree of swelling. The metaplast melds or bonds all particles and is therefore particle size independent. Therefore, swelling is linearly proportional to vitrinite content and independent of particle size. For inertinite rich coal maceral concentrates, the low content of vitrinite decreases the extent of metaplast, and the swelling correspondingly decreases.

- Densities of cokes from high vitrinite concentrates decreased with increasing vitrinite content; however, cokes from high inertinite concentrates did not match this relationship due to the high ash contents. In addition, there was no distinct difference between vitrinite content and coke density when vitrinite content was above 90% due to its high extent of swelling and low ash content. Optical microscopy results indicate that cokes from high vitrinite concentrates were more porous than that from low vitrinite concentrates.

Chapter 7 Estimated permeability from the measured pressure drop

7.1 Introduction

Understanding in the development of swelling, permeability and heats of pyrolytic reactions and their correlations between each other during carbonization of coal maceral concentrates will help in revealing the various mechanisms involved in the transformation of coal to coke. However, there is only few literature available that correlated physical changes, such as swelling and permeability, and thermal reactions, such as heat of coal devolatilisation.

Swelling, endothermic and exothermic reactions and thermal conductivity individually as well as their correlation between each other for heating coals and coal maceral concentrates have been evaluated in Chapters 4-6. Chapter 6 revealed that the vitrinite rich concentrates separated from high swelling coal showed a large intergranular swelling due to large plasticity. The intermediate plastic phase is considered to be the result of thermal chemical reactions [20, 36]. During the primary devolatilisation (400-600°C), chemical pyrolysis produces a number of gases and tars; however, not all gases and tars can escape from the viscous plastic material immediately [20]. The difficulty of gases and tars passing through the heating coal pellet relates to higher molecular weight tars vapour pressure [20], and the low permeability of heating coal pellet [145]. Coal permeability can be defined by a lumped index of how well fluid passes through coal [79]. With the increase of viscosity, permeability of the heating coal pellet decreases; it becomes difficult for gases and tars to escape from the heating coal pellet. Therefore, gas bubbles with very high internal pressure may form to swell the viscous mass. When primary devolatilisation is complete, the viscosity decreases so that the corresponding permeability increases. Therefore, low permeability is very important when determining the ability of a specific coal to give rise to high coking pressure and volumetric swelling [58, 111]. However, it is difficult to directly estimate the permeability of the heating coal pellet experimentally. Since it was shown that the low permeability can lead to an increase of the pressure drop of gas flowing through the coal sample [17, 72, 105, 106], the measurement of pressure drop of gas flowing through the sample has been employed to estimate the permeability of the heating coal pellet. The transient permeability coefficient k (m^2) of the heating coal pellet can be estimated using the Darcy's law, which has been described in Chapter 3. The equation is as follows

$$\frac{\Delta P}{L} = \frac{1}{k}\mu U$$

ΔP is the pressure drop of gas flowing through the coal sample expressed in Pa, μ is the viscosity of the carrier gas of argon expressed in Pa.s, changes of argon viscosity with temperature was based on data in Perry's chemical engineer's handbook [168]. U is the carrier gas velocity in m/s, L is the length of the packed bed of coal in m, which was calculated according to the LVDT measurement. Down stream pressure was assumed to be atmospheric. The effect of the release of volatile matter during coal devolatilisation on gases flow for the estimation of permeability is also discussed.

This Chapter correlates the swelling and permeability along with thermal properties including endothermic and exothermic reactions and thermal conductivity for heating coal maceral concentrates. Experiments were performed on the basis of the novel CATA technique with simultaneously introducing a Linear Variable Displacement Transducer (LVDT) and a pressure transducer, which is capable of investigating the swelling and pressure drop of gas flowing through the coal sample besides the apparent specific heat and thermal conductivity. Permeability of the heating coal pellet was estimated based on the Darcy's law with the combination of instantaneous pressure drop, swelling, viscosity and velocity of the carrier gas of argon.

A suite of coal maceral concentrates separated from the 106-212 μm size cuts of coal sample B were selected for the evaluations of swelling and pressure drop of gas flowing through coal sample, along with synchronised identification of endothermic and exothermic reactions and thermal conductivity during coke formation. All pyrolysis experiments were conducted at a heating rate of 10°C/min from 25 to 1000°C. Two coal maceral concentrates of vitrinite contents 86.4% and 64.4% were selected to emphasize the correlations between swelling, pressure drop of gas flowing through coal sample, endothermic and exothermic reactions and thermal conductivity. These two coal maceral samples were named B_8 (86.4% vitrinite) and B_6 (64.4% vitrinite) for Gieseler Plasticity analysis, the results are summarized in Table 7.1. As the swelling characteristics of inertinite concentrates are insignificant, the permeability of inertinite concentrates was not evaluated here. The results for the relative density, ash content and petrographic analysis for all the samples were presented in Chapter 6.

Table 7.1. Coal maceral concentrates properties.

Maceral Name	B_8	B_6
Vitrinite (% mmf)	86.4	64.4
Inertinite (% mmf)	13.6	35.6
R_{vMax}, %	1.47	1.51
Relative density (g/ml)	1.31	1.38
Ash, %	2.0	9.6
Gieseler Plasticity		
Initial softening temperature (°C)	425	435
Maximum fluidity temperature (°C)	470	475
Resolidification temperature (°C)	500	495
Plastic range (°C)	75	60
Maximum fluidity (ddpm)	90	10

7.2 Reproducibility of swelling, pressure drop, permeability, apparent specific heat and thermal conductivity

To check the reproducibility, the experiments were repeated three times and the experimental results showed good reproducibility. The results from the three runs for swelling, pressure drop, permeability along with apparent specific heat and thermal conductivity for the 86.4% vitrinite concentrate are shown in Figures 7.1-7.5. The graphs clearly showed the repeatability. The temperatures for characterising apparent specific heat and thermal conductivity in Figures 7.4 and 7.5 were estimated based on the control temperature and measured surface and centre temperatures of sample (section 3.1.2.2). The temperatures for describing swelling, pressure drop of gas flowing through the coal sample, permeability of coal pellet in Figures 7.1-7.3 are the measured surface temperatures of sample, which may be 5-10°C higher than the temperature estimated for characterising the apparent specific heat and thermal conductivity.

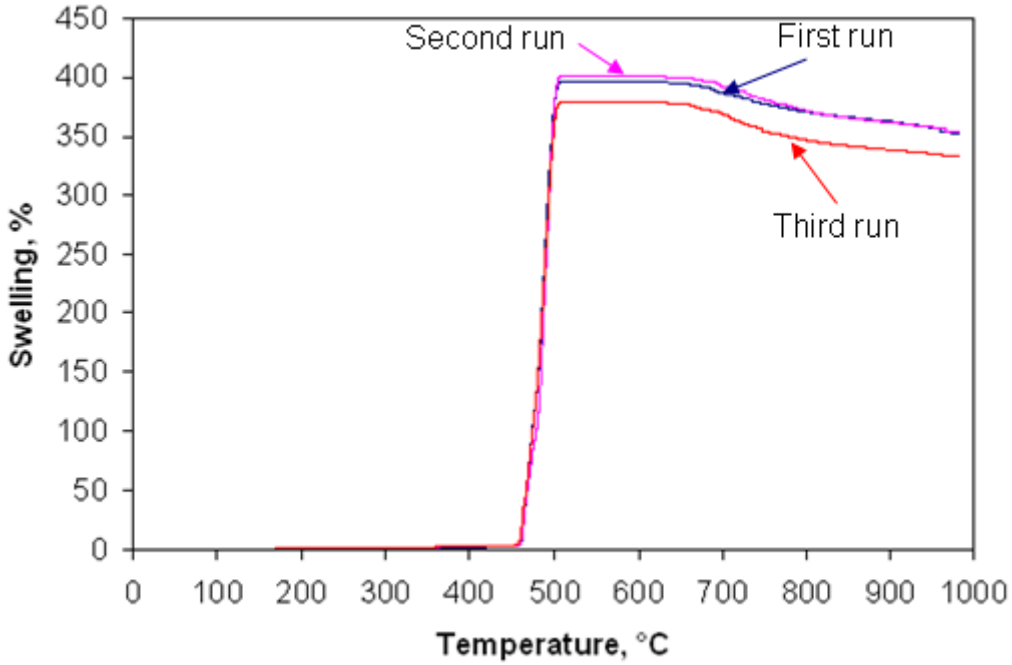

Figure 7.1. Swelling of the 86.4% vitrinite concentrate at a heating rate of 10°C/min from 25 to 1000°C for three replicate experiments.

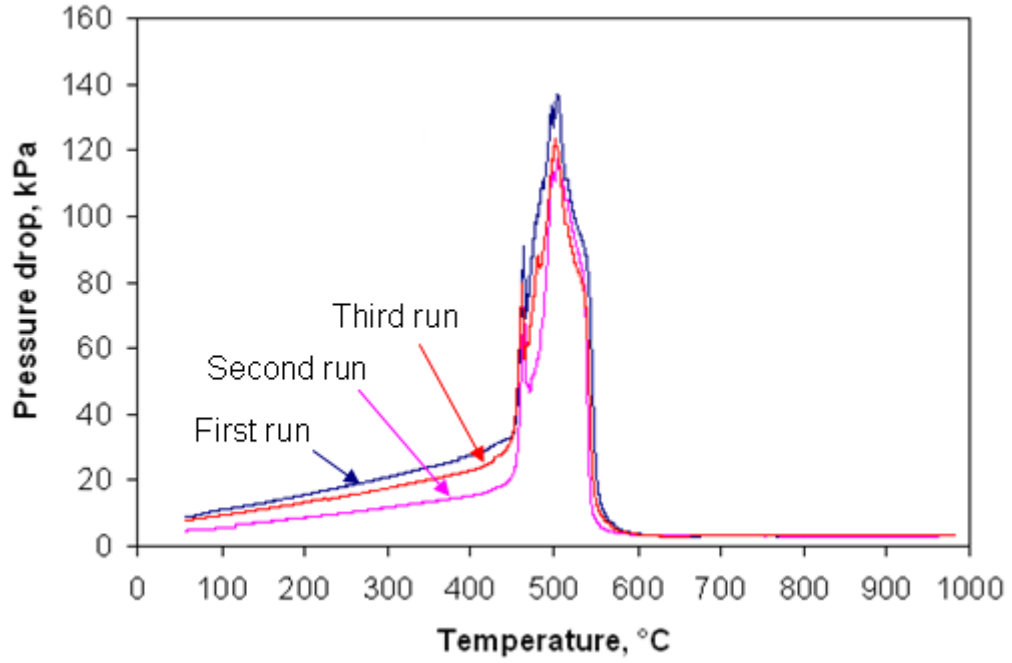

Figure 7.2. Pressure drop of the 86.4% vitrinite concentrate at a heating rate of 10°C/min from 25 to 1000°C for three replicate experiments.

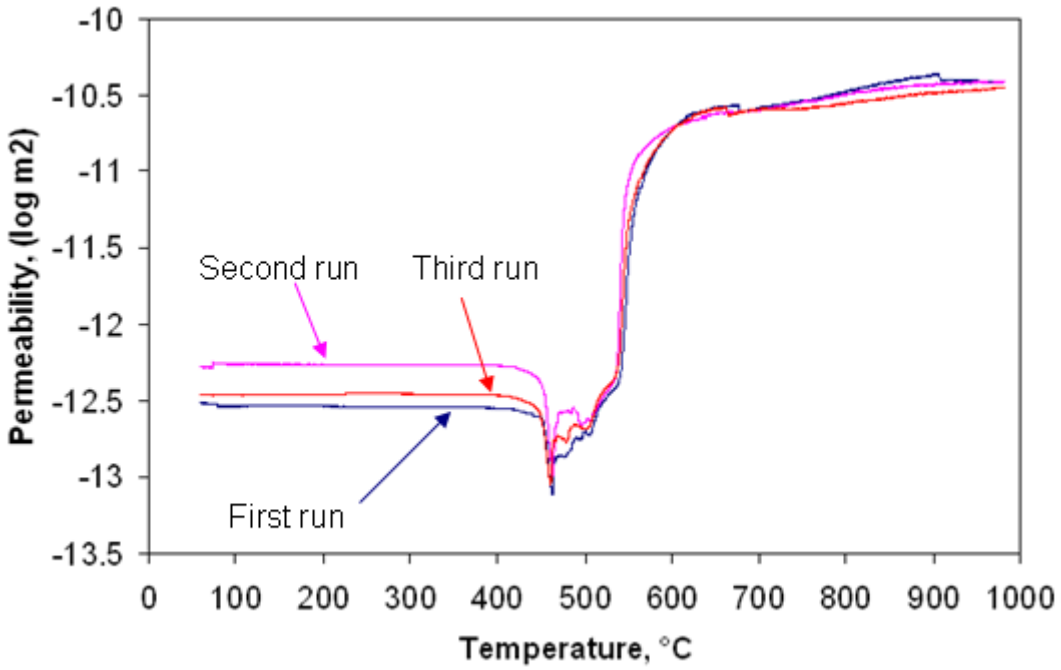

Figure 7.3. Permeability of the 86.4% vitrinite concentrate at a heating rate of 10°C/min from 25 to 1000°C for three replicate experiments.

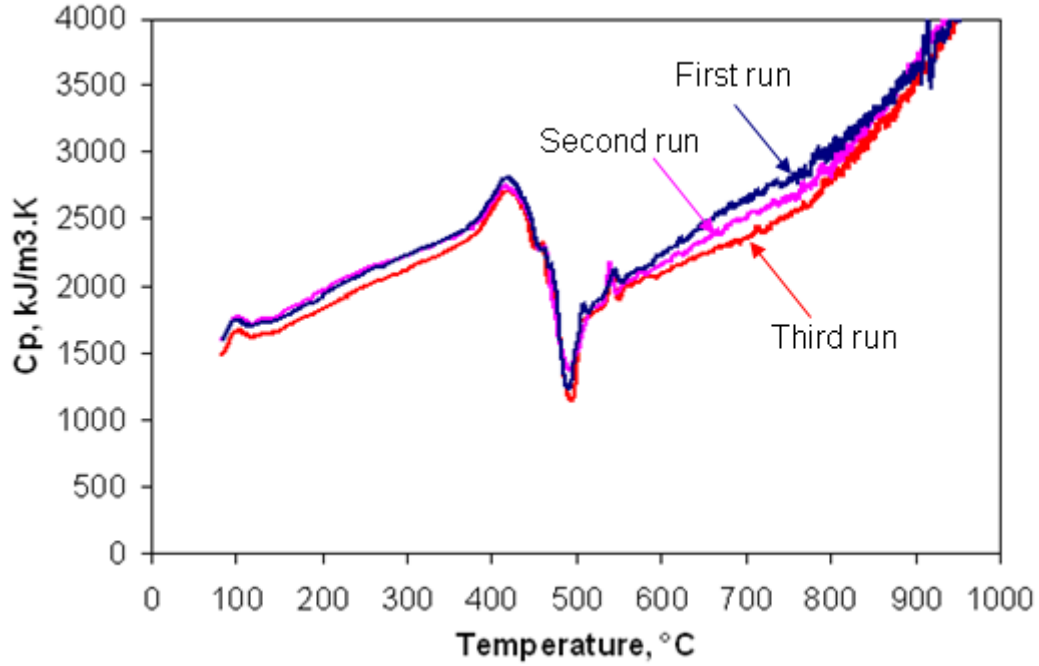

Figure 7.4. Apparent specific heat of the 86.4% vitrinite concentrate at a heating rate of 10°C/min from 25 to 1000°C for three replicate experiments.

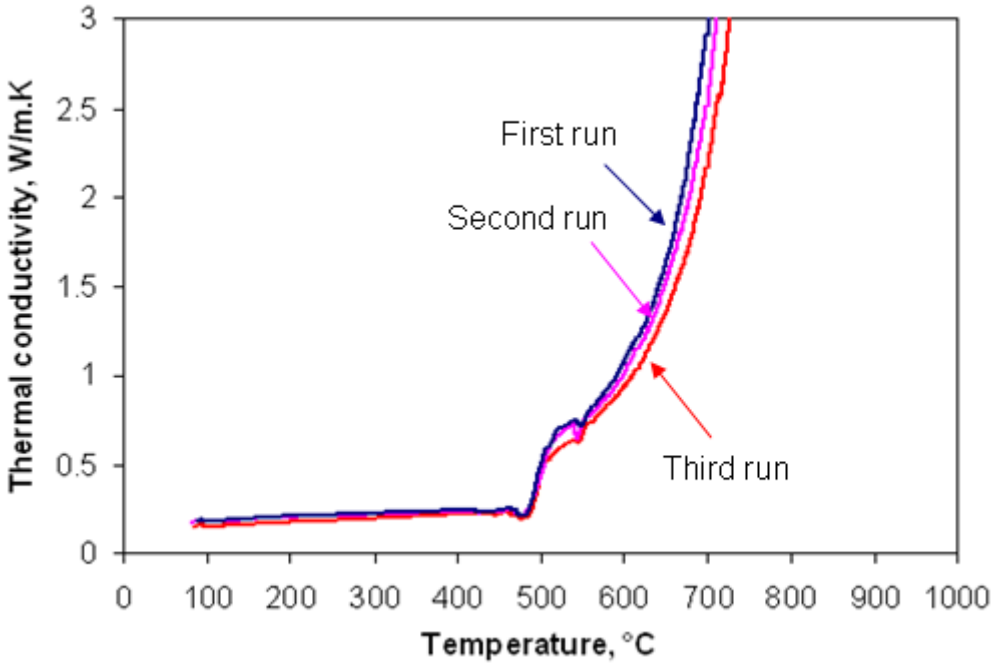

Figure 7.5. Thermal conductivity of the 86.4% vitrinite concentrate at a heating rate of 10°C/min from 25 to 1000°C for three repeated experiments.

Figure 7.1 indicates that the 86.4% vitrinite concentrate began to swell at 453°C and reached the maximum of about 400% at 506°C. Above 676°C, a high temperature contraction was observed up to 1000°C. The results obtained from the three runs for the maximum swelling at 506°C showed a maximum difference of 20% between them indicating a relative error of ±5%. The initial temperature of swelling was almost the same in all three experiments and the trends in swelling and shrinkage with temperature were also similar. Two main peaks for pressure drop of gas flowing through the coal sample were observed with increasing temperature, as seen in Figure 7.2. The temperatures at which peaks pressure drop appeared were almost the same in all three repeated experiments. Combining Figure 7.1 and Figure 7.2, the first peak about 80 kPa occurred at 464°C, which was 10°C higher than the initial swelling temperature. The second peak about 120 kPa occurred at 506°C corresponding to the maximum swelling temperature. Although the trends of pressure drop with temperature were the same for all three experiments, differences in absolute values of pressure drop existed because of experimental errors associated with the initial packed kaowool on both sides of the packed sample. The trends in permeability with temperature were similar with the results published earlier [106], although absolute values of permeability coefficient k (m^2) of the heating coal pellet differed from the reported data because of the difference in coal properties and experimental conditions, i.e., coal bed expansion was previously limited [106]. The permeability of the heating coal pellet began to decrease at 405°C and reached a minimum at 464°C corresponding to the first peak pressure drop. It slowly increased between 464 and

494°C due to consecutive swelling. Between 494 and 506°C, the permeability slightly decreased again because the low swelling rate in this stage. At 506°C, swelling and the primary exothermic reaction identified by the apparent specific were complete, permeability began to increase again but at a low rate. Between 546 and 676°C, permeability rapidly increased followed by a slow increase above 676°C, as seen in Figure 7.3. As permeability of the heating coal pellet was estimated based on Darcy's law, it can be affected by the velocity and viscosity of flowing gas. Therefore, the effect of the release of volatile matter on gases flow for the calculation of permeability was also discussed. It was found that about 4.50% error can be observed if the release of volatile matter with temperature was considered as carrier gas argon to calculate the transient permeability.

Figure 7.4 shows that the apparent specific heat of the 86.4% vitrinite concentrate obtained from all the three runs shows good reproducibility. It has been described in Chapter 4 that the peak of the apparent specific heat represents endothermic reactions while the trough indicates exothermic reactions. Below 100°C, the apparent specific heat is about 1500 kJ/m^3·K. A trough in the apparent specific heat from 450 to 510°C is attributed to the primary devolatilisation, which is an exothermic reaction stage. This was discussed detailedly in Chapters 4-6. Prior to this exothermic trough, an endothermic peak at around 415°C was observed. Another endothermic peak at about 545°C appeared, and this peak corresponded to the rapid fall in the pressure drop in Figure 7.2. Thermal conductivity obtained from all the three runs showed a constant value of 0.23 W/m·K until the exothermic reactions occurred. A slight decrease in thermal conductivity was obtained prior to its quick increase at around 480°C due to volumetric swelling which affected the concentration of liquid in the plastic material. The thermal conductivity reached 3 W/m·K at about 700°C, as shown in Figure 7.5.

7.3 Correlations of pressure drop, swelling and thermal changes

This section correlates the pressure drop, swelling and thermal properties for two coal maceral concentrates with vitrinite contents 86.4% and 64.4%, respectively. Figures 7.6 and 7.7 show the correlations between swelling, pressure drop, apparent specific heat and thermal conductivity for two coal maceral concentrates on heating. It can be seen that both the coal maceral concentrates showed two main peaks in pressure drop within 450 to 580°C. Swelling began to develop prior to the first peak in pressure drop and reached the maximum at the second peak. Endothermic and exothermic reactions and the successive changes of thermal conductivity were observed with the progress of the two peaks of pressure drop. This indicates the association of physical changes with thermal reactions. The changes in pressure drop, swelling and thermal conductivity are mainly attributed to the release of volatiles (gases

and tars) that affected the viscosity, fluidity and internal pressure of the metaplast during thermal reactions.

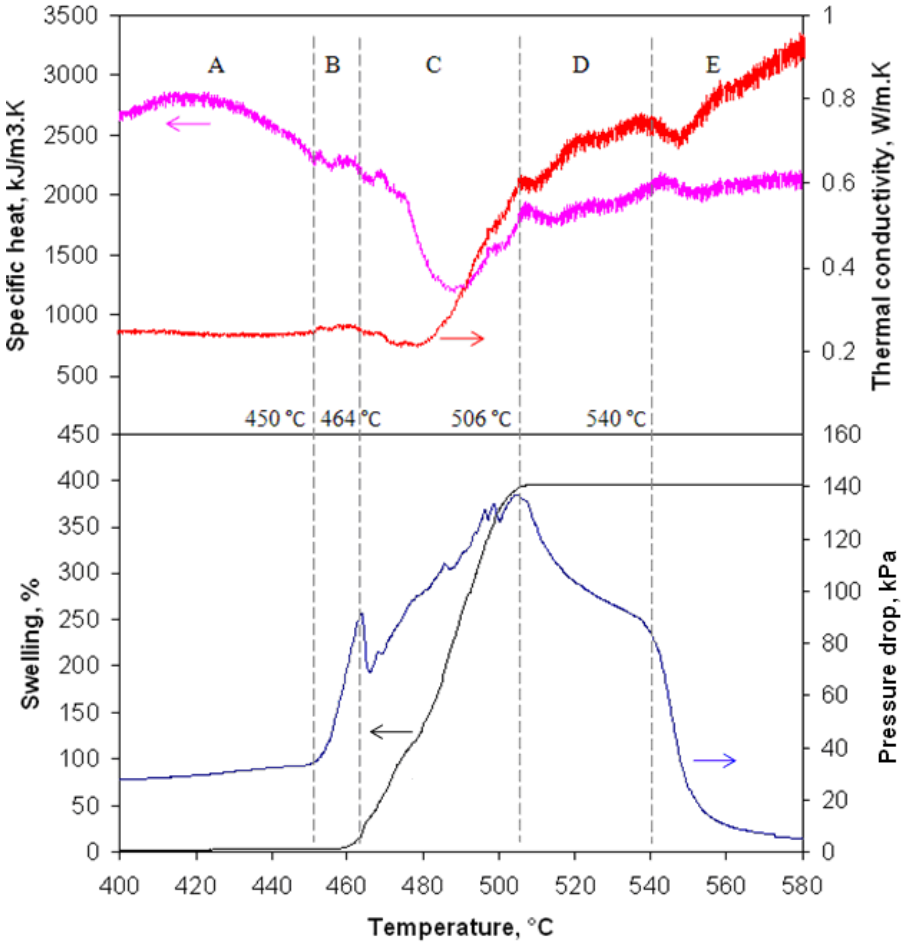

Figure 7.6. Correlation between swelling, pressure drop of gas flowing through the coal sample, apparent specific heat and thermal conductivity for the 86.4% vitrinite concentrate at a heating rate of 10°C/min.

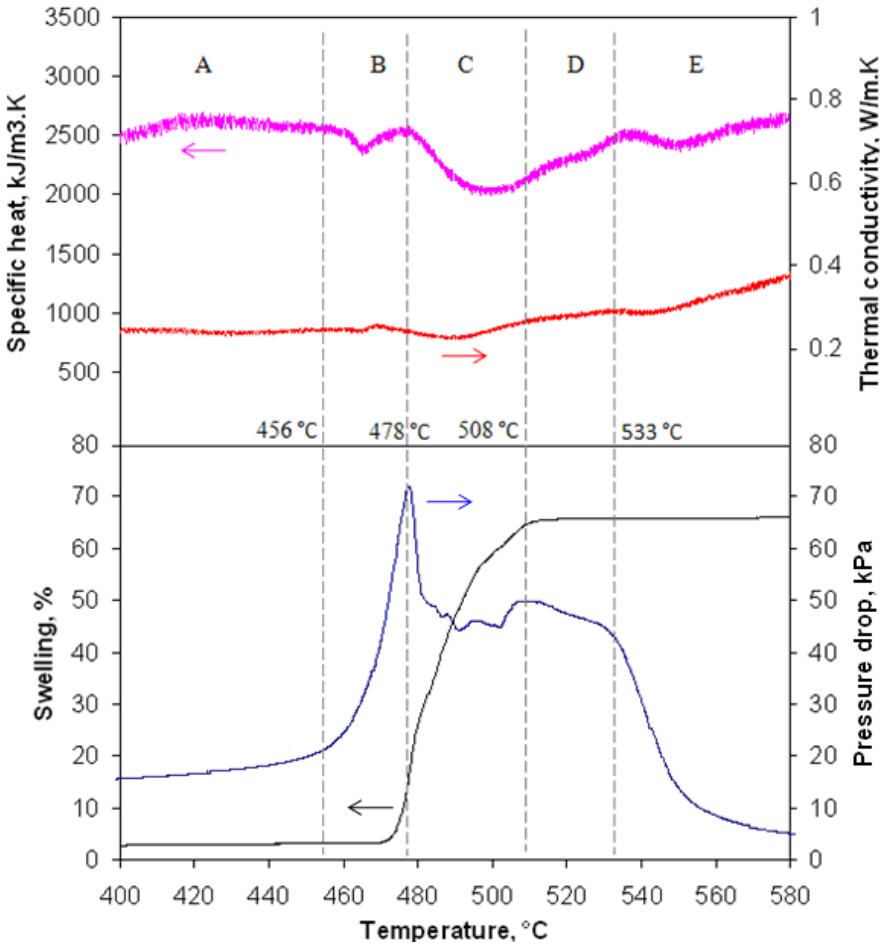

Figure 7.7. Correlation between swelling, pressure drop of gas flowing through the coal sample, apparent specific heat and thermal conductivity for the 64.4% vitrinite concentrate at a heating rate of 10°C/min.

According to the results in Figures 7.6 and 7.7, the pressure drop, swelling, apparent specific heat and thermal conductivity can be divided into five regions (A to E), they are presented as follows

- In region A (below 450°C), there is an endothermic peak at around 415°C for both the coal maceral concentrates, which relates to softening and the primary devolatilisation. There is little change for thermal conductivity, swelling and pressure drop.
- In region B (450-480°C), a small exothermic trough is observed due to the partial evolution of volatiles. Pressure drop and thermal conductivity slightly increase with temperature and swelling begins. The partial evolution of volatile matter was evidenced by the observation of tars in the inner surface of the outlet of the quartz when the heating sample was quenched at 450°C for the 86.4% vitrinite concentrate. The quenched sample was agglomerating as a continuous material rather than remaining as discrete particles. This indicates that the softening and partial evolution

of volatile matter has commenced prior to the increase of pressure drop and thermal conductivity. In Gieseler Plasticity test, the softening temperature at a heating rate of 3°C/min is 425°C for the 86.4% vitrinite concentrate and 435°C for the 64.4% vitrinite concentrate, respectively. In addition, the first derivative curve of TG curve from TG-DTG experiments also shows that at a heating rate of 10°C/min the primary devolatilisation starts to develop at around 400°C, as shown in Figure 7.8.

- In region C (480-510°C), a large trough for apparent specific heat is observed, which indicates the primary exothermic reaction. For the 86.4% vitrinite concentrate, a large amount of tars adhered to the inner surface of the outlet of the quartz when the heating sample was quenched at 506°C. DTG curve shows that the weight loss rate of the heating sample continues to increase, reaches the maximum at 506°C, and then decreases, as seen in Figure 7.8. Pressure drop firstly decreases due to rapid swelling followed by an increase due to a large number of volatile matter release. Thermal conductivity firstly undergoes a slight decrease followed by a rapid increase due to the changes of the concentration of liquid in the metaplast.

- In region D (510-540°C), weight loss rate decreases after peak devolatilisation, heating sample approaches the resolidification temperature [17]. The swelling is complete and the pressure drop decreases. An overlap of the endothermic and exothermic processes relates to heat reactions and tar vaporization due to the primary devolatilisation. Thermal conductivity keeps on increasing with temperature, but at a relatively low rate.

- In region E (540-580°C), pressure drop keeps on decreasing, and the process is at a higher rate than that in region D due to tar evaporation and the end of the primary devolatilisation. A small peak of the apparent specific heat is observed relating to tar vaporization and the secondary reaction, correspondingly, a small dip in thermal conductivity appears. Beyond region E, the thermal conductivity shows a continuous increase with temperature, the reasons have been discussed in Chapters 4. They include: (a) radiant heat transfer across pores and cracks; (b) changes in the thermal conductivity of the coals due to pyrolysis; (c) changes in the intrinsic conductivity with temperature of char [20, 85], (d) a numerical artefact (the estimated thermal conductivity is affected by heats of reactions) associated with heat build-up in the packed bed. When thermal conductivity reached 2-3 W/m·K and beyond [19], the difference between measured surface and centre meta-plastic material temperatures was in a very narrow range or thermal inversion between surface and centre of heating sample occurred, hence results became unstable. The correlations of pressure drop, swelling, endothermic and exothermic reactions (identified by apparent specific

heat) and thermal conductivities of heating coal maceral concentrates are also summarized in Table 7.2.

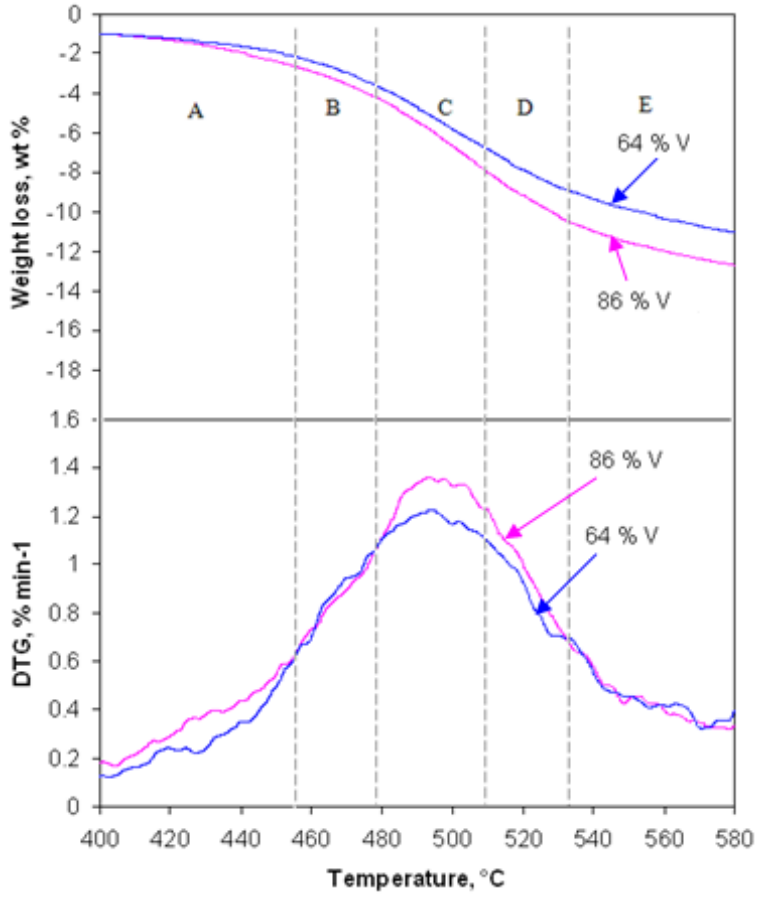

Figure 7.8. TG-DTG results for the 86.4% and 64.4% vitrinite concentrates at a heating rate of 10°C/min.

Table 7.2. A summary of thermal-swelling properties for heating coal maceral concentrates.

Regions	Note
A	Pre-pyrolytic event, endothermic process relates to softening and the primary devolatilisation; little change in thermal conductivity, swelling, and pressure drop.
B	Pyrolytic event, exothermic process due to softening and partial devolatilisation; thermal conductivity and pressure drop show a slight increase relating to fluidity and plasticity, swelling begins to develop.
C	Pyrolytic event, exothermic process relates to the primary devolatilisation; thermal conductivity decreases first then increases relating to liquid concentration; rapid increase in swelling; pressure drop decreases first due to rapid swelling followed by an increase due to a large number of volatile matter release.
D	An overlap of the endothermic and exothermic processes relates to heat reactions and tar vaporization due to the primary devolatilisation; thermal conductivity continues to increase but at a relatively low rate due to the decrease of the liquid concentration, pressure drop decreases and swelling is complete.
E	Endothermic process relates to tar vaporization and the secondary devolatilisation, correspondingly, a small dip for thermal conductivity appears; pressure drop decreases at a higher rate than that in region D due to tar evaporation and the end of the primary devolatilisation.

7.4 Effect of coal maceral components on pressure drop and permeability

Chapters 5-6 revealed that during the primary devolatilisation high vitrinite concentrates caused a higher swelling and a larger exothermic reaction as well as a higher thermal conductivity than the high inertinite concentrates. The initial temperatures at which the physical and thermal changes occurred decreased with increasing vitrinite content. These were consistent with the plasticity properties from Gieseler Plastometer analysis, although the results were measured at a heating rate of 3°C /min. Figure 7.9 indicates that the high vitrinite concentrate initiated the increase of pressure drop at a lower temperature than the low vitrinite concentrate from 450 to 580°C. The pressure drop at the second peak was larger than that in the first peak for the 86.4% vitrinite concentrate but an opposite trend for the 64.4% vitrinite concentrate was observed. Figure 7.10 indicates that the second pressure drop at the maximum swelling (510°C) increased linearly with the vitrinite content, which is the similar trend with swelling against the vitrinite content in Chapter 6, indicating the relevance of pressure drop and swelling.

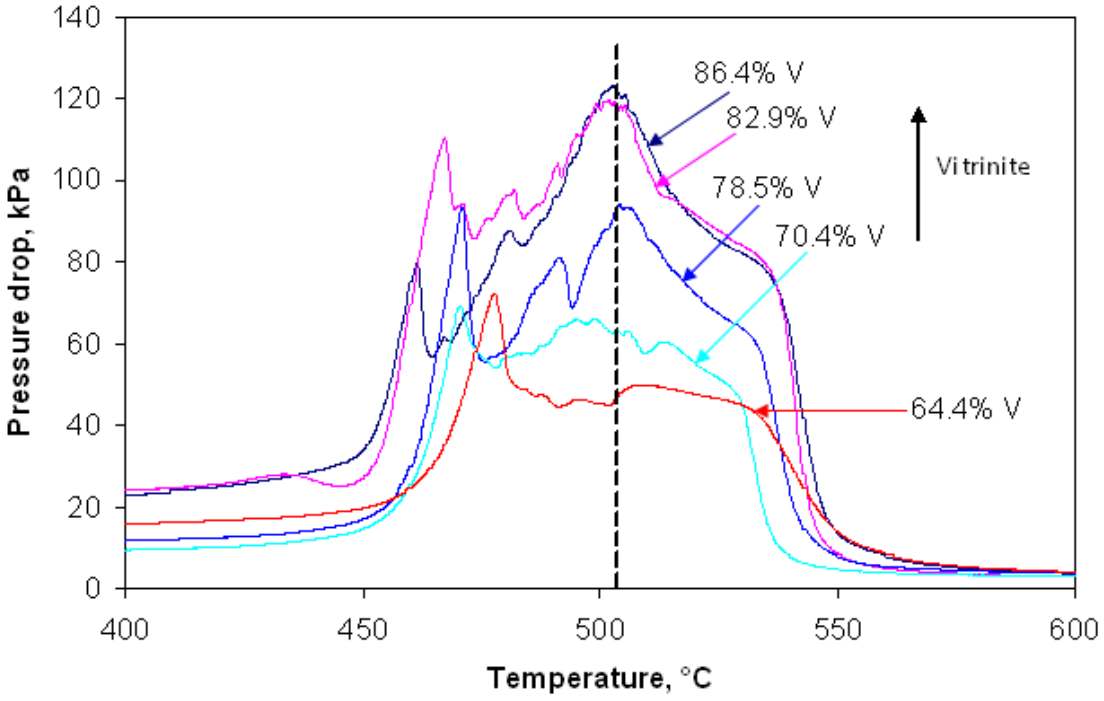

Figure 7.9. Pressure drop of gas flowing through the coal maceral concentrates at a heating rate of 10°C/min.

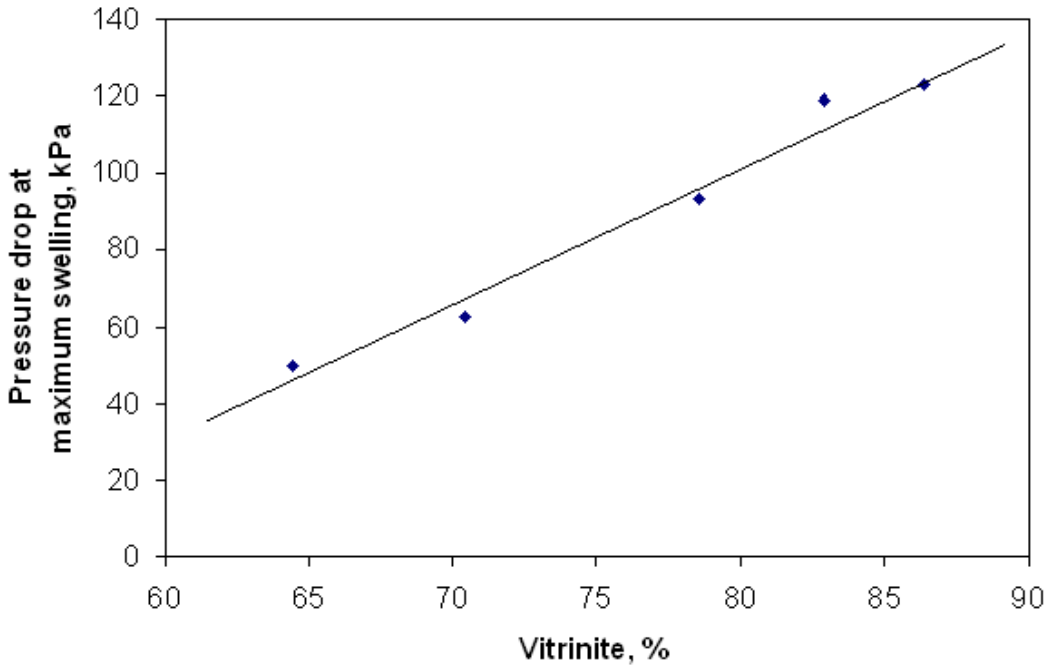

Figure 7.10. Relationship between pressure drop of gas flowing through the coal sample at maximum swelling and vitrinite content for coal maceral concentrates at a heating rate of 10°C/min.

The changes of permeability with temperature for two coal maceral concentrates with vitrinite contents 86.4% and 64.4% are presented in Figure 7.11. It can be seen that the permeability began to decrease at a lower temperature for the 86.4% vitrinite concentrate than that of the 64.4% vitrinite concentrate. The minimum permeability occurred at 464°C for the 86.4% vitrinite concentrate and 478°C for the 64.4% vitrinite concentrate, corresponding to the first peak pressure drop. By comparison, Nomura et al. [17] previously considered the maximum pressure drop of gas flowing through the heating coal sample as the minimum permeability of the heating coal pellet. This may be attributed to the difference in the coal properties and the experimental conditions. Nomura restricted the expansion of coal sample in a constant volume cell. By comparison, the heating samples in these experiments showed a high extent of swelling. The swelling opened up the paths through which gas may escape. Also, swelling weakened the barrier from the fluid phase generated in the heating coal pellet, causing coalescence and decreasing the thickness of bubble wall. Thus, the permeability of heating coal pellet began to increase after somewhat swelling, corresponding the first peak pressure drop. Figure 7.8 indicates that prior to the first peak pressure drop the 86.4% vitrinite concentrate showed a higher volatile evolution rate than the 64.4% vitrinite concentrate. Therefore, a lower permeability for the 86.4% vitrinite concentrate was observed, as shown in Figure 7.11.

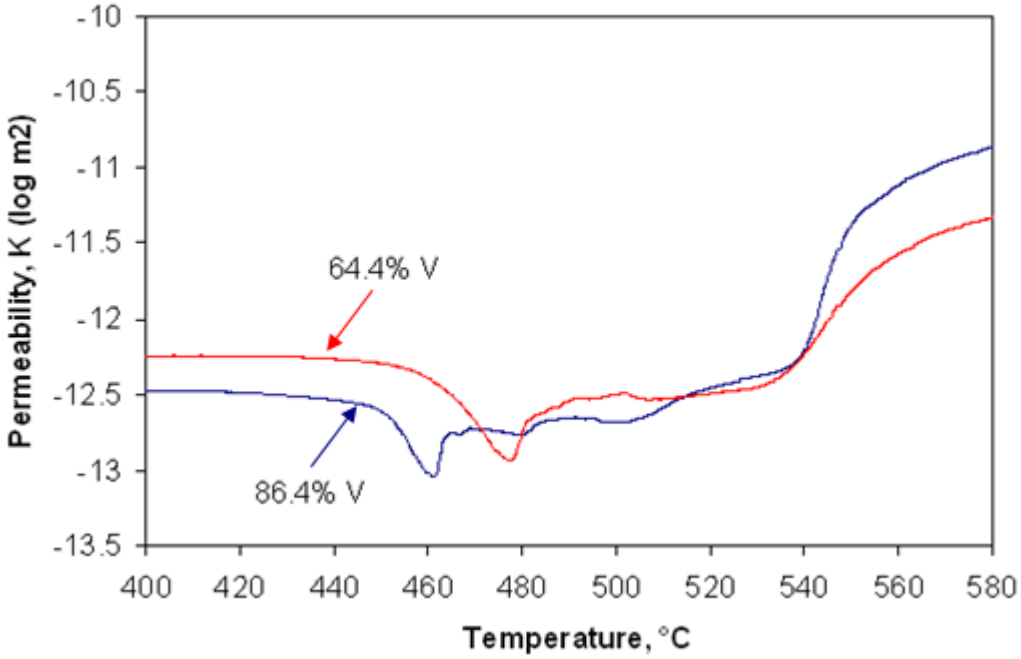

Figure 7.11. Estimated permeability based on Darcy law for coal maceral concentrates at a heating rate of 10°C/min.

7.5 Development of coke porosity and its association with swelling, permeability and thermal changes

The 64.4% vitrinite concentrate was used to investigate the development of porosity for the heating sample. Optical microscopy images of the sectioned sample at four different temperatures in Figure 7.12 indicate the development of pore network structure. The four different temperatures were the critical points applied to differentiate the five regions for physical and thermal changed of heating coal in Figure 7.7. At the early stage of devolatilisation at around 451°C (see Figure 7.8), the individual coal maceral particles were clearly distinguishable, and retained their angular shape. Some small micropores within the coal maceral particles were apparent. A large proportion of the porosity at this stage was inter-granular, and can be identified by the dark regions surrounding each particle. This porosity allowed some gas flow to occur, but the permeability remained relatively low due to the high packed density of the sample (~900 kg/m^3). At around 483°C, after the first observed peak of pressure drop, the coal particles fused with swelling rapidly increasing. Much of the inter-granular porosity visible at 451°C disappeared, while most of the newly formed pores remained closed. Consequently there was an overall drop in permeability (as seen in Figure 7.11) and correspondingly there was an increase in swelling (as seen in Figure 7.7) and weight loss rate (as seen in Figure 7.8). When the temperature reached the resolidification temperature (at around 512°C), the maximum weight loss rate and maximum swelling were observed; the apparent specific heat increased slowly with temperature after an exothermic

trough, with a similar trend for thermal conductivity being observed. At this temperature there was an apparent increase in porosity. However, the permeability was still lower than that at 451°C, which implies that the pore structure can still not facilitate gas escape. At 583°C, the permeability increased dramatically because of the decrease of plasticity of semi-coke.

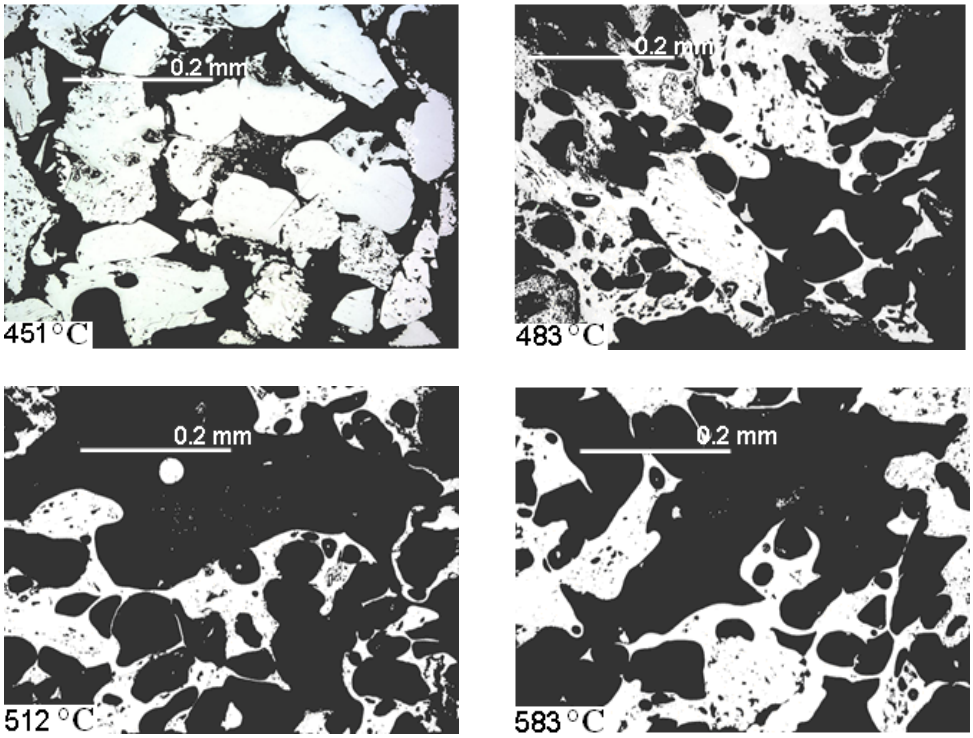

Figure 7.12. Optical microscopy images for the 64.4% vitrinite concentrate quenched at critical temperature points.

7.6 Conclusions

A suite of coal maceral concentrates separated from a bituminous coking coal with the same particle size distribution 106-212 μm but different vitrinite contents were employed to correlate thermo-physical aspects of heating coal maceral concentrates.

The conclusions from this Chapter may be summarised as follows

- The coal maceral concentrates gave two peaks in the pressure drop of gas flowing through the coal sample. The first peak was observed at softening and the early stage of the primary devolatilisation with slight volumetric swelling. The second peak was observed during the primary exothermic reaction associated with rapid swelling. The permeability of the heating coal pellet began to decrease prior to the onset of swelling and reached a minimum at the first peak pressure drop. A rapid increase in permeability did not occur until the beginning of the second exothermic reaction.

- The exothermic reaction during the primary devolatilisation can be further divided into two exothermic troughs, the first one being associated with particle softening and inter-granular agglomeration of particles, which caused a decrease in permeability and the onset of volumetric swelling of softened sample. The second trough was associated with the successive volumetric swelling and the increase of thermal conductivity, following the onsets of resolidification and the slow increase of permeability.

- Between 450 and 580°C, the high vitrinite concentrate showed a higher pressure drop, corresponding to a higher swelling, a larger exothermic reaction trough and a higher extent of increase in thermal conductivity than the low vitrinite concentrate. The initial temperatures, at which the pressure drop began to increase, decrease with the increasing vitrinite content. This complements the relationship of the initial temperature for swelling with the vitrinite content.

Chapter 8 The elemental compositions of volatiles evolved from heating size cuts of coal maceral concentrates

8.1 Introduction

The swelling and thermal properties of heating coals and coal maceral concentrates were evaluated in Chapters 4-7. It was found that at the temperature between 420 and 580°C the heating coal underwent the primary exothermic reaction identified by apparent specific heat. The primary exothermic reaction was accompanied by a rapid swelling and an increase of thermal conductivity. The changes in swelling, specific heat and thermal conductivity on heating coal relate to coal maceral softening and resolidification, such as the phase transformation of solid-metaplast-solid, and chemical reactions, such as depolymerisation and repolymerisation of organic molecules [20, 36]. A number of tars and gases were evolved during the depolymerisation and repolymerisation of organic molecules. The properties of gases and tars formed due to depolymerization of organic molecules determine the fluidity and viscosity of the plastic material, permeability of heating coal pellet and the release of gases and tars themselves [20, 36]. Therefore, the understanding in the properties of gases and tars is one of the keys in revealing the thermo-plasticity of heating coal and coal maceral concentrates. This Chapter uses the Dynamic Elemental Thermal Analysis (DETA) technique to investigate the chemical compositions of gases and tars formed during heating coal maceral concentrates. Identical coal maceral concentrates separated from the 106-212 μm size cuts of coal sample B were used in this investigation. Vitrinite content of these coal maceral concentrates varied from 32.4 to 86.4%. Details for the preparation of these samples were reported in Chapter 6.

The description, procedure and the calibration of the DETA technique have been detailed in Chapter 3. With this technique, the real-time elemental compositions of the released gases and tars from the heating coal maceral concentrates can be quantitatively estimated. The boiling point and elemental compositions of condensed and extracted tars from the heating coal maceral concentrates can also be estimated. The condensable tars were the condensable liquid rather than gases during coal devolatilisation. The extracted tars were the tars that can not be released during coal devolatilisation, but they can be extracted from semi-coke by some solvents [3]. In addition to analysing the properties of gases and tars, the DETA technique is capable of back calculating the instantaneous elemental distributions of pyrolytic residue of char. Figure 8.1 shows the typical results for the instantaneously elemental compositions of C, H, N, S and O by combusting the volatiles that were released by heating the 86.4% vitrinite

concentrate (106-212 μm) at a heating rate of 10°C/min from 25 to 1000°C. These results could be considered equivalent to an elemental TGA, though from a molar basis (as derived from a gas composition) rather than mass basis (as derived from a solid mass loss). Peaks for the total carbon and total hydrogen show that there are two main thermal regions: the primary devolatilisation at around 505°C and the secondary devolatilisation at around 745°C. The first region is dominated by the release of C and H, while the second region is dominated by H only. The consumption of oxygen during combusting the evolved gases and tars is shown in the upper half of the graph in volume percentage, which represents the oxygen concentration introduced to the combustion system. The curve at the lower half of the graph gives the instantaneous compositions of H (calculated from H_2O), C ($CO+CO_2$), S (SO_2) and N ($NO+NO_2$). The instantaneous oxygen concentration from the combusted products was obtained on the basis of the concentrations of H_2O, CO, CO_2, SO_2, NO and NO_2 as a function of temperature. Oxygen concentration evolved from volatile matter (gases and tars) or gases only with temperature was calculated based on the difference of oxygen between the produced oxygen concentration from combusted products and introduced (consumed) oxygen concentration. The results indicated that, when the total gas flow rate was 1564 mL/min, the maximum concentrations for hydrogen and carbon at 505°C were about 28000 and 14000 ppm per gram of sample, respectively. Nitrogen and sulphur concentrations were about 100 and 30 ppm per gram of sample, respectively.

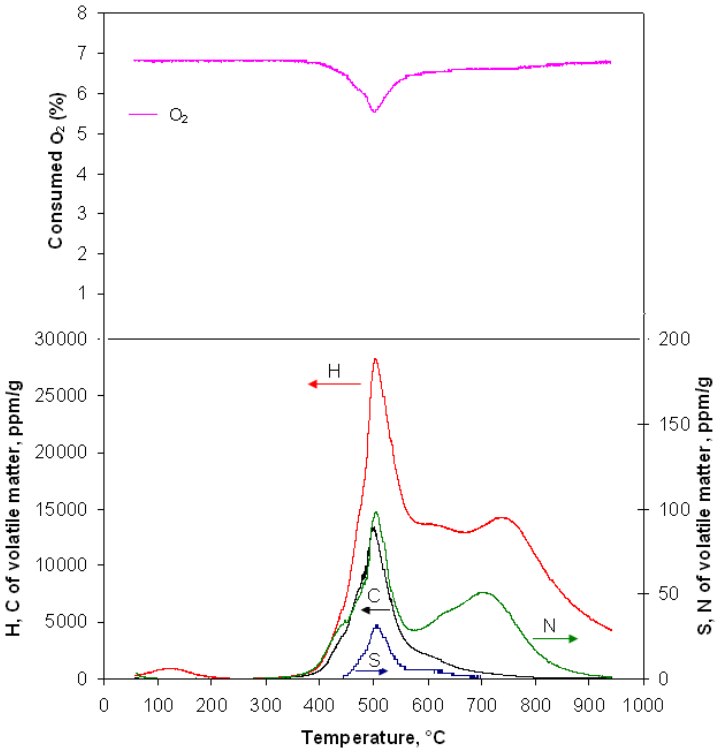

Figure 8.1. Instantaneous elemental compositions of C, H, N, S and O by combusting volatiles released from heating the 86.4% vitrinite concentrate at a heating rate of 10°C/min from 25 to 1000°C.

8.2 Elemental compositions of volatiles for various coal maceral components

8.2.1 Elemental compositions of volatiles

This section reports the elemental compositions of the evolved gases and tars for various coal maceral components. The literature review in Chapter 2 revealed that the dominant elements released during the transformation of coal to coke are carbon and hydrogen. Also, the same conclusions were observed in Figure. 8.1. The major release of gases and tars occurs at the primary devolatilisation (400-550°C). During the secondary devolatilisation, only light gases, such as H_2 and CO are released [20, 36]. Figures 8.2 and 8.3 give a comparison of the total hydrogen and carbon concentrations produced by combusting the total volatiles as they evolved from heating coal maceral concentrates with different vitrinite contents from 32.4% to 86.4%. The coal maceral concentrates with the same particle size of 106-212 μm but different vitrinite contents were heated at a heating rate of 10°C/min from 25 to 1000°C. Three peaks for hydrogen (H) concentration were observed for all heating coal maceral concentrates. The first peak appeared at around 110°C corresponding to moisture release, the second peak occurred at around 505°C relating to the primary exothermic reaction and contributing to the maximum swelling, the third peak was observed at 745°C and it is attributed to the secondary exothermic reaction with hydrogen released. However, there was only one peak for carbon (C) concentration at around 505°C, which corresponds to maximum swelling and primary exothermic reaction. The absence of a carbon peak at around 750°C indicates that only a low CO concentration was released during the secondary exothermic reaction. Peaks for hydrogen and carbon concentrations per gram of heating sample increased with vitrinite content except for the peak H at 110°C, which indicated that a high vitrinite content corresponds to a high evolution rate of volatiles.

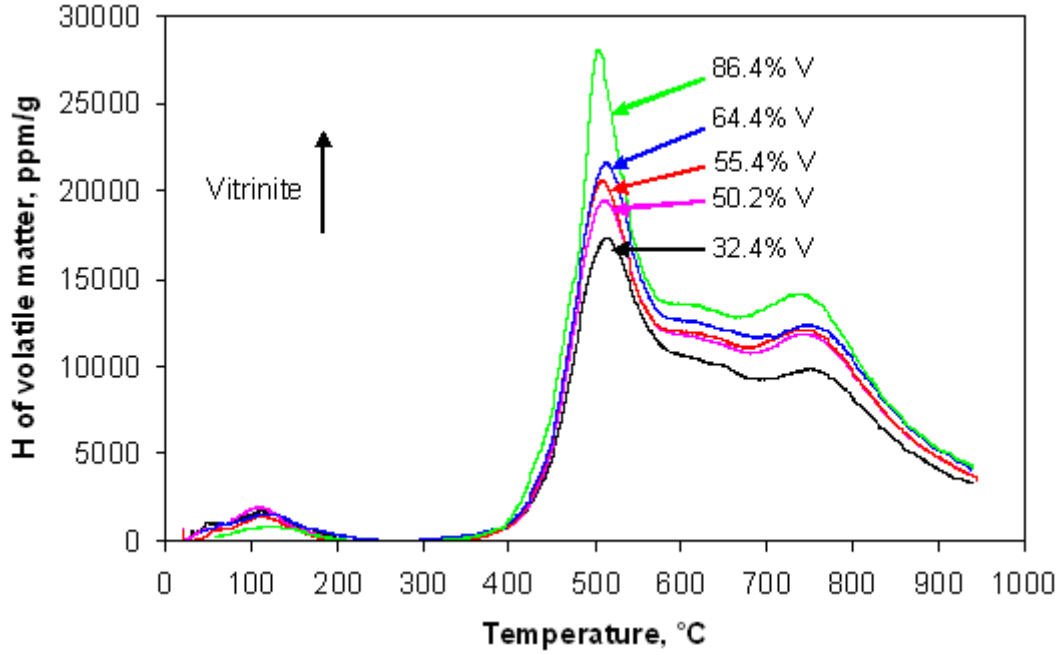

Figure 8.2. Hydrogen concentration of total volatiles for various coal maceral concentrates at a heating rate of 10°C/min from 25 to 1000°C.

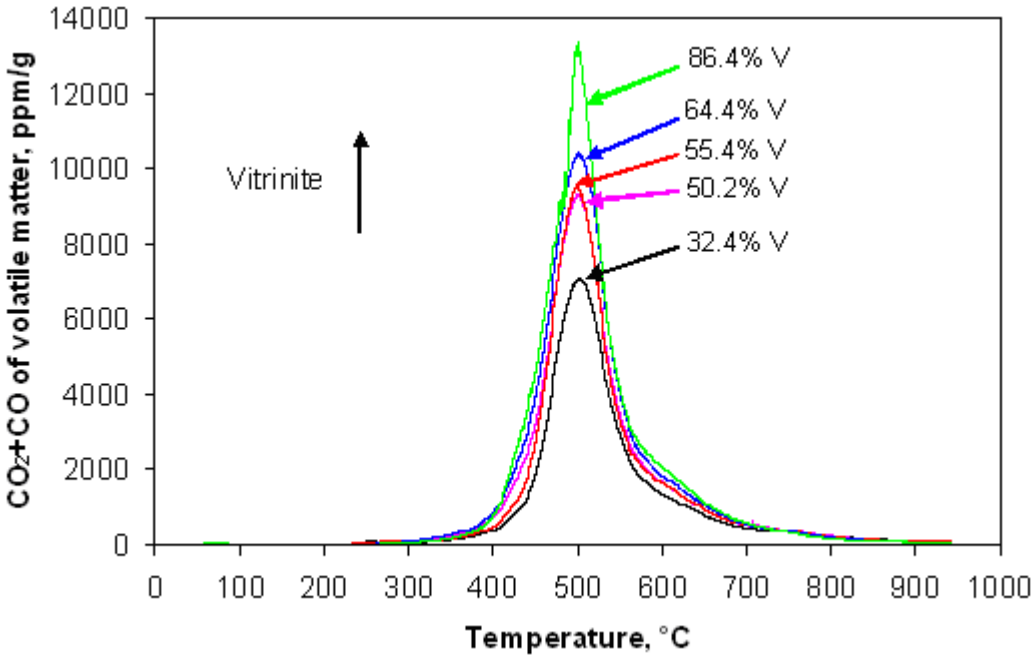

Figure 8.3. Carbon concentration of total volatiles for various coal maceral concentrates at a heating rate of 10°C/min from 25 to 1000°C.

Figure 8.4 (a) and (b) show the relationship between H/C of total volatiles and vitrinite content for various coal maceral concentrates with different vitrinite contents from 32.4% to 86.4%. Figure 8.4 (b) is a re-scaled result of Figure 8.4 (a) to exhibit H/C in the temperature from 400 to 600°C. During swelling and the primary exothermic reaction (400-510°C), it is difficult to differentiate the ratios of H/C from different coal maceral concentrates, except that

the 32.4 % vitrinite concentrate exhibited a higher H concentration, as seen in Figure 8.4 (b). Above 550°C, H/C exhibited the trend to decrease with vitrinite content. During the second exothermic reaction (700-950°C), higher the vitrinite content, higher the H/C was observed, as seen in Figure 8.4 (a). Since the main products during the second exothermic reaction are H_2 and CO [20, 36], this observation indicated that, during the secondary exothermic reaction, the vitrinite rich concentrates contain a higher ratio of organic bonds that tend to release H_2 rather than CO in comparison with the inertinite rich concentrates. Above 850 °C, the decrease of H/C for all coal maceral concentrates relates to the end of the secondary devolatilisation.

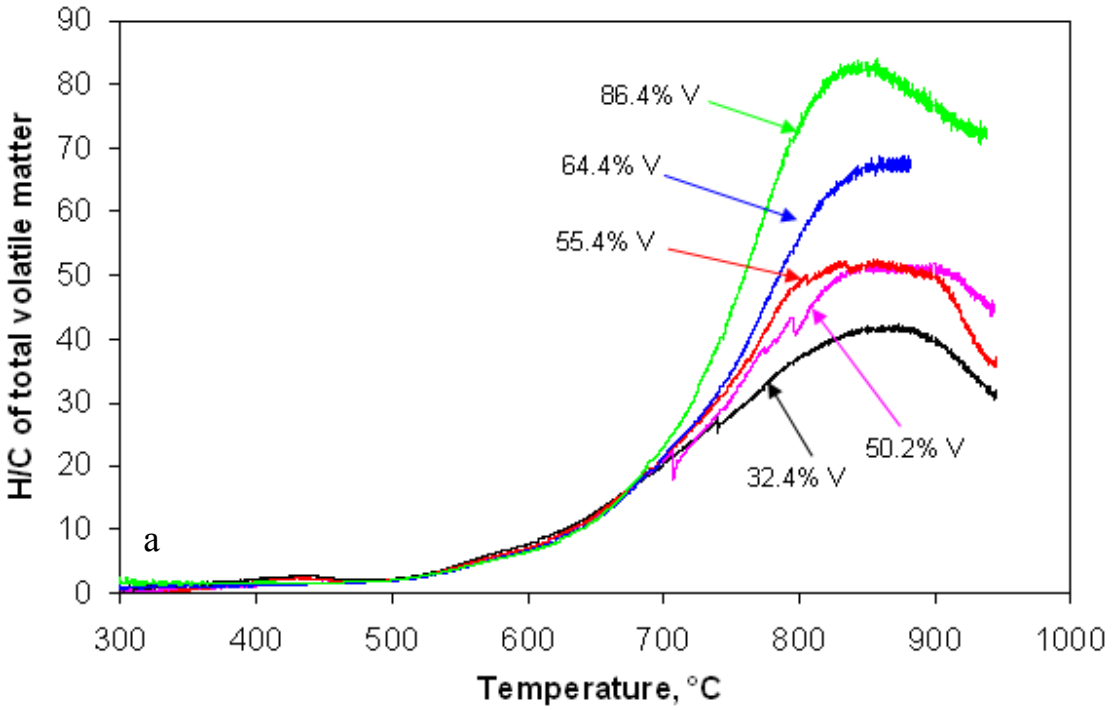

Figure 8.4 (a). The H/C of total volatiles for various coal maceral concentrates at a heating rate of 10°C/min from 25 to 1000°C.

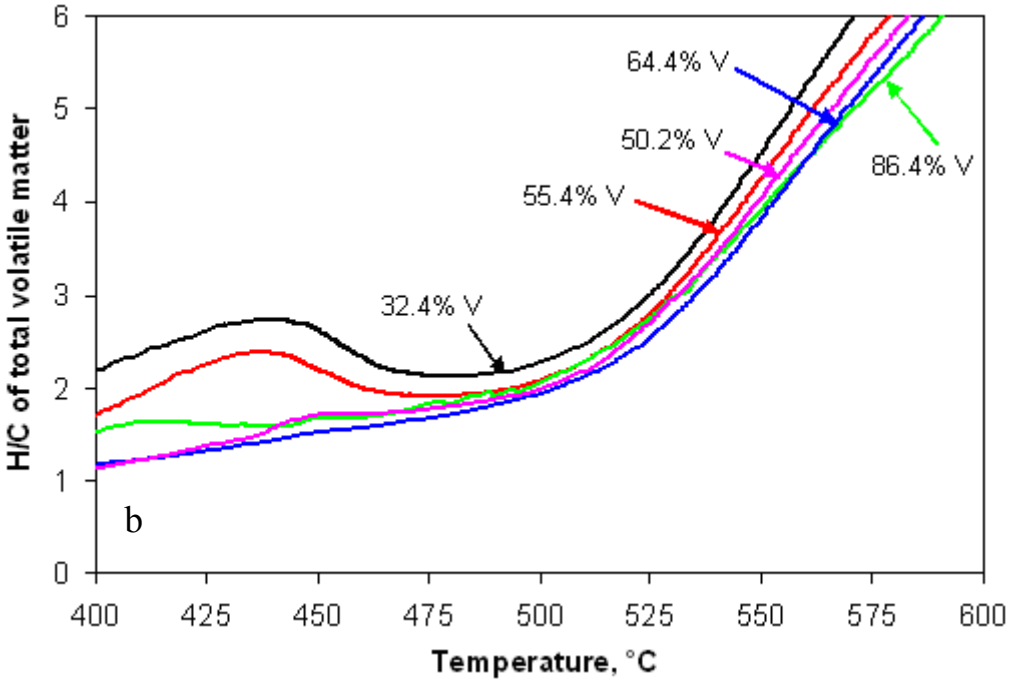

Figure 8.4 (b). A re-scaled H/C during the primary devolatilisation for Figure 8.4 (a).

8.2.2 Elemental compositions of gases and tars components of volatiles

This section analyses the elemental compositions of "gases only" and "tars only". The different modes of analysis in DETA technique was detailed in Chapter 3. Mode 3 represents the gas only combustion. By condensing out the tars and combusting the evolved gases in a secondary reactor in this mode in the DETA technique, the total volatiles may be further deconstructed into a "gas only" and a calculated "tar only" fraction or *"dynamic tars by difference"*. Three coal maceral concentrates comprising of one vitrinite rich concentrate (86.4% V), one medium vitrinite concentrate (64.4% V) and one inertinite rich concentrate (32.4% V) were used to study the release of carbon and hydrogen in volatiles, gas only and tar only. The results are shown in Figures 8.5-8.10. From these Figures, it can be observed that the initial volatile evolution consists predominantly of carbon heavy condensable tar species beginning at around 300°C, with hydrogen rich light gases production beginning at 380°C. The maximum evolution rate of tars and gases was observed at around 505°C. As there was no carbon in the *"dynamic tars" (Figure 8.6),* the secondary exothermic reaction evolved mainly hydrogen (H_2) (Figure 8.5), a small amount of H_2O (Figure 8.5) and CO (Figure 8.6).

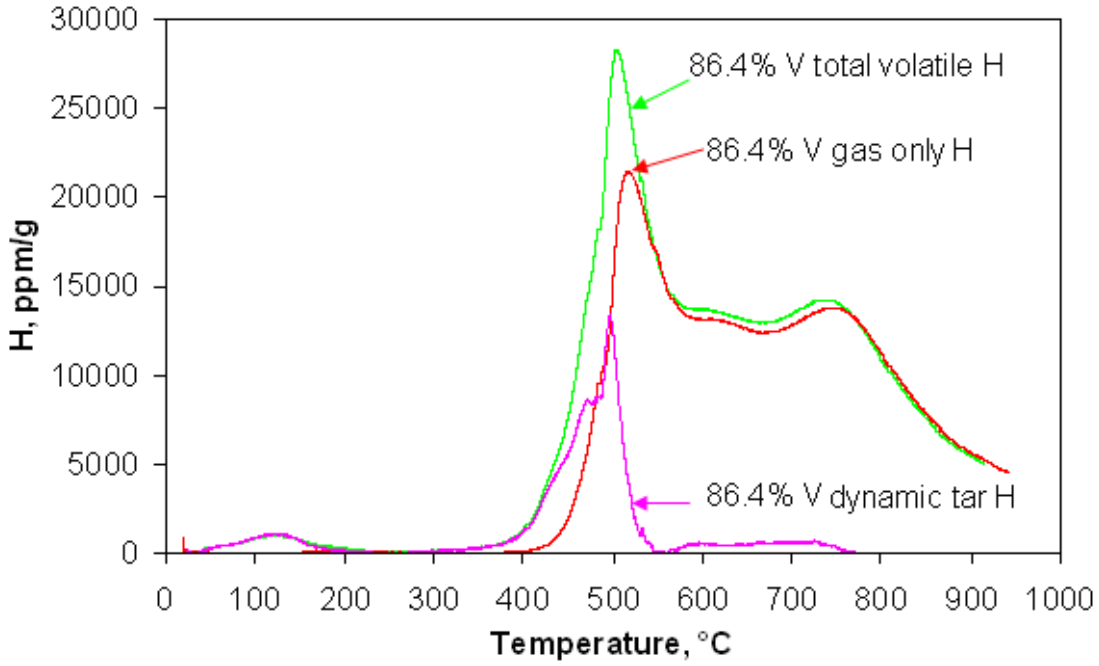

Figure 8.5. Hydrogen concentration for total volatile, gas only and mathematically derived dynamic tar for the 86.4% vitrinite concentrate at a heating rate of 10°C/min from 25 to 1000°C.

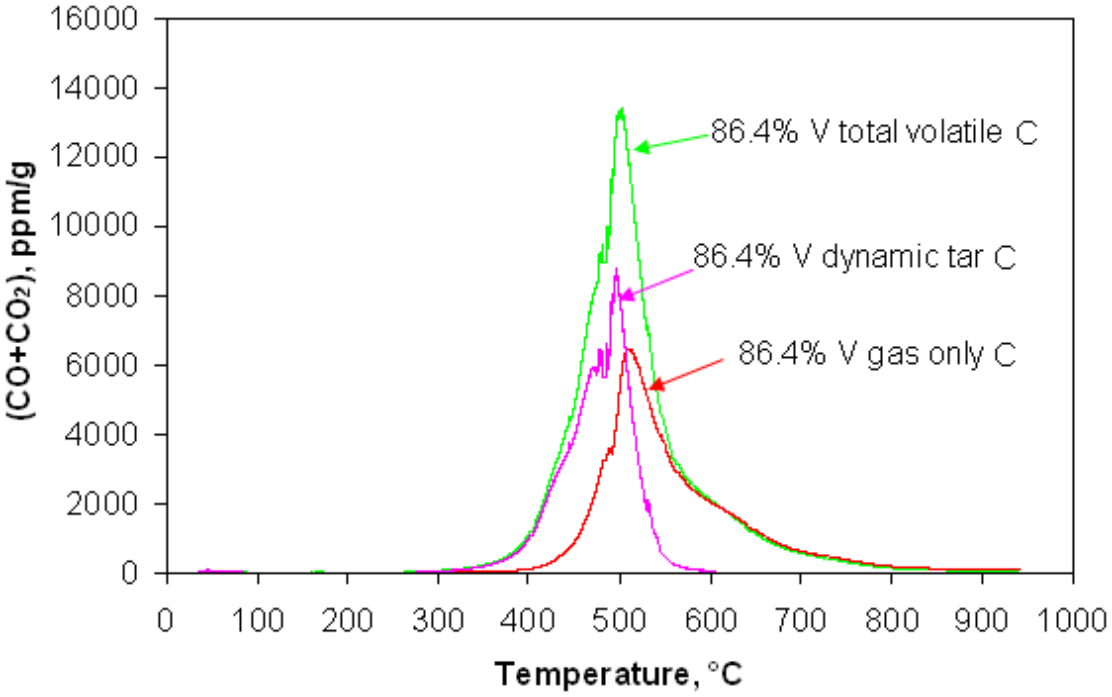

Figure 8.6. Carbon concentration for total volatile, gas only and mathematically derived dynamic tar for the 86.4% vitrinite concentrate at a heating rate of 10°C/min from 25 to 1000°C.

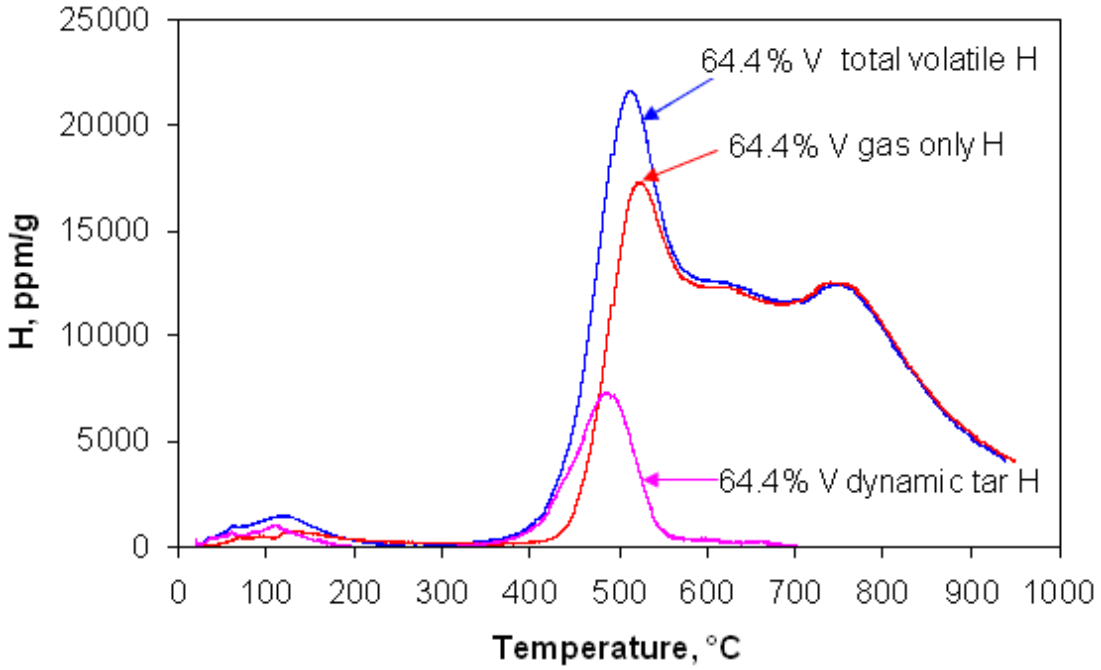

Figure 8.7. Hydrogen concentration for total volatile, gas only and mathematically derived dynamic tar for the 64.4% vitrinite concentrate at a heating rate of 10°C/min from 25 to 1000°C.

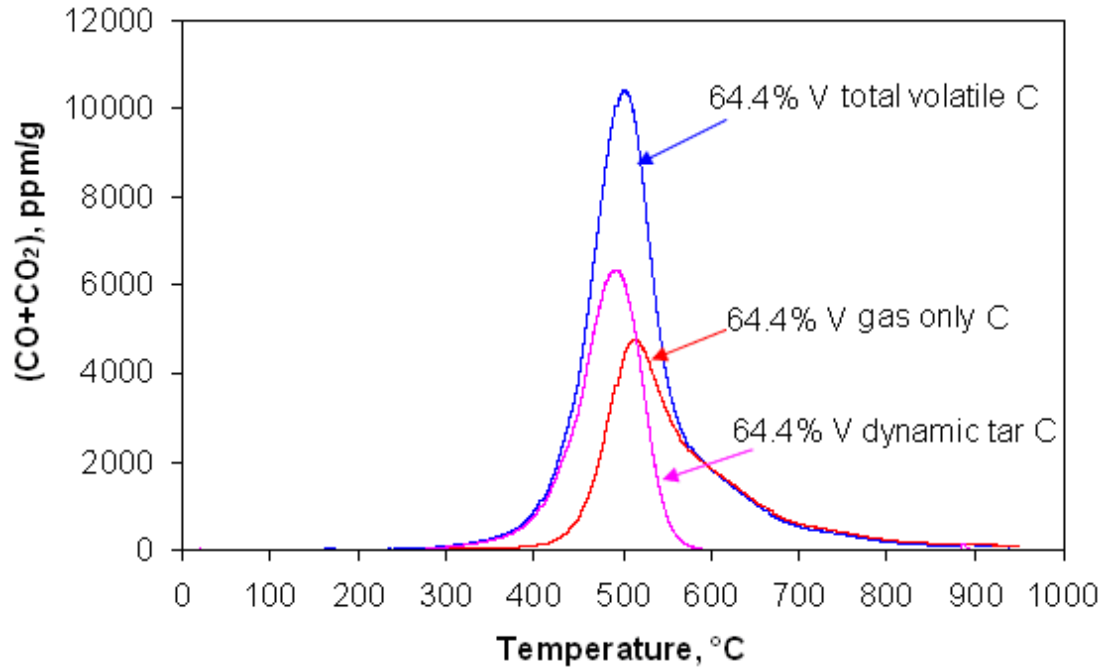

Figure 8.8. Carbon concentration for total volatile, gas only and mathematically derived dynamic tar for the 64.4% vitrinite concentrate at a heating rate of 10°C/min from 25 to 1000°C.

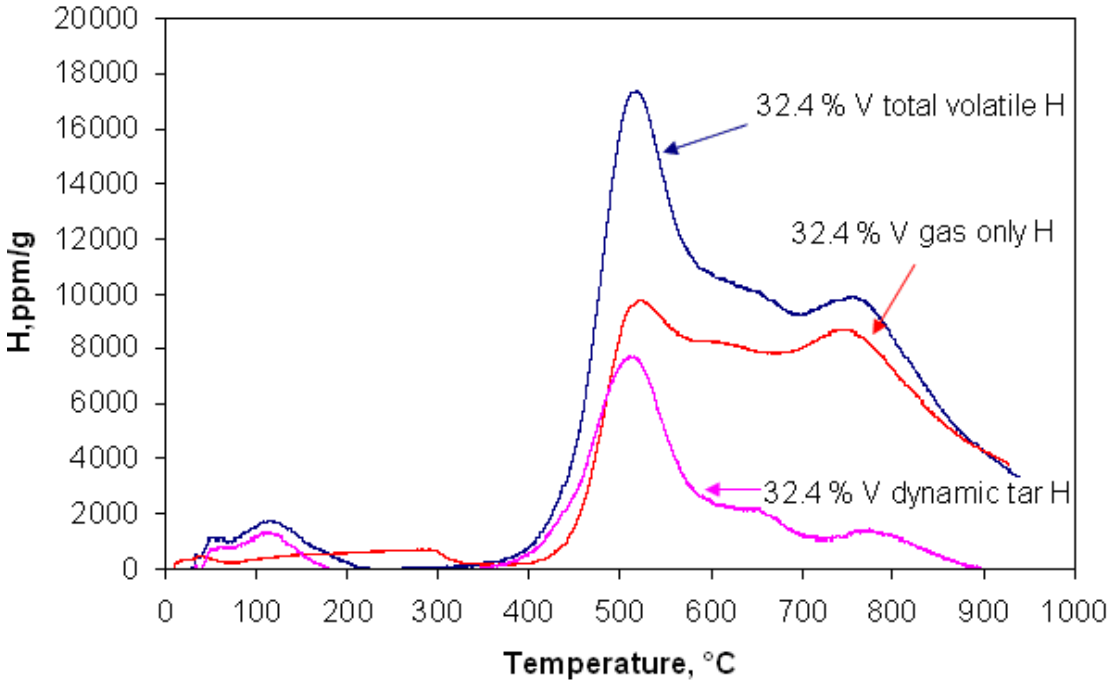

Figure 8.9. Hydrogen concentration for total volatile, gas only and mathematically derived dynamic tar for the 32.4% vitrinite concentrate at a heating rate of 10°C/min from 25 to 1000°C.

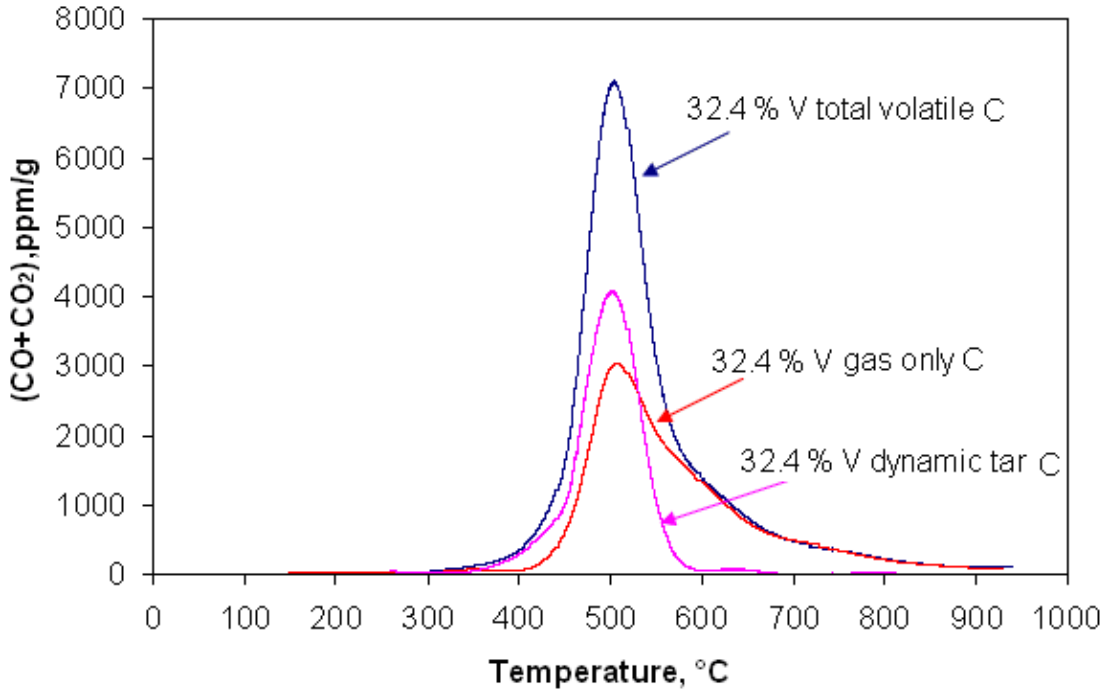

Figure 8.10. Carbon concentration for total volatile, gas only and mathematically derived dynamic tar for the 32.4% vitrinite concentrate at a heating rate of 10°C/min from 25 to 1000°C.

Comparing the evolution of tar only for three different coal maceral concentrates, during the primary devolatilisation, the vitrinite rich concentrate began to evolve condensable tars at a lower temperature than the inertinite rich concentrate. Meanwhile, considering the overlap of

H and C concentrations between volatiles and gases only, the evolution of condensable tars for the vitrinite rich concentrate was also complete at a lower temperature than that of the inertinite rich concentrate, as seen in Figures 8.11 and 8.12. The carbon concentration of dynamic tar per gram of sample increased with vitrinite content. However, above 500°C, the hydrogen concentration of dynamic tar per gram of inertinite rich concentrate (32.4% V) is higher than that of medium vitrinite concentrate (64.4% V). This indicated that the condensed tar from the inertinite rich concentrate (32.4%) may contain a higher ratio of H rich aliphatic structures or more water than that of the medium vitrinite concentrate (64.4% V). Only the inertinite rich concentrate (32.4% V) showed a certain concentration of C at about 655°C in Figure 8.12, corresponding to a small peak of H concentration in Figure 8.11. Above 690°C, the disappearance of C concentration and the decrease of H concentration for the inertinite rich concentrate (32.4% V) indicated that the condensable product at higher temperature was only H_2O. Overall, during the secondary devolatilisation, the inertinite rich concentrate (32.4% V) produced more H_2O than the other concentrates (64.4% V and 86.4% V). Since inertinite rich concentrate (32.4% V) has a high ash content (25.3%), water evolved from this concentrate during secondary devolatilisation may be attributed to the decomposition of mineral components. However, further work needs to be justified to prove this theory.

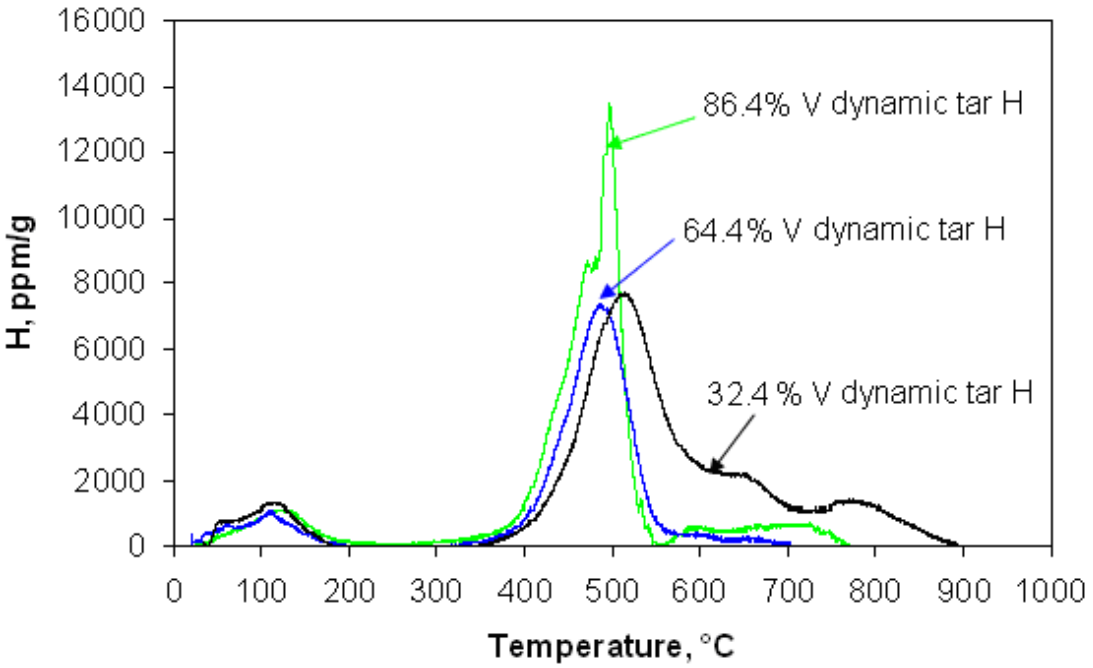

Figure 8.11. Comparison of H for mathematically derived dynamic tar for the 86.4%, 64.4% and 32.4% vitrinite concentrates at a heating rate of 10°C/min from 25 to 1000°C.

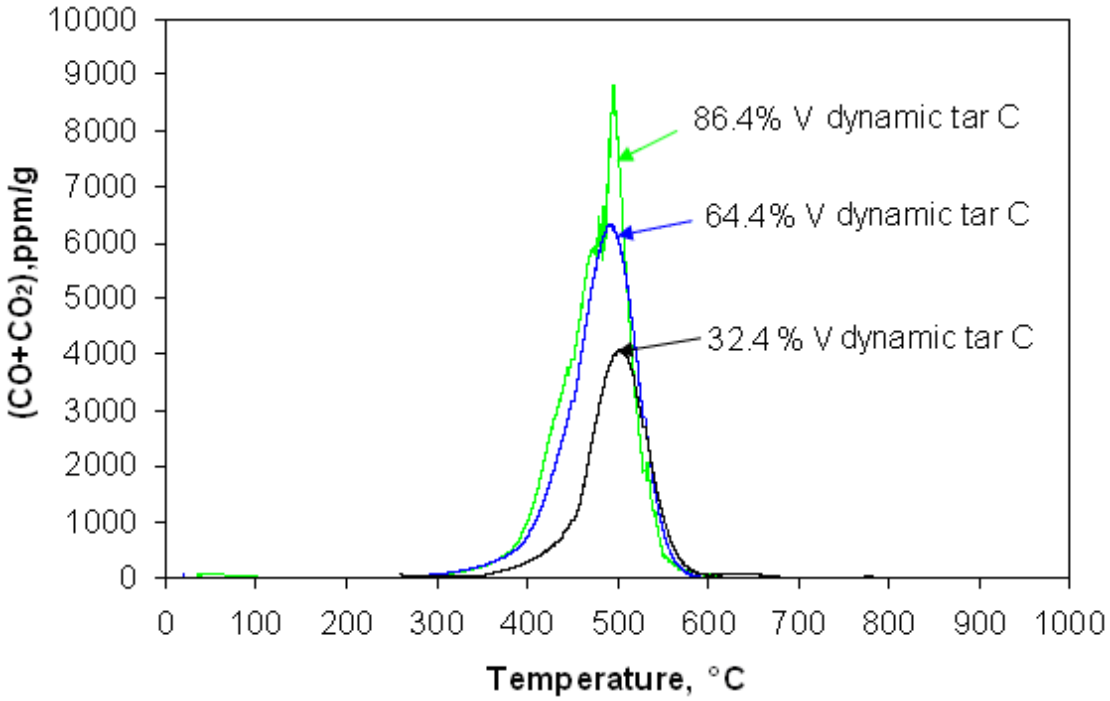

Figure 8.12. Comparison of C for mathematically derived dynamic tar for the 86.4%, 64.4% and 32.4% vitrinite concentrates at a heating rate of 10°C/min from 25 to 1000°C.

Figure 8.13 shows the changes of H/C of dynamic tars only with temperature for three different coal maceral concentrates. During primary devolatilisation, the H/C curves show a small peak at around 445°C, implying that the tars produced at this temperature contain a high ratio of H which is a characteristic of aliphatic rich structures. The values of H/C of dynamic tar from the inertinite rich concentrate (32.4% V) are larger than that of the vitrinite rich (86.4% V) and the medium vitrinite (64.4% V) concentrates, although the trends observed were the same. This may be attributed to the higher ratio of H rich aliphatic structures or more water in the dynamic tar for the 32.4% vitrinite concentrate.

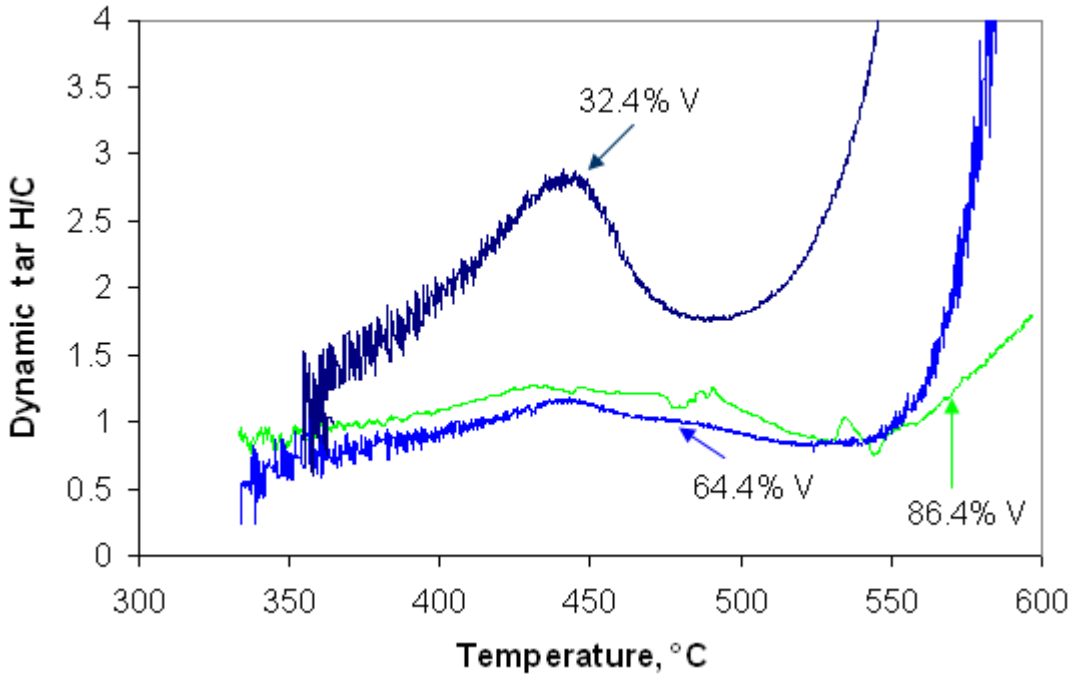

Figure 8.13. Comparison of H/C for mathematically derived dynamic tar for the 86.4%, 64.4% and 32.4% vitrinite concentrates at a heating rate of 10°C/min from 25 to 1000°C.

Table 8.1 shows the mass distributions of H, C and O in gas only and dynamic tar only modes (including condensed water when tars were condensed). The mass of individual element in volatile matter and gas only was estimated based on the integrations of H, C and O concentrations in the temperature between 280 and 900°C, which eliminated the effect of moisture in coal. In terms of a single element of H, C and O, its mass percentage is considered 100% in volatile matter. The mass of a single element in gas divided by its mass in volatile matter is its mass percentage in gas. The content of a single element in tar is the difference of its mass percentage between in volatile matter and in gas. The results indicated gas from the 86.4% vitrinite concentrate contains more hydrogen and oxygen but less carbon than that from the 32.4% vitrinite concentrate, whereas opposite results were observed for dynamic tar. The 86.4% vitrinite concentrate has a lower H/C (mole ratio) in dynamic tar than the 32.4% vitrinite concentrate. This implied that tars from the vitrinite rich concentrate are more aromatic than that from the inertinite rich concentrate [20]. The oxygen content may relate to the organic structure in tar and water. The instantaneous oxygen distributions in volatile matter and gas only modes for vitrinite rich and inertinite rich concentrates are shown in Figures 8.14 and 8.15. The dynamic difference of oxygen contents between volatile matter and gas only is the oxygen content of condensed tar and water.

Table 8.1. Mass distributions of C, H and O in gas only and tar only for vitrinite rich and inertinite rich concentrates.

	86.4% vitrinite					32.4% vitrinite				
	H%	C%	O%	H/C	Mass,%	H%	C%	O%	H/C	Mass,%
Volatile matter	100	100	100	4.7	100	100	100	100	5.8	100
Gas only	85.9	45.2	90.3	11.7	31.2	75.8	59.0	48.6	7.5	34.8
Dynamic tar & water	14.1	54.8	9.7	1.2	68.8	24.2	41.0	51.4	3.4	65.2

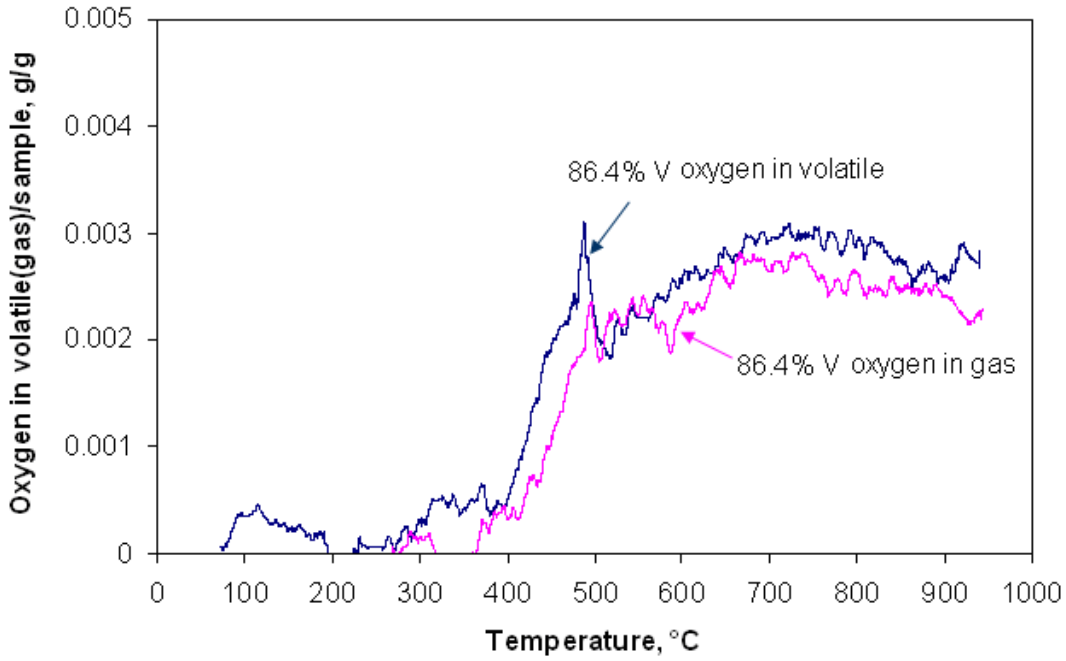

Figure 8.14. Oxygen in volatile matter and gas only for the 86.4% vitrinite concentrate at a heating rate of 10°C/min from 25 to 1000°C.

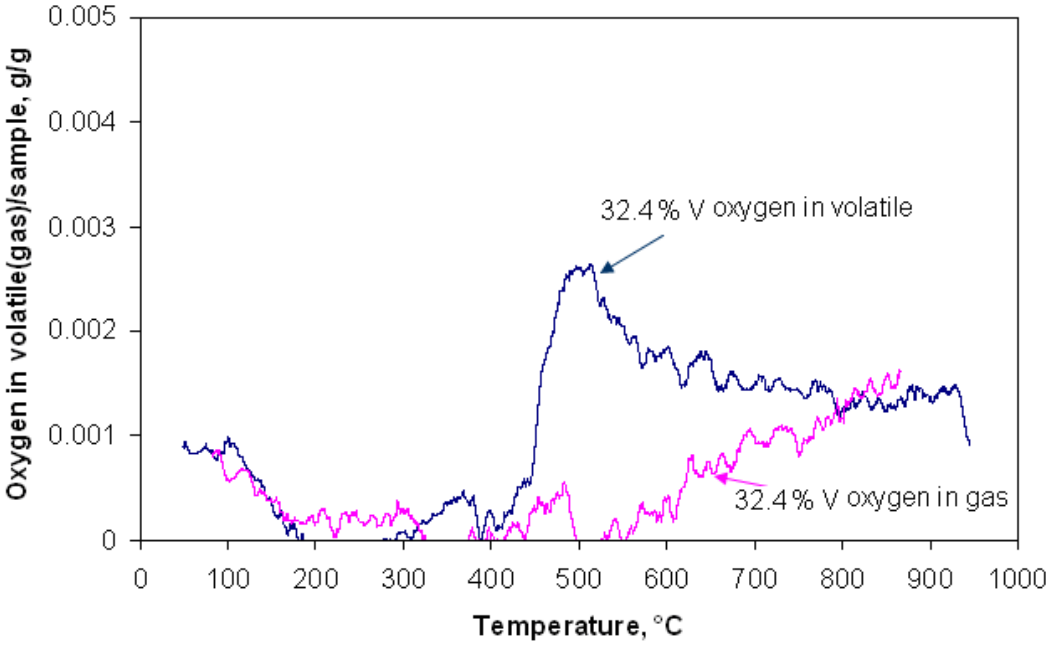

Figure 8.15. Oxygen in volatile matter and gas only for the 32.4% vitrinite concentrate at a heating rate of 10°C/min from 25 to 1000°C.

8.2.3 Elemental compositions of coke

In addition to elemental compositions of gases only and tars only, the instantaneous elemental compositions of the char can also be back-calculated using the DETA technique. After devolatilisation, the final coke obtained at 1000°C was combusted using mode 2 of the DETA technique (adding an O_2 stream to the front end of the furnace to combust the residual coke/char, the details of this mode can be seen in Chapter 3). The instantaneous char elemental fraction with increasing temperature is the percentage of a single element left in the pyrolytic residue against the total mass of all elements of C, H, N, S and O calculated based on the combusted products of volatile matter and char. Figures 8.16 and 8.17 show the results of the instantaneous elemental compositions of chars for the 86.4% and 32.4% vitrinite concentrates (the re-scaled concentrations of O, H, S and N in Figures 8.16 and 8.17 can be seen in Appendix C). It can be observed that despite undergoing significant devolatilisation (i.e., peak tar and gas evolution), the majority of the elemental variation did not occurr until 505°C. This is predominantly due to the high temperature evolution of H_2. For different coal maceral concentrates, char from the vitrinite rich concentrate showed higher C and lower O contents than that from the inertinite rich concentrate. The initial contents of H in the vitrinite rich and the inertinite rich concentrates were similar, 4.6% in the 86.4% vitrinite concentrate and 4.5% in the 32.4% vitrinite concentrate, respectively.

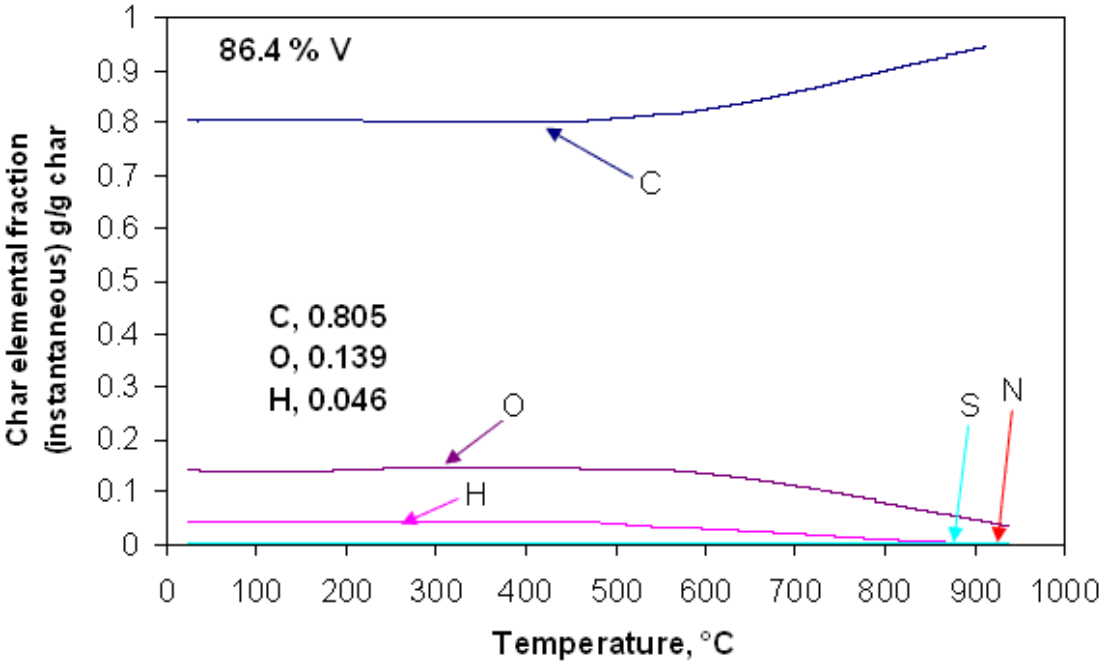

Figure 8.16. Calculated elemental compositions of the residue as a function of temperature for the 86.4% vitrinite concentrate at a heating rate of 10°C/min from 25 to 1000°C.

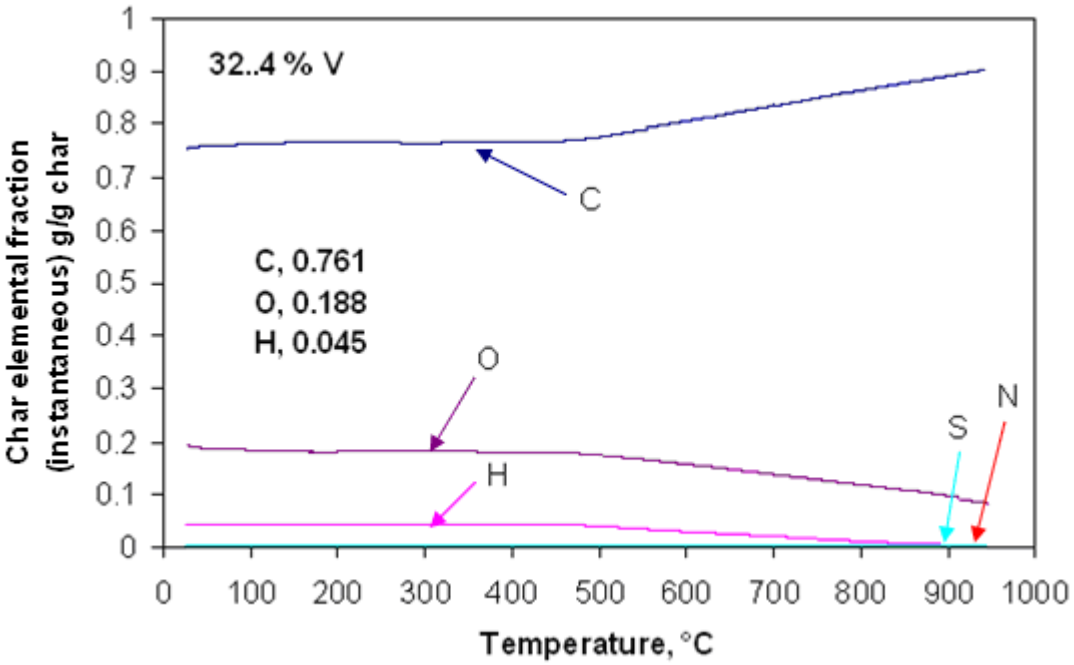

Figure 8.17. Calculated elemental compositions of the residue as a function of temperature for the 32.4% vitrinite concentrate at a heating rate of 10°C/min from 25 to 1000°C.

8.2.4 Mass balance for volatile matter, char and coal maceral concentrates

Using DETA technique, one vitrinite rich (86.4% V) and one inertinite rich (32.4% V) concentrates were used to estimate the mass balance of heating coal maceral concentrates. The mass of individual elements of C, H, N and S per gram of sample in the evolved volatile matter was estimated based on its concentration integration in combustion products of CO_2, H_2O, SO_2, NO and NO_2 during combusting volatiles. Similarly, the mass of individual elements of C, H, N and S per gram of sample in the residue of char was estimated based on its concentration integration in combustion products of char. The mass of O in volatile matter or char was obtained by the difference of the concentration integration of the consumed (introduced) oxygen for combusting volatile matter or char and the produced oxygen in the combustion products. The mass of individual element of C, H, N, S and O per gram of sample in coal maceral concentrate (volatile matter plus char) was the sum of its mass in volatile matter and char.

Table 8.2 shows the results of the proximate and ultimate analysis for these two coal maceral concentrates under study. Both the samples selected have similar moisture contents. The vitrinite rich concentrate under study has a lower ash content but higher volatile matter and fixed carbon contents than the inertinite rich concentrate. The ultimate analysis shows that the vitrinite rich concentrate has higher C and H contents but a lower O content than the inertinite rich concentrate.

Table 8.2. Proximate and ultimate analysis for the vitrinite rich (86.4% V) and inertinite rich (32.4% V) concentrates.

Sample	86.4% Vitrinite	32.4% Vitrinite
Proximate analysis, %		
Air Dried Moisture	1.4	1.2
Ash	2.1	25.3
Volatile Matter	20.9	16.3
Fixed Carbon	75.7	57.2
Ultimate analysis, %		
Carbon	89.3	86.7
Hydrogen	4.88	4.57
Nitrogen	2.25	1.94
Sulphur	0.49	0.62
Oxygen (by difference)	3.0	6.2

The mass of volatile matter based on the sum of the mass of individual elements of C, H, N, S and O in volatile matter per gram of sample was 0.2532 g for the 86.4% vitrinite concentrate and 0.1891 g for the 32.4% vitrinite concentrate, namely, the estimated volatile matter contents are 25.32% and 18.91%, respectively, as seen in Table 8.3. These estimated volatile matter contents were higher than the results for the proximate analysis in Table 8.2. The reason for this difference may attribute to the error that caused by estimating oxygen content using the DETA technique. Table 8.3 indicated that the oxygen content from the volatile matter was 10.59% (0.1059 g per gram sample) for the 86.4% vitrinite concentrate and 8.47% (0.0847 g per gram sample) for the 32.4% vitrinite concentrate, respectively, which were even higher than the oxygen contents in the ultimate analysis for the coal maceral concentrates in Table 8.2. Similarly, the oxygen contents in char in Table 8.3 for both concentrates were also higher than the results in the ultimate analysis in Table 8.2. In the current study, the oxygen contents in volatile matter and char were estimated by the difference between the consumed (introduced) oxygen and the produced oxygen. The consumed (introduced) oxygen concentrations for combusting the volatile matter and char were measured in volumetric percentage, while the produced oxygen was estimated in ppm based on the combusted products of CO_2, H_2O, SO_2, NO and NO_2. Therefore, it is considered that the estimation of introduced oxygen concentration by volumetric percentage is responsible for the errors in calculating volatile matter content in coal maceral concentrates.

Table 8.3. Mass of C, H, N, S and O in volatile matter and char per gram of vitrinite rich (86.4% V) and inertinite rich (32.4% V) concentrates, elemental compositions (daf) based on DETA results and Ultimate analysis of concentrates are also reported in this table.

Sample / Element	86.4% Vitrinite			32.4% Vitrinite		
	Volatile matter (g)	Char (g)	Elemental compositions (%daf)	Volatile matter (%daf)	Char (g)	Elemental compositions (%daf)
C	0.1022	0.7183	85.03	0.0709	0.4974	77.33
H	0.0430	0.0043	4.90	0.0320	0.0018	4.60
N	0.0016	0.0044	0.62	0.0011	0.0020	0.41
S	0.0005	0.0029	0.34	0.0004	0.0013	0.23
O	0.1059	0.0394	15.06	0.0847	0.0856	23.17
Sum	0.2532	0.7693	105.95	0.1891	0.5881	105.74

Based on the estimated mass of individual elements in volatile matter and char, the contents of individual elemental compositions for the air dry and ash free basis were further calculated based on the proximate analysis in Table 8.2. The results were shown in Table 8.3. It can be seen that the H contents in two different coal maceral concentrates based on the DETA technique were similar with the results from the ultimate analysis. The C content was lower than that of the ultimate analysis but a higher O content was observed. The errors for the high O content are attributed to the experimental error in measuring the introduced oxygen (as discussed in elemental compositions of volatile matter and char) and also due to the transformation of oxygen from minerals during char combustion [173]. The oxygen content in char was calculated by the difference between the produced oxygen in products of CO_2, CO, H_2O, NO, NO_2 and SO_2 and the introduced oxygen for combusting the char using mode 2 in Figure 3.5. Figure 8.18 shows that the instantaneous release of oxygen from char for the 32.4% vitrinite concentrate is higher than that from the char for the 86.4% vitrinite concentrate. This may be attributed to the higher ash content of the 32.4% vitrinite concentrate in comparison with the 86.4% vitrinite concentrate, higher ash content the char, more oxygen transformation from minerals the char had during char combustion.

Using the DETA technique, for the two coal maceral concentrates, the total mass of all elements based on the integrated mass per gram of sample (dry and ash free basis) was about 1.06 g (105.95% in elemental compositions daf for 86.4% vitrinite concentrate and 105.74% for 32.4% vitrinite concentrate) rather than 1.0 g (100%), which was also relevant to the errors of the measured oxygen content. Comparing the results for the two coal maceral concentrates in Table 8.3, the 86.4% vitrinite concentrate has higher C and H contents but a lower O content than the 32.4% vitrinite concentrate, which are consistent with the results of the ultimate analysis in Table 8.2.

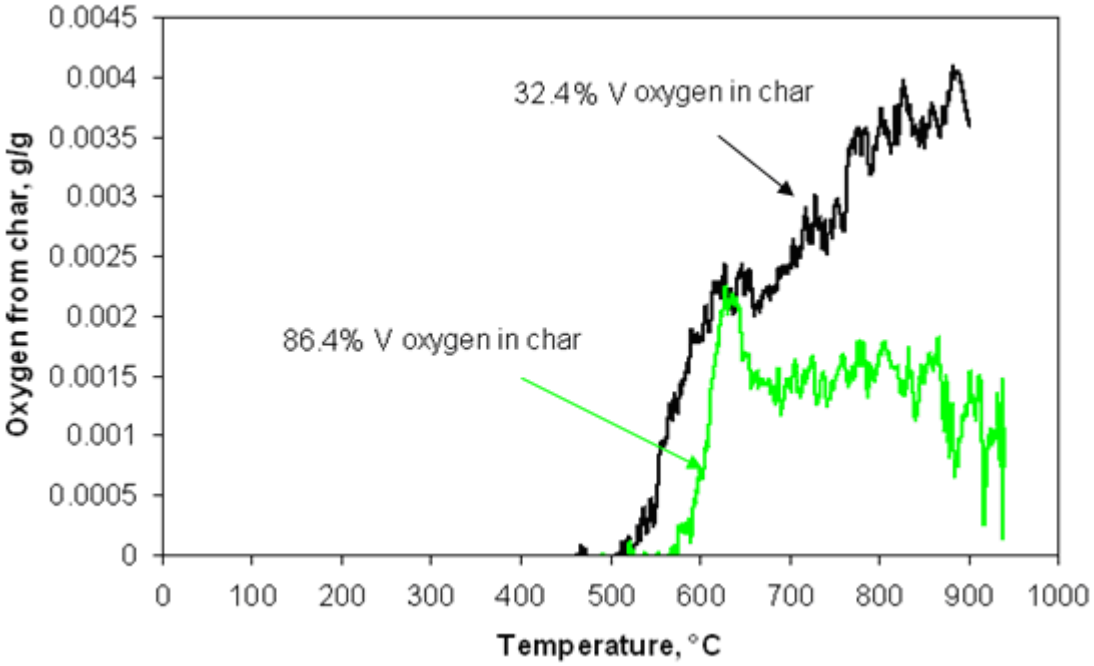

Figure 8.18. Oxygen released from chars for the 86.4% and 32.4% vitrinite concentrates at a heating rate of 10°C/min from 25 to 1000°C.

Since the primary elemental compositions of coal are C and H [27], the current work focuses only on C and H rather than all elements in coal maceral concentrates. If C and H are considered the only elements in char neglecting other elements, the instantaneous concentrations of C and H from char with increasing temperature were found to be similar for both the vitrinite rich and inertinite rich concentrates, as shown in Figure 8.19. The results implied that the difference in elemental compositions for these two coal maceral concentrates was mainly characterised by the volatile matter components rather than char components.

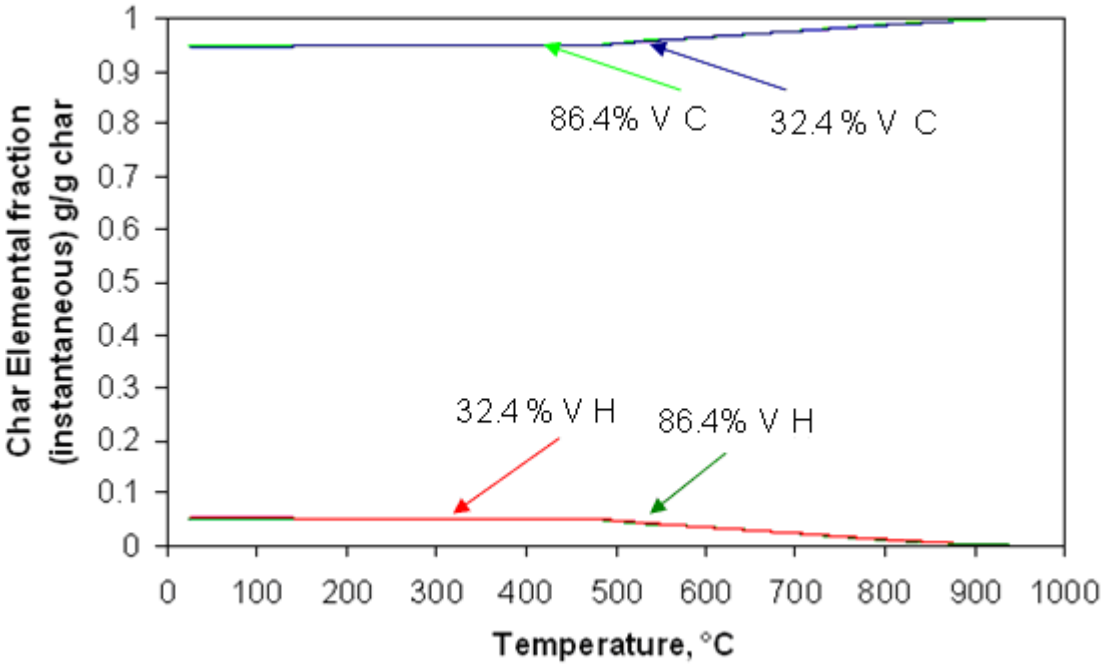

Figure 8.19. Calculated elemental compositions of the residue as a function of temperature for the 86.4% and 32.4% vitrinite concentrates at a heating rate of 10°C/min from 25 to 1000°C (with carbon and hydrogen only considered).

8.3 Tar properties

8.3.1 Properties of condensable tars

In addition to the estimated dynamic tar based on the difference by volatile matter and gas only, the condensable tars from one vitrinite rich concentrate (86.4% V) and one inertinite rich concentrate (32.4% V) were also evaluated using the DETA technique. These tars were condensed using a tar condenser sitting in an ice bath during the gas only experiments that were conducted from 25 to 1000°C at a heating rate of 10°C/min. For condensable tars analysis, they were firstly washed out of the apparatus and dissolved in acetone. A portion of the dissolved tars were reloaded into the quartz crucible and allowed to sit until all the

acetone had evaporated. In this way the tars were re-concentrated and placed back into the furnace for analysis. As they re-vaporised at a heating rate of 10°C/min from 25 to 1000°C, the tars were combusted to form carbon and hydrogen distributions against boiling point. The results for the concentrations of H and C with temperature were shown in Figures 8.20 and 8.21. The H/C ratio concentrations with temperature are shown in Figure 8.22. For this analysis the concentrations of the combustion products were the representative of the amount of tars reloaded into the furnace rather than being indicative of the total amount of tars. Because some tars were lost during washing (the following experiments for tars analysis are the same, unless otherwise specified). The results showed that there are two significant tar groups that have peaks at 209°C and 355°C for tars from the 86.4% vitrinite concentrate and 192°C and 328°C for tars from the 32.4% vitrinite concentrate. For the first group, tars from the vitrinite rich concentrate had H/C<1 while tars from the inertinite rich concentrate had H/C>1. One possible explanation could be that the condensed tars from the inertinite rich concentrate are more aliphatic than condensed tars from the vitrinite rich concentrate. The second group tars with boiling point up to 400°C for both coal maceral concentrates were similar and they showed H/C<1. However, comparing the C and H peaks at about 200 and 350°C in Figures 8.20 and 8.21, it can be seen that the vitrinite rich concentrate has a higher ratio of high boiling point tars than the inertinite rich concentrate. It was noted that these coal maceral concentrates produced a small amount of high molecular weight material with boiling points within the range of thermoplastic behaviour (440-500°C for the parent coal). It was expected that such material could be formed during decomposition to produce the fluid phase, i.e., a “meta-plastic tar”, which would then be vaporised and present in the condensed tar. However, the material that was re-vaporised within this range appeared to show a cross-linking (repolymerization) reaction rather than being directly re-vaporised. Figures 8.20 and 8.21 indicate that from 500 to 950°C, a small amount of H was detected with minute traces of C. Residue in the crucible was obtained when the experiments were finished, indicating some large molecules were present in the condensed tar which showed the similar properties with the original coal, with a high temperature cross-linking (repolymerization) resulting in H_2 release leaving residue as a solid of coke.

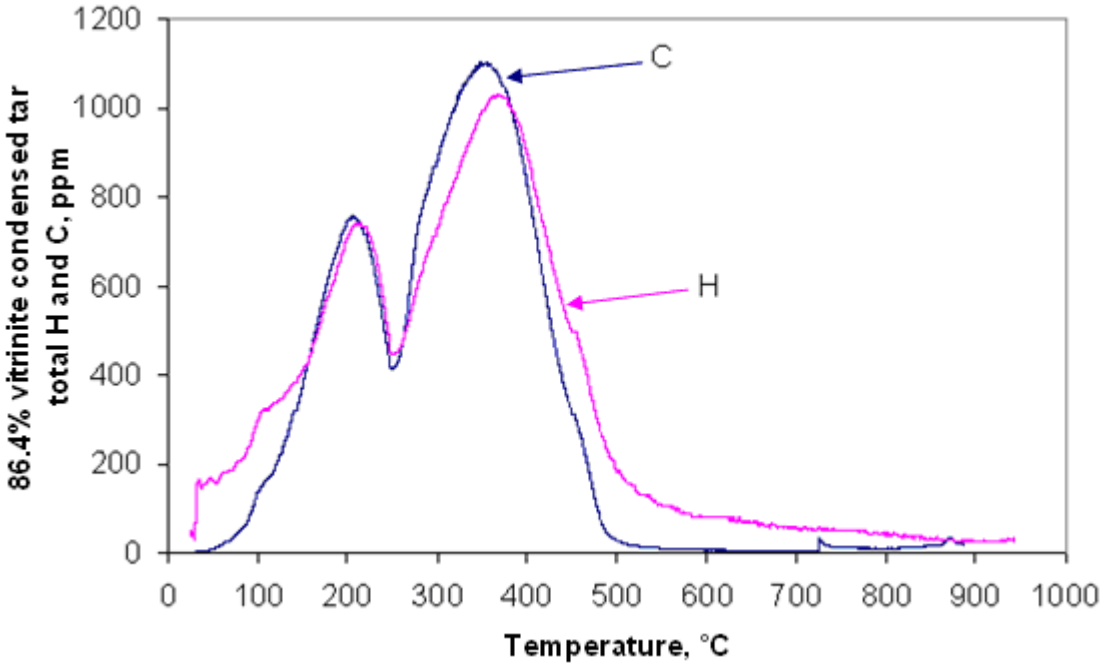

Figure 8.20. Properties of condensed tar obtained from the 86.4% vitrinite concentrate at a heating rate of 10°C/min from 25 to 1000°C.

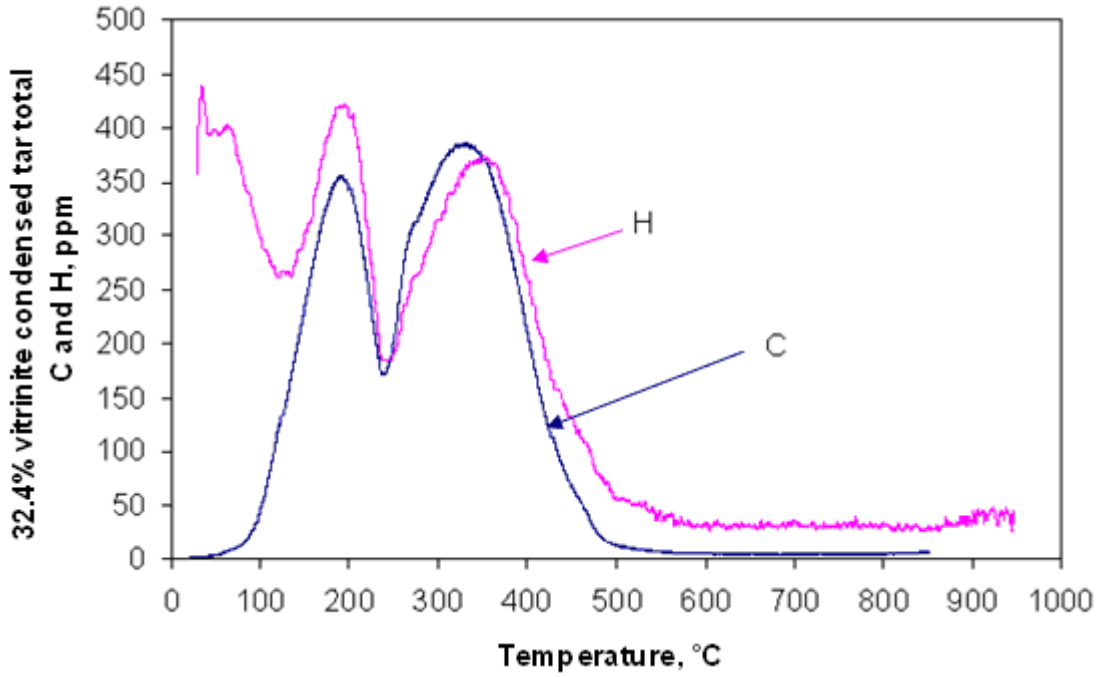

Figure 8.21. Properties of condensed tar obtained from the 32.4% vitrinite concentrate at a heating rate of 10°C/min from 25 to 1000°C.

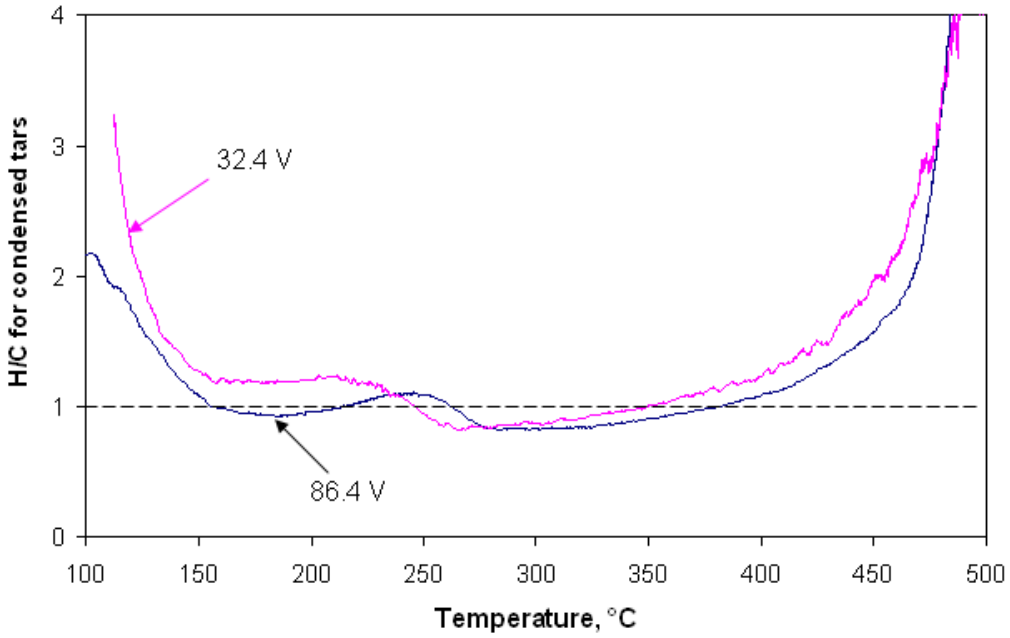

Figure 8.22 H/C for condensed tar obtained from the 86.4% and 32.4% vitrinite concentrates at a heating rate of 10°C/min from 25 to 1000°C.

8.3.2 Physical and chemical properties of the condensed and extracted tars from semi-coke

During the primary devolatilisation, the weakest bonds of coal molecular can break producing molecular fragments, part of the molecular fragment will be released as tars if they are small enough to vaporize and be transported out of the char particles, this part of tars can be condensed as condensable tar [20]. However, large molecular fragments may not be able to immediately escape from the heating coal pellet as they are formed. Therefore, they would not be vaporised until higher temperatures. To analyse these tars, pyrolysis experiments for the 86.4% vitrinite and 32.4% vitrinite concentrates were conducted at a heating rate of 10°C/min. The heating samples were quenched at the dynamic tar peak (at around 505°C) to extract the tars that did not vaporise when they formed. In the meanwhile, the vaporised tars were condensed by a tar condenser and washed out using acetone by repeating the step in section 8.3.1 for the total condensed phase during coal maceral concentrates pyrolysis from 25 to 1000°C. The tars that are not able to escape from the heating samples were firstly extracted out of semi-coke and dissolved in acetone. This was followed by a second-step extraction with toluene as the solvent to dissolve heavier tars. The re-vaporization and combustion of the condensed and extracted tars were carried out in the same procedure as that conducted for the condensable tars in section 8.3.1. Due to the high boiling point of toluene (111°C), the tar dissolved by toluene was warmed from 25 to 70°C and held up until all the toluene had evaporated.

8.3.2.1 Condensed tars from semi-coke

Prior to the extracted tars, the condensable tars condensed from the heating samples were analysed first as they were revaporised and combusted at a heating rate of 10°C/min from 25 to 1000°C. Figures 8.23 and 8.24 indicate that the similar trends for C and H concentrations can be seen on re-heating condensable tars that were condensed by heating the 86.4% vitrinite and 32.4% vitrinite concentrates from 25 to 505°C at a heating rate of 10°C/min. Neglecting the peak for H_2O below 100°C, two peaks for C and H concentrations were observed. The first small peak at about 160°C appeared at a narrow temperature range while the second peak at about 280°C included a broad temperature range with higher C and H concentrations. Tars with boiling points between 160 and 230°C exhibit H/C >1, whereas tars with higher boiling point between 230 and 420°C exhibit H/C <1. This implies that the high boiling point tars are more aromatically structured than the low boiling point tars.

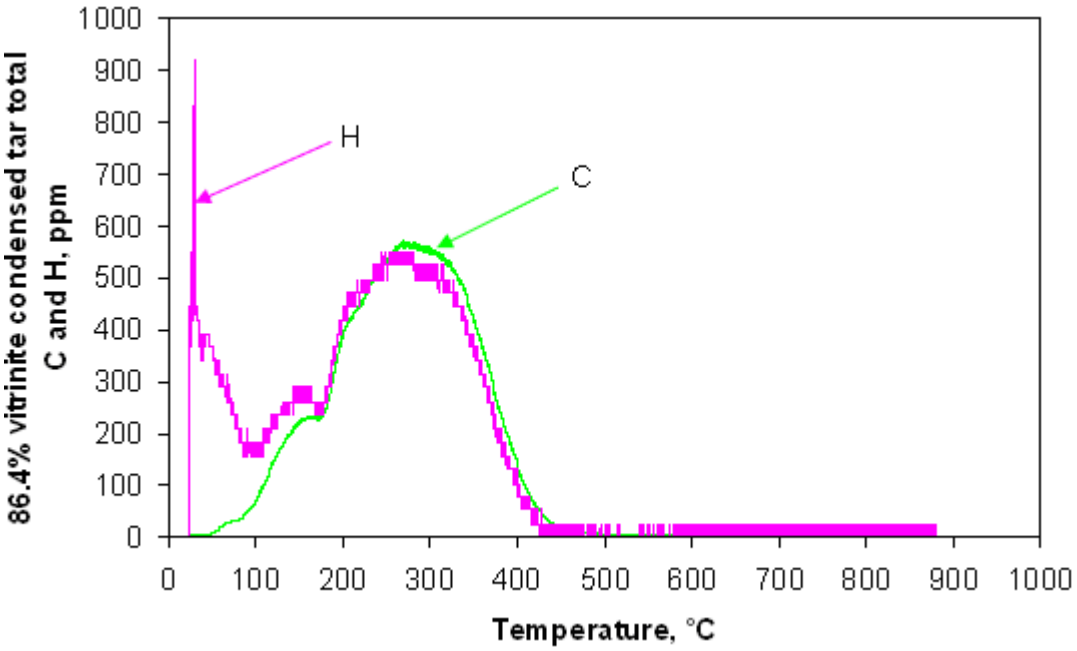

Figure 8.23. Properties of condensed tar obtained from the 86.4% vitrinite concentrate at a heating rate of 10°C/min from 25 to 505°C.

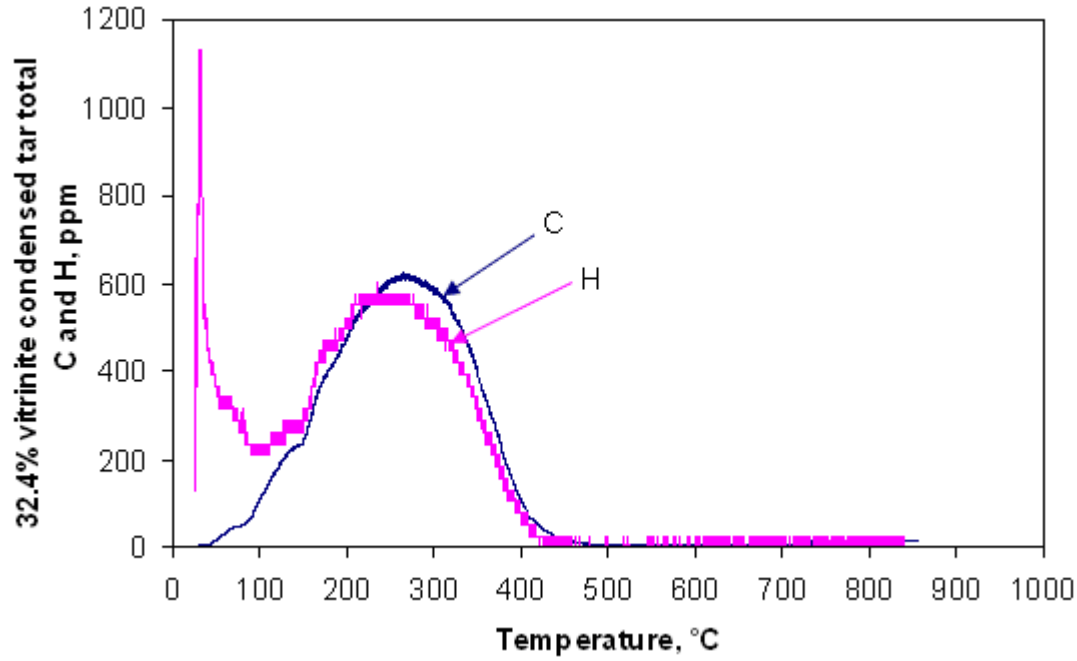

Figure 8.24. Properties of condensed tar obtained from the 32.4% vitrinite concentrate at a heating rate of 10°C/min from 25 to 505°C.

8.3.2.2 Acetone extracted tar

After the condensed tars, the extracted tars from semi-coke were analysed. Figures 8.25 and 8.26 show the results of the acetone extracted tars as they were revaporised and combusted to form carbon and hydrogen distributions against boiling point. The results indicated that the

acetone extracted tar that originated from the 86.4% vitrinite concentrate showed four peaks at 170°C, 198°C, 315°C and 435°C, whereas the acetone extracted tar that originated from the 32.4% vitrinite concentrate had only three peaks at 164°C, 196°C and 320°C. This implies that for acetone extracted tars only that originated from vitrinite rich concentrate contain high molecular weight materials with boiling points within the range of thermoplastic behaviour (400-500°C). The tars with high boiling point may affect the fluidity and viscosity of metaplast, further affect the thermal conductivity and swelling of the heating vitrinite rich concentrate. Thermal conductivity and swelling of vitrinite rich concentrates and inertinite rich concentrates were reported in Chapters 5-7. In addition, it can be observed that the acetone extracted tar that originated from the vitrinite rich concentrate had a higher ratio of H content than that from the inertinite rich concentrate. A possible explanation for this is such tars that originated from the vitrinite rich concentrate may have more or longer alkyl side chains linked to the aromatic rings. Further work is needed to justify this theory.

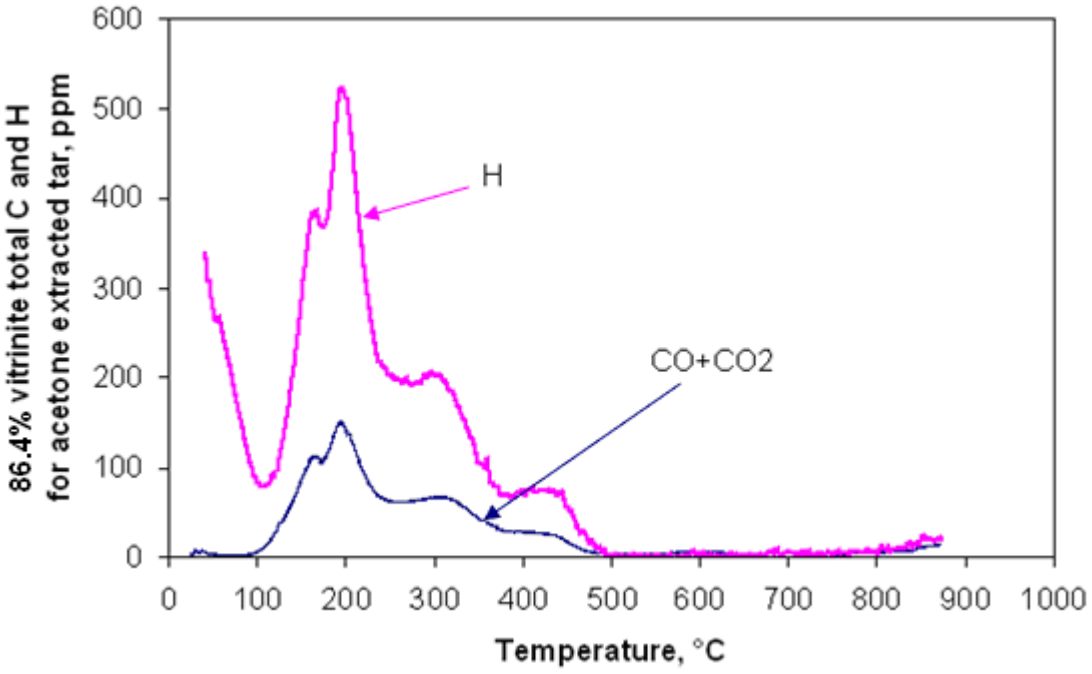

Figure 8.25. Properties of acetone extracted tar obtained from the 86.4% vitrinite concentrate at a heating rate of 10°C/min from 25 to 505°C.

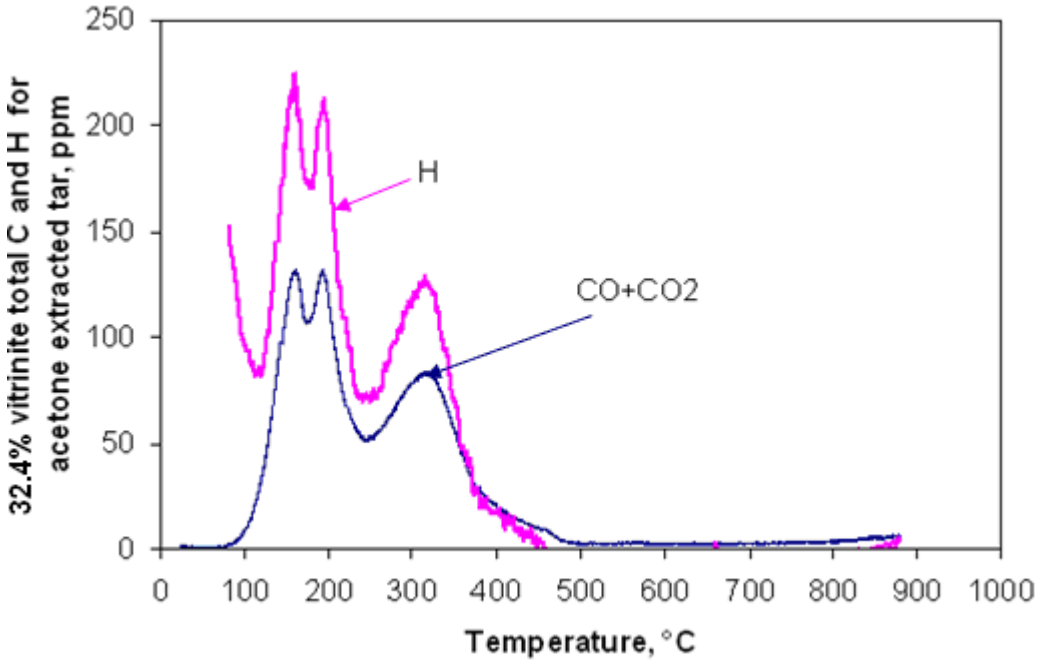

Figure 8.26. Properties of acetone extracted tar obtained from the 32.4% vitrinite concentrate at a heating rate of 10°C/min from 25 to 505°C.

8.3.2.3 Toluene extracted tar

After the first-step extracted tar using the solvent of acetone, a second-step extracted tar using the solvent of toluene was analysed. Figures 8.27 and 8.28 show the development of carbon and hydrogen concentrations with temperature for the reheated toluene extracted tar from semi-cokes. Tar extracted from semi-coke that originated from the 86.4% vitrinite concentrate showed C and H peaks at 230°C. Between 280 and 425°C, the C and H concentrations showed a plateau with a slight change. The H/C changed from 1.55-1.75 and the re-vaporization of these tars was complete at 470°C. By comparison, tar extracted from semi-coke that originated from the 32.4% vitrinite concentrate showed peaks for C and H concentrations at 325°C and 430°C, and the high boiling point tar at the second peak was at a higher proportion than the low boiling point tar at the first peak. The H/C was in the range between 2.05-2.20; the re-vaporization for these tars was not complete until 485°C. The reasons for the different properties of the toluene extracted tar that originated from two different coal maceral concentrates are not clearly understood and need more work in this front. For better understanding in extracted tars, analyses of tars from various concentrates using different solvents need to be carried out in future as the solvent may influence the extraction of tars from semi-coke.

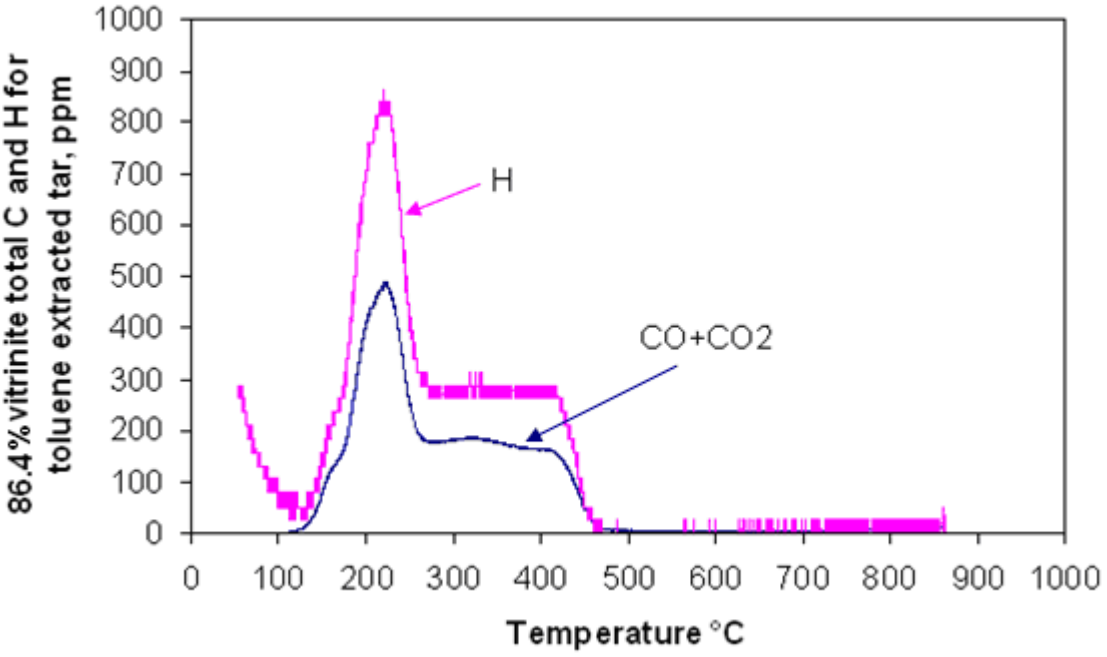

Figure 8.27. Properties of toluene extracted tar obtained from the 86.4% vitrinite concentrate at a heating rate of 10°C/min from 25 to 505°C.

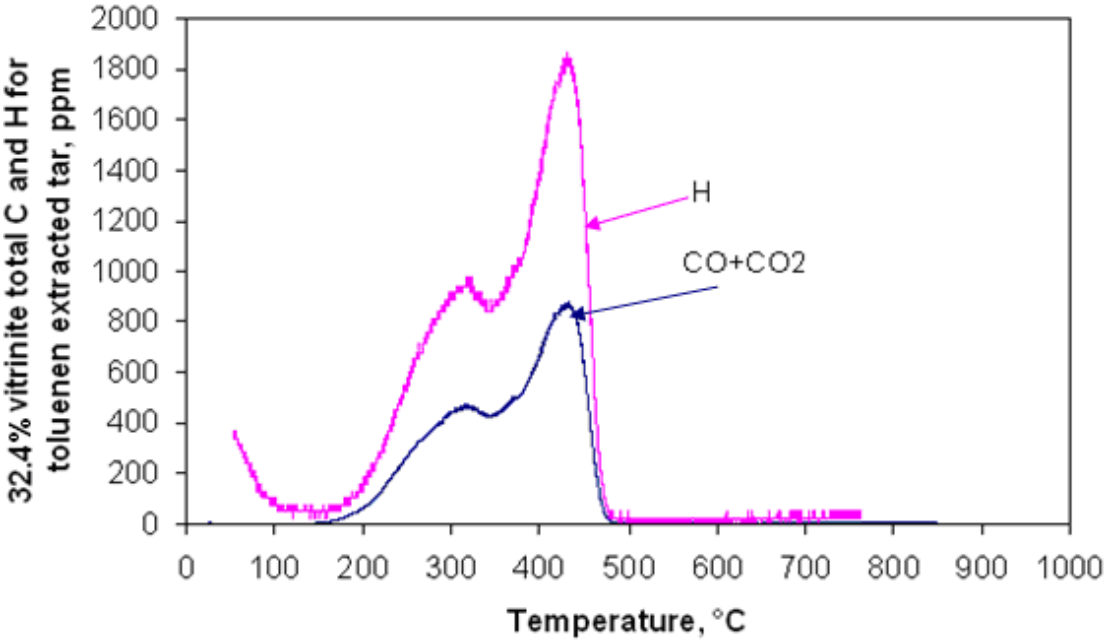

Figure 8.28. Properties of toluene extracted tar obtained from the 32.4% vitrinite concentrate at a heating rate of 10°C/min from 25 to 505°C.

8.4 Discussion

DETA technique

The Dynamic Elemental Thermal Analysis (DETA) technique was employed to evaluate the volatile evolution between different coal maceral concentrates. These results could be

considered equivalent to an elemental Thermogravimetirc Analysis (TGA). In addition, this technique is also able to show the dynamic elemental evolution of gas only and tar only as a function of temperature. The results from DETA tests showed that the volatile evolution during the primary devolatilisation consists mainly of carbon heavy condensable tars and hydrogen rich gases. The secondary devolatilisation consisted mainly of gaseous hydrogen (H_2), a small proportion of condensable hydrogen (H_2O) and gaseous CO. The tars and gases evolutions are indicative of the decomposition mechanism of molecular fragments during coal pyrolysis. The H/C of the total volatiles or dynamic tars for heating coal maceral concentrates indicated the aliphatic and/or aromatic properties and is indicative of elemental compositions of tars from different coal maceral concentrates. Combining the chemical compositions (H and C contents) and physical properties (evaporated) of tars obtained from vitrinite rich and inertinite rich concentrates, the DETA technique provides an insight into understanding the fundamental mechanisms in revealing the thermo-plasticity during the transformation of coal to coke.

Tar properties

All tars for condensed portion and extracted portion from coke and semi-coke evaporated in the temperature range between 140 and 500°C. The known tar compounds in the coal tar book [62] mainly include a) aliphatic structures connected to carbonyl, carboxyl and ether group, b) aromatic ringed structures connected to carbonyl, carboxyl and ether group or O, N and S ring or aliphatic. The aliphatic and/or aromatic frame and N, S and O containing radicals play a dominant role in determining the boiling point of tar; the more the aromatic rings, the higher the boiling point of tar has. In addition, the alkyl chains connected to the frame of tar molecules may cause a distinct influence in characterising the elemental ratio, such as H/C. For example, a longer H rich alkyl chain can result in a higher H/C. Based on the known tars compounds [62], results for the tar analysis in Figures 8.20 to 8.28 indicated that tars evaporated at around 200°C are mainly aliphatic structured or 1-2 ringed aromatic structured. Tars evaporated at around 280°C are also classified one or two ringed aromatic structured compounds. Heavier tars, such as the tars evaporated at around 350°C, belong to 3-4 ringed aromatic structured compounds. The heavy tars from vitrinite rich concentrate evaporated at around 435°C are 3-4 ringed aromatic structured or 4-6 aromatic rings compounds [62].

8.5 Conclusions

The Dynamic Elemental Thermal Analysis (DETA) technique provides a fundamental understanding in the mechanism in the transformation of coal to coke by offering quantitative elemental analysis of volatiles (gases and tars) and instantaneous elemental distributions of

pyrolytic residue of char. In addition, this technique can also be used to evaluate the physical (temperature for evaporation) and chemical (elemental compositions) properties of condensed and extracted tars. The main conclusions for this Chapter are summarized below

- Volatiles evolved during the primary devolatilisation of heating coal in the temperature range 300 to 600°C consist mainly of carbon heavy condensable tars and hydrogen rich gases. The secondary devolatilisation in the temperature range 600 to 1000°C releases mainly gaseous hydrogen (H_2) and a small proportion of condensable hydrogen (H_2O) and gaseous CO. The evolution rates of volatiles and dynamic tars that are characterised by hydrogen and carbon from vitrinite rich concentrate are higher than that from inertinite rich concentrate.

- The mass integrated based on the concentrations of individual elements of C, H, N, S and O in volatile matter and char balanced the mass (daf) of the original coal maceral sample with explicable errors. The elemental distributions of volatile matter and char for coal maceral concentrates obtained from DETA technique matched the results from the Proximate and Ultimate analysis with explicable errors.

- The difference in temperatures for the onsets of the evolution of gas and dynamic tar is indicative of the mechanism of volatiles evolution during the transformation of coal to coke. The H/C of dynamic tars is indicative of the aliphatic/aromatic content of coal tars.

- When heating to 1000°C, the vitrinite rich concentrate has a higher ratio of condensable tars that evaporated at relatively high temperatures than the inertinite rich concentrate. When heating to 505°C, condensable tars from both the vitrinite rich and inertinite rich concentrates evaporated at similar temperatures and showed similar chemical compositions. For the acetone extracted tars from semi-coke (obtained by quenching heating coal maceral concentrates at 505°C), only tars from the vitrinite rich concentrate evaporated at higher temperatures (a peak at 435°C), indicating that heavy tars can only be produced from the vitrinite rich concentrate. However, for the toluene extracted tars, a higher ratio of tars that evaporated at high temperature zone were extracted from the inertinite rich concentrate in comparison with the vitrinite rich concentrate. Further studies for the extracted tars from different coal maceral concentrates using different solvents are needed to justify the findings from this work.

Chapter 9 Mechanisms and reactions in the transformation of coal to coke

The transformation from coal to coke involves complex physical changes, thermal behaviour and co-occurring chemical reactions. The development of thermo-plasticity, endothermic and exothermic reactions and the evolution of gases and tars with temperature are strongly dependent on coal maceral components and coking conditions. This study aims to investigate the mechanism of swelling and shrinkage, endothermic and exothermic reactions and the evolution of tars and gases during the transformation of coal to coke based on a suite of coals and coal maceral concentrates. The correlations between physical, chemical and thermal changes during cokemaking were also simultaneously discussed based on the experimental observations. In Chapter 4, correlations between swelling, endothermic and exothermic reactions (identified by apparent specific heat) and thermal conductivity during coal heating were studied. Chapters 5 and 6 revealed that vitrinite rich concentrates are responsible for swelling, exothermic activities and the increase of thermal conductivity during primary devolatilisation. Corresponding to a high degree of swelling, Chapter 7 reported that vitrinite rich concentrates showed a higher pressure drop of gas flowing through the coal sample than inertinite rich concentrates. Chapter 8 found that vitrinite rich concentrates release more tars and gases than inertinite rich concentrates.

This Chapter will summarise the associations of physical, chemical and thermal changes of heating coal and coal maceral concentrates.

9.1 Associations of physical, chemical and thermal changes in the transformation of coal to coke

This study aims to reveal the mechanisms and reactions in the transformation of coal to coke. As vitrinite concentrates are responsible for swelling, heat of exothermic reactions and the release of tars and gases, one high vitrinite concentrate (86.4% V) and one medium vitrinite concentrate (64.4% V) were employed to correlate the physical, chemical and thermal changes during coke formation. The changes of the physical, chemical and thermal behaviour for both the two samples were correlated by a sequence of 9 events, as shown in Figures 9.1 and 9.2 and summarized in Table 9.1. For both samples, during the transformation of coal to coke, liquid tars initially began to evolve prior to distinct specific heat changes (event 1). At about 380°C (for the 86.4% vitrinite concentrate, the following temperatures are also for this coal maceral concentrate, unless otherwise specified), tars were rapidly evolving, while endothermic reactions and the evolution of gases had just began (event 2). The permeability

of heating sample pellet began to decrease at the endothermic peak at about 405°C, with the increase of plasticity due to the rapid evolution of tars (event 3). With increasing temperature, swelling began and permeability continued to decrease (event 4). Permeability reached the minimum after a certain of swelling; with increasing temperature, swelling increased rapidly along with the release of gases and tars. Meanwhile, thermal conductivity rapidly increased due to the release of tars (events 4-5). A tar peak appeared corresponding to the primary exothermic trough (event 5). Tar evolution rate decreased, while gas evolution rate continued to increased (events 5-6). Swelling was complete at maximum gas evolution rate. An overlap of the endothermic and exothermic processes related to heat reactions and tar vaporization due to the primary devolatilisation (event 6). Once the evolution of tar was complete, the permeability began to rapidly increase. Correspondingly, the thermal conductivity showed a small trough accompanied by a small endothermic peak, indicating the onset of secondary exothermic reaction (event 7). Above 676°C, the char started to shrink with the evolution of the light gas (H_2) due to secondary exothermic reaction, permeability slowly increased (event 8). Thermal conductivity continued to rapidly increase due to coal pyrolysis and structural changes of char. However, when the thermal conductivity was in the range of 2-3 W/m·K or higher, it became unstable due to thermal inversion between the measured surface and centre temperatures of char. At 746°C, maximum contraction rate and secondary gases evolution were observed, corresponding to secondary exothermic reaction trough, permeability continued to slowly increase (event 9). Beyond event 9, the secondary exothermic reaction was complete, and the final coke was formed. Based on the sequence of 9 events, it can be seen that the evolution of gases and tars determined the development of fluidity, permeability and swelling, as well as the heats of chemical reactions and the changes in thermal conductivity.

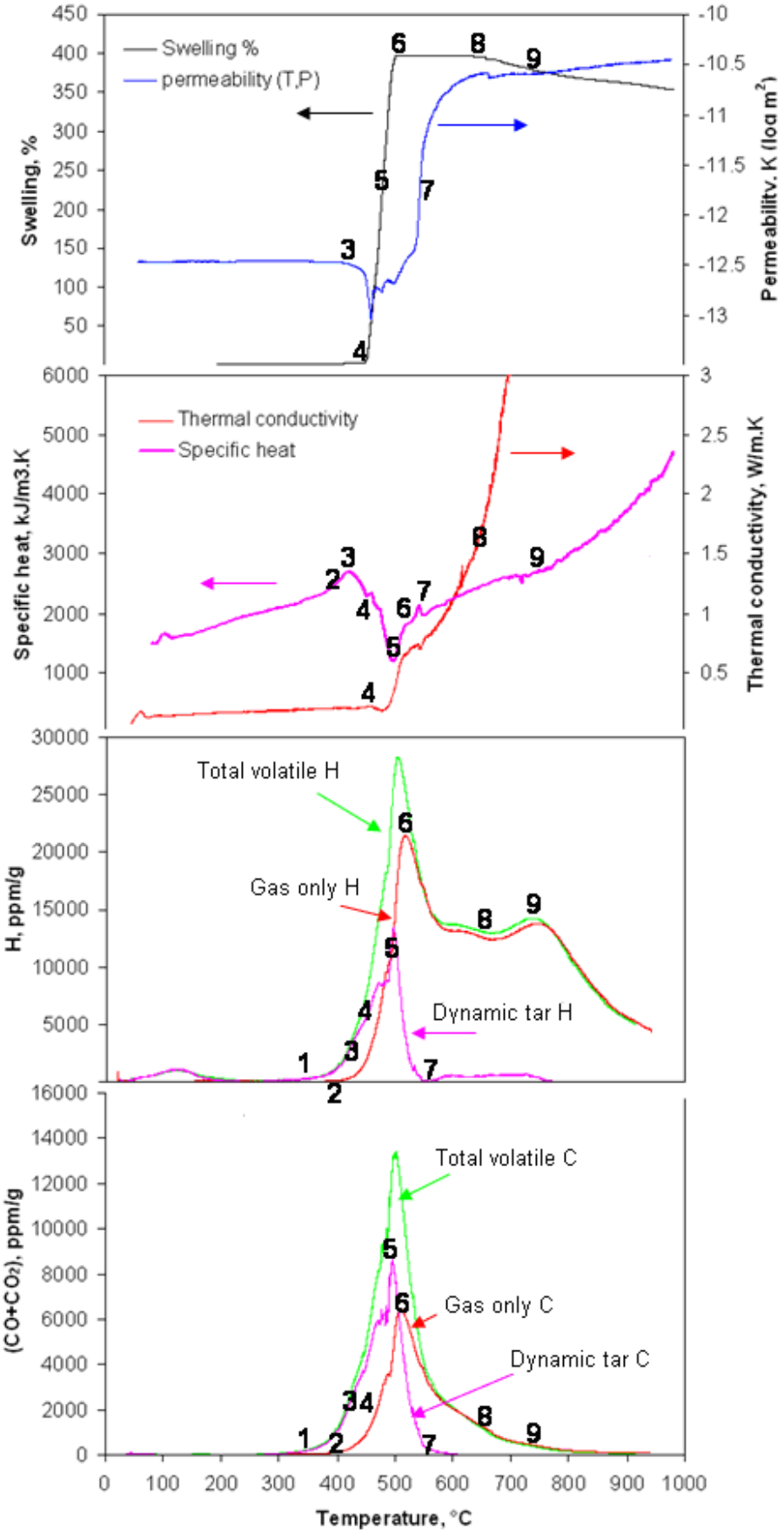

Figure 9.1. Correlations of physical, chemical and thermal changes during coke formation for the 86.4% vitrinite concentrate.

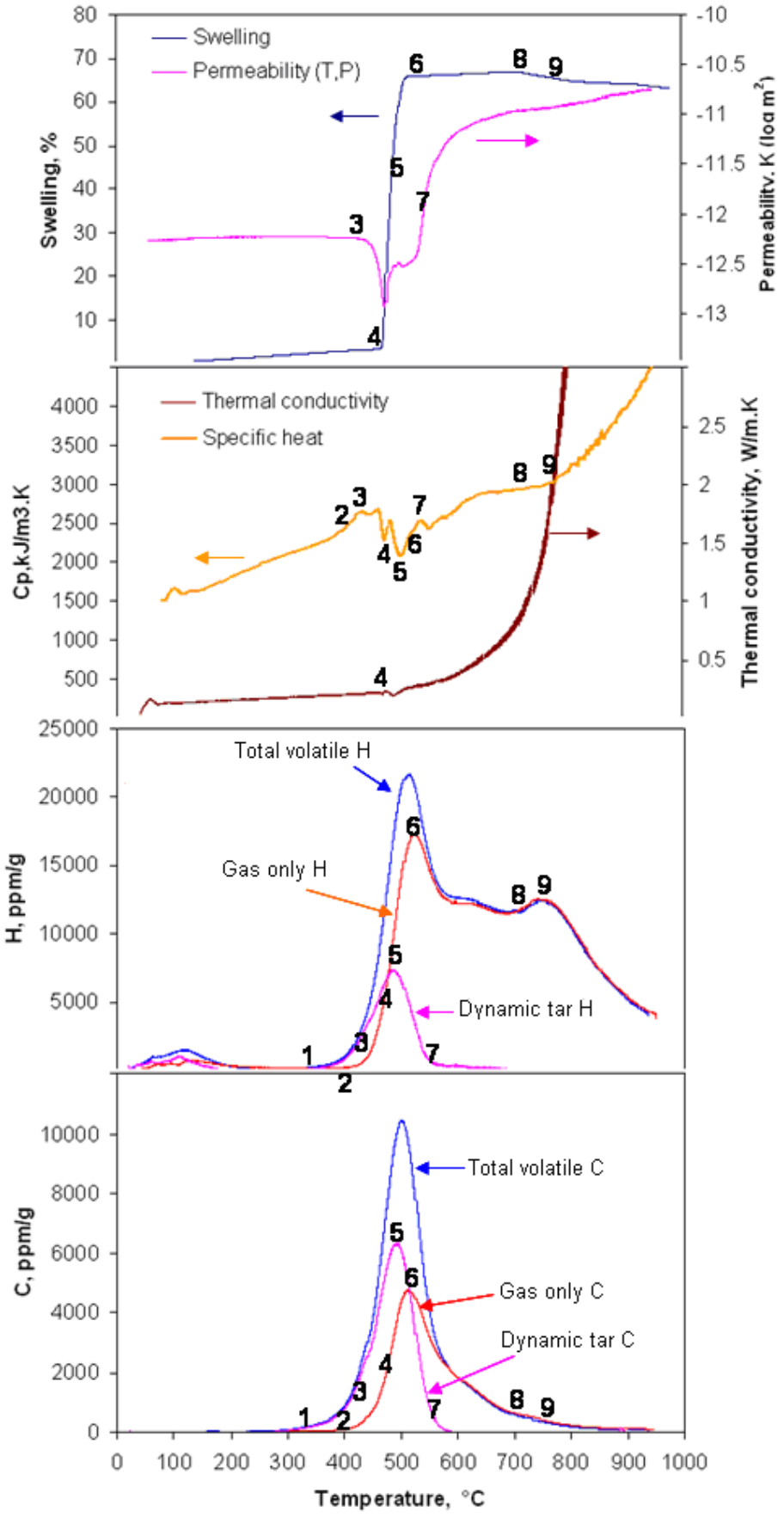

Figure 9.2. Correlations of physical, chemical and thermal changes during coke formation for the 64.4% vitrinite concentrate.

Table 9.1. Correlations between physical, chemical and thermal changes during coke formation, for the events indicated on Figures 9.1 and 9.2.

Event	Temperature, °C		Physical	Thermal	Chemical	Comments on associations
	Sample 86.4V	Sample 64.4V				
1	275	335	---	---	Tars began to slowly evolve	Tars evolution prior to swelling
2	380	390	---	Endothermic reactions began	Tars rapidly evolved, gases began to slowly evolve	
3	405	420	Permeability began to decrease	Endothermic peak appeared	Tars rapidly evolved, gases slowly evolved	
4	453	472	swelling began; permeability continued to decrease	Small thermal conductivity peak and exothermic trough	Tars and gases both rapidly evolved	Rapid gas/tar evolution ~ onset of swelling ~ low permeability
5	494	500	Max swelling rate; permeability slightly decreased again after an increase	Exothermic trough appeared, thermal conductivity rapidly increased	Peak tars appeared	Max swelling rate and tar evolution rate ~ exothermic trough
6	506	515	Swelling completed; permeability began to slowly increase	Overlap of exothermic and endothermic reactions	Peak gases appeared	Swelling ended as peak gases appeared
7	546	550	Permeability rapidly increase	Small endothermic peak and thermal conductivity trough	Rapid tars evolution ended	Char structure became porous, rapid increase of permeability, tars fully evolved
8	676	696	High temperature contraction began, permeability slowly increase	Thermal conductivity rapidly increased	Gas (H_2) evolution rate began to increase	Onset of contraction and secondary reactions with gases evolution
9	746	753	Contraction continued, permeability slowly increased	Exothermic reaction for secondary devolatilisation	Secondary peak gas (H_2) appeared	Max contraction rate and max secondary gases evolution rate

9.2 Differences between vitrinite and inertinite concentrates during coking

Based on the observations and conclusions from Chapters 5 to 8, the differences in maceral concentrates for events 1 to 9 are shown in Figures 9.1 and 9.2 and Table 9.1. The summary of the differences are as follows

- The occurrence of events 1-9 shifted to higher temperatures with decreasing vitrinite content.

- During events 2-6, vitrinite rich concentrates contribute to exothermic reactions, the increase of thermal conductivity and swelling of heating coal. For the blend of two vitrinite rich concentrates (81.8% and 81.6% vitrinite) and one inertinite rich concentrate (29.0% vitrinite) of 1:1:1 by mass, inertinite rich concentrate suppressed nearly 50% of the swelling compared the expected value (events 4-6) but did not have a significant influence on high temperature contraction (events 8-9).

- During events 3-6, for the vitrinite rich concentrates separated from a high swelling coal, the maximum swelling, heats of exothermic reactions and thermal conductivity at the maximum swelling all showed a linear increase with vitrinite content independent of particle size. In addition, the pressure drop of gas flowing through the coal sample in event 6 and high temperature contraction during events 8-9 also showed the similar relationship with vitrinite content. However, there was no particular trend observed with inertinite rich concentrates.

- For events 5-6, the evolutions of tars and gases increased with increasing vitrinite content. Tars evolved from vitrinite rich concentrates showed higher boiling points than that from inertinite rich concentrates.

9.3 New insight into coking mechanisms gained from this study

The present study is the first to conduct experiment to simultaneously measure swelling, pressure drop of gas flowing through the coal sample, endothermic and exothermic reactions, thermal conductivity and the release of gases and tars for heating coal and coal maceral concentrates. This study further correlates the physical, chemical and thermal changes during the transformation of coal to coke. In comparison with the previous studies, the new insights into coking mechanism gained from this study are summarized as follows

Previous work has suggested [59, 140] that blocked CO_2 and CH_4 are driven off at about 200°C, while tar formation begins at around 300-400°C. Strezov et al. [20] also reported that gases species such as CO_2 and CO evolved at lower temperature than tars. Saxena [59] and Solomon et al. [20] concluded that during primary pyrolysis, the weakest bonds can break by producing molecular fragments, the fragments abstract hydrogen from the hydroaromatics or aliphatics to form tars. By comparison, this study found that tars began to evolve at lower temperature than gases. In addition, there was no endothermic or exothermic reaction indentified by the changes in specific heat during the initial evolution of tars between 275 and 380°C, as seen in events 1-2 in Figure 9.1. However, tars evolved at above 380°C are associated with exothermic reactions, as seen in events 3-7 in Figures 9.1 and 9.2.

Swelling is expected to be associated with increasing internal pressure due to the trapped gases in a viscous material during primary exothermic reaction [73]. This study has further revealed that swelling did not begin until some of the tars and gases are released. The maximum swelling rate appeared at the temperature of maximum tar evolution, and swelling is complete at peak gases evolution, as seen in events 3-6 in Figures 9.1 and 9.2

It has previously been reported that the swelling of heating coal increases as the sample size of coal increased [3, 111]. The present study also showed the increase in swelling with increasing coal particle size. However, this trend was not observed for all the current vitrinite rich concentrates separated from a high swelling coal. In Chapter 6 it was suggested that, for vitrinite rich concentrates obtained from a high swelling coal, the maximum swelling in event 6 in Figures 9.1 and 9.2 is determined only by vitrinite content independent of particle size.

Strezov et al. [19] found that high fluidity coking coals show higher thermal conductivity than low fluidity coking coals during primary devolatilisation. This study found that vitrinite rich concentrates showed higher thermal conductivity and a higher tar evolution rate than inertinite rich concentrates during primary exothermic reaction. As fluidity relates to the concentration of liquid tars, this implies that thermal conductivity is dependent on the evolution of tars. In events 4-6 as shown in Figures 9.1 and 9.2, the thermal conductivity rapidly increased with the evolutions of tars while showing a small dip at event 7 as the evolution of tars was complete.

9.4 Implications for coal quality assessment for coking

The implications of the present study in assessing coal properties for coking are discussed below

- During primary devolatilisation, the vitrinite rich concentrates show larger heats of exothermic reactions corresponding to larger swelling, while the inertinite rich concentrates show smaller heats of exothermic reactions with smaller swelling. This provides a potential methodology for assessing the swelling of coking coal based on heats of reactions.

- Thermal conductivity, the release rate of tar and gas and the measured pressure drop of gas flowing through the coal sample increase with increasing vitrinite content. The changes of thermal conductivity relates to the evolution of tars. Therefore, thermal conductivity during the formation of metaplast may be used to assess fluidity of coking coal.

- During primary devolatilisation, vitrinite rich concentrates evolved more gases and tars than inertinite rich concentrates, corresponding higher swelling, larger heats of exothermic reactions and higher thermal conductivity. Condensed tars evolved from vitrinite rich concentrates have higher boiling points and lower H content than that from inertinite rich concentrates. Therefore, the tar and gas evolution rates and their properties during coal heating may be useful for evaluating coal quality for coking.

Chapter 10 Conclusions and Recommendations

10.1 Findings from the literature survey

This study includes a critical review of the literature for the transformation of coal to coke. The significant findings from the literature study are listed as follows

- During the transformation of coal to coke, the heating coal undergoes coal devolatlisation with the release of gases and tars; the residue after coal devolatlisation is coke. The major release of gases and tars occurs in the temperature range between 400 and 550°C, which is named the primary devolatilisation. At the higher temperature range between 550 and 1000°C, the release of volatiles mainly includes light gases, such as H_2 and CO, which is named the secondary devolatilisation.

- Coals have a complex combination of physical, thermal and chemical changes during coking, which includes softening, fluidity, resolidification, swelling, shrinkage, endo/exothermic reactions and the release of tars and gases. The correlations between these changes during the transformation of coal to coke are somewhat uncertain and techniques for determining their associations during coke formation are lacking.

- Vitrinite fractions from coal show greater softening, fluidity and swelling than inertinite fractions during coal heating. However, differences in the endothermic and exothermic reactions between vitrinite fractions and inertinite fractions during coke formation are still unknown.

- The separation of vitrinite and inertinite rich concentrates from coals has been previously achieved by using some inorganic or organic media solutions based on the difference in densities between vitrinite rich and inertinite rich concentrates. However, media solutions may also have a deleterious effect on coking behaviour. A new technique for separating coal maceral concentrates is required to study the real behaviour of coal maceral concentrates during coking without any foreign substance's intervention. This will eradicate the errors involved with the experimental technique or analysing method.

10.2 Conclusions from experimental techniques

- The reflux classifier can successfully separate coal maceral concentrates on the basis of an alternative water based method which eliminates the intervention of the dense media.

- The novel Computer Aided Thermal Analysis (CATA) technique is capable of synchronously evaluating the physical (swelling/shrinkage and permeability through the heating coal pellet) and thermal changes (apparent specific heat and thermal conductivity) during coal coking.

- The Dynamic Elemental Thermal Analysis (DETA) is able to quantify the elemental compositions of volatiles by an analysis of gases and tars measured in real-time during coal heating. It can also be used to evaluate the physical (boiling point) and chemical (elemental compositions) properties of condensed and extracted tars, and it is capable of back calculating the instantaneous elemental distributions of pyrolytic residue of char.

10.3 Conclusions from experiments for coal macerals separation

- The separated coal maceral concentrates from the reflux classifier are heterogeneous and contain vitrinite up to 90% or inertinite up to 70%.

- The separation for coal maceral concentrates is mainly affected by density and particle size of the coal sample.

- By comparison with separation for the original coal slurry without particle size controlled, size cuts of coal can obtain more coal maceral concentrates with various vitrinite contents, particularly, more concentrates with various medium vitrinite contents can be separated, which indicated that the separation of coal macerals is better when size cuts of coal are completed first.

- The ash content and relative density of separated coal maceral concentrates tend to decrease with increasing vitrinite content. It has been found that the particle size has little effect on ash content and density for coal maceral concentrates with vitrinite content above 63%. However, for coal maceral concentrates with vitrinite content below 63%, ash content and density increase with particle size.

10.4 Conclusions from experiments for swelling and thermal properties of coals

- All the samples studied underwent an endothermic reaction prior to the onset of rapid swelling. Between 400 and 550°C, the primary exothermic reaction and a distinct increase of the thermal conductivity along with rapid swelling were observed. Between 550 and 600°C, an endothermic reaction accompanied by a slight decrease of thermal conductivity was observed. Above 600°C, the secondary exothermic reaction occurred, which was accompanied by volumetric shrinkage of semi-coke and a rapid increase of thermal conductivity.

- The effects of heating rate on thermal and swelling properties of heating coals were evaluated at three different heating rates of 3, 5 and 10°C/min. Between 400 and 550°C, increasing heating rate shifted the initial endothermic and exothermic reactions and swelling to occur at higher temperatures, increased the maximum swelling, exothermic reactions trough and the thermal conductivity. Between 550 and 1000°C, the initial temperatures for the onsets of the endothermic and exothermic reactions and the rapid increase of thermal conductivity also increased with increasing heating rate.

- Two different particle size samples of 0-212 μm and 0-500 μm were employed to study the effects of particle size on thermal and swelling properties of heating coal. The experimental results indicated that, between 400 and 550°C, the large particle size sample showed a wider temperature range for swelling and the primary exothermic reaction. The swelling and primary exothermic trough increased with increasing particle size. Between 550 and 1000°C, the small particle size sample showed a larger exothermic trough than the large particle size sample.

10.5 Conclusions from the correlations between physical, chemical and thermal changes of heating coal

The dominant event associated with coke formation is swelling. The new findings of the present study related to the temperature sequence of events on heating prior to the first-detected onset of swelling and the temperature of rapid swelling during the formation of coke from heating coal are

- **Measured tar release** identified by DETA technique was initiated at almost 180°C prior to the measured onset of swelling and is associated with endothermic and exothermic reactions identified by CATA technique.

- **Measured gas release** was initiated at less than 100°C prior to the onset of swelling.

- **The measured pressure drop** of gas flowing through the coal sample indicated liquid formation and the pressure drop increased at about 30°C prior to the onset of swelling, decreased after this onset and increased again during rapid swelling.

- **The estimated thermal conductivity** identified by CATA technique increased slightly at about 30°C prior to the onset of swelling, apparently also due to liquid formation (but with less sensitivity than pressure drop), and to a greater degree during rapid swelling.

- **Measured rapid swelling** occurred over a temperature interval after the onset of swelling of about 40°C and was associated with an additional exothermic reaction and the release of gases.

- A suggested mechanism for rapid swelling requires the formation of metaplast, with the measured increases of pressure drop and thermal conductivity (at about 70°C prior to the onset of rapid swelling) being indicators of the onset of metaplast formation. A second requirement is the release of gases after sufficient metaplast has formed. The current measurements for gas and tar evolution, with the associated changes of pressure drop and thermal conductivity, support such a mechanism.

The contribution of the present work is to provide the sequence of multiple indicators of the chemical, physical and thermal events and estimates of heats of reactions and pressure drop to a general sequence that has been previously proposed. The new insights into the contributions of maceral fractions to the transformation of coal to coke are

- **With decreasing vitrinite content,** the sequence of events with the evolution of tars and gases, the onset of the increase of pressure drop of gas flowing through the coal sample, the onsets of swelling and endothermic and exothermic reactions and the increase of thermal conductivity during coking were shifted to higher temperatures.

- **Vitrinite rich concentrates** exhibited a higher release rate of gases and tars, higher pressure drop of gas flowing through the coal sample, higher swelling, higher thermal

conductivity and larger heats of exothermic reactions during the primary devolatilisation **than inertinite rich concentrates**.

- **For vitrinite rich concentrates separated from high swelling coal,** particle size (112-212 μm and 212-500 μm) was found to have insignificant effect on swelling and thermal changes during heating. The sequence of events of pressure drop of gas flowing through the coal sample, maximum swelling, heat of exothermic reactions during the primary devolatilisation, and thermal conductivity at the maximum swelling all increased linearly with vitrinite content independent of particle size of samples. However, no specific trend was observed by the inertinite rich concentrates.

- **Addition of inertinite rich concentrate to vitrinite rich concentrate** suppressed swelling during the primary devolatilisation and shifted the swelling to a higher temperature. However, it did not cause a significant effect on heat of exothermic reactions and thermal conductivity during rapid swelling event, but increased the heat of endothermic reactions and decreased thermal conductivity prior to high temperature contraction. Also, the addition of inertinite rich concentrate to vitrinite rich concentrate did not show a significant effect on high temperature contraction, heat of exothermic reactions and thermal conductivity during the secondary devolatilisation.

10.6 Recommendations for future research

- The laboratory scale coal heating furnace employed in the study has some short-comings: the size being too small to accommodate coke size used in coke ovens; the escaping of the evolved gases and tars along with the carrier gas flow were not controlled; the heating coal samples were permitted only to swell in one dimension. Practically, particle size of charged coal, the immigration of tars and gases and swelling of heating coal in the industrial cokemaking ovens are different from the laboratory scale furnace. The effects of coal particle size and coke oven on swelling, apparent specific heat, thermal conductivity and the immigration of gases and tars need to be considered. It is recommended that a comparative study between different heating furnaces of various scales should be undertaken.

- In terms of the parent coal, the large particles showed larger swelling and exothermic reactions during the primary devolatlisation than the small particles. By comparison, for vitrinite rich concentrates separated from high swelling coal, the swelling was

only determined by vitrinite content independent of particle size of sample. However, these conclusions were only drawn from the high swelling vitrinite rich concentrates that have particle size ranges of 106-212 μm and 212-500 μm. Vitrinite rich concentrates separated from different parent coals, such as medium swelling coal, and larger particle size, such as 2-4 mm or larger, need to be considered.

- The individual effects of fluidity, porosity of char and density of carbon in char on instantaneous thermal conductivity need to be further studied.

- The effects of vitrinite and inertinite rich concentrates on pressure drop of gas flowing through the coal sample, swelling, the release of gases and tars, endothermic and exothermic reactions and thermal conductivity have been studied. However, the effects of minerals in coal maceral concentrates on the physical, chemical and thermal changes, particularly the apparent specific heat, thermal conductivity and release of H_2O during the secondary devolatilisation need further studied.

- Further work for the pyrolysis behaviour of the blends of vitrinite tars and inertinite rich concentrates needs to be studied to investigate the specific contributions of high boiling point vitrinite tars to the swelling of inert matter.

References

1. Gupta, S., D. French, R. Sakurovs, M. Grigore, H. Sun, T. Cham, et al. Minerals and iron-making reactions in blast furnaces. Progress in Energy and Combustion Science, 2008; 34: 155-197.
2. Yao, Z. and M. Zheng. Cokemaking. Metallurgy Industry, Beijing, 2005, 6.
3. Loison, R., P. Foch, and A. Boyer. Coke quality and production. London, Butterworth, 1989.
4. Young, D.J. and D.J. Harris. Effect of alkalis on high temperature degradation of coke, 1987.
5. Díez, M.A., R. Alvarez, and C. Barriocanal. Coal for metallurgical coke production: predictions of coke quality and future requirements for cokemaking. International Journal of Coal Geology, 2002; 50(1-4): 389-412.
6. Menéndez, J.A., R. Alvarez., and J.J. Pis. Determination of metallurgical coke reactivity at INCAR: NSC and ECE-INCAR reactivity tests. Ironmak. Steelmak, 1999; 26: 117-121.
7. Nakamura, N., Y. Togino, and T. Tateoka. Behaviour of coke in large blast furnace. Coal, Coke and Blast Furnace. The Metals Society, London, 1977; 1-18.
8. Couch, G. R. Metallurgical Coke Production 2001; IEA coal research.
9. Kaegi, D.D., H.S.Valia, and Ch. H. Harrison. Maceral behaviour and coal carbonisation. Proc. 47th Ironmaking Conf. ISS-AIME, 1988; 339-349.
10. Košina, M. and P. Heppner. Macerals in bituminous coals and the coking process: Part 1: Effect of basic coal properties on the process of thermal degradation. Fuel, 1984; 63(6): 838-846.
11. Sakurovs, R., D. French, and Grigore. M. Quantification of mineral matter in commercial cokes and their parent coals. International Journal of Coal Geology, 2007; 72: 81-88.
12. Grigore, M., R. Sakurovs, D. French, and V. Sahajwalla. Mineral matter in coals and their reactions during coking. International Journal of Coal Geology, 2008; 76(4): 301-308.
13. Krebs, V., G. Furdin, J.-F. Maréché, and D. Dumay. Effects of coal moisture content on carbon deposition in coke ovens. Fuel, 1996; 75(8): 979-986.
14. Nomura, S. and A. Takashi. The cause of the uneven carbonization process in wet coal charging in coke oven chamber. Fuel, 2008; 87(15-16): 3240-3246.
15. Yu. J.L., V. Strezov, J. Lucas, and W. Terry. Swelling behaviour of individual coal particles in the single particle reactor. Fuel, 2003; 82(15-17): 1977-1987.
16. Nishioka, K. and S. Yoshida. Index for true dilatation of coal and its usefulness Tranction. ISIJ, 1983; 23: 381-386.
17. Nomura, S., M. Mahoney, K. Fukuda, K. Kato, A.L. Bas, and S. McGuire. The mechanism of coking pressure generation I: Effect of high volatile matter coking coal, semi-anthracite and coke breeze on coking pressure and plastic coal layer permeability. Fuel, 2010; 89(7): 1549-1556.
18. Mahoney, M., S. Nomura, K. Fukuda, K. Kato, A. Le Bas, D.R. Jenkins, et al. The mechanism of coking pressure generation II: Effect of high volatile matter coking coal, semi-anthracite and coke breeze on coking pressure and contraction. Fuel, 2010; 89(7): 1557-1565.

19. Strezov, V., A. Morrison., and P.F. Nelson. Thermal study of the coking behaviour of Australian Thermoplastic coals, Final ACARP report. Macquarie Univeristy, 2007; Report No: C15067.
20. Solomon, P.R., M.A. Serio, and E.M. Suuberg. Coal pyrolysis: Experiments, kinetic rates and mechanisms. Progress in Energy and Combustion Science, 1992; 18(2): 133-220.
21. Strezov, V., J.A. Lucas, and L. Strezov. Quantifying the heats of coal devolatilization. Metallurgical and materials transactions B 2000; 31B: 1125-1131.
22. Amamoto, K. Coke strength development in the coke oven : 1. Influence of maximum temperature and heating rate. Fuel, 1997; 76(1): 17-21.
23. Amamoto, K. Coke strength development in the coke oven. 2. Homogenizing the strength of coke throughout the coke oven chamber. Fuel, 1997; 76(2): 133-136.
24. Osinski, E.J., P.V. Barr, and J.k. Brimavombe. Mathematical Model for Tall Coke Oven Battery. Part 1 The Development of the Thermal Model for Heat Transfer Within the Oven Charge. Ironmaking and Steelmaking, 1993; 20: 350.
25. Nomura, S. and T. Arima. Coke shrinkage and coking pressure during carbonization in a coke oven. Fuel, 2000:79(13): 1603-1610.
26. Elliott, M.A. and G.R. Yohe. The coal industry and coal research and development in perspective, in Chemistry of coal utilization, Elliott.M.A, Editor. 1981, Wiley-interscience: New York, Chichester, Brisbane, Toronto: 1-53.
27. Van Krevelen, D.W. Coal, typology-chemistry-physics-constitution. Amsterdam, London, New York, Tokyo, Elsevier, 1993.
28. Zimmerman, R.E. Evaluating and testing the coking properties of coal. San Francisco, California 94105, USA: Miller Freeman Publications, 1979.
29. Howard, J.B. Fundamentals of coal pyrolysis and hydropyrolysis, in Chemistry of coal utilization, Elliott. M. A, Editor, 1981, Wiley-interscience: New York, Chichester, Brisbane, Toronto: 665-784.
30. Valković, V. Trace elements in coal Volume Vol. I: CRC press; 1983: 30-56.
31. Speight, J.G. The Chemistry and Technology of Coal. New York and Basel, 1983.
32. Given, P.H. The distribution of hydrogen in coals and its relations to coal structure. Fuel, 1960; 39: 147.
33. Shinn, J.H. From coal to single-stage and two-stage products: A reactive model of coal structure. Fuel, 1984; 63(9): 1187-1196.
34. Berkowitz, N. The chemistry of coal. Amsterdam, New York: Elsevier, 1985.
35. Neavel, R.C. Original, Petrography, and Classification of Coal, in Chemistry of coal utilization, Elliott. M. A, Editor. 1981, Wiley-interscience: New York, Chichester, Brisbane, Toronto: 91-158.
36. Yu, J.L., J.A. Lucas, and T.F. Wall. Formation of the structure of chars during devolatilization of pulverized coal and its thermoproperties: A review Progress in Energy and Combustion Science, 2007; 33(2): 135-170.
37. Teichmüller, M. The genesis of coal from the standpoint of coal petrology. Int. J. Coal Geology, 1989; 12: 1-87
38. Dyrkacz, G.R. and Horwitz, E.P. Separation of coal macerals. Fuel, 1982; 61(1): 3-12.

39. Xie, K.C., Y.F. Zhang, C.Z. Li, and D.Q. Ling. Pyrolysis characteristics of macerals separated from a single coal and their artificial mixture. Fuel, 1991; 70(3): 474-479.
40. Das, T.K. Evolution characteristics of gases during pyrolysis of maceral concentrates of Russian coking coals. Fuel, 2001; 80(4): 489-500.
41. Zhao, Y.P., H.Q. Hu, L.J. Jin, X.F. He, and B. Wu. Pyrolysis behavior of vitrinite and inertinite from Chinese Pingshuo coal by TG-MS and in a fixed bed reactor. Fuel Processing Technology, 2011; 92(4): 780-786.
42. Jones, R.B., C.B. McCourt, C. Morley, and K. King. Maceral and rank influences on the morphology of coal char. Fuel, 1985; 64(10): 1460-1467.
43. Dormans, H.N.M, F.J. Huntjens, and D.W. van Krevelen. Fuel, 1957; 36: 221.
44. Iveson, S. and K. Galvin. Influence of organic liquids on coal carbonisation properties. 2010, Nov, Final ACARP report. University of Newcastle; Project No: C17051.
45. Galvin, K.P., J. Zhou., and K. Walton. Application of closely spaced inclined channels in gravity separation of fine particles. Minerals Engineering, 2010; 23(4): 326-338.
46. Galvin, K.P., E. Doroodchi, A.M. Callen, N. Lambert, and S.J. Pratten. Pilot plant trial of the reflux classifier. Minerals Engineering, 2002;15(1-2): 19-25.
47. Galvin, K.P., A. Callen, J. Zhou, and E. Doroodchi. Performance of the reflux classifier for gravity separation at full scale. Minerals Engineering, 2005;18(1): 19-24.
48. Borrego, A.G., G. Marban, M.J.G. Alonso, D. Alvarez, and R. Menendez. Maceral effects in the determination of proximate volatiles in coals. Energy & Fuels, 2000; 14: 117-126.
49. Sun, Q.L., W. Li, H.K. Chen, and B.Q. Li. The variation of structural characteristics of macerals during pyrolysis. Fuel, 2003; 82(6): 669-676.
50. Averitt, P. Coal resources, in Chemistry of coal utilization, Elliott.M.A, Editor. 1981, Wiley-interscience: New York, Chichester, Brisbane, Toronto: 57.
51. Whitehurst, D.D. A primer on the chemistry and constitution of coal, in Orginal chemistry of coal, Gould R.F., Editor. 1978, Washington, American Chemistry Society: 1-35.
52. Fletcher, H.T., A.R. Kerstein, R.J. Pugmire, M.S. Solum, and D.M. Grant. Chemical Percolation model for develatilization. 3. Direct Use of 13C NMR Data To Predict Effect of Coal Type. Energy & Fuels, 1992; (6): 414-431.
53. Freihaut,J.D., W.M. Proscia, and D.J.Seery. Chemical Characteristics of Tars Produced in a Novel Low-Severity, Entrained-Flow Reactor. Energy & Fuels, 1989; 3(6): 692-703.
54. Solomon, P.R., T.H. Fletcher, and R.J. Pugmire. Progress in coal pyrolysis. Fuel, 1993; 72(5): 587-597.
55. Suuberg, E.M., D. Lee, and J.W. Larsen. Temperature dependence of crosslinking processes in pyrolysing coals. Fuel, 1985; 64(12): 1668-1671.
56. Huntington, H.D. Coal properties-measurement and application to cokemaking. Iron and steel Engineer, 1997; 74(11): 28-33.
57. Zhang, Q., X. Wu, A. Feng, and M. Shi. Prediction of coke quality at Baosteel. Fuel Processing Technology, 2004; 86(1): 1-11.
58. Minkina, M., F.L.G. Oliveira, and V. Zymla. Coal lump devolatilization and the resulting char structure and properties. Fuel Processing Technology, 2010; 91(5): 476-485.

59. Saxena, S.C. Devolatilization and combustion characteristics of coal particles. Progress in Energy and Combustion Science. 1990; 16(1): 55-94.
60. Aristoff, E., R.W. Rieve, and H. Shalit. Low-temperature Tar, in Chemistry of coal utilization, Elliott M.A., Editor. 1981, Wiley-interscience: New York, Chichester, Brisbane, Toronto: 983-1002.
61. Mcneil, D. High-temperature coal tar, in Chemistry of coal utilization, Elliott.M.A, Editor. 1981, Wiley-interscience: New York, Chichester, Brisbane, Toronto: 1006-1083.
62. The coal tar book. Leeds, 1953.
63. Strezov, V., J.A. lucas, T.J. Evans, and L. Strezov. Effect of heating rate on the thermal properties and devolatilization of coal. Journal of Thermal Analysis and Calorimetry. 2004; 78: 385-397.
64. Carangelo, R.M., P.R. Solomon, and D.J. Gerson. Application of TG-FT-i.r. to study hydrocarbon structure and kinetics. Fuel; 1987, 66(7): 960-967.
65. Whelan, J.K., P.R. Solomon, G.V. Deshpande, and R.M. Carangelo. Thermogravimetric Fourier Transform Infrared Spectroscopy (TG-FTIR) of Petroleum Source Rocks Initial Results. Energy & Fuels, 1988; 2(1): 65-73.
66. Seebauer, V., J. Petek, and G. Staudinger. Effects of particle size, heating rate and pressure on measurement of pyrolysis kinetics by thermogravimetric analysis. Fuel, 1997; 76(13): 1277-1282.
67. van Krevelen, D.W, F.J. Huntjens, and H.N.M. Dormans. Chemical structure and properties of coal. XVI. Plastic behaviour on heating. Fuel, 1956; 35: 462-475.
68. Solomon, P.R., D.G. Hamblen, R.M. Carangelo, M.A. Serio, and G.V. Deshpande. Models of tar formation during coal devolatilization. Combustion and Flame. 1988; 71(2): 137-146.
69. Miura, K., H. Tomobe, and T. Fujisawa. Quantitative estimation of metaplast in heat-treated coal by solvent extraction, in Structure and thermoplasticity of coal, Komaki, I., S. Itagaki, and T, Miura, Editors. 2005, Nova Science, New York: 77-88.
70. Marzec, A., S. Czajkowska, and J. Moszynski. Mass Spectrometric and Chemometric Studies of Thermoplastic Properties of Coals. 1. Chemometry of Conventional, Solvent SwellinG, and Extraction Data of Coals. Energy & Fuels, 1992; (6): 97-103.
71. Schulten, H-R., A. Marzec, and S. Czajkowska. Mass spectrometric and chemometric
studies of thermoplastic properties of coals. 2. Field ionization mass spectrometry of coals. Energy & Fuels, 1992; (6): 103-108.
72. Duffy, J.J, K. Steel, O. Scholes, and M. Mahoney. The use of high temperature rheometry to study the foaming behaviour of coal and elucidate the mechanisms for oven wall pressure. Metec Insteel Con, 2011.
73. Habermehl, D., F. Orywal, and H-d. Beyer, Plastic properties of coal, in Chemistry of coal utilization, Elliott.M.A, Editor. 1981, Wiley-interscience: New York, Chichester, Brisbane, Toronto: 317-368.
74. Waters, P.L. Rheological properties of coal during the early stage of thermal softening. Fuel, 1962; 41 XLI: 3-14.
75. Lynch, L.J., D.S. Webster, R. Sakurovs, W.A. Barton, and T.P. Maher. The molecular basis of coal thermoplasticity. Fuel, 1988; 67(4): 579-583.
76. Gavalas, G.R. Coal pyrolysis: Amsterdam, Oxford, New York: Elsevier Scientific publishing company, 1982.

77 Sasaki, M., R. Takahashi, and I. Mochida. Relation between the fluorescence intensity of vitrinites and the fluidity of coals. Fuel, 1990; 69(4): 529-532
78. Kidena, K., M. Katsuyama, S. Murata, M. Nomura. Study on Plastcity of Maceral Concentrates in terms of their Structural Features. Energy & Fuels, 2002;16(5):1231-1238.
79. Shen, J., Y. Qin, G.X. Wang, X. Fu, C.T. Wei, and B. Lei. Relative permeabilities of gas and water for different rank coals. International Journal of Coal Geology, 2011;86(2-3): 266-275.
80. Khan, M.R. and R.G. Jenkins. Influence of weathering and low-temperature oxidation on the thermoplastic properties of coal, in Chemistry of coal weathering, Nelson, C.R., Editor, 1989: Amsterdam: 109.
81. Brown, H.R., W.R. Hesp, and P.L. Waters. J. Inst. Fuel (April 1964):130-138.
82. Stanger, R. A mechanistic study of coal behaviour during pyrolysis, gasification and direct iron reduction. Phd thesis; 2008
83. Glass, H.D. Differential Thermal Analysis of Coking Coals. Fuel, 1955; 34: 253.
84. Rosenvold, R.J., J.B. Dubow, and K. Rajeshwar. Thermal analyses of Ohio bituminous coals. Thermochimica Acta, 1982; 53(3): 321-332.
85. Butorin, V.I. and Matveeva, G.N. Computerized investigation of temperature distributions in coke-oven chambers. Coke and Chemistry, 1975; 10: 20-24.
86. Sakurovs, R., L.J. Lynch, and T.P. Maher. The prediction of the fusibility of coal blends. Fuel Processing Technology, 1994; 37(3): 255-269.
87. Sakurovs, R. Direct evidence that the thermoplastic properties of blends are modified by interactions between the component coals. Fuel, 1997; 76(7): 615-621.
88. Duffy, J.J., M.R. Mahoney, and K.M. Steel. Influence of thermoplastic properties on coking pressure generation: Part 1 - A study of single coals of various rank. Fuel, 2010; 89(7): 1590-1599.
89. Duffy, J.J., M.R. Mahoney, and K.M. Steel. Influence of coal thermoplastic properties on coking pressure generation: Part 2 - A study of binary coal blends and specific additives. Fuel, 2010; 89(7): 1600-1615.
90. Duffy, J.J., M. Castro Díaz, C.E. Snape, K.M. Steel, and M.R. Mahoney. Understanding the mechanisms behind coking pressure: Relationship to pore structure. Fuel 2007; 86(14): 2167-2178.
91. Sakurovs, R. Some factors controlling the thermoplastic behaviour of coals. Fuel, 2000; 79(3-4): 379-389.
92. Lewitt, M.W. and A.J. Lowe. Proton magnetic resonance thermal analysis in coal research: A users overview. Thermochimica Acta. 1997; 294(1): 13-21.
93. Supaluknari, S., F.P. Larkins, P. Redlich, and W.R. Jackson. Determination of aromaticities and other structural features of Australian coals using solid state 13C NMR and FTIR spectroscopies. Fuel Processing Technology, 1989; 23(1): 47-61.
94. VanderHart, D.L. and H.L. Retcofsky. Estimation of coal aromaticities by proton-decoupled carbon-13 magnetic resonance spectra of whole coals. Fuel, 1976; 55(3): 202-204.
95. Harmer, J., T. Callcott, M. Maeder, and B.E. Smith. A novel approach for coal characterization by NMR spectroscopy: global analysis of proton T1 and T2 relaxations. Fuel, 2001; 80(3): 417-425.
96. Suggate, R.P. and W.W. Dickinson. Carbon NMR of coals: the effects of coal type and rank. International Journal of Coal Geology, 2004; 57(1): 1-22.

97. Solomon, P.R., M.A. Serio, R.M. Carangelo, and R. bassilakis. Coal analysis by TG-FTIR. Advanced Fuel Research, Inc: 334.
98. Kawashima, H., Y. Yamashita, and I. Saito. Studies on structural changes of coal density-separated components during pyrolysis by means of solid-state 13C NMR spectra. Journal of Analytical and Applied Pyrolysis, 2000; 53(1): 35-50.
99. Hefta, R.S., H.H. Schobert, and t.l.W.R. Kube. Calorimetric pyrolysis of a North Dakota lignite. Fuel, 1986; 65(9): 1196-1202.
100 Janikowski, S.K. and V.I. Stenberg. Thermal analysis of coals using differential scanning calorimetry and thermogravimetry. Fuel, 1989; 68(1): 95-99.
101. Elder, J.P. and M.B. Harris. Thermogravimetry and differential scanning calorimetry of Kentucky bituminous coals. Fuel, 1984; 63(2): 262-267.
102. Feng, J. Laser pulse heating method of measuring the thermal diffusivity, specific heat and thermal conductivity of coal. Coal combustion science and technology of industrial and utility applications, 1988: 325.
103. Strezov. V., J.A. Lucas, and L. Strezov. Computer aided thermal analysis. Journal of Thermal Analysis and Calorimetry, 2003; 72: 907-918.
104. Australian Standard: Coal and coke-Analysis and testing, Part 12.4.1 High rank coal-caking and coking properties-Plasticity-Continuous-torque Gieseler method, 1996.
105. Barriocanal, C., D. Hays, J.W. Patrick, and A. Walker. A laboratory study of the mechanism of coking pressure generation. Fuel, 1998; 77(7): 729-733.
106. Casal, M.D., E. Díaz-Faes, R. Alvarez, M.A. Díez, and C. Barriocanal. Influence of the permeability of the coal plastic layer on coking pressure. Fuel, 2006; 85(3): 281-288.
107. Koch, A., R. Gruber, D. Cagniant, J. Pajak, A. Krzton, and J.M. Duchène. A physicochemical study of carbonization phases. Part I. Tars migration and coking pressure. Fuel Processing Technology, 1995; 45(2): 135-153.
108. Australian Standard Coal and coke-analysis and testing part 12.1: higher rank coal-caking and coking properties-crucible swelling number. 2002.
109. Australian Standard Coal and coke-analysis and testing Part 12.3: higher rank coal-caking and coking properties-dilatation. 2002.
110. Strezov, V., J.A. Lucas, and T.F. Wall. Effect of pressure on the swelling of density separated coal particles. Fuel, 2005; 84(10): 1238-1245.
111. Fu, Z., Z. Guo, Z. Yuan, and Z. Wang. Swelling and shrinkage behavior of raw and processed coals during pyrolysis. Fuel, 2007; 86(3): 418-425.
112. Versan Kök, M., E. Özbas, O. Karacan, and C. Hicyilmaz. Effect of particle size on coal pyrolysis. Journal of Analytical and Applied Pyrolysis, 1998; 45(2): 103-110.
113. http://en.wikipedia.org/wiki/Matrix-assisted_laser_desorption/ionization.
114. John, P., C.A.F. Johnson, J.E. Parker, G.P. Smith, A.A. Herod, C.-Z. Li, et al. Molecular masses up to 270 000 u in coal and coal-derived products by matrix assisted laser desorption ionization mass spectrometry (MALDI-m.s.). Fuel, 1994; 73(10): 1606-1616.
115. Arenillas, A., F. Rubiera, J.J. Pis. Simultaneous thermogravimetric-mass spectrometric study on the pyrolysis behaviour of different rank coals Journal of Analytical and Applied Pyrolysis, 1999; 50(1): 31-46.

116. Nali, M., F. Corana, L. Montanari, and L. Pellegrini. A pyrolysis-gas chromatography/mass spectrometry study on coals. Journal of Analytical and Applied Pyrolysis, 1994; 29(1): 15-23.
117. Strezov, V., J.A. Lucas, and L. Strezov. Experimental and modelling of the thermal regions of activity during pyrolysis of bituminous coals. Journal of Analytical and Applied Pyrolysis, 2004; 71(1): 375-392.
118. http://en.wikipedia.org/wiki/Carbon-13_NMR.
119. Nomura, M., K. Kidena, S. Murata, S. Yoshida, and S. Nomura, Molecular structure and thermoplastic properties of coal, in Structure and thermoplasticity of coal, Komaki, I., S. Itagaki, and T. Miura, Editors. 2005, Nova Science, New York: 1-34.
120. http://en.wikipedia.org/wiki/Differential_thermal_analysis.
121. Watson, E.S., M.J. O'Neill, J. Justin, and N. A. Brenner. A differential Scanning Calorimeter for quantitative differential thermal analysis. Anal. Chem, 1964; 36: 1233.
122. Tromp, P.J.J., F. Kapteijn, and J.A. Moulijn, Characterization of coal pyrolysis by means of differential scanning calorimetry.1. quantitative heat effects in an inert atmosphere, in Coal characterisation for conversion processes, 1986, Jacob A.M., K. Freek, Editors. 1987, Elsevier: Amsterdam-Oxford-New York-Tokyo: 46-57.
123. Liu, G.S, V. Strezov, J.A. Lucas, LJ. Wibberley. Thermal investigations of direct iron ore reduction with coal. Thermochimica Acta, 2004; 410(1-2): 133-140.
124. Strezov, V. Iron ore reduction using sawdust: Experimental analysis and kinetic modelling. Renewable Energy, 2006; 31(12): 1892-1905.
125. Australian Standard (AS1038.13-1990), Methods for the analysis and testing of coal and coke, part 13: tests specific to coke, section 3. determination of coke reactiviry index and coke strength after reaction. 1990.
126. Varma, A.K. Thermogravimetric investigations in prediction of coking behaviour and coke properties derived from inertinite rich coals. Fuel 2002; 81(10): 1321-1334.
127. Hays, D., J.W. Patrick, and A. Walker. Pore structure development during coal carbonization. 1. Behaviour of single coals. Fuel, 1976; 55(4): 297-302.
128. White, A., M.R. Davies, SD. Jones. Reactivity and characterization of coal maceral concentrates. Fuel, 1989; 68(4): 511-519.
129. Zeng, D., M. Clark, T. Gunderson, W.C. Hecker, and T.H. Fletcher. Swelling properties and intrinsic reactivities of coal chars produced at elevated pressures and high heating rates. Proceedings of the Combustion Institute, 2005; 30(2): 2213-2221.
130. Strugnell, B. and J.W. Patrick. Rapid hydropyrolysis studies on coal and maceral concentrates. Fuel, 1996; 75(3): 300-306.
131. MacPhee, J.A., L. Giroux, J.F. Gransden, and J.T. Price. The synergistic effect between macerals of different coals during coking. Fuel, 2005; 84(14-15): 1998-1999.
132. Hilding, T., S. Gupta, V. Sahajwall, B. BJorkman, and J.-O. Wikstrom. Degradation Behaviour of a High CSR Coke in an Experimental Blast Furnace: Effect of Carbon Structure and Alkali Reactions. ISIJ International, 2005; 45(7): 1041-1050.
133. Lundgren, M., B. BJorkman, and L.-S. Okvist, Coke reactivity under blast furnace condition and in the CSR/CRI test.

134. Pusz, S., B. Kwiecinska, A. Koszorek, M. Krzesinska, and B. Pilawa. Relationships between the optical reflectance of coal blends and the microscopic characteristics of their cokes. International Journal of Coal Geology, 2009; 77(3-4): 356-362.
135. Wang, J., J. Du, L. Chang, and K. Xie. Study on the structure and pyrolysis characteristics of Chinese western coals. Fuel Processing Technology, 2010; 91(4): 430-433.
136. Liu, Q., H. Hu, Q. Zhou, S. Zhu, and G. Chen. Effect of inorganic matter on reactivity and kinetics of coal pyrolysis. Fuel, 2004; 83(6): 713-718.
137. Shi, L., Q. Liu, X. Guo, W. Wu, and Z. Liu. Pyrolysis behavior and bonding information of coal-A TGA study. Fuel Processing Technology; 108(0): 125-132.
138. Serio, M.A, D.G. Hamblen, J.R. Markham, and P.R. Solomon. Kinetics of volatile product evolution in coal pyrolysis:Experiment and theory. Energy & Fuels, 1987; 1: 138-152.
139. Solomon, P.R., D.G. Hamblen, R.M. Carangelo, M.A. Serio, and G.V. Deshpande. General model of coal devolatilization. Energy & Fuels, 1988; 2: 405-422.
140. Smith, K.L. The structure and reaction processes of coal. New York: Plenum Press; 1994.
141. Wang, H., X. Jiang, H. Liu, S. Wu. Fast pyrolysis comparison of coal-water slurry with its parent coal in Curie-point pyrolyser. Energy Conversion and Management, 2009; 50(8): 1976-1980.
142. Wachowska, H. and W. Pawlak. Effect of cleavage of ether linkages on physicochemical properties of coals. Fuel, 1977; 56(4): 422-426.
143. Das, T.K. Thermogravimetric characterisation of maceral concentrates of Russian coking coals. Fuel, 2001; 80(1): 97-106.
144. Nomura, S. and K.M. Thomas. The effect of swelling pressure during coal carbonization on coke porosity. Fuel, 1996; 75(2): 187-194.
145. Harpalani, S.and R.A. Schraufnagel. Shrinkage of coal matrix with release of gas and its impact on permeability of coal. Fuel, 1990; 69(5): 551-556.
146. Strezov, V., J.A. Lucas, and L. Strezov. Investigation of the swelling pressure development during slow pyrolysis of thermoplastic coals. Journal of Analytical and Applied Pyrolysis, 2005; 74(1-2): 88-95.
147. Marzec, A. and S. Czajkowska. Studies on Generation of Excessive Coking Pressure. 2. Field Ionization Mass Spectrometry of Coals Showing Different Contraction during Carbonization. Energy & Fuels, 1997; 11: 982-986.
148. Gao, H., S. Murata, M. Nomura, M. Ishigaki, M. Qu, and M. Tokuda. Experimental observation and image analysis for evaluation of swelling and fluidity of single boal particles heated with CO2 laser. Energy & Fuels, 1997; 11(3): 730-738.
149. Marsh, H. and R.C. Neavel. Carbonization and liquid-crystal (mesophase) development. 15. A common stage in mechanisms of coal liquefaction and of coal blends for coke making. Fuel, 1980; 59(7): 511-513.
150. Spiro, C.L. Space-filling models for coal: a molecular description of coal plasticity. Fuel, 1981; 60(12): 1121-1126.
151. Gagarin, S.G. Pressure generation in coking furnaces: A review. Coke and Chemistry, 2011; 54(6): 193.

152. Koch, A., R. Gruber, D. Cagniant, and J.M. DuchÃ¨ne. A physicochemical study of carbonization phases, Part II: quenching experiments at the pilot scale. Fuel Processing Technology, 1996; 48(1): 29-37.
153. Zubkova, V. Some peculiarities of formation mechanism of metallurgical coke from polish coals. Fuel, 2004; 83(9): 1205-1214.
154. Nomura, S., T. Arima, and K. Kato. Coal blending theory for dry coal charging process. Fuel, 2004; 83(13): 1771-1776.
155. Stewart, I.M. Coal properties, analysis and effective use. 1982: 2-1-12.
156. Cai, H.Y., A.J. Güell, I.N. Chatzakis, J.Y. Lim, D.R. Dugwell, and R. Kandiyoti. Combustion reactivity and morphological change in coal chars: Effect of pyrolysis temperature, heating rate and pressure. Fuel, 1996; 75(1): 15-24.
157. Ward, C.R. Coal characteristics and resources for ironmaking. 2005.
158. Horrocks, K.R.S., R.B. Cunningham, J.F. Ellison, and R.J. Nightingale, Coke quality at BHP Steel Port Kembla, in 4th European Coke and Ironmaking Cong., ATS-RM. 2000, Paris, 167-173.
159. Alvarez, R., J.J. Pis, M.A. Diez. Studies on Generation of Excessive Coking Pressure. 1. Semicoke Contraction versus Thermoplastic Properties of Coals. Energy & Fuels, 1997; (11): 978-981.
160. Hanrot, F., D. Ablitzer, J.L. Houzelot, and M. Dirand. Experimental measurement of the true specific heat capacity of coal and semicoke during carbonization. Fuel, 1994; 73(2): 305-309.
161. Merrick, D. The thermal decomposition of coal: mathematical models of the chemical and physical changes, in Coal Science and Chemistry, Volborth A., Editor. 1987; Amsterdam: 307-342.
162. Agroskin, A.A., E.I. Goncharov, V.M. Tyangunov, I.G. Zubilin, and V.B. Gleibman. Thermal properties of coals in relation to bulk density, carbonizing rate and isothermal period. Coke and Chemistry, 1977; 8: 14.
163. Lopez-Peinado, A.J., P.J.J. Tromp, and J.A. Moulijn. Quantitative heat effects associated with pyrolysis of coals, ranging from anthracite to lignite. Fuel, 1989; 68(8): 999-1004.
164. Badzioch, S., D.R. Gregory, and M.A. Field. Investigation of the temperature variation of the thermal conductivity and thermal diffusivity of coal. Fuel, 1964; 43: 267.
165. Dindi, H., X.-h. Bai, and W.B. Krantz. Thermal and electrical property measurements for coal. Fuel, 1989; 68(2): 185-192.
166. Zhou, J., K. Walton, D. Laskovski, P. Duncan, and K.P.Galvin. Enhanced separation of mineral sands using the Reflux Classifier. Minerals Engineering, 2006; 19(15): 1573-1579.
167. Incropera, F.P., D.P. Dewitt, T.L. Bergman, and A.S. Lavine. Fundamentals of heat and mass transfer. 6th ed 2005.
168. Green, D.W. and R.H. Perry. Perry's chemical engineers' handbook. 2008.
169. Weber, J.V., M. Schneider, M. Darif, M. Swistek, E. Yax, and R. Bertau. Contribution to the study of copyrolysis. Correlation of additives analytical data with optical texture of resultant cokes. Fuel Processing Technology, 1990; 24: 27-33.
170. Aoki, H., T. Miura, S. Itagaki, K. Fukuda, Analysis of dilatation and contraction of coal during carbonization, in Structure and thermoplasticity of coal, Komaki I., S. Itagaki, and T. Miura, Editors. 2005, Nova Science, New York: 109-117.

171. Attar A. Bubble nucleation in viscous material due to gas formation by a chemical reactions: application to coal pyrolysis. AIChE, 1978; 24(1): 106-115.
172. Agroskin, A.A., E.I. Goncharov, and N.S. Gryaznov. Thermal properties of coals in the plastic state. Coke Chem, 1972; 9: 3-5.
173. Tomeczek, J. and H. Palugniok. Kinetics of mineral matter transformation during coal combustion. Fuel, 2002; 81(10): 1251-1258

Publications

Journals

1. W. Xie, R. Stanger, J. Lucas, T. Wall, M.R. Mahoney, Coal macerals Separation and the preliminary thermo-swelling analysis based on the Computer Aided Thermal Analysis. Fuel, Volume 103, pages 1021-1031

2. Rohan Stanger, **Wei Xie**, Terry Wall, John Lucas, Merrick Mahoney, Dynamic behaviour of coal macerals during pyrolysis – Associations between physical, thermal and chemical changes. Proceedings of the Combustion Institute, 34(2) Pages 2393-9400

3. Rohan Stanger, **Wei Xie**, Terry Wall, John Lucas, Merrick Mahoney, Dynamic Elemental Thermal Analysis: A technique for continuous measurement of carbon, hydrogen, oxygen chemistry of tar species evolved during coal pyrolysis. Fuel, Volume 103, pages 764-772

Conferences

1. **W. Xie,** R. Stanger, J. Lucas, T. Wall, M.R. Mahoney, Influence of heating rate and particle size on thermo-swelling properties of heating coal, Proceedings of the Australian Combustion Symposium. Newcastle, November, 2011 (in CD)

2. Rohan Stanger, **Wei Xie**, Terry Wall, John Lucas, Merrick Mahoney, Dynamic behaviour of coal macerals during pyrolysis- associations of thermal and physical phenomena with the tar and gas evolution and C-H-N-S-O chemistry. 34th International Symposium on Combustion, Poland, July, 2012 (in CD)

3. Rohan Stanger, **Wei Xie**, Terry Wall, John Lucas, Merrick Mahoney, Dynamic measurement of coal thermal properties and elemental composition of volatile matter during coal pyrolysis. 6th International Congress on the Science and Technology of Ironmaking, Brazil, 2012 (in CD)

Appendix A, Calibration

All calibration Figures in Chapter 3 are included here.

A1, Furnace temperature distribution

Figure A.1 shows the temperature distribution of Sin-ku Riko Gold Image infrared heating furnace. The thermocouple sat first in one side of the furnace detecting the *in situ* temperature; it was gradually moved towards the other side of the furnace with instantaneous temperature detected. The relationship between displacement of thermocouple and detected temperature in Figure A.1 shows that more than 15 cm in the furnace can be considered a stable temperature region. This guarantees that the measured samples can sit in the stable temperature zone even if a huge swelling occurs.

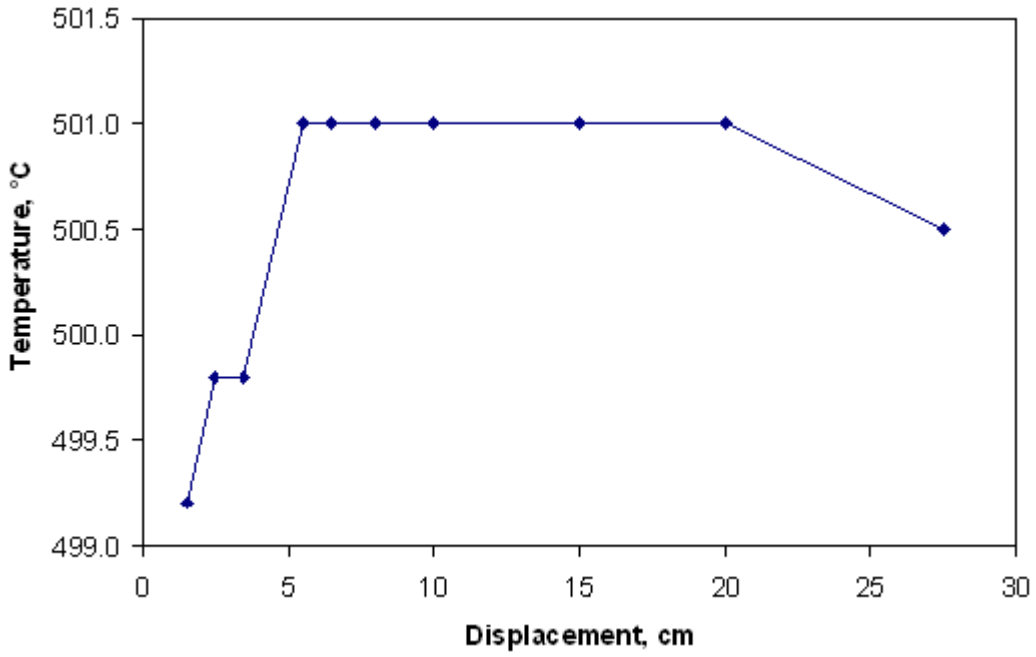

Figure A.1. Temperature distribution of the Sin-ku Riko Gold Image infrared heating furnace.

A2, Compressible spring

Figure A.2 indicates that the spring employed for the experiments can be compressed up to 45 mm. For coals and coal maceral concentrates, if they are expected to have a huge swelling that is over the measured range of one spring, two springs would be connected together to measured the actual swelling of heating samples.

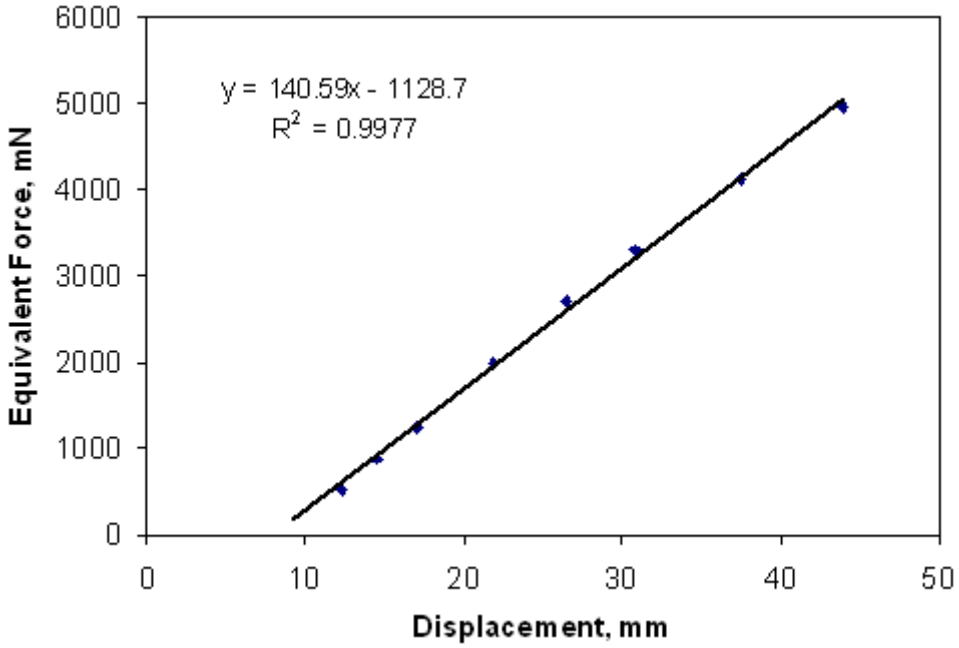

Figure A.2. Relationship between spring compression and equivalent force.

A3, Apparent thermal resistance

Figure A.3 shows the changes of heat rate with temperature for copper at three different heating rates of 3, 5 and 10°C/min. The cylindrical copper is 30 mm long with a diameter 11.5 mm sooted by carbon. During calibration, there was only one thermocouple used in the centre of the copper cylinder. Since the copper has a very high thermal conductivity [167], the surface temperature is considered exactly the same as the measured centre temperature. Carrier gas was kept 30 ml/min, which is the same as the gas flow used for cokemaking.

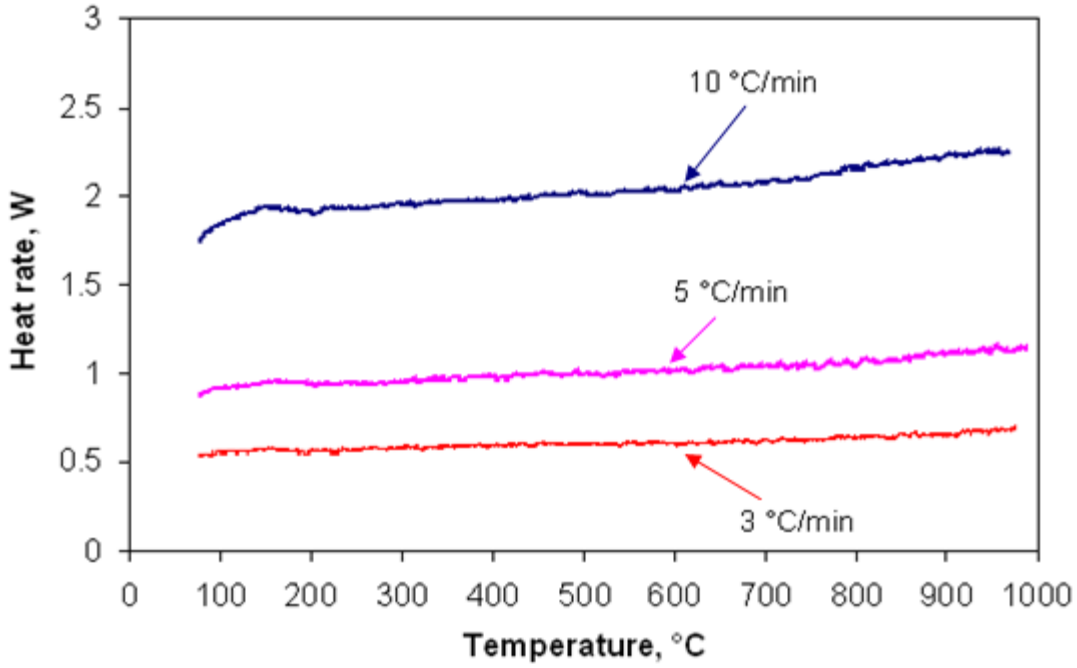

Figure A.3. Heat rate of heating furnace at three different heating rates calibrated by a copper.

Following equation 3-1 (section 3.1.2.1), the heat rate from graphite to the sample surface is:

$$Q = \frac{2\pi Lk(T_g - T_s)}{\ln(r_2 / r_1)} \qquad \text{(A-1)}$$

Where Q is the heat rate (W); k is the thermal conductivity of the graphite (W/m·K); L (m) is the length of the sample; r_1 is the distance from the centre to the surface of the sample and r_2 is the distance from the centre of the sample to the graphite surface where the graphite control thermocouple is positioned (m). T_g and T_s are the temperatures of the graphite and the surface of the samples (K), respectively.

For calibration using copper, at a fixed heating rate, heat rate equals:

$$Q = m \times C_p \times \frac{\Delta T}{\Delta t} \qquad \text{(A-2)}$$

Where Q is the heat rate (W), C_p is specific heat of copper at transient temperature, $\Delta T/\Delta t$ is heating rate.

Combine equations (A-1) and (A-2),

$$\frac{2\pi Lk}{\ln(r_2 / r_1)} = \frac{Q}{(T_g - T_s)} \qquad \text{(A-3)}$$

Therefore, the reciprocal value of the apparent thermal resistance $\ln(r_2/r_1)/2\pi Lk$ at a fixed heating rate can be obtained based on equation (A-3), as shown in Figure A.4. The relationships between the reciprocal value of the apparent thermal resistance *(Y)* and the instant temperature *(X)* at three different heating rates of 3, 5 and 10°C/min are reported here.

3°C/min heating rate

$$y = 3.98077E(-13)x4 - 7.10084(-10)x3 + 3.34200E(-7)x2 + 1.60128E(-5)x + 5.57080E(-2)$$

5°C/min heating rate

$$y = 3.00605E(-14)x4 + 1.25195E(-10)x3 - 2.71341E(-7)x2 + 1.63596E(-4)x + 5.02967E(-2)$$

10°C/min heating rate

$$y = 1.25613E(-13)x4 - 8.31703E(-11)x3 - 7.43118E(-8)x2 + 1.50475E(-4)x + 5.55541E(-2)$$

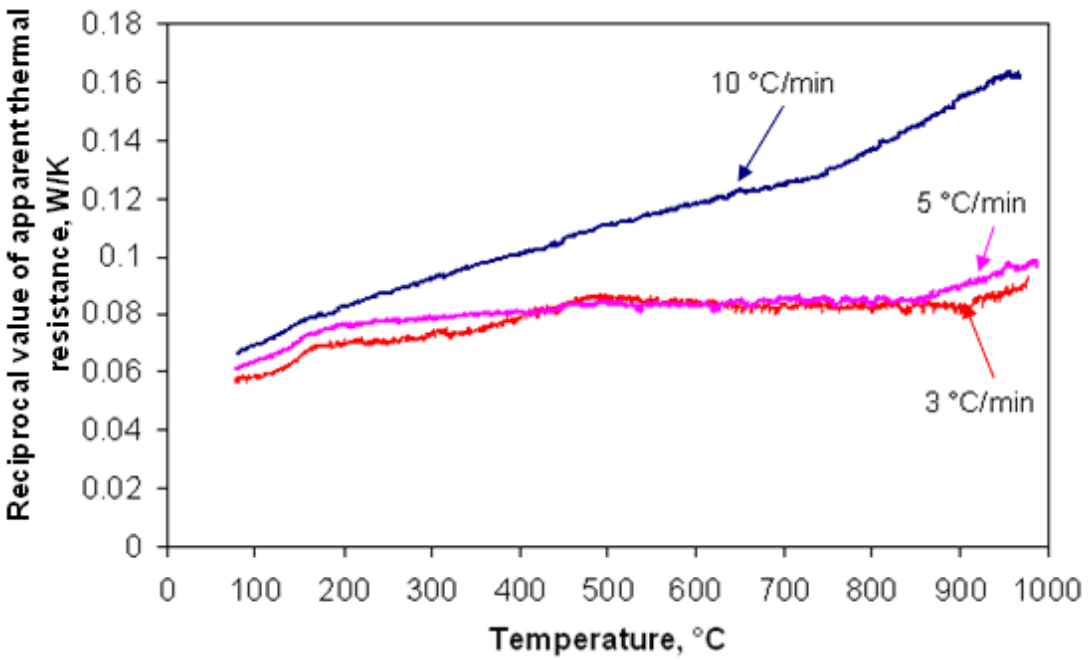

Figure A.4. Reciprocal value of the apparent thermal resistance of heating furnace at three different heating rates calibrated by a copper.

The reciprocal values of the apparent thermal resistances obtained from the calibration were used for numerically calculating the volumetric apparent specific heat and thermal conductivity of heating coal samples. Application of apparent thermal resistance to solid material of Al_2O_3 with known Cp was carried out at a heating rate of 10°C/min. The result in Figure A.5 indicates that the calculated Cp is very close to the real Cp of Al_2O_3 [167], only some errors exist when the temperature is over 700°C.

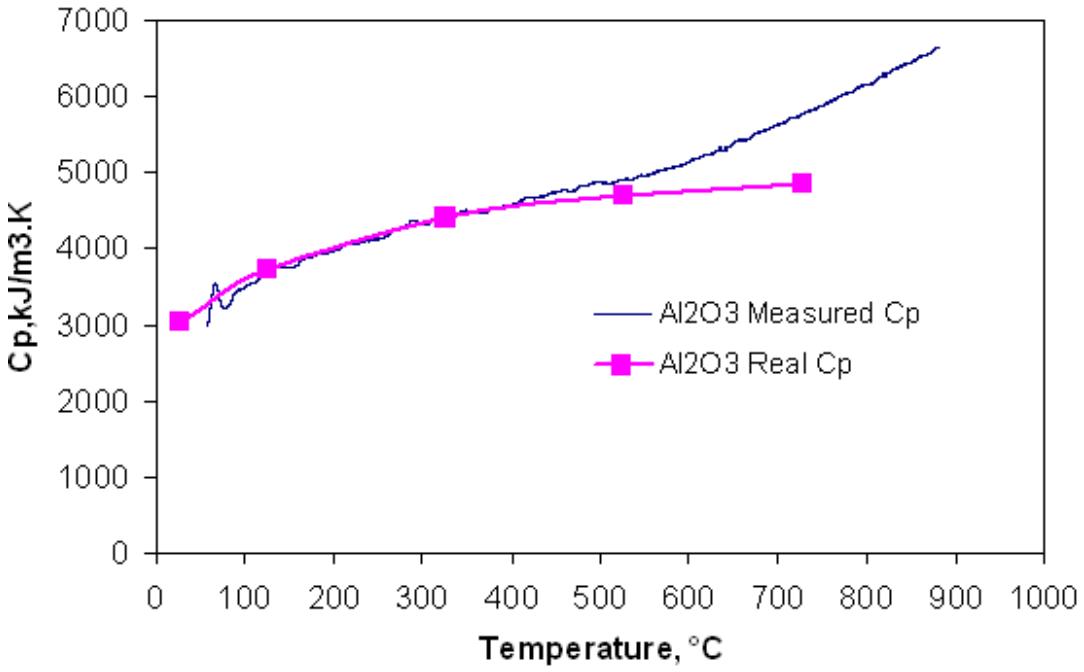

Figure A.5. Calculated Cp comparing to real Cp of Al2O3 at a heating rate of 10°C/min.

A4, Dynamic Elemental Thermal Analysis (DETA) calibration

The calibration of elemental compositions for Benzoic acid ($C_7H_6O_2$) is shown in Figure A.6. Benzoic acid ($C_7H_6O_2$) was vaporized and combusted in a crucible in the Sin-ku Riko Gold Image infrared heating furnace. The products of CO_2, CO and H_2O from combusted Benzoic acid ($C_7H_6O_2$) were detected each second. C concentration was based on the concentrations of CO and CO_2, H concentration was obtained from the detected H_2O concentration. Oxygen concentration evolved from Benzoic acid ($C_7H_6O_2$) with temperature was calculated based on the difference of oxygen between the produced oxygen concentration from combusted products and introduced (consumed) oxygen concentration. The ratios of elemental H and O with elemental C are shown in Figure A.6. It can be seen that the measured H and O concentrates match the theoretical values. The mass of all elements was calculated based on the integrated volumetric concentrations and total gas flow rate. The original mass of Benzoic acid ($C_7H_6O_2$) is 0.1584 g, the measured mass from C, H and O is 0.1565 g, which only has an error of 1.2%. Therefore, it is considered that the instruments for measuring CO_2, CO and H_2O were calibrated.

After the calibration for C, H and O, elements S and N were calibrated based on Diphenylamine ($C_{12}H_{11}N$) and Sulfolane ($C_4H_8O_2S$), as shown in Figure A.7 and Figure A.8. S and N concentrations were obtained by combusted products of SO_2, NO and NO_2. The measured S concentration in Figure A.7 matches the theoretical S concentration against the C

concentration in Sulfolane ($C_4H_8O_2S$). The relationship between N concentration and C concentration for Diphenylamine ($C_{12}H_{11}N$) in Figure A.8 was calibrated with a factor introduced, which made the measured results match the theoretical values.

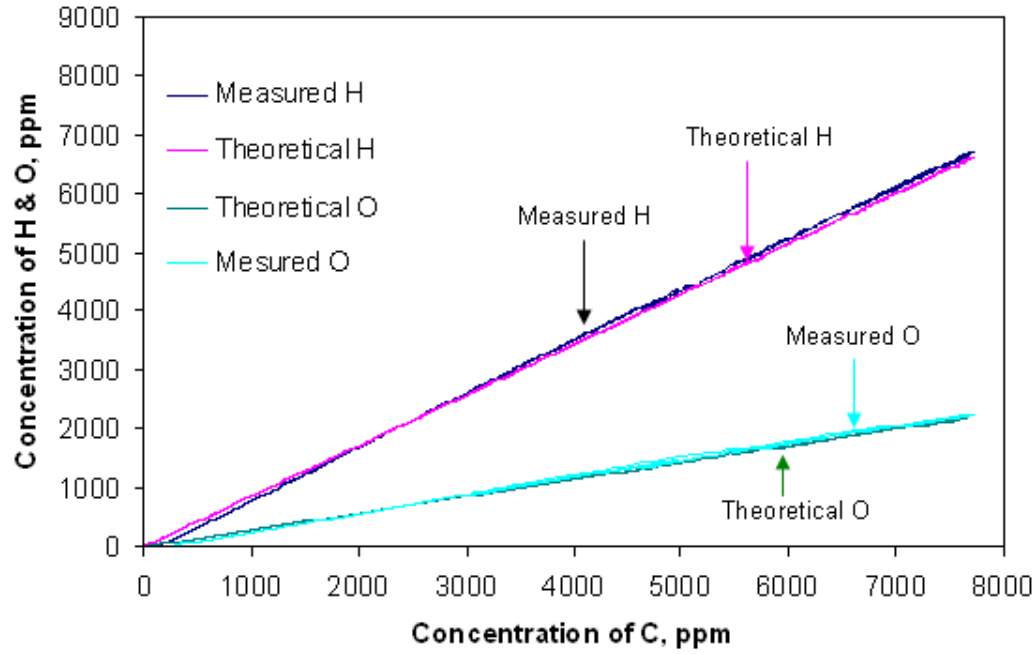

Figure A.6. Elemental evolutions for benzoic acid combustion at a heating rate of 10°C/min.

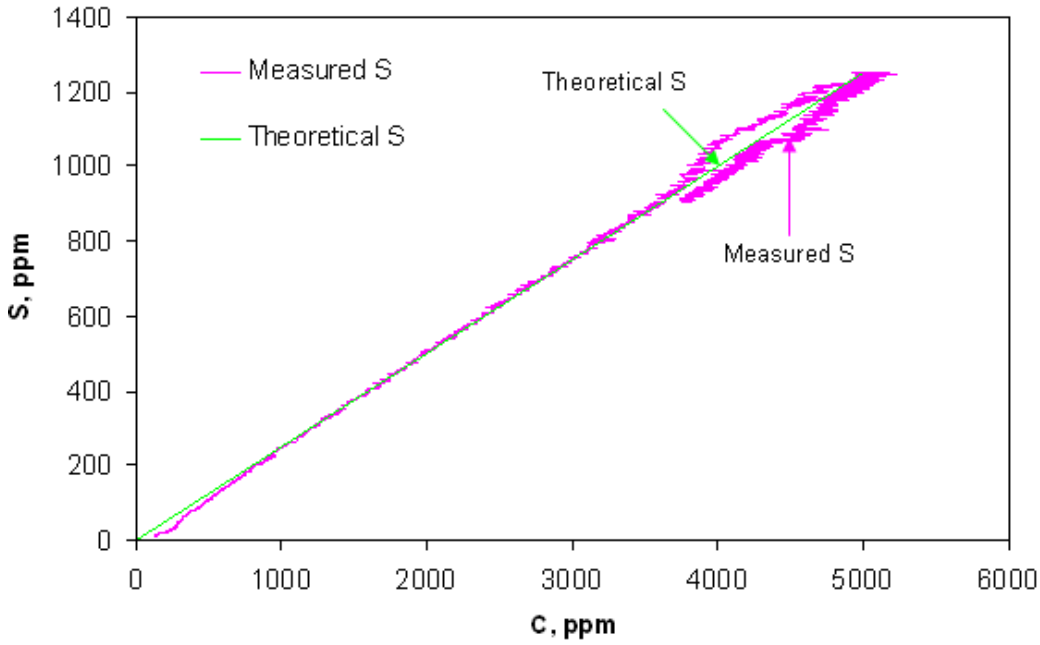

Figure A.7. Calibration of S concentration evolution with C concentration

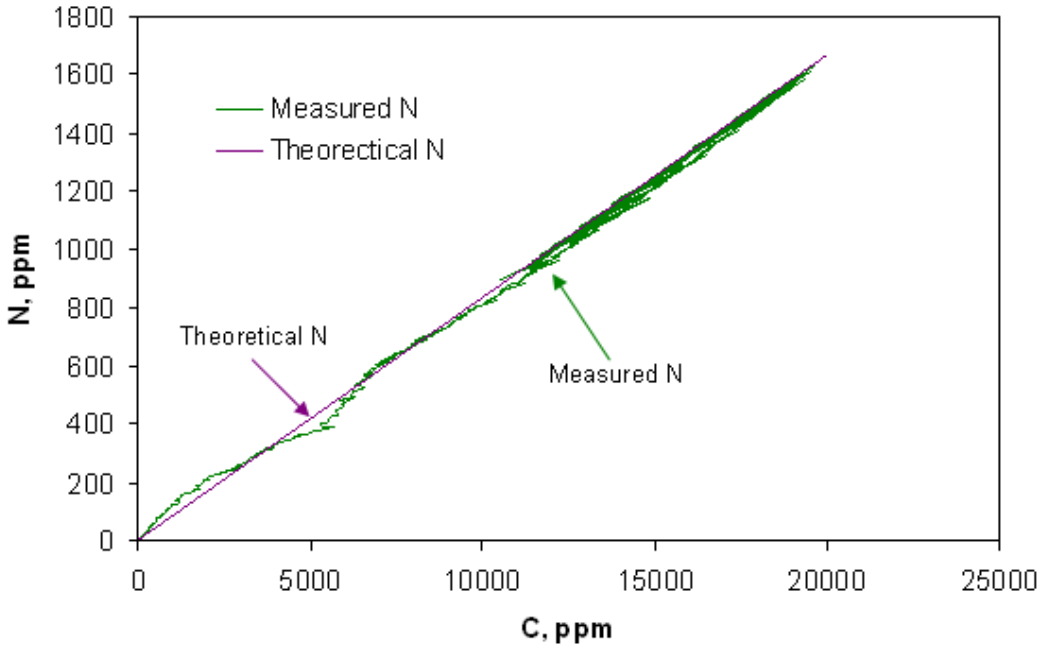

Figure A.8. Calibration of N concentration evolution with C concentration

Appendix B, Effect of coal bed length on swelling, apparent specific heat and thermal conductivity

Figures B.1-3 are the results of swelling, apparent specific heat and thermal conductivity for coal sample E at a heating rate of 10°C/min with three different coal bed lengths of 20, 30 and 40 mm. The results indicate that coal with different packed lengths show the similar swelling exception for a higher extent of high temperature contraction for 40 mm packed length. The specific heat during primary exothermic reaction for 40 mm coal bed length also decreases more than that of 20 and 30 mm coal bed lengths. The apparent specific heat of heating coal is calculated based on the measured control, surface and centres temperatures of heating sample (in Chapter 3), therefore, it can be concluded that the difference between surface and centre temperatures for 40 mm coal bed length sample is larger than that of 20 and 30 mm coal bed length samples. After primary devolatilization, the temperature for the onset of rapid increase of thermal conductivity decreases with increasing coal bed length. The possible explanation is as follows

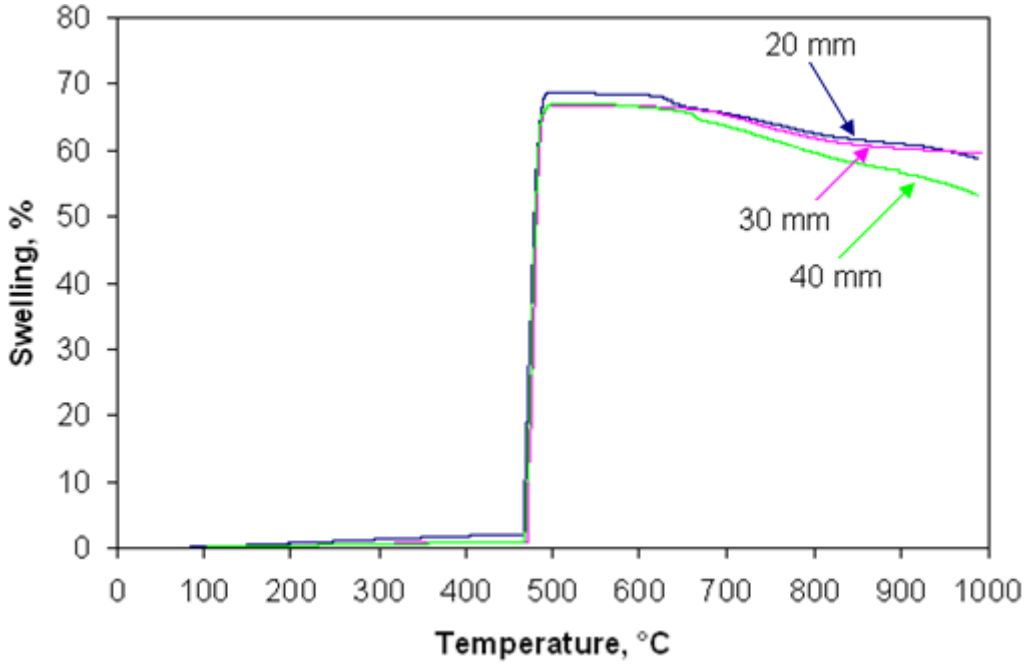

Figure B.1. Swelling of coal sample E at a heating rate of 10°C/min with different coal bed lengths.

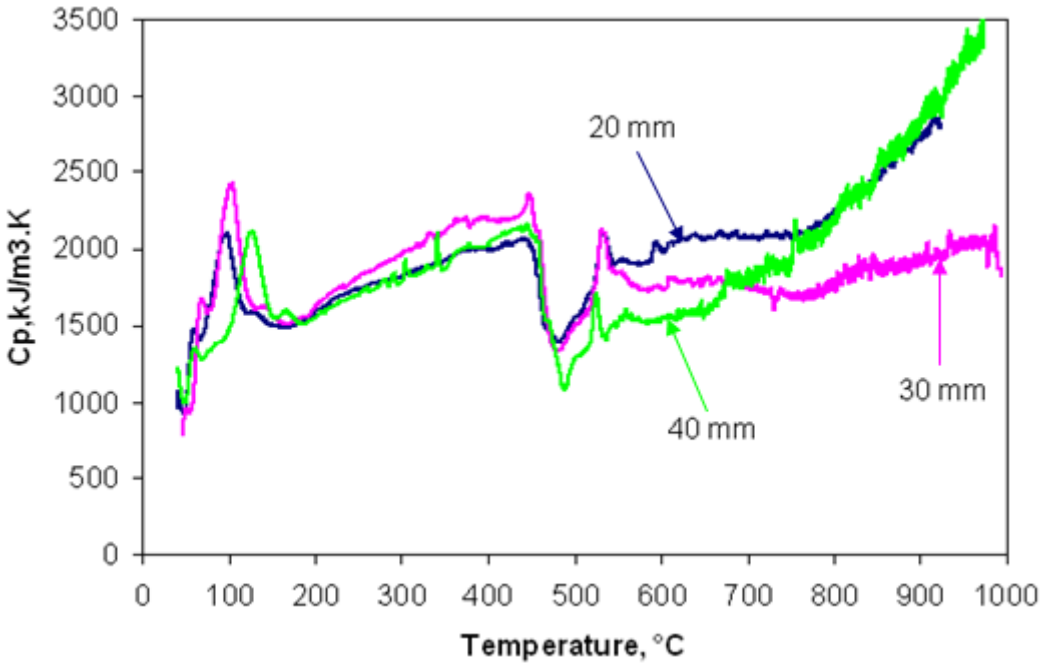

Figure B.2. Specific heat of coal sample E at a heating rate of 10°C/min with different coal bed lengths.

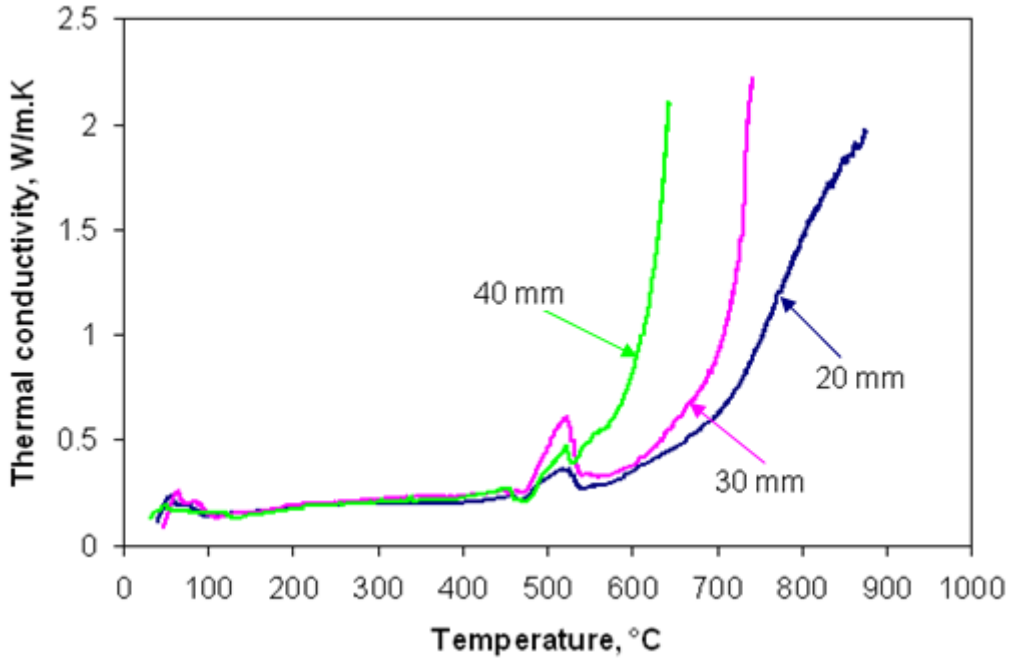

Figure B.3. Thermal conductivity of coal sample E at a heating rate of 10°C/min with different coal bed lengths.

B.1 From graphite to sample surface

The experimental schematic representation for coal pyrolysis is followed in Figure B.4, the appropriate form of the heat equation for heat conduction in the cylinder without heat generation is

$$\frac{1}{r}k\frac{\partial}{\partial r}\left(r\frac{\partial T}{\partial r}\right)=0 \qquad (1)$$

$$q_r=-kA\frac{dT}{dr}=-k(2\pi rL)\frac{dT}{dr} \qquad (2)$$

Since equation 1 indicates that the quantity *kr(dT/dr)* is independent of r, it follows from equation 2 that the conduction heat transfer rate q_r is a constant in the radial direction, although the q_r may be affected by the length of the cylinder, *L*.

The temperature distribution may be determined by assuming the value of *k* to be constant, equation 1 may be integrated twice to obtain the general solution, $T(r)=C_1 lnr+C_2$, solving for C_1 and C_2 and substituting into the general solution, the temperature distribution may be obtained,

$$T(r)=\frac{T_{graphite}-T_{surface}}{\ln(r_1/r_2)}\ln\left(\frac{r}{r_2}\right)+T_{surface} \qquad (3)$$

Where r_1 and r_2 are the radius from the cylinder axis to sample surface and graphite, respectively; if the temperature distribution, equation 3, is used with Fourier's law, equation 2, the heat transfer rate can be expressed as,

$$q_r=\frac{2\pi Lk(T_{graphite}-T_{surface})}{\ln(r_2/r_1)} \qquad (4)$$

Equation 4 indicates the heat transfer rate from graphite to sample surface is linear with packed sample length.

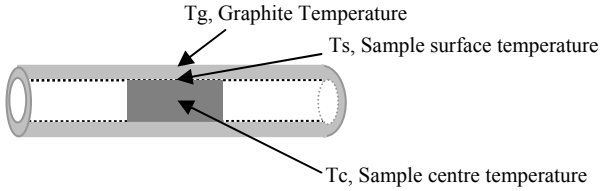

Figure B.4. Schematic representation of measured temperatures for heating sample.

B.2 From sample surface to sample centre

If the packed sample length is L_1 and L_2 and ($L_1>L_2$), respectively, heat transfer rate may be expressed as,

$$q_{L_1}=\frac{L_1}{L_2}q_{L_2} \qquad (L_1>L_2) \qquad (5)$$

Thermal conductivity of heating sample at any radius r close to the axis of cylinder with rising temperature may be expressed as,

$$k = \frac{q_r \ln(r_2/r)}{2\pi L(T_{surface} - T_r)} \quad (6)$$

Equation 5 combines with equation 6, the difference of the thermal conductivity for heating sample with various packed length is determined by ($T_{surface}$-T_r), for different packed sample length L_1 and L_2 (L_1>L_2), heat transfer rate obtained from graphite may be expressed as equation 5.

Total heat (E_g) generated by exothermic reaction of heating coal with different packed length, L_1 and L_2 is,

$$E_{g_{L_1}} = \frac{L_1}{L_2} E_{g_{L_2}} \quad (L_1 > L_2) \quad (7)$$

However, total heat is carried out by carrier gas argon under fixed gases flow rate, no matter what the packed sample length,

$$E_{Loss_{L_1}} = E_{Loss_{L_2}} \quad (8)$$

In terms of equations 5, 7 and 8, energy stored per volume unit of sample,

$$E_{store_{L_1}} > E_{store_{L_2}} \quad (9)$$

It may be concluded, for equations 6 and 9, the sample centre temperature will be higher at longer sample packing, namely ($T_{surface}$-T_r) decreases with the increase of packed sample length, therefore, the rapid increase of thermal conductivity will occur at lower temperature with increasing packed sample length. For three different packed lengths, from sample surface to centre, the relationship between thermal conductivity and ($T_{surface}$-T_{centre}) is shown in Figure B.5.

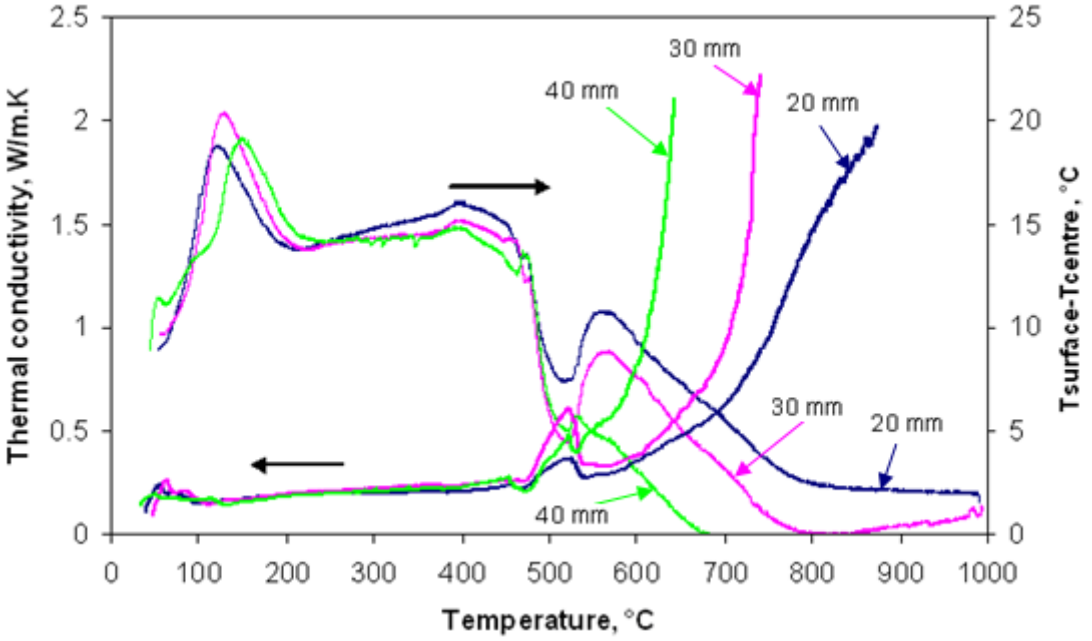

Figure B.5. The relationship between thermal conductivity and ($T_{surface}$-T_{centre}) with different packed lengths under same heating conditions for coal sample E.

Appendix C, Scaled elemental compositions for residue of 86.4 V and 32.4 V

Figure C.1 and Figure C.2 are the re-scaled elemental compositions of H, O, N and S for Figure 8.16 and Figure 8.17, so that it is easier to observe the instantaneous elemental compositions of the residue.

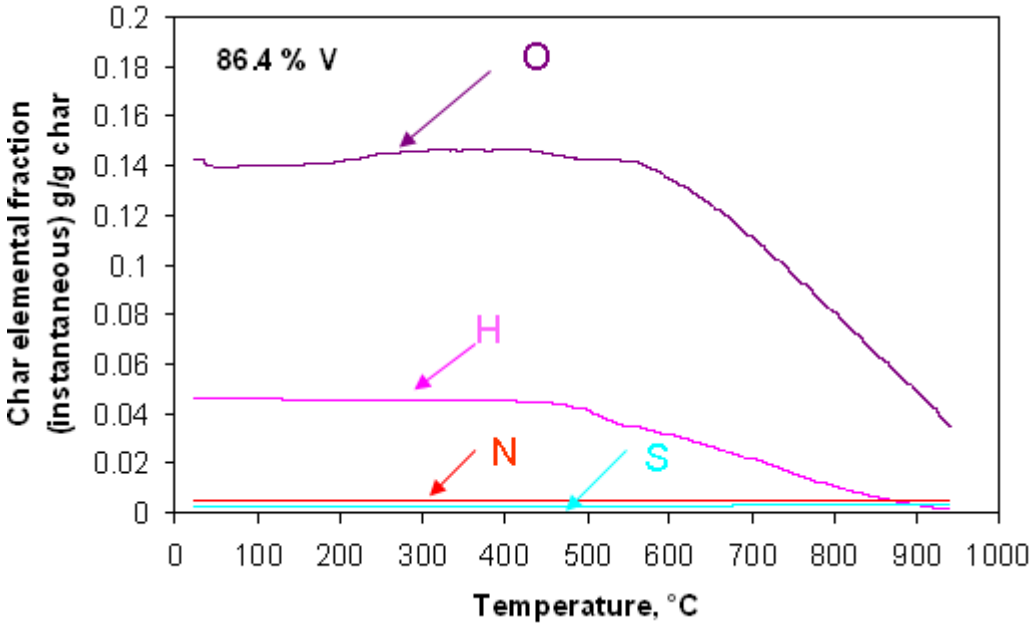

Figure C.1. The re-scaled Figure 8.16

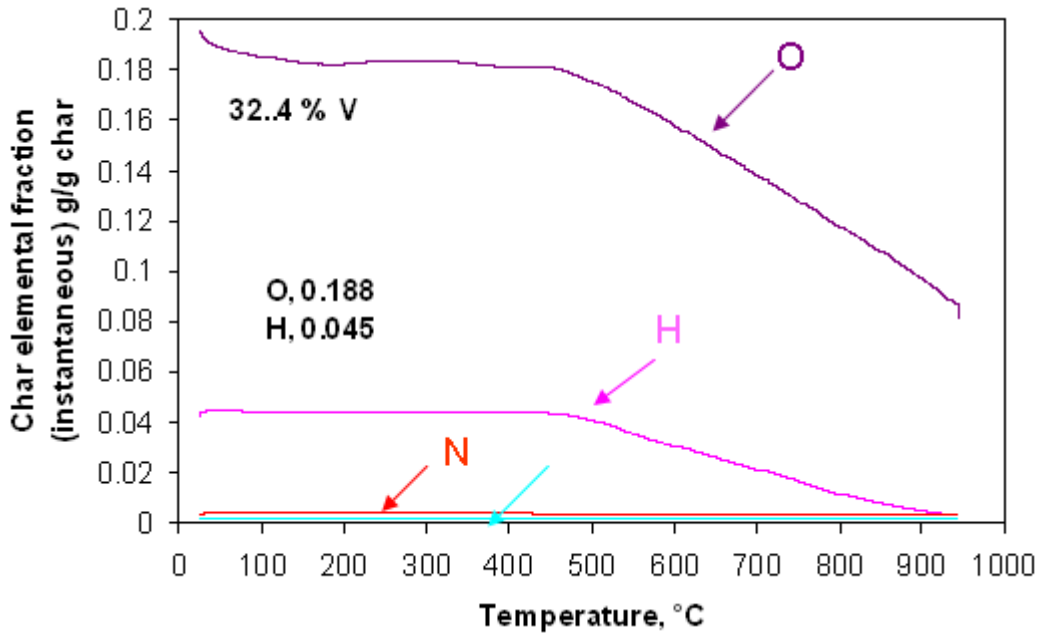

Figure C.2. The re-scaled Figure 8.17